University of Alberta

Geothermics of the Phanerozoic strata of Saskatchewan

by

Tibor Lengyel

A thesis submitted to the Faculty of Graduate Studies and Research
in partial fulfillment of the requirements for the degree of

Master of Science

Department of Earth and Atmospheric Sciences

Fall 2013
Edmonton, Alberta

Legyen Tiéd [...] a dicsőség

Abstract

New data and revised processing methods yielded a revised understanding of the geothermics of the Phanerozoic strata in Saskatchewan. Temperatures increase with depth from 5 °C at 100 m to 120 °C at 3200 m. Average integral geothermal gradients range between 25 and 30 °C·km^{-1}. Geothermal gradients are higher than average between the Cypress Hills and Swift Current; in the Weyburn-Estevan area; and at Yorkton. Anomalously cold areas are present near the Alberta border and at Saskatoon. Hot anomalies are present due to excess basement heat generation, the insulating effect of low thermal conductivity shale packages, and topographic effects. Colder than average areas coincide with areas of low heat flow. No extremely high geothermal gradients (>50 °C·km^{-1}) or significant vertical heat flow differences (>10 mW·m^{-2}) exist along the outcrop edge, therefore heat conduction is considered the main heat transfer method in the basin.

Acknowledgements

In the course of research I have received help from a vast number of people. First, I would like to acknowledge Dr. Ben Rostron, my supervisor for his continued support and patience while I have been carrying out the never-seem-to-ending quality control and the rest of the work. I have learned a lot about scientific attitude and scientific writing from him. Should I ever continue on an academic career it will be a lot due to what I have learned from him. I would also like to acknowledge the very useful comments made by my exam committee members Dr. Inga Möck and Dr. Carl Mendoza. These comments helped improve the final copy of my thesis a lot. Carl and Ben also introduced me to many concepts, ideas in hydrogeology throughout my studies, which are not just fascinating, but also, highly useful.

The open door policy of Dr. József Tóth, his continuing support, and also his connections, which made participating in this research possible for me on the first place, are gratefully acknowledged. Sharing an office for years with him is my honour, and it let me learn, what kind of passion a true scientist has towards his research. Another very influential scientist throughout my studies was Dr. Jacek Majorowicz: the countless times I could consult with him, his never-ending help with my ideas, his help of pointing me into the right direction proved to be instrumental in development of my geothermal knowledge and are gratefully acknowledged.

The geologists and geoscientists of the Saskatchewan Ministry of Economics provided the framework that I could build on. I am especially grateful for Melinda Yurkowski, Gavin Jensen and Arden Marsh. Our semi-annual meetings in Regina with them and with the rest of the research team were a great force to move my project forward. I would also like to acknowledge the help of Brian Brunskill, who has been always willing to help me and provided me with means to answer my questions.

Several people helped me on various occasions and topics: Munir Sharar and Gregg Peterson from Weatherford, Melanie Bridgeman from ERCB, James Lawson from PotashCorp, Dr. Yoram Eckstein from the Kent State University and Dr. Jon Busby from BGS assisted greatly me with understanding, how different temperature measurements are taken, which knowledge proved to be crucial in quality controlling temperature data. Dr. Lorraine Manz from the NDGS and Dr. Matt Grobe from ERCB provided me with information on thermal conditions outside my study area helping to constrain the edges of my maps. Dr. Alan Jessop helped me out with high quality data for my study area. Caroline Barnes helped me with information on soil surface temperature measurements, while Bruce Bauer and Shaopeng Huang helped with shallow heat flow measurements. I would like to also acknowledge the help I have received from Anna Crowell and Dr. Will Gosnold from the UND with regards to thermal conductivity data. I am also grateful for the various companies providing our group and my research project with data and/or software to work with. I would like to acknowledge: Accumap (IHS), geoSCOUT (Geologic Systems), temperature logs from MJ Systems and net rock analysis from CanStrat.

My friends and colleagues at the University of Alberta Hydrogeology Group and outside made this journey much easier, much more fun to take part in. I am especially grateful for Brigitta Czauner, Judit Déri-Takács, Rares Bistran and Anatoly Melnik for helping me in all of my academic endeavours, like abstracts, talks, posters. Listening to me countless times have probably made you experts on the geothermics as well.

Finally, I would like to acknowledge my hinterland, people who provided me with support. My friends helped me staying on the right track. I am especially indebted to Csaba Tóth for his continued support and to Márton Kelemen for his attempts to cut through some of the Gordian knots I have been facing. My family, my Mom and my Dad taught me work ethic and were inspirational in so many different ways... Talking to you has always been the source of joy during my days! The encouragement I have received from you, Mom, whenever I was facing

challenges helped me through the rough times. Miki, I am glad that even if we were this far apart, but we were at least on the same continent, and we could talk frequently and you gave advice with so many questions. You are probably those, who have listened almost the most time to my presentations. I really miss you, Nagyi, but I hope you can still see and are happy about my results. And last, but not least, I would like to acknowledge Andi: I am not sure how I would have completed this part of my life without you - you have listened literally hundreds of times to my presentations, you have stayed up late to help me, when I had to stay up late, provided me with whatever I needed for success. My success is your success as well... Thank you!

Table of contents

List of tables

List of figures

List of abbreviations

BHT – Bottom hole temperature measurement. A borehole temperature measurement conducted in conjunction with geophysical logs. Records only a single temperature value with a maximum thermometer.

DSL – Dominion Land Survey

DST – Drill stem test. A borehole temperature measurement method conducted while drill-stem testing, (formation testing) with usually repeated cycles of shut-in and flow periods.

masl – metres above sea level

mbsl – metres below sea level

m KB – metres below kelly bushing

SPFPS - Saskatchewan Phanerozoic Fluids and Petroleum Systems assessment.

WCSB – Western Canadian Sedimentary Basin

WPS – Well pressure survey, a category of borehole temperature measurement methods. It has several different subtypes, but they are all usually conducted after the well has started producing.

1 Introduction

Temperature has a significant impact on the rate of the subsurface biological, physical and chemical processes. Temperature generally increases with depth; however the rate of this increase depends on the local geothermal conditions. The knowledge of the local geothermal conditions is important for various fields of geosciences and engineering, including petroleum geology, hydrogeology, and drilling engineering.

The Western Canadian Sedimentary Basin (WCSB) is a large sedimentary basin with significant hydrocarbon reserves (National Energy Board, 2012) extending from the Northwest Territories to Manitoba and covering more than 1 400 000 km^2 (Mossop and Shetsen, 1994, Figure 1.1). It has two sub-basins: the Alberta Basin and the Williston Basin. They are separated by the Sweetgrass Arch (Figure 1.1). The Williston Basin straddles over the international border with the US.

Previous studies

The geothermal conditions of the WCSB are important for most subsurface activities in the basin (e.g., hydrocarbon production, geological storage of CO_2, and potential geothermal energy utilization). Therefore, numerous geothermal studies have been published previously on the WCSB since the 1960's including: Anglin and Beck, 1965; Bachu and Burwash, 1994; Jones and Majorowicz, 1987; Garland and Lennox, 1962; Majorowicz and Jessop, 1981. However, the majority of the studies focused on the western part, i.e., on the Alberta Basin (e.g., Bachu, 1988; 1999; Beach *et al.*, 1987; Jones *et al.*, 1984; Lam and Jones, 1984; Majorowicz *et al.*, 1985a, 1985b), and not the eastern portion, the Williston Basin (locations: Figure 1.1).

It is important to note that most of these regional geothermal studies in the WCSB utilized dominantly bottom hole temperature measurements, which are of questionable quality (e.g., Bachu (1999) questions their quality).

The study of Majorowicz *et al*., (1986) is the only detailed, Saskatchewan wide study known that focused on deep geothermal conditions. They mapped temperatures at 1 and 2 km beneath ground surface. The mapped temperatures increase with depth (30- 40 °C at 1 km, and 55- 70 °C at 2 km). Highest values were identified near Swift Current and in the Weyburn-Estevan area. They have also calculated heat flow density (in short: heat flow) for both the Paleozoic and the younger strata using thermal conductivities estimated based on lithology. Regions of high heat flow (>100 $mW \cdot m^{-2}$) were observed in the Paleozoic rock package in the Weyburn-Estevan area extending north from the US border, and along the basin edges in the younger strata, in the northeast. Therefore, Majorowicz *et al.,* (1986) concluded based on the distribution of heat flow, and vertical heat flow differences that regional groundwater flow has a significant effect on the redistribution of subsurface heat.

In the most recent, detailed, WCSB wide, geothermal study, Bachu and Burwash (1994) identified several regions with anomalously high geothermal gradients (>50 $°C \cdot km^{-1}$) close to the Precambrian outcrop edge. These high geothermal gradients were explained as possibly being the result of local scale convection.

The role of regional groundwater flow, previously suggested to be an important factor in basin wide heat redistribution (e.g., Hitchon, 1984, Majorowicz *et al*., 1986) was questioned based on dimensional analysis. For example, Bachu (1988) calculated Peclet numbers (Pe) for the hydrostratigraphic units of the Alberta Basin and found that the Pe is several orders of magnitude smaller than 1[1]. Therefore he identified heat conduction to be the dominant heat transfer method in the Alberta Basin. Therefore, Bachu and Burwash (1994) explained the basin scale geothermal features of the WCSB to be determined by the large scale basement tectonic features, as the heat redistribution effects of regional groundwater flow became controversial in the basin.

[1] If Pe>>1, the system is convection dominated, if Pe<<1, the system is conduction dominated. At Pe~1 conduction and convection have similar importance in heat transfer.

More recent, detailed, local scale, deep geothermal studies of the WCSB are available only for the Alberta Basin (e.g., Bachu, 1999; Majorowicz *et al.*, 1999) and not for the Williston Basin. These also concluded that regional groundwater flow cannot explain the high geothermal gradients observed along the edges of the basin. Majorowicz *et al.* (1999; 2012) concluded that extremely high geothermal gradient values next to the edges of the Alberta Basin are probably the result of incorporating erroneous measurements in previous studies. However, the cause of the trends observed on geothermal maps (e.g., geothermal gradients, heat flow) and the contribution of regional groundwater to the large scale geothermal patterns in the Williston Basin remained unidentified.

In contrast to the Canadian part of the Williston Basin, more recent geothermal studies of the basin have been completed on the US portion (e.g., Crowell *et al.*, 2011; Gosnold, 1990; 1999; Gosnold *et al.*, 2010; 2012). Newly measured thermal conductivities are of special importance. Gosnold (1990) revised previous heat flow calculations on the US side of the basin using newer, measured thermal conductivities and concluded that the previously identified heat flow anomaly (>100 $mW \cdot m^{-2}$) extending into Canada was the result of overestimated shale thermal conductivities. A similar revision has not been done for Saskatchewan yet.

Finally, an additional motivation for a new, comprehensive geothermal study of the Williston Basin is to incorporate newly available data. The amount of new data is especially significant for the deeper strata of Saskatchewan: many new deep wells have been drilled, since the enactment of deep rights reversal in 1998[2]. For example, before the discovery of the prolific Red River Midale oil pool in December 1995 (Haidl *et al.*, 1996) only 189 wells were drilled into the basement over a period of about 50 years[3]. Following the discovery of this pool, the rate of

---

[2] http://www.gov.sk.ca/news?newsId=d4bed916-7f3d-479c-b6ca-e81c8b05f113), [Last accessed: 2012.12.18]

[3]First commercial oil well drilled in Saskatchewan in 1943. http://www.gov.sk.ca/Default.aspx?DN=4a57f37e-88de-4da5-b6a8-411793a739d5 [Last accessed: 2012.12.31]:

drilling wells into the basement has more than doubled due to the renewed interest in deep formations: another 148 new wells have reached the basement by 2011.12.31 (data from Accumap®). In addition to new geothermal data, a new, detailed stratigraphy has been also developed for the Phanerozoic strata of Saskatchewan (Marsh and Love, 2013).

Thus, an opportunity exists that by utilising the newly available and better quality data (see Chapter 3.1), and new methods (e.g., Chapter 3.3) the understanding of the geothermal conditions of the Phanerozoic strata of Saskatchewan could be improved, and also the much debated geothermal pattern of Saskatchewan could potentially be explained.

1.1 Study area and objectives

This study was initiated as part of a larger scale, Saskatchewan wide, multidisciplinary study: the Saskatchewan Phanerozoic Fluids and Petroleum Systems Assessment (SPFPS, Whittaker *et al.*, 2009). The previously mentioned newly-developed stratigraphy of Saskatchewan (Marsh and Love, 2013) has been also developed within the framework of this multidisciplinary study. Results of this geothermal study can be used for multiple purposes including potential facilitation of geothermal energy utilization, basin modeling, understanding hydrocarbon maturation, migration and entrapment, and assessing CO_2 sequestration potential.

The area of interest for this study is bounded to the north by the outcrop edge of the Precambrian shield and to the east, south and west by the political boundaries of Saskatchewan (Figure 1.1). The underlying Precambrian basement forms the lower stratigraphic boundary of the studied sediments, as this study analyses only the geothermal conditions of the Phanerozoic rock strata. There is a mild topographic gradient from the elevated southwest towards the low lying northeast in the study area (Figure 1.2).

The study area was surveyed in the Dominion Land Survey system and was divided into Townships and Ranges with respect to certain marked Meridians. The grid used for the maps produced in this study (e.g., Figure 3.10, Figure 4.1 to Figure 4.18 (except for Figure 4.13) and maps in the Appendices) is the grid created within this land survey.

Data from two Townships outside the boundaries of the study area were collected and utilized during mapping to reduce the artificial effects of contouring near map edges. The properties of various data types and the methods of handling them are described in Chapter 3.

The study has the following objectives:

- Creation of a comprehensive database of pre-existing temperature data from commercial and public sources;
- Characterization of the subsurface thermal conditions as illustrated by a set of temperature maps at various depths, elevations, and at the top of major regional aquifers identified by recent studies;
- Estimation of the regional heat flow density field.

The next chapter will provide a detailed review of the current knowledge of the study area.

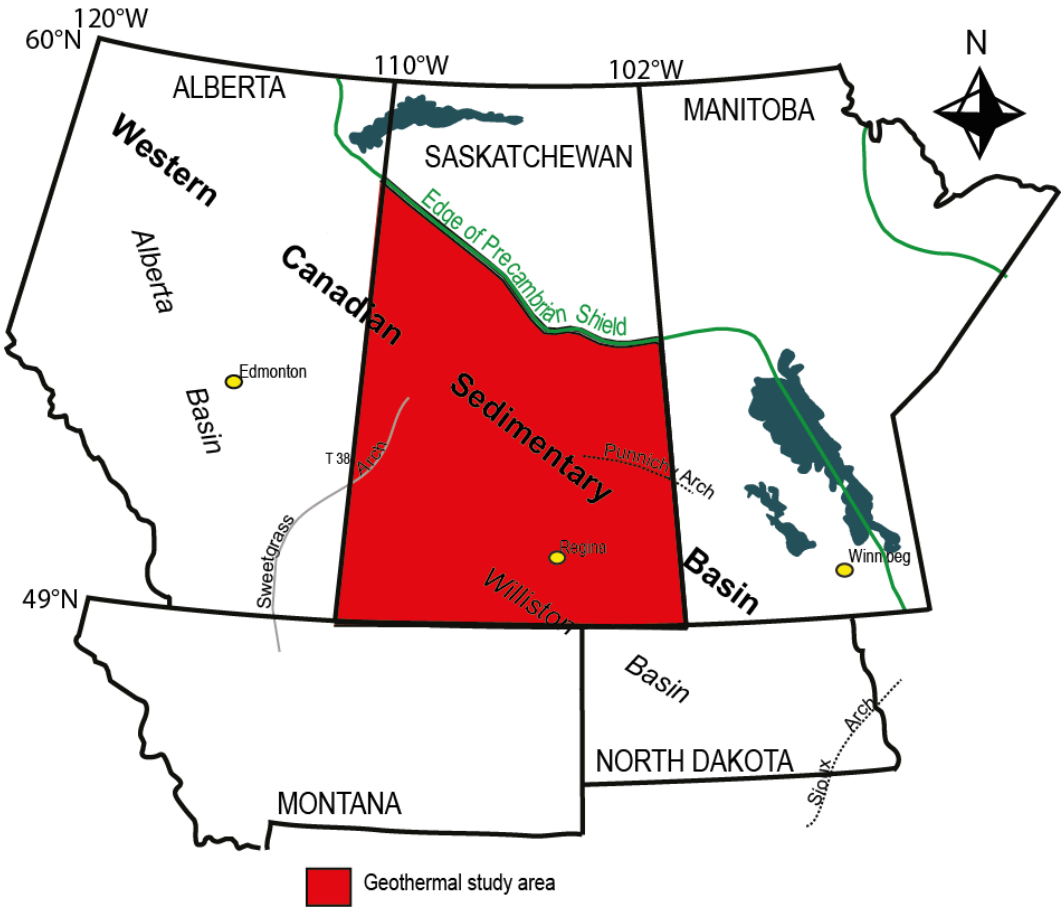

Figure 1.1 Location of the study area, the Western Canadian Sedimentary Basin and its two sub-basins, i.e., the Alberta Basin and the Williston Basin.

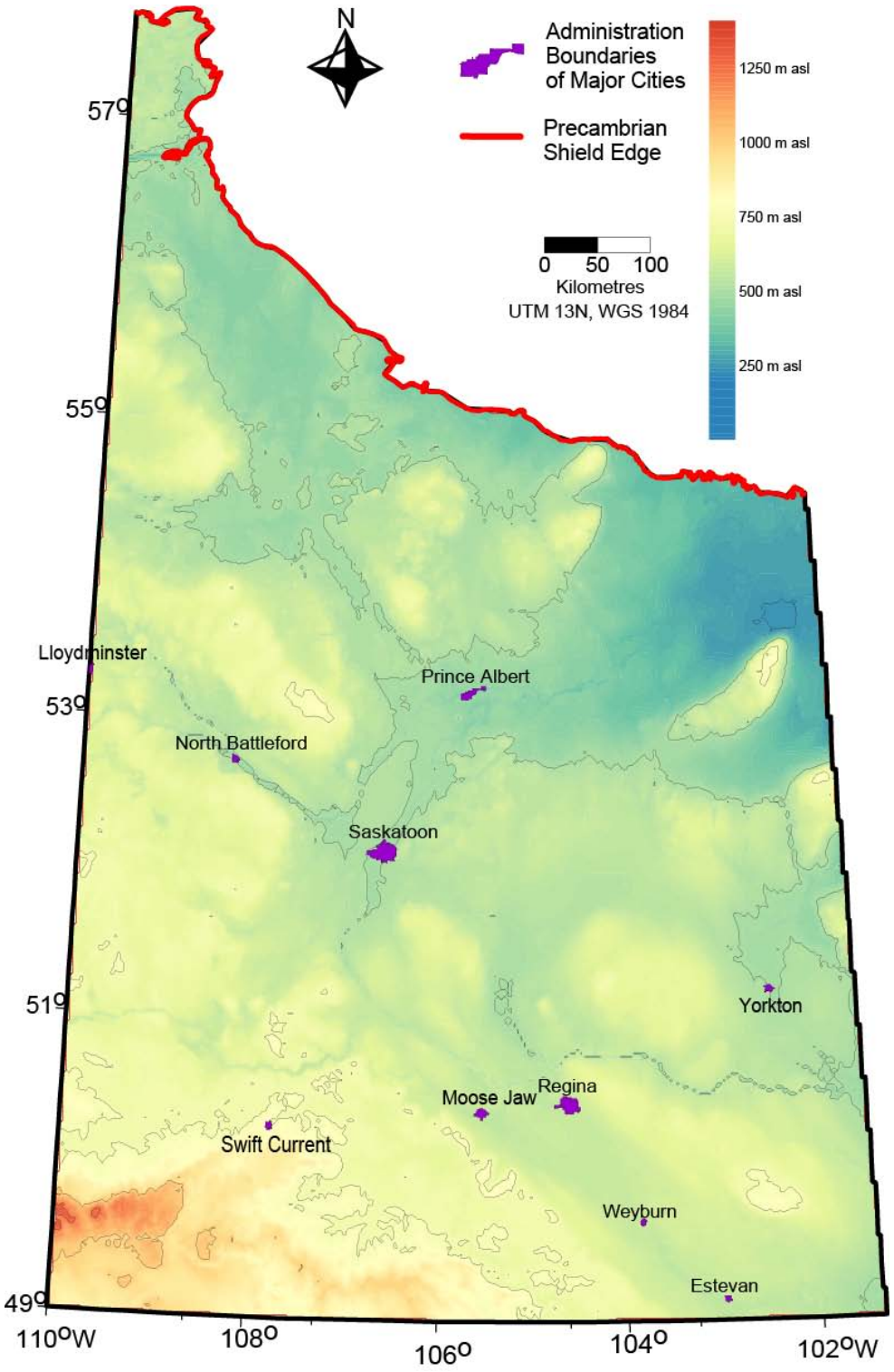

Figure 1.2 Topographic map of the study area. (DEM data from GeoBase®).

2 Background

2.1 Regional geology

Lithology influences the geothermal conditions; for example different types of rocks, with various thermal conductivity values (e.g., shale: 1.1 $W \cdot m^{-1} \cdot °C^{-1}$, limestone: 3 $W \cdot m^{-1} \cdot °C^{-1}$), result in different geothermal gradients (e.g., if heat flow is 60 $mW \cdot m^{-2}$, then the geothermal gradient in the shale is ~54.5 $°C \cdot km^{-1}$ and 20 $°C \cdot km^{-1}$ in the limestone). Therefore, the regional geology and stratigraphy of the Phanerozoic rocks of the study area will be summarized here briefly.

The study area covers the northern portion of the Williston Basin. The Williston Basin is an ellipsoidal intracratonic basin with maximum Phanerozoic sediment thickness of over 4500 m (e.g., Peterson and MacCary, 1987, Burgess, 2008). The thickness of the Phanerozoic sediments in the Canadian portion of the basin ranges from 0 m at the Precambrian outcrop edge to ~3200 m in southeast Saskatchewan at the international border (Kent and Christopher, 1994).

The Phanerozoic strata of the Williston Basin can be divided up into five major transgressive-regressive sequences bounded by unconformities (Carlson and Anderson, 1965; Kent and Christopher, 1994). One of these major regional unconformities is the sub-Mesozoic unconformity (Figure 2.1).

This sub-Mesozoic unconformity is used in this study to divide the rocks into two intervals with markedly different lithologies: The Paleozoic sediments are dominated by carbonates and evaporites with only minor amounts of sandstones and shales; while the Mesozoic and Cenozoic sediments are dominated by clastic sediments (Figure 2.1).

Stratigraphy

The stratigraphy of the Williston Basin and adjacent areas has been described in great detail elsewhere (e.g., Gerhard *et al.*, (1982); Kent and Christopher, (1994);

Kreis *et al.*, (2004); or Peters and MacCary (1987)). Here only a brief overview of the stratigraphy will be given.

The first deposition sequence lasted for the Cambrian period. The Cambrian clastic sediments with minor amounts of carbonate unconformably overly the Precambrian basement in the Williston Basin (Kreis *et al.*, 2004). The Deadwood Formation represents the first major marine transgression after a long period of aerobic exposure of western North America. In the mid-Ordovician a major regression exposed these rocks resulting in widespread erosion of Cambrian rocks (Peters and MacCary, 1987).

The second transgression-regression sequence covered the time interval between the Ordovician and Silurian periods. The depocentre of the basin became clearly defined during this period (Gerhard *et al.*, 1982, Peters and MacCary, 1987). The Ordovician sediments and the Cambrian rocks are separated by a major erosional unconformity.

The first part of this sequence is dominated by marine siliciclastic sediments (Burgess, 2008) similar in make-up to the Cambrian sediments, i.e., the rocks of the Winnipeg Formation and the basal beds of the Red River Formation are mostly sandstones, siltstones and shales (Peters and MacCary, 1987). These Cambrian-Ordovician sediments together form the clastic base of the Paleozoic strata.

The rest of this sequence is dominated by carbonate-evaporite strata (Burgess, 2008). They were formed in warm shallow sea (Kreis *et al.*, 2004) and sabkha environments (Gerhard *et al.*, 1982). These rocks are characterized by repeated cycles of carbonates and evaporites (brining upwards sequences). These repetitive cycles can be explained by tectonism, cycles of Ordovician continental glaciations and climatic changes (Peters and MacCary, 1987). While the lower Red River Formation is mostly characterized by limestone, dolomites are dominant in the Interlake Formation (Peters and MacCary, 1987).

Following the deposition of the Silurian rocks, a major regression event affecting most of interior North America ended this deposition cycle. This regression event spanned the Middle Silurian to Early Devonian period (Burgess, 2008; Kent and Christopher, 1994), and resulted in widespread erosion of the pre-Devonian rocks (Peters and MacCary, 1987).

The third sediment deposition cycle lasted between the Devonian and the Mississippian. Shallow water carbonates, argillaceous carbonates and evaporites are characteristic of this interval (Peters and MacCary, 1987) with repetitive shallowing upward cycles (Kent and Christopher, 1994).

The first shallowing upward cycle started with red dolomites, siltstones and shale beds, which represent the erosion of earlier Paleozoic rocks (Ashern Formation, Gerhard *et al.,* 1982). Reef carbonates of the Winnipegosis Formation (Peters and MacCary, 1987) developed over this erosional base. This sub-cycle completed with the deposition of the evaporites of the basin infill Prairie Formation (Kent and Christopher, 1994).

The Middle and Upper Devonian formations (Dawson Bay, Souris River, Duperow, Birdbear) overlying the Prairie Formation all form similar shallowing upward carbonate cycles capped by bioclastic bank or sabkha facies sediments (Burgess, 2008). These carbonate cycles are capped by the siliciclastic sediments of the Three Forks Group.

The deposition of the Three Forks Group marked a smaller regression phase. This regression was caused by the increased sediment transport from the west due to the uplift of the Ancient Rockies (Peters and MacCary, 1987).

The clastic sediments of the Three Forks Group also form the initial phase of the next transgression: this starts with the clastic sediments of the Bakken Formation. The Bakken Formation has three units: a middle unit dominated by siltstone and sandstone, bounded by upper and lower organic rich shale units.

The Bakken Formation is overlaid by the carbonates of the Mississippian Madison Group deposited under relatively stable tectonic conditions (Peters and MacCary, 1987). Three formations comprise the Madison Group: the thin to medium bedded, argillaceous to silty Lodgepole Formation, the thick bedded to massive Mission Canyon Formation, and the Charles Formation consisting of carbonates interbedded with halite and anhydrite. The maximum transgression occurred near the end of the Lodgepole Formation (Gerhard *et al.*, 1982). Therefore the younger a Mississippian formation is, the more south its current subcrop is located[4].

The fourth major regression transgression cycle was constricted to the central parts of the basin. A long erosional hiatus lasted from late Mississippian to late Triassic (Kent, 1987) on the northern margin of the basin due to tectonic uplift of the surrounding areas (Gerhard *et al.*, 1982; Burgess, 2008).

The fifth, major deposition sequence starts with Jurassic strata, which are still carbonate dominated (Gerhard *et al.*, 1982; e.g., Shaunavon Formation). However, the Cretaceous strata are dominated by clastic sediments (Burgess, 2008) with thick shale packages (e.g., Colorado Group). The relative thickness of these sediments varies by location.

2.2 Hydrogeology

Understanding hydrogeology in conjunction with geothermal studies is important for several reasons. On the one hand, a geothermal study may assist hydrogeological studies (e.g., with calculating density for density dependent flow analysis, Bachu, 1995). On the other hand, the flow of water can significantly alter the geothermal field under appropriate conditions (e.g., Deming *et al.*, 1992; Smith and Chapman, 1982). In addition, the availability of water influences the economics of geothermal energy utilization (i.e., the amount of geothermal energy that can be produced is linearly dependent on the yield of the confined aquifer,

[4] E.g., Mississippian maps: <http://www.manitoba.ca/iem/mrd/geo/willistontgi/maps.html#> [Last accessed: 2012.12.31]

Čermák and Haenel, 1988). Thus, hydrogeological conditions of the study area are of importance.

Hydrogeology of the Williston Basin has been extensively studied (e.g., Bachu and Hitchon, 1996; DeMis, 1995, Hannon, 1987). Regional groundwater systems of the Williston Basin flow dominantly from the elevated recharge areas in the southwest (Figure 1.2) towards the low-lying discharge areas along the northern, northeastern edges of the basin (e.g., DeMis, 1995, Hannon, 1987). The latest complete, province-wide hydrogeological investigation of Saskatchewan identified seven major aquifer systems in the deep subsurface (Bachu and Hitchon, 1996).

The University of Alberta Hydrogeology Group has carried out more recent, detailed studies of the hydrogeology of various parts of the Williston Basin (Al-Kalali, 2002; Iampen, 2003; Khan, 2006; Margitai, 2002; Melnik, 2012; Palombi, 2008). A province wide integration is planned (Whittaker *et al.,* 2009), but remains in progress. These studies have significantly refined previous hydrostratigraphy and identified between 12 and 19 regional aquifers, depending on the studied region (Figure 2.1).

These more recent hydrogeological studies indicate for their respective areas that the main direction of regional fluid flow is similar to that identified previously, i.e., from the southwest towards the low-lying areas in the northern, northeastern parts of the Williston Basin. However, Al-Kalali (2002), Palombi (2008) and Melnik (2012) have identified areas, where the regional flow of groundwater can actually change direction or become sluggish due to density effects. In addition, Grasby and Betcher, (2000) proposed Pleistocene flow reversal in the discharge areas of the Williston Basin. Flow rates inferred by these two observations are low and thus they are not likely to be sufficient to significantly impact geothermal conditions.

2.3 Previous geothermal investigations of the WCSB and the Williston Basin

Geothermal conditions have been studied in the WCSB since the 1960's: the first studies were conducted by Garland and Lennox (1962) and Anglin and Beck (1965). However, it was not until the early 1980's following the investigations of the 1960's that the interest in the geothermal conditions of the WCSB rose again as part of the National Geothermal Energy Program (Grasby *et al.*, 2012). During this period several studies were published describing geothermal conditions of the WCSB. However, most of these studies investigated the western half of the basin (e.g., Bachu, 1985; 1988; Jones *et al*., 1984; Lam and Jones, 1984; Majorowicz *et al.*, 1985a, 1985b). The results of this period of research were summarized in the chapter on geothermics in the Geological Atlas of the Western Canada Sedimentary Basin (Bachu and Burwash, 1994). Only few studies have been published on the geothermics of the WCSB since then (e.g., Bachu, 1999; Majorowicz *et al*., 1999; 2012). In the following the results of these previous investigations will be detailed.

Temperature

On a regional scale the temperature in the WCSB "shows a striking similarity to and correlation with the isopach of the sedimentary cover on top of the Precambrian basement" (Bachu and Burwash, 1994, pg. 450, illustrated by Figure 2.2). They found that temperatures range from over 140 °C in the deepest part of the basin to less than 20 °C at the edges at the Precambrian surface in the WCSB (Figure 2.2). However, in the study of Bachu and Burwash (1994) it is hard to determine, whether any of the regions have anomalous temperature values (i.e., areas, where temperature values are significantly higher or lower than at the same depth in its surroundings), as the depth of the Precambrian surface varies along the WCSB from deeper than 3000 m below sea level to above sea level (Figure 2.3).

Majorowicz *et al.*, (1986) studied the temperature distribution at 1 and 2 km below the surfaces for the eastern portion of the basin. In such a representation it is much easier to identify anomalous regions. For example, they recognized a temperature high anomaly in the Weyburn-Estevan area. The temperature map at 1 km shows temperature values over 40 °C in this area, while the rest of their study area is colder than this (30- 35 °C, see Figure 2.4). They explained this anomaly to be the result of the insulation of the thick package of low-conductivity shale in the shallower strata.

Geothermal gradient

Previous studies identified a regional increase of geothermal gradients from less than 20 °C·km^{-1} in the southeast to over 50 °C·km^{-1} along the edges of the basin (e.g., Bachu and Burwash, 1994, also see Figure 2.3). Early on it has been recognized that this trend correlates with the Phanerozoic sediment thickness (e.g., Majorowicz and Jessop, 1981), i.e., high geothermal gradients coincide with areas, where the sedimentary package is thin, and low geothermal gradients correspond to areas, where the sedimentary package is thick.

There is a controversy with regards to the origin of the observed basin scale trend of geothermal gradients. Some origins proposed to cause it are: heat redistribution by regional groundwater flow (e.g., Hitchon, 1984; Majorowicz and Jessop, 1981); variable basement heat generation (e.g., Bachu and Burwash, 1991); or measurement errors of shallow data (Majorowicz *et al.*, 1999). Intermediate scale features, like the higher than average geothermal gradients near Swift Current were explained by locally increased basement heat generation (e.g., Bachu and Burwash, 1994).

Thermal conductivity

There are only few studies that have published measured thermal conductivity values for the rocks of the WCSB (these are: Jessop and Vigrass, 1989; Jones *et al.*, 1984; Kushigbor, 1984) and thus most regional geothermal studies have estimated thermal conductivities based on net rock analysis (e.g., Bachu, 1993;

Bachu and Burwash, 1994; Majorowicz and Jessop, 1981). The estimated thermal conductivities for the entire sedimentary package range between 1.9 $W \cdot m^{-1} \cdot °C^{-1}$ and 2.9 $W \cdot m^{-1} \cdot °C^{-1}$ in the Alberta Basin (Majorowicz and Jessop, 1981). No apparent trends could be identified on thermal conductivity maps.

While a major gap of data exists in the WCSB with regards to measured thermal conductivities, an effort has been undertaken in the US portion of the Williston Basin to make up for this lack of measurements. Especially important are the shale thermal conductivities measured and published by the University of North Dakota geothermal group (e.g., in Gosnold, 1990; 1999; Gosnold *et al.*, 2010; 2012). These measured values (ranging from 0.9 to 1.2 $W \cdot m^{-1} \cdot °C^{-1}$ for shale) proved that shale thermal conductivities previously used for net rock analysis in the WCSB (e.g., 1.5 $W \cdot m^{-1} \cdot °C^{-1}$ in Majorowicz and Jessop, 1981) were overestimated.

Deep heat flow

Heat flow calculated for the entire sedimentary package shows similar features to the geothermal gradient maps, i.e., an increase from the southwest from <40 $mW \cdot m^{-2}$, towards the areas, where the Phanerozoic sediments of the basin pinch out, where it can be >80 $mW \cdot m^{-2}$ (e.g., Bachu and Burwash, 1994, also see Figure 2.5).

Paleozoic and Mesozoic-Cenozoic heat flow have been also investigated in the WCSB (e.g., Majorowicz *et al.*, 1985a; 1985b). In the Williston Basin (Majorowicz *et al.*, 1986) heat flow in the Paleozoic strata decreases from the south-southwest from values of >100 $mW \cdot m^{-2}$ towards the basin edges to values of <40 $mW \cdot m^{-2}$. In the Mesozoic-Cenozoic sediments the opposite is observed, i.e., an increase of heat flow from <60 $mW \cdot m^{-2}$ in the southwest to >100 $mW \cdot m^{-2}$ along the edges of the basin. Thus, a heat flow deficit is present in the shallow strata compared to the deep strata in the topographically elevated southwest (Figure 1.2), while a heat flow surplus is present along the low-lying edges of the

basin. A similar trend with regards to topography was observed in the Alberta Basin (Majorowicz *et al.,* 1985a; 1985b).

Jessop and Vigrass (1989) calculated heat flow for a research well in Regina based on measured thermal conductivity of rock samples and previously recorded high precision temperature logs. They also found a difference between the shallow and the deep heat flow. However, they explained it by potential issues with measuring shale thermal conductivities. Therefore, they considered the heat flow calculated for the Paleozoic strata valid for the location (51 $mW \cdot m^{-2}$).

In the US portion of the Williston Basin, Gosnold (1990) revised previous heat flow calculations based on newly measured thermal conductivity values, and identified that a previously identified major heat flow anomaly (>100 $mW \cdot m^{-2}$) in northern North Dakota was the result of overestimating shale thermal conductivities. Such revision of heat flow in the Canadian portion of the basin is yet to be done.

Shallow heat flow

Shallow heat flow determinations can also be in error due to effects of climate change. Some recent, local studies (e.g., Majorowicz and Safanda, 1998; 2001; Majorowicz *et al*., 2002; 2005; 2006) investigated the shallow geothermal conditions and showed a temperature transient being present due to recent warming. Majorowicz and Wybraniec (2011) proposed a correction for heat flow values for both the short term warming, and for the anomaly existing due to the long lasting effects of the previous ice age. Such correction has not been used on deep heat flow determinations in Saskatchewan to date.

Heat generation

Heat generation of the basement rocks of the WCSB was calculated from radioactive element concentration measured on cores (e.g., Bachu and Burwash,

1994). However, such values were measured only in two studies of the WCSB (these are: Bachu and Burwash, 1991; Burwash and Cumming, 1976[5]).

Bachu and Burwash (1994) calculated heat generation values to range between <1 $\mu W \cdot m^{-3}$ and >10 $\mu W \cdot m^{-3}$ in the latest analysis of heat generation in the WCSB. They identified two regions of higher than average heat generation to extend through Saskatchewan (the Edmonton anomaly, between T70-26W3 and T90-25W3 >4 $\mu W \cdot m^{-3}$; and the Swift Current anomaly, with a major high of >10 $\mu W \cdot m^{-3}$ in T16-17W3). The high anomaly at Swift Current reflects igneous rocks crystallised from highly differentiated magmas enriched in potassium, uranium and thorium (Burwash and Cumming, 1976).

Sedimentary heat generation has not been estimated previously for the eastern portion of the WCSB.

Room for improvement

Bottom hole temperature (BHT) measurements, which are the most commonly used source of temperature data in the WCSB (used by e.g., Bachu and Burwash, 1994; Jones *et al.*, 1985; Majorowicz *et al.*, 1985b) are subject to errors. Most of these studies acknowledged that such data bear error, but did not quantify it.

Jessop (1990) compared BHT data to high precision temperature logs, and concluded that individual data points may be in error as much as 30 °C. However, by sheer volume, BHTs may provide useful information (i.e., errors of fitted linear trends were <10 °C) on the geothermal conditions. Thus, using different sources of data would result in a better characterization of the geothermal conditions.

Shallow temperature data are especially prone to errors. Majorowicz *et al.*, (1999) proposed that these extremely high geothermal gradient values along the edges of the basement (e.g., Figure 2.3) are potentially just the result of erroneous

[5] potassium data published in Beach, 1985

measurements. Later, the issue with shallow bottom hole temperature data was confirmed in the Alberta Basin (e.g., Majorowicz *et al.*, 2012). However, an investigation of shallow data in the Williston Basin is yet to be implemented.

Improvements could also be made with regards to thermal conductivity. Previous estimates of thermal conductivity (e.g., Majorowicz and Jessop, 1981) used values to calculate thermal conductivity, which were proved later to be too high (e.g., by Gosnold, 1990). Therefore, a revision of thermal conductivity estimates in the Williston Basin needs to be undertaken.

Also a controversy exists with regards to the interpretation of the observed geothermal gradient and heat flow distributions. Majorowicz and Jessop (1981) compared the observed geothermal gradient and heat flow pattern to the distribution of radioactive heat generation and the distribution of calculated thermal conductivities, and found no obvious correlation between them.

However, they identified an apparent correlation with the hydrogeological maps, i.e., higher geothermal gradients and heat flow are in discharge areas (see Figure 2.6), while lower geothermal gradients are in recharge areas. Similar results were shown for Saskatchewan by Majorowicz *et al.*, (1986). Thus, several studies (including Hitchon, 1984; Majorowicz and Jessop, 1981; Majorowicz *et al.*, 1986) concluded that regional groundwater flow plays an important role in determining the geothermal conditions in the WCSB.

The results of these studies, including the vertical differences in heat flow identified both in Alberta and Saskatchewan (Majorowicz *et al.*, 1985a; 1985b; 1986) correspond to the predictions of theoretical models of coupled heat and groundwater flow (e.g., Domenico and Palciauskas, 1973; Smith and Chapman, 1982). However, in the WCSB this relationship was determined solely on a qualitative basis.

Bachu (1985) disagreed with the groundwater flow hypothesis. He was the first to use independent hydrogeological data in conjunction with the geothermal data to investigate geothermal conditions in the Cold Lake area of the Alberta Basin. He

concluded based on dimensional analysis that groundwater flow rates are too low on a regional scale to create the geothermal anomalies observed. He also suggested that convection might be important only on a local scale determining the geothermal patterns, in areas where permeabilities are enhanced. Later other studies have shown similar results (Bachu, 1988; 1999; Bachu and Burwash, 1991; 1994).

Thus, regional groundwater flow as an explanation of the observed geothermal pattern remains controversial. Revising previously used temperature measurements, calculated thermal conductivities also allows for the revision of heat flow calculations, potentially contributing to the interpretation of the observed geothermal gradient and heat flow patterns.

The previous paragraphs provide information on the current knowledge of the geothermal conditions, lithology and hydrogeology of Saskatchewan. The methods and the data used in this study to investigate the geothermal conditions of Saskatchewan will be detailed in the next chapter.

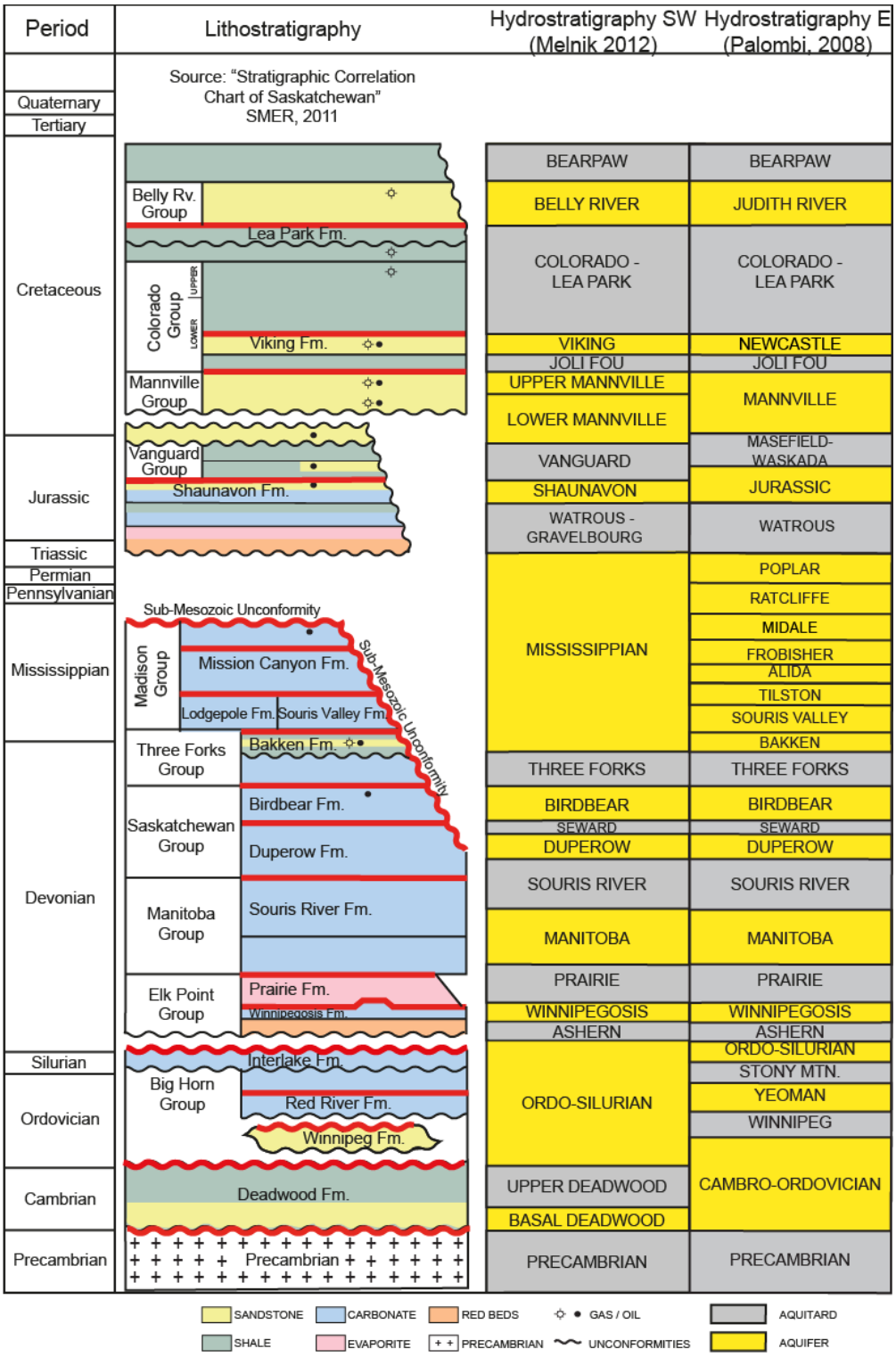

Figure 2.1 Lithostratigraphic and hydrogeologic chart of the study area. Thick red line marks formation tops, for which strata specific temperature maps were generated.

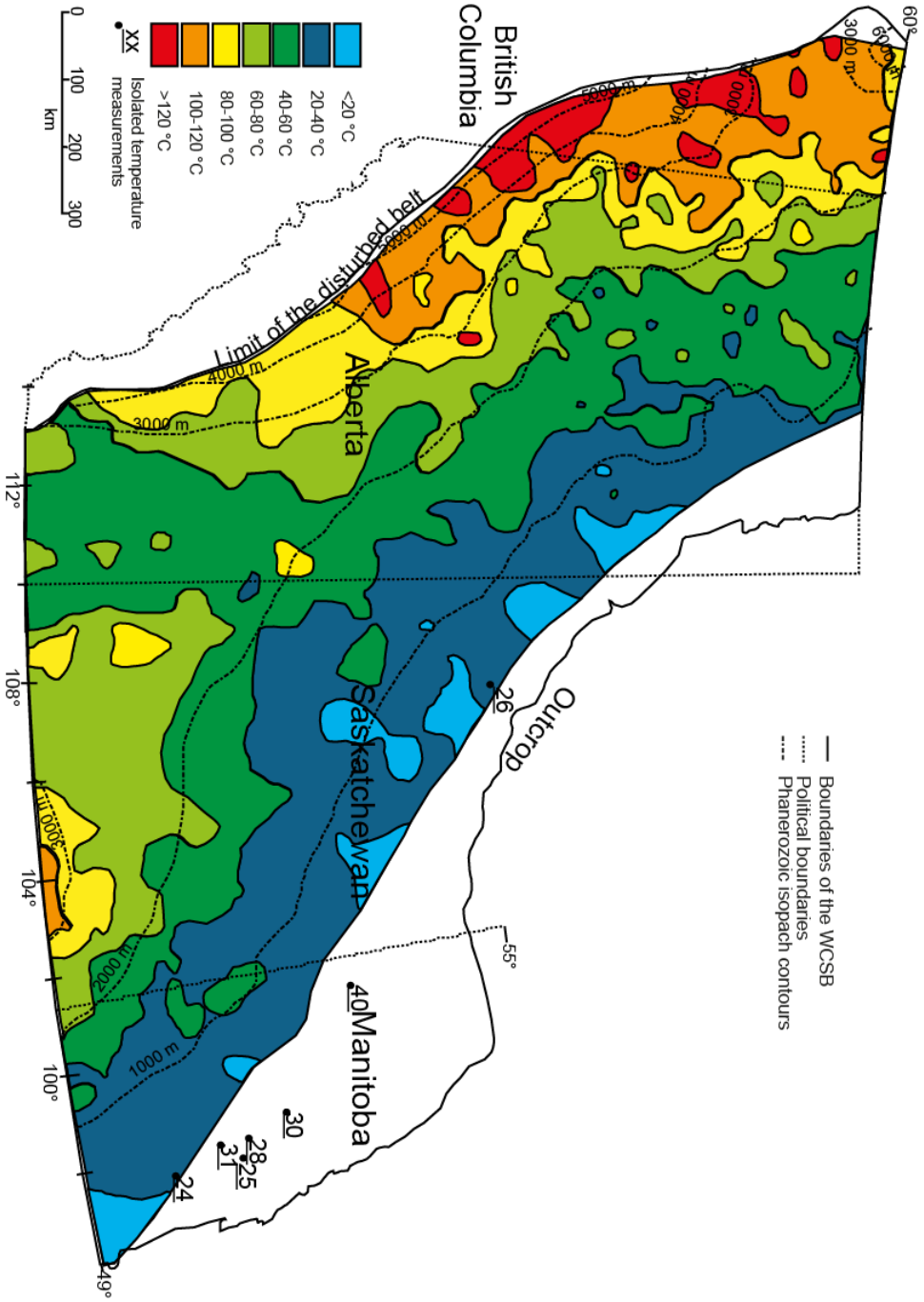

Figure 2.2 Temperatures at the Precambrian surface of the WCSB south of 60°N. Phanerozoic isopach contours are also shown. Modified after: Bachu and Burwash, 1994; Wright *et al.*, 1994.

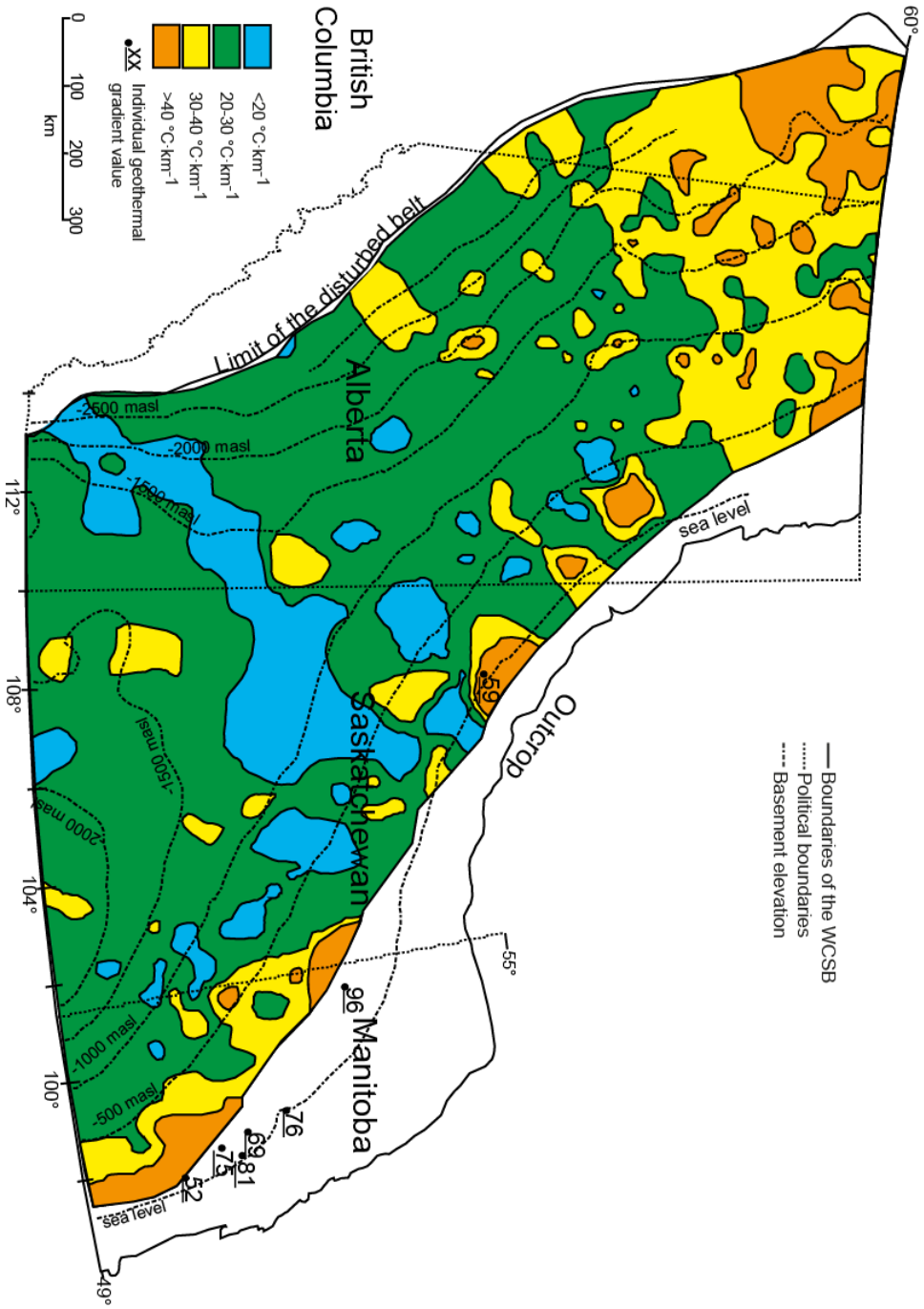

Figure 2.3 Integral geothermal gradient of the WCSB south of 60°N. Basement elevation contours are also shown. Modified after: Bachu and Burwash, 1994; Burwash *et al.*, 1994.

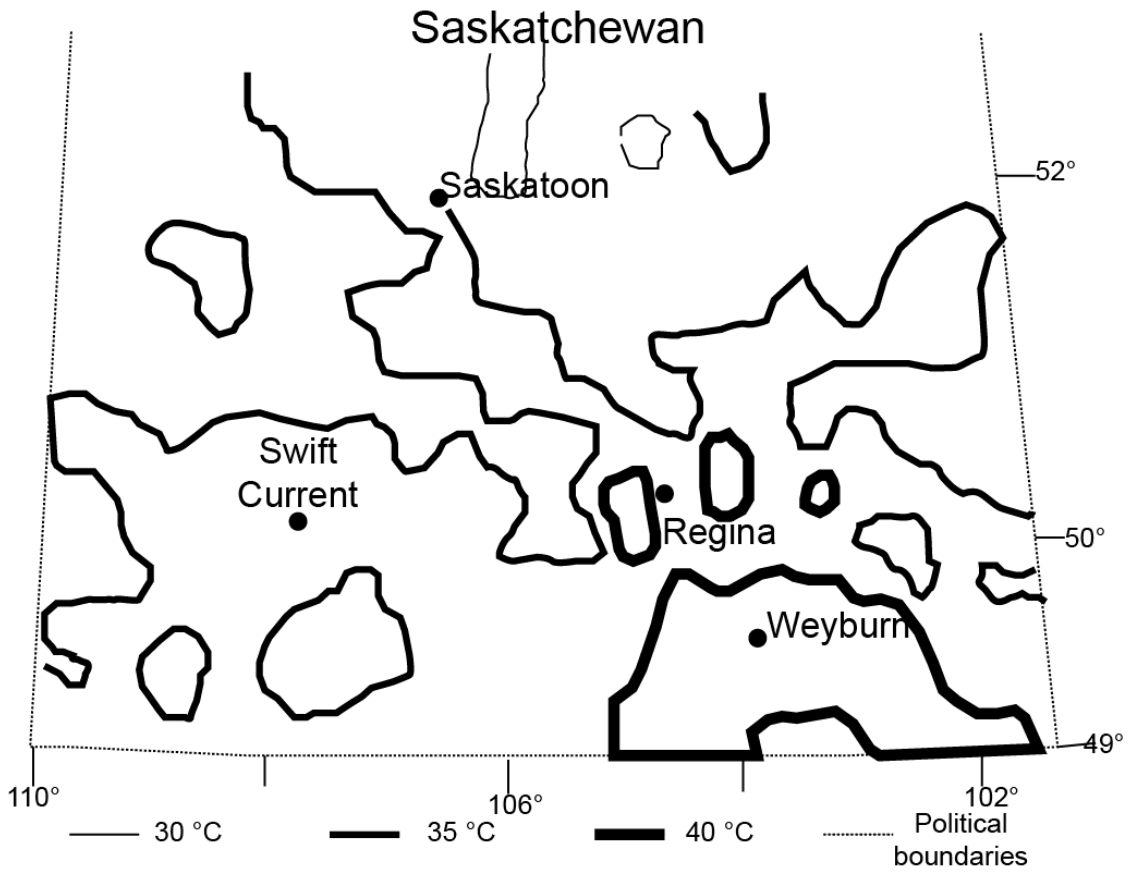

Figure 2.4 Temperatures at 1 km depth in Saskatchewan. Modified after Majorowicz *et al.*, 1986.

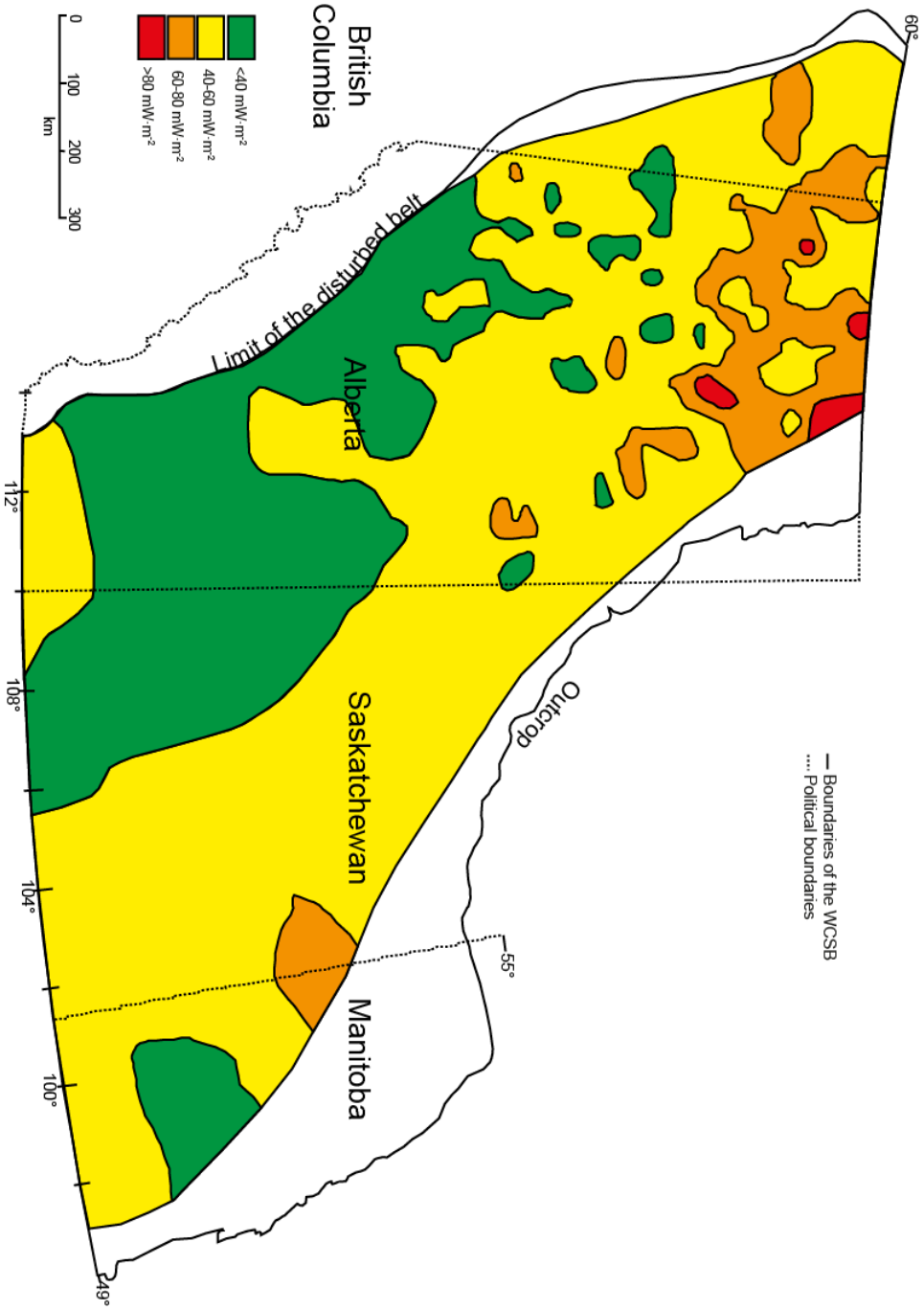

Figure 2.5 Heat flow in the Phanerozoic strata of the WCSB south of 60°N. Modified after: Bachu and Burwash, 1994.

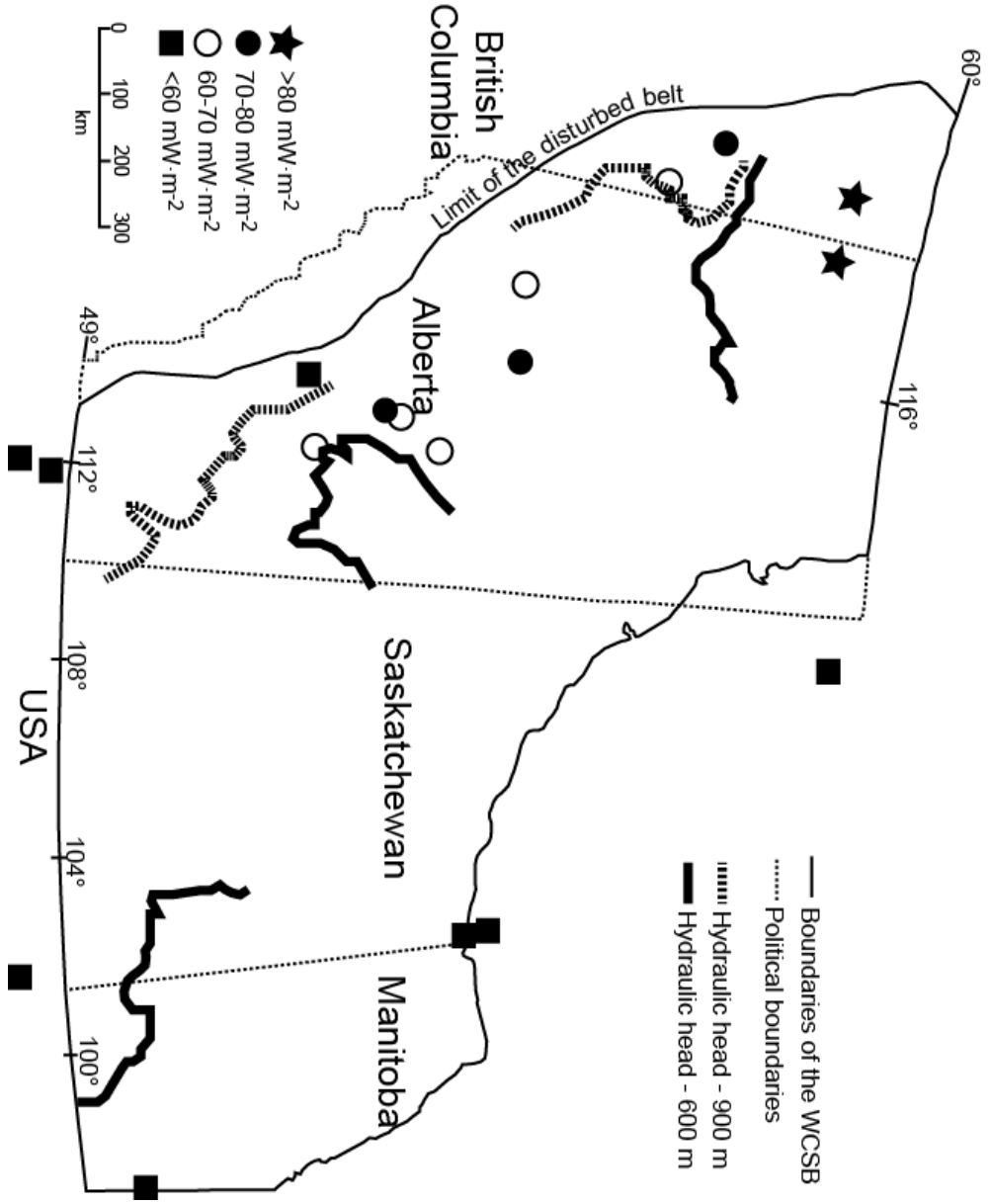

Figure 2.6 Heat flow calculated for the WCSB and correlation with the hydrogeological regime. Hydraulic heads decrease towards the northeast. Modified after Majorowicz and Jessop, 1981.

3 Data and methodology

A geothermal investigation studies the subsurface temperature distribution, and the explanation of the patterns observed. Temperature data are the primary variable needed for initial geothermal investigations. There are direct and indirect measurements of temperature (see Beardsmore and Cull (2001) for more details). In this study direct measurements of temperature were used since they are available in large numbers from the measurements of the petroleum industry. However, such temperature data often contain errors (e.g., Jessop, 1990). Thus, the various sources of temperature data and their possible associated errors will be described first.

Temperature data were quality controlled ("culled"), and mapped. Maps created from the culled temperature data allowed for easier identification of outliers. These were individually inspected and were removed if found to be erroneous. Thus, culling and mapping became an iterative process until only anomalies not proved to be erroneous remained on the temperature distribution maps.

Later, the processed temperature data were used for geothermal gradient calculations. Thermal conductivity had to be estimated due to the scarcity of measured values. Then thermal conductivity and geothermal gradients were used together to determine heat flow, required in order to assess the natural geothermal conditions. Finally, the amount of heat produced in the basement and in the sediments was determined to see how much upper crustal heat generation influences heat flow. The data needed for all of these calculations and the methods applied in this study will be detailed in this chapter.

3.1 Temperature data

The types of temperature data used in this study are:

- BHT: bottom hole temperature measurements
- DST: temperature measurements conducted while drill-stem testing
- Log: continuous temperature logs
- WPS: well pressure survey temperature measurements.

Bottom hole temperature data are the most abundant source of data in this study similarly to previous studies using petroleum industry data. However, other types of temperature data also form a significant portion of the database, unlike most previous studies. Table 3.1 illustrates the data distribution by the type of temperature data before and after culling. Logs are not included since they are continuous thus the amount of data points from a log depends on digitization. However, the number of logs used in the study has decreased through the culling process from over 900 to 204.

Table 3.1 Quantity of various data types prior and after quality control. BHT: Bottom-hole temperature, DST: drill-stem test, WPS: well-pressure surveys. Logs are not shown since they are continuous source of data, while the rest of the data types are point sources.

	Original (Nr. of points)	Original (%)	After culling (Nr. of points)	After culling (%)
BHT	44884	82.98	15698	70.36
DST	7167	13.25	5162	23.14
WPS	2039	3.77	1451	6.50
Total	54090	100	22311	100

The various types of data used in this study are measured in different ways, under different conditions, and provide temperature values of different reliability. Therefore the various conditions and ways of measurements will be described along with their potential associated errors.

3.1.1 The characteristics of temperature data

Bottom Hole Temperature

BHTs are temperature measurements taken in conjunction with geophysical logs (e.g., Beardsmore and Cull, 2001). They are measured with a maximum thermometer attached to a logging tool, when it is lowered into the hole in order to provide the required temperature data for the interpretation of various logs (e.g., resistivity or SP; Beck and Balling, 1988). They are by far the most common, readily available source of temperature data in areas of hydrocarbon exploration (e.g..; Rollin, 1995 for the UK). However, they are known to be of poor quality (Bachu, 1999; Jessop, 1990).

A maximum thermometer records only a single value: the highest temperature reached. This temperature is assigned to the greatest depth, which has been reached during the run of the log. However, the recorded greatest depth may be in error due to mud settling out at the bottom of the hole, which would not allow the probe to pass (Anglin and Beck, 1965) or the unaccounted stretching of the cable connecting the tool to the surface. It is important to mention, that most logs are taken while open hole conditions still exist, i.e., shortly after drilling, when the borehole is still out of thermal equilibrium due to the circulation of drilling mud.

Previous studies of the geothermics of the WCSB (e.g., Bachu and Burwash, 1991; 1994; Majorowicz and Jessop, 1981) mainly used bottom hole temperature measurements to investigate the subsurface thermal conditions, since they are readily available in vast amounts for large areas.

Drill Stem Tests

A drill-stem test (DST) is the temporary completion of a formation; it is used to investigate the fluid content, the original pressures, the permeability and productivity of the formation (e.g., Stewart, 2011). The tested interval is isolated by inflated packers and formation fluids are allowed to flow into the tool followed

by a shut-in period. The flow and shut-in cycles are generally repeated, to gain a representative pressure reading and fluid samples.

Temperature values are also recorded during DSTs. Several studies (Beardsmore and Cull, 2001; Peters and Nelson, 2009) consider DST values the most accurate representation of the original formation temperature measured shortly after drilling due to potentially sampling formation fluids thermally not modified by the drilling procedure

Thermometers used in conjunction with DSTs have changed over the years. No formal references were found describing this evolution of thermometers, thus measurements have been separated into three generations via examining numerous DST reports available throughout the various decades.

The first generation of DSTs (measured in the 1950's and 1960’s) were recorded similarly to BHTs, i.e., they used a maximum thermometer to record the temperature during the test, if temperatures were recorded at all.

The second generation of DSTs, used chiefly in the 1970's, were capable of continuously recording temperature. These thermometers consisted of a mechanical handle that expanded outward due to the increase of temperature. The continuous temperature readings were recorded on a rotating metal plate, with a pin attached to a mechanical handle. Thus, it became possible with these thermometers to record the temporal variation, or “evolution”, of temperature values.

The third generation of DSTs were recorded with digital thermometers. The first digital temperature gauges appeared in about 1980 and are still used today. These gauges are capable of continuously recording the change of temperature while conducting a DST with a dense sample interval (i.e., very short times between the measurements) and are thus the most desired in a geothermal investigation.

The exact depth of the measurement is not always documented in a DST. It is common to assign the top or bottom of the tested interval to the recorded

temperature measurement. More recent DSTs often contain the depth of the recording gauge (i.e., the actual depth of the measurement). However, this value is not always available in the digital databases used as sources of data in this study. Thus, if the actual value was not stated the middle of the tested interval (i.e., the average of the upper and lower depth) is assigned as depth of the measurement. DSTs with large tested interval (>50 m)[6] were removed from the database due to possible error associated with the lack of properly known depth of measurement.

Temperature logs

Temperature logs are geophysical logs measuring the temperature distribution of a borehole. A tool capable of recording the temperature continuously with depth (e.g., a thermistor) is used to measure the temperature values.

There are two subsets of temperature logs. Those logs belong to the first set which are conducted for research purposes in wellbores generally left shut-in for an extended period of time to allow for the dissipation of the temperature influencing effects (including the thermal effects of drilling)[7]. These measurements were conducted using high resolution equipment. For example, Jessop (1990) claims that the instrumental precision of the tools used in his study was better than ±0.01 °C with regards to temperature.

The other set of temperature logs has been conducted in wells, which were generally not shut-in for extended periods. These logs are typically used in steaming operation or cold water injection, and their main purpose is monitoring of the propagation of the induced thermal anomaly (Sharar, 2012, pers. comm.). The tool used for measuring these logs is not generally stated, and no studies have detailed the accuracy of these measurements. However, Ben Dhia (1988) suggests

[6] Over this distance, depending on lithology and local heat flow a change in temperature as large as 3.6 °C can occur (Table 3.4). To avoid such additional errors, such DSTs were removed.
[7] The two sources for these wells were the Canadian Geothermal Data Compilation (Jessop *et al.*, 2005), and the logs measured by Dr.-s W. Gosnold and J. Majorowicz; data archived at the World Data Center for Paleoclimatology. URL<http://www.ncdc.noaa.gov/paleo/wdc-paleo.html >, [Last accessed: 2011.12.13].

that one type of these logs (i.e., those monitoring the success of cementing) is not more reliable than BHTs, as both types of data are recorded in the drilling mud.

Some of these logs are measured in cased holes (e.g., injection logs). These wells are theoretically closer to the natural thermal conditions, since more time has passed since the circulation of the drilling fluid. However, other effects (like production) might still influence the thermal field.

The depths assigned to the temperature measurements in the case of these logs could potentially be in minor error for the same reasons as BHTs (i.e., unaccounted stretching of the cable, bridging of the borehole). However, Jessop (1990) claims that the accuracy of depth control is better than 1 m for the high resolution equipment.

Well Pressure Surveys

Well pressure surveys (WPSs) are a group of different types of measurements, with variable characteristics. One of the common features of these measurements is that they are generally conducted in producing wells, after a shut-in period, in order to characterize the effects of production on the reservoir. The two main types of these measurements are static gradient, and flow and build-up tests. They are frequently conducted following each other.

These values are not readily available for Saskatchewan,[8] since they do not form part of the commercial and public digital well information databases. For this study several thousand well files were investigated and temperature values were digitized into a database.

Temperature values show improvement over time: the earliest measurements in the 1950's-1960's were done with a maximum thermometer. Fortunately, these make up only a small portion of the data. Digital gauges were introduced similarly

[8] Unlike in Alberta – there they were previously used as an additional data source in a few studies. They were used for the first time by Majorowicz and Jessop, 1981.

to DSTs from the 1980's on[9]. These gauges often record several temperature values (for the static gradients vertically, for flow and build-up tests for the tested elevation).

There is very limited amount of information available on the accuracy of depth and temperature measurements of the well pressure surveys. According to Peters and Nelson (2009) these measurements ("long term static tests") are reliable, but rare[10]. Furthermore, the measurements conducted since the 1980's often record the variation of temperature values to the third decimal, thus implying a high instrumental precision.

3.1.2 Culling temperature data

Quality control processes were used in order to remove erroneous data from the databases. Culling is such a quality control process, when a database is cleared from non-representative data, in order to retain only values, which reflect the initial, natural conditions.

Previous geothermal studies have infrequently utilized culling methods (e.g., in Majorowicz *et al.,* 1984, where the only data culling criteria was to have a uniform spatial data distribution). In some studies the erroneous values are removed, but the method of removal and the culling criteria are not explained in detail. For example, Förster (2001, pg. 245) states that: "In the analysis of the BHTs care was taken to discard obviously erroneous values, for example values that do not increase with increasing time of temperature relaxation and probably are the result of incorrect recordings." Considerable time has been spent in this study to identify and compile the errors associated with the various measurements to allow for a comprehensive quality control.

[9] This classification is based only on the study examination of the WPS reports

[10] In some places (e.g., Alberta) WPSs are more frequent due to legal requirements mandating hydrocarbon producers to conduct them time to time.

Three quality categories were developed: Qualities A, B and C. Quality A measurements are the best measurements used in this study, which very closely represent the original formation temperature. Those measurements were sorted into Quality B, which contain useful information on the original formation temperature, but are known to be altered from the original formation temperature to a smaller degree (e.g., BHTs are altered due to circulation of the drilling fluid). Quality C represents those measurements, which are completely erroneous for some reason and contain no signal of the natural conditions (e.g., due to steaming) or never had any relation to the virgin rock temperature (e.g., estimated values).

A two-step culling process was used to improve the quality of the temperature database. The first step of the process is the removal of erroneous data (Quality C). The second step of quality control was the removal of Quality B data (e.g., DSTs recovering only drilling mud, or having low recoveries) to improve the quality of the database if Quality A data (e.g., DSTs with high recoveries) were available close to them. This process will be detailed below.

3.1.2.1 Quality C data

Erroneous (Quality C) data are temperature values which do not represent natural conditions. There are two types of general errors which could corrupt all types of measurements, and several more errors, which are more dependent on the method and tools of the measurement. The two types of errors, which are potential for all measurements, are tool failure (e.g., Hermanrud *et al.*, 1991) and recording errors.

Recording errors

One example of a recording error is due to the change of imperial to metric measurements system. Sometimes values are measured in imperial values, but the units in the report cards are already metric[11]. These values are easy to identify,

[11] E.g., measuring 130 °F, and recording it as "130" on a form with unit of °C. A correct record would either indicate the measurement unit (i.e., 130 °F) or would be converted to 54.45 °C.

especially if several other temperature measurements in the area are available, and the outliers, if changed to metric values, would conform to the rest of the data.

A similar recording error can be present in some DSTs measured since the 1980's. Depth errors occur if the drill hole is bridged off, and the tools cannot pass, but the intended depths are recorded for the measurement. This results in significantly cooler temperature values than expected in the measured depth. However, bridging off is generally recorded in the test notes and thus it is easy to identify, and to account for it. If the recording errors can be corrected, these data are considered Quality B, if they cannot be corrected they are Quality C.

BHT - Maximum thermometer error

In the case of BHTs, there were two possible sources for the recorded value to be completely erroneous. The first one is related to the tool of measurement: as BHTs are measured with maximum thermometer, shallow measurements are potential candidates for a "maximum thermometer anomaly". This error represents the case, when the highest temperature was recorded outside of the borehole, because the atmospheric temperature was higher than the subsurface temperature at the bottom of the hole. The tool records only the highest temperature, thus if the surface temperature is higher than the subsurface temperature, the measured value will be erroneous.

There are several ways to identify such errors. The most direct way is, if this maximum thermometer error is recorded on the log header (see Figure 3.1). However, such direct proof is rarely available.

If such direct proof was not available a combination of factors were investigated to ensure the identification and removal of BHTs with maximum thermometer error. The first indicator is the season of measurement. If shallow BHTs were measured in the months (mostly summer), when the temperature on average is higher than the expected temperature value, they are potentially erroneous.

Two different approaches were taken depending on data availability to confirm or contradict whether these shallow summer BHTs are erroneous. If data measured with other equipment than maximum thermometer was available in the vicinity[12] of the questionable BHT, the temperature data were compared and if the BHT was considerably higher it was culled.

If no other data were available nearby, then the geothermal gradient of the BHT values were observed. The BHT measurement was culled, if the calculated geothermal gradient was found to be very high[13], since the introduced errors are positive and are scaled up by the shallow depths.

This maximum thermometer anomaly was known previously (e.g., Vaught 1980). However, Majorowicz *et al.,* (1999) were the first to suspect this to be the possible source of the very high geothermal gradients in the shallow parts of the WCSB. Recently, similar anomalies have been identified as the source of shallow geothermal anomalies on the edges of the Alberta Basin (Gray *et al.*, 2012; Majorowicz *et al.*, 2012).

BHT - Guesstimates

Another possible source for a BHT to be unrepresentative of the original formation temperature is that BHTs are sometimes estimated and not measured (Erdlac, 2006; Vaught, 1980). This kind of error is more common and more readily identifiable in the case of DSTs, thus they will be detailed in the next paragraphs investigating the possible sources of errors for DST measurements.

DST maximum thermometer errors

Earliest DSTs are likely candidates for the same maximum thermometer error as the BHTs if measured at shallow depths, since the oldest DST values were recorded with a maximum thermometer. This is potentially a significant source of error, as about half of the DST temperature values used in this study were

[12] In this study 3x3 townships centered on the measurement is considered the vicinity.
[13] "High" is areaand depth dependent.

measured before 1970, and a significant proportion of the measurements (above 20 %) are shallower than 900 m[14] (Figure 3.2). Shallow old measurements are potential candidates for maximum thermometer error. Methods similar to those used to cull BHTs were applied to identify and remove DSTs with this error.

DST Guesstimates – Second generation DSTs

Another source of error characterizes the second generation of DSTs (i.e., from the 1970's): large number of the temperature values reported for these DSTs were not measured, but estimated. A large number of measurements are potentially affected, since a significant portion of the DSTs were measured in the 1970's (Figure 3.2). Similar "guesstimates" were suspected to exist for BHTs (e.g., Erdlac, 2006; Vaught 1980), but to the knowledge of this author, they have never been identified in the case of DSTs.

Estimated measurements can sometimes be directly identified in the case of DSTs. The reported temperature values are sometimes accompanied by either of the following notes: calc. (i.e., calculated) or est. (i.e., estimated). In the case of some DST headers even a separation was made between measured and estimated values (e.g., Figure 3.4.b).

However, checking the report of all DSTs is inefficient, thus to identify potentially erroneous values the frequency distribution of DST temperature values was analyzed (Figure 3.5). On Figure 3.5 depth values were averaged for 10 m intervals, thus the number of bins for depth intervals is lower than the number for the temperature values (303 vs. 824). However, some temperature values still show a disproportionate abundance compared to the frequency of the depth values. Table 3.2 illustrates the most frequent values in the original DST database. The DSTs reporting these temperature values were manually checked and a significant proportion of them were found to be guesstimates.

[14] 900 m is used here since as Figure 3.3. shows, from 700- 800 m on the BHTs are starting to be colder than other types of measurements, i.e., until this depth the impact of maximum thermometer error raises the fitted trend of the BHTs above the other fitted trends.

Table 3.2 Temperature values occurring more than 100 times in the original DST database.

Rank	T (°C)	T (°F)	Frequency	Rank	T (°C)	T (°F)	Frequency
1	37.78	100	472	18	42.22	108	135
2	43.33	110	365	19	71.11	160	135
3	48.89	120	332	20	35	95	134
4	30	86	263	21	31.11	88	132
5	54.45	130	221	22	36.67	98	132
6	60	140	219	23	58.89	138	130
7	47.78	118	202	24	53.33	128	128
8	32.22	90	199	25	28	82.4	124
9	40	104	188	26	20	68	121
10	26.67	80	179	27	28.89	84	120
11	27	80.6	161	28	45.56	114	117
12	25.56	78	156	29	38.89	102	116
13	44.44	112	155	30	29.44	85	114
14	50	122	155	31	33.33	92	114
15	65.56	150	136	32	55.56	132	114
16	27.78	82	135	33	25	77	105
17	40.56	105	135	34	26	78.8	102

However, sometimes it could not be verified whether a DST is an estimate or a real measurement (e.g., the report card of the DST was not available, or no note was recorded in conjunction with the temperature). In this case, and in the case of BHTs an indirect approach was used to identify guesstimates.

It has been noted while doing the frequency analysis of values that most of the frequent temperature values are round figures in Fahrenheit degrees. Thus, if a reported temperature was a round number in Fahrenheit, and it was an outlier compared to data in its vicinity (e.g., 100 °F or 37.78 °C on Figure 3.4), they were identified to be affected by this errors.

DST Guesstimates – Third generation of DSTs

Similar recording error occurs sometimes in the case of DSTs measured since the 1980's. These reports often include calculated formation parameters. Some of these calculations require the knowledge of formation temperature. However, if temperature was not recorded while conducting the DST for some reason, the temperature values utilized for various calculations are estimated.

Sometimes these estimated temperature values were found to be entered into the digital database as if they would have been measured temperature values. These values can be readily identified by checking the DST reports.

Logs - Purposes

The source of the major errors masking the natural formation temperatures depend on the purpose of the logs. Most temperature logs are conducted not to characterize the natural thermal conditions, but to monitor the induced anthropogenic effects on the temperature field. The natural conditions were masked, if the logs were conducted for the following purposes:

- Cementing;
- Channeling;
- Injecting and storing natural gas in subsurface caverns
- Steaming.

Logs - Cementing

As the setting of cement is an exothermic process, the heat generated due to bonding is examined in order to locate the top of the cement. This excess heat is generally expected to quickly dissipate (Sharar, 2011, pers. comm.). However, no studies have investigated the rate of decrease of this thermal anomaly. Taking the dissipation of the thermal effects of drilling as analogy (e.g., Lachenbruch and Brewer, 1959) a quick thermal recovery is questionable. This could potentially result in higher than expected temperature measurements. Logs with this error were recognized by looking at the log headers and were rejected.

Logs – Channeling

Channeling is a process when portion of the produced fluids in the well are flowing behind the casing due to poor cement job. If channeling is suspected to occur in a well, the production is halted, and a baseline log (generally temperature and gamma-ray) is run. After recording the baseline situation, a radioactive tracer fluid is injected, which have significantly different temperature than the surrounding formations. Then the progress of this temperature anomaly is monitored to determine, whether the fluids are channelling. If channelling occurs, it is also determined, where the fluids are flowing.

Any temperature logs, measured after injection, are not reliable due to the impact of the injected fluids on the thermal field and were not used in this study. For similar reasons the logs of injected gas storage caverns are not representative of the original formation temperature either and they were also rejected. However, the baseline logs might potentially be useful if the temperatures are not distorted by production and they were considered Quality B data.

Logs – Enhanced oil recovery methods

Steaming operations in heavy oil areas and other secondary and tertiary production methods can also seriously influence the temperature fields (e.g., Figure 3.6). These wells were all removed from the database.

Logs – Production influence

Vasseur *et al.,* (1991) noted in a well after a one month pumping test that the shallow temperature values were seriously increased. Similarly, if production has already commenced before the temperature log was recorded, the shallower temperatures will be impacted.

If there is no record about previous production this situation can be identified based on elevated temperature in the shallower parts of the well compared to other measurements at shallower depths, if available. Also, since the temperatures are elevated in the shallower parts of the well, the geothermal gradient in the well is

reduced. Therefore, the shallow parts of production influenced wells were rejected in this study. The deeper parts were considered Quality B.

WPS - Maximum thermometer error

Older, shallow well pressure surveys might be possibly influenced from the surface for the same reason as BHTs and DSTs are, i.e., due to the tool of measurement. However, newer data are generally more reliable than other types of measurements.

The previously summarized Quality C data are such, that the original formation temperature is completely obscured, i.e., these measurements do not represent initial, natural conditions in any sense. Measurements affected by any of these errors were culled. Table 3.3 provides a summary of these errors.

Table 3.3 Errors associated with the different data types. The symbol "?" means that other errors are possible, but have not been identified.

	BHT	DST	Log	WPS
Tool Failure	Yes	Yes	Yes	Yes
Recording errors	Yes; E.g., mixing imperial-metric units, recording the same value in consecutive measurements	Yes; e.g., Intended depth recorded in a bridged off hole	Yes	Yes
Maximum thermometer error	Yes	Yes	No	Yes
Guesstimates	Yes	Yes; both for second and third generation DSTs	No	?
Other	?	?	Yes, monitoring cementing, channeling or enhanced oil recovery methods	?

3.1.2.2 Quality B data

Quality B temperature measurements contain potentially useful information on the original formation temperature. They were only culled, if Quality A data were available in the same area. Conditions impacting the quality B measurements deteriorating their quality and making them less representative follow below.

DSTs – The type of recovery

DSTs attempt to sample original formation fluids. The quantity and the quality of the DST recovery have important implications for the general quality of the temperature measurements recorded during the test. Considering the type of the recovery, several different possibilities exist. A recovery may consist of:

- Drilling fluid/mud;
- Formation water;
- Oil;
- Gas;
- Fluid cushion.

From these formation water, oil, and gas represent the original formation fluids, thus their presence is desirable in the recovery.

Drilling fluids are used in a borehole among other purposes to cool the drill bit (e.g., ASME Committee, 2004). Thus, if drilling fluids are sampled during a recovery the measured temperature is likely to be colder than the original formation temperature (Figure 3.7).

Fluid cushions are applied generally in deeper measurements [15] to provide additional pressure to balance the formation pressures (Black, 1956; Stewart, 2011). They can be of various fluid and gas types, but most often water is used as cushion. When a fluid cushion is injected into the hole from the surface, it is

[15] Measurements deeper than 2000 m used fluid cushion in the study area.

cooler than its surroundings. Although it stays in the drill pipe, it may impact the formation temperature through conduction (Figure 3.7). However, the influence of fluid cushion has been overlooked so far.

The only other work questioning the quality of DSTs with fluid cushion is that of Nativ (1990). She compared the DST temperatures to BHTs in deep aquifers. Her conclusions were similar to that of this study: DSTs sampling fluid cushion are likely to record colder temperature than the original formation temperature. Thus, DST measurements with fluid cushion are considered Quality B measurements.

DSTs – The amount of recovery

The amount of recovery also influences how representative the DST temperature is. It is possible that the drill stem test does not recover anything for various reasons (e.g., tool failure, the low permeability of the formation or the skin damage of the wellbore, e.g., Stewart, 2011). It has been determined on a test database of wells with WPS measurements (Figure 3.7) that the larger the recovery of original formation fluids is, the hotter the measured temperatures are, i.e., the larger the recovery the more likely the original formation temperature is measured. This is similar to what Nativ (1990) identified empirically. Therefore, DST's with recoveries <50 m of original formation fluids were considered Quality B measurements.

DSTs – The season of measurement

In addition the role of the amount and nature of recovery, the season of the measurement has an impact on the consistency of DST data (Figure 3.8). Older, shallow data were expected to be less consistent in the summer due to being measured with a maximum thermometer. However, surprisingly even those measurements, which were not measured with maximum thermometer, are less consistent if measured during summer (Figure 3.8). Thus, summer measurements were deemed Quality B measurements.

DST – Misruns

Some DST reports are classified as "misruns". A misrun can happen for various reasons, including, packer failure (i.e., interval cannot be separated), plugging, not being able to produce fluids, not reaching intended depth due to bridging of the hole[16]. These measurements are generally not good for pressure determination (e.g., Melnik (2012) discarded them).

However, they are not considered automatically erroneous with regards to temperature measurement, since they may provide useful information on the temperature field. In several cases, where both misruns and properly measured DSTs were available at the same depth, the temperatures of the misruns were similar to the proper DSTs (within 2-3 °C). However, their Quality is classified as "B".

WPS – Production influence

Well pressure surveys, are usually conducted in producing fields. Thus, any kind of secondary or tertiary thermal hydrocarbon production effects may influence the nearby temperature field. However, records of these effects are rarely available.

In addition to this, similarly to temperature logs, the production of the well can also influence shallower temperature values. Thus, only the temperatures measured at the depth of the production were used. If these Quality B temperatures were significantly higher (>10 °C) than other measurements they were rejected to avoid including anthropogenic effects.

WPS – Thermal mass

In addition to these both for WPS, and for logs the thermal mass of the measuring tool is of question (Beck and Balling, 1988): the temperature of the tool may not have enough time to readjust with its surroundings since the tools are lowered and

[16] E.g., see: The quality code of the American Institute of Formation Evaluation: <http://dstdata.com/dstpress.htm> [Last accessed: 2012.12.31].

raised with significant velocity (especially in the case of static gradient tests). This would show up theoretically similar to the effects of production, i.e., the gradient of the log is lowered. Thus, the same solution was used to improve the quality of the database, as in the case of production influenced WPS.

BHTs

BHTs are probably the most studied and the most commonly used source of temperature data (e.g., Deming, 1989; Förster, 2001). It is also well known that their quality is poor (e.g., Bachu, 1999; Jessop, 1990). The poor quality has been related by many studies to the thermal effects of the circulation of drilling mud. This circulation generally heats the shallower parts of the wellbore, and cools the deeper parts, i.e., transports heat vertically up (as illustrated by the temperature logs published by Förster, 2001 and Lachenbruch and Brewer, 1959). Therefore, all BHTs not considered to be Quality C were classified Quality B.

BHT correction methods

Several corrections have been derived for BHTs to account for the cooling effects of drilling fluid (e.g., Kutasov and Eppelbaum, 2005; Middleton, 1979; 1982). Such corrections will be described in the following section to determine whether they could improve the quality of BHTs used in this study.

BHT correction methods are hindered by a lack of necessary data. Both simpler (e.g., Horner, 1951) and more advanced (e.g., Shen and Beck, 1986) methods require data often not recorded when measuring BHTs. Even if the required data are recorded, they are not available from the commercial and public databases used in this study.

This lack of data has been often overcome by developing regional correction factors using only a few local measurement points (e.g., Ben Dhia, 1988). However, Deming (1989) pointed out that these regional, empirical corrections bear an unknown amount of error for the areas outside of the regions, where they have been developed.

The most common corrections were summarized by Hermanrud *et al.*, (1990) who showed that simpler temperature corrections are significantly underestimating the virgin rock temperature values, while more complex models result in better estimates but still with very significant standard deviations.

Therefore, in this thesis no such BHT corrections were applied for the lack of necessary data and for the uncertainty of correction methods. Thus, the quality of BHTs could not be improved. Other types of measurements were preferentially used compared to BHTs, i.e., if an area had a better quality data (e.g., quality A DSTs) covering a significant depth range (>500 m), linear regression trends were fitted to them. The less representative BHT data were removed over the depth interval covered by the better quality data, if they were more than 5 °C from the fitted trend.

Finally, an effort has been also undertaken to remove points, which showed inverse temperature depth relations (i.e., temperature decreased with greater depth), when comparing temperature data on temperature depth plots in these areas. This was also conducted via using Quality A data to constrain Quality B data. Data not affected by any of the previous issues is considered Quality A data.

This way the temperature data were processed to ensure that only representative data are used for further evaluation of the geothermal conditions of the province. The improvements made on a test database of Precambrian wells after using the previously mentioned methods are illustrated by Figure 3.3.

3.1.3 Temperature maps

3.1.3.1 Generating temperature maps

Four types of temperature maps were generated from the processed temperature data: formation, depth and elevation specific temperature maps and isothermal depth maps. The method of gridding is described in greater detail in Chapter 3.5.

Formation specific temperature maps

Eighteen temperature maps were generated for the tops of selected formation and two unconformity surfaces (Figure 2.1) according to the previously described methods (Appendix A). Formations were chosen to assist with the hydrogeological mapping of Saskatchewan conducted within SPFPS, taking into account data availability, thickness of formations and regional significance.

Additional strata were chosen for various reasons: For example, the Prairie Formation (Figure A.7) to facilitate potash mining by solution mines; or the Precambrian (Figure 4.2) and sub-Mesozoic unconformity temperature maps (Figure A.14) to calculate geothermal gradients across the study area.

Elevation specific temperature maps

Fourteen elevation specific temperature maps were generated for elevations between 750 masl (above sea level) and 2500 mbsl (below sea level) with an elevation difference of 250 m between the maps (Appendix B). These maps were produced in conjunction with the depth specific maps in order to emphasize temperature anomalies by illustrating temperature at a single depth/elevation, unlike strata specific temperature maps.

The maps produced for the elevations above the sea level are restricted in area due to topography (Figure B.3, the 250 masl is also restricted in the extreme northwest by the elevation of the basement).

Depth specific temperature maps

Thirteen depth specific temperature maps were generated between 250 m KB (metres below kelly bushing) and 3250 m KB, with a distance of 250 m between the maps (Appendix C). An additional temperature map was also generated from the shallow data for the 100 m depth surface (Figure 3.10) to provide surface boundary condition for the geothermal gradient calculations. These maps are used as an input for geothermal exploration as they illustrate where it is more economic to drill, i.e., where higher temperatures are located at the same depth.

Isothermal depth maps

Four isothermal depth maps were produced (Appendix D). These maps depict how deep one would have to drill to reach a selected temperature value. For this characteristic, they are also of direct use for geothermal prospecting similar to depth specific maps, i.e., they can answer the question, where is a specific temperature located at the shallowest depths. Also, they proved to be very useful for highlighting erroneous temperature measurements during the iterative phase of the culling process.

Correction for interval thickness

One potential approach to creating temperature maps is generating the maps by extrapolation of geothermal gradients or heat flow (e.g., Majorowicz and Grasby, 2010). However, the uncertainties of extrapolation increase with the increasing distance from the known value. Another approach commonly used for generating temperature maps is that only temperature data measured at the mapped surface (e.g., Bachu and Burwash, 1994) are used. However, temperature data are rarely measured right at the surface, thus this approach is limited by data availability.

To be able to overcome the limits of these approaches, the two were combined in this study: First, temperature data were sorted into 250 m thick depth intervals centered on the selected surfaces (i.e., depth, elevation, formation top) to provide enough data for mapping. And then temperature data were extrapolated to the mapped surface to account for the difference in elevation between the measurement point and the mapped surface (illustrated on Figure 3.11). Thus, the uncertainty of the extrapolation was limited by the interval thickness.

If the lithology between the data point and the mapped surface was not known, the average continental geothermal gradient (33.3 $°C \cdot km^{-1}$) was used for correction.

If the lithology of the depth interval between the data point and the mapped surface could be readily estimated (i.e., in the case of the stratigraphic temperature maps) the following corrections were applied for the maximum distance of 125 m[17]:

carbonates, siltstones and sandstones: 2.25 °C;

shale or glacial till: 5 °C;

evaporite: 2 °C.

Table 3.4 Calculated temperature change over an interval of 125 m for various lithologies with various heat flows. Maximum, average and minimum heat flows of 80, 60, and 30 mW m^{-2}. Potential temperature change calculated via the Fourier equation (i.e., equation (8) in Chapter 3.3).

	K ($W \cdot m^{-1} \cdot °C^{-1}$)	ΔT_{Qmax} (°C)	ΔT_{Qave} (°C)	ΔT_{Qmin} (°C)
Anhydrite	5.7	1.75	1.32	0.66
Dolomite	3.3	3.03	2.27	1.14
Glacial till	1.2	8.33	6.25	3.13
Gypsum	3.1	3.23	2.42	1.21
Limestone	3	3.33	2.50	1.25
Marlstone	2.3	4.35	3.26	1.63
Salt	6	1.67	1.25	0.63
Sandstone	3.2	3.13	2.34	1.17
Shale	1.1	9.09	6.82	3.41
Siltstone	2.5	4.00	3.00	1.50
Average		4.19	3.14	1.57

Both types of these corrections were based on calculating potential temperature differences occurring in the case of various lithologies with various, potential heat flow values for the study area. The results of this calculation are shown in Table 3.4.

A more accurate correction is not possible on the scale of this study due to the lack of a priori knowledge of heat flow, and detailed knowledge of site specific lithology.

[17] If the distance was smaller, the correction was accordingly linearly decreased.

From the data corrected in this manner strata, depth and elevation specific temperature maps were generated (Appendix A, B, C and D). It is important to note that in the case of the depth and elevation specific temperature maps, the northern boundary of the maps is marked by the isopach line of the shallowest depth/elevation of the sample interval.

Correction for temperature difference for isothermal depth maps

A correction, similar to the one previously described, was applied to the data used for mapping the isothermal depth maps (i.e., depth maps for a selected temperature surface). First, temperature data were selected, which fell into 5 °C temperature interval centered on the temperature value of the mapped surface. Then a depth correction was applied to the mapped depth (62.5 m for the maximum difference of 2.5 °C between the mapped value and the measured value). Due to the lack of a priori knowledge of heat flow, and for the lack of site specific lithological knowledge no better correction could be applied. The northern boundary of the maps was determined in a way to include all measurement points providing data for the selected surface.

3.1.3.2 Analysing temperature maps

Depth and conductivity of the overlying strata are the two main factors determining temperature in a purely conductive situation with no significant heat sources or sinks (e.g., Bachu and Burwash, 1994). The effect of refraction due to thermal conductivity differences is minimal (e.g., Jessop, 1989), since the Phanerozoic strata are mostly continuous in Saskatchewan without major lateral lithological changes. Therefore temperatures at any specific elevation level should be theoretically at the same temperature value.

Anomalous temperature regions were identified on the formation specific temperature maps by comparing the distribution of the isotherms to the respective formation top depth maps. Regions where the isopachs and isotherms are not parallel were considered to be anomalous.

Anomalous regions in the case of the elevation and depth specific maps were defined with regards to the background temperature of the map. The temperature value, covering most of the province was considered the background value, and any major change (>5 °C) from this temperature was considered anomalous. Similar definition of anomaly was used for the isothermal depth maps with regards to depths, i.e., regions deeper than the background depth represent colder than average geothermal conditions, while shallower intervals represent hotter than average geothermal areas.

If an identified anomaly was caused by a single point and/or is present only on a single surface, it was deemed to be not a regionally characteristic anomaly (e.g., it could be the result of an erroneous measurement remaining in the database after the careful culling process, or it could suggest something affecting mainly a single surface, like a steaming event).

The generated temperature distribution maps provide very useful information on the horizontal distribution of temperature values. Isothermal depth maps also contain some vertical information. However, geothermal gradients much more readily represent the vertical distribution of temperatures. The way they were calculated will follow.

3.1.4 Geothermal gradient calculations

Geothermal gradient values represent the rate of the temperature increase with depth. They are important for several reasons, e.g., providing vertical information on the temperature distribution, unlike temperature maps (Chapter 4.1), which bear information only on the horizontal distribution of temperature.

Two ways of determining geothermal gradients were used in this study:

- individually for points;
- for groups of data points.

Geothermal gradient determination for individual points

Individual geothermal gradients were calculated by:

$$\frac{dT}{d\boldsymbol{d}} = \frac{T_1 - T_2}{D_1 - D_2} \quad (1)$$

where *T* and *D* are temperature and depth, and 1 and 2 in subscripts represent the deeper and the shallower measurement respectively and $\frac{dT}{d\boldsymbol{d}}$ is geothermal gradient.

Integral geothermal gradient, representing the temperature gradient of the entire Phanerozoic strata, were calculated by this method. The temperature measured at the Precambrian surface and the temperature calculated for 100 m depth surface were used for calculating the integral geothermal gradients (Figure 4.5).

This two point method was also utilized for mapping *interval geothermal gradients*, representing the geothermal gradient of a smaller interval than the whole Phanerozoic package. The temperature gradient was calculated between the 100 m depth surface and the sub-Mesozoic unconformity for the Mesozoic-Cenozoic interval (Figure 4.6), and the sub-Mesozoic unconformity and the Precambrian surface for the Paleozoic interval (Figure 4.7).

Although this method of determining geothermal gradient is straightforward, two issues have to be accounted for. First, this method provides only an average geothermal gradient value for the interval, and therefore it will lack the details of variation of gradient within the formations (e.g., Bachu and Burwash, 1994; Majorowicz *et al.*, 1986).

Second, representative ground surface temperature values, which would be required both for the Mesozoic-Cenozoic and the integral geothermal gradient calculations are not readily available for two reasons. On the one hand, only very few meteorological stations record ground surface temperature in Saskatchewan. Previous studies (e.g., Bachu and Burwash, 1991; 1994; Majorowicz and Jessop, 1981) often determined ground surface temperature from more readily available air temperature measurements with various corrections. However, the conversion

from air temperature to ground surface temperature is hard to determine due to the several factors influencing it, like snow cover (Mann and Schmidt, 2003).

On the other hand, current ground surface temperature values would not be appropriate for gradient calculations even if they could be easily determined from air temperature measurements, since the deep temperatures are still equilibrated with colder paleoclimate. This is proved by temperature transients observed in numerous shallow boreholes (e.g., Majorowicz, 1993; Majorowicz and Skinner, 2001 and Figure 3.9). Thus using the current, increased ground surface temperature value would decrease the calculated geothermal gradients (see eq. (1)).

Therefore instead of taking the ground surface temperature as the upper boundary condition, the temperature at 100 m depth[18] was used as top boundary in this study. A temperature map was generated for the 100 m depth level for the study area from the processed data (Figure 3.10). From the grid of this map the temperature at 100 m depth was determined in every well[19] and this value was used for calculating the geothermal gradients via the two point method.

Geothermal gradient determination for groups of data points

Geothermal gradients with this method were determined by fitting linear trend lines to points of data on a temperature depth plot in 3x3 Township areas. The slope of the fitted line reveals the geothermal gradient. The integral and the interval geothermal gradients defined this way were used in this study only in heat flow calculations.

There are two major advantages of this method over the two point method. First, the effect of any remaining outliers (i.e., erroneous measurements) is reduced compared to calculating geothermal gradients for individual data points. Second,

[18] 100 m was chosen as the upper boundary, since this depth was found to be deeper than the depth of the temperature inversion commonly occurring in shallow, precise temperature logs. Therefore gradient calculation to this depth does not result in negative gradients.
[19] With inverse distance weighing; distances were measured from the grid points.

variations in geothermal gradient with depth can be easily recognized as data between the two end points are plotted.

However, there are two major hurdles of applying this more accurate but more time consuming method in the entire study area. First, more data points are required for it, i.e., in areas of low data density it cannot be used. Second, data should be distributed over a wide range of depths, since the poor vertical data distribution "contributes more to the uncertainty than the quality of individual data" (Jessop, 1990, pg. 257). Thus, even in areas, which have high data density but low vertical range, this method cannot provide a reliable gradient.

The geothermal gradient determined in these two ways is a useful representation of vertical change in temperature. However, its magnitude depends on thermal conductivity. Therefore, geothermal gradients should not be used without determining thermal conductivity to predict temperatures at depth.

3.2 Thermal conductivity

Thermal conductivity is a material property revealing how easily it transports heat, or how well it insulates (e.g., Beardsmore and Cull, 2001). Knowledge of this parameter is required for the determination of heat flow from geothermal gradients. It is also an important parameter when thermally enhanced oil recovery methods are applied (e.g., Boberg, 1988).

Measured thermal conductivity from the study area

Although thermal conductivity is an important parameter for geothermal studies, it is not regularly measured on the chips and cores of wells, thus very few measured values are available in Saskatchewan. To the knowledge of this author there are only six wells in the study area, which have measured thermal conductivity values. Four of these wells are located in the extreme northeast, in the shallowest part of the basin, where the amount of Phanerozoic sediments is insignificant. The reported thermal conductivity values in these wells are those of igneous and metamorphic rocks of Precambrian age and thus are no use for

estimating thermal conductivity of the Phanerozoic sedimentary rocks. However, they can be used for calculating heat flows in those wells.

There are only two wells among these six, where the thermal conductivity was measured on rocks of Phanerozoic age (in Regina and Winslow, published in Jessop *et al.*, 2005). A few additional thermal conductivity measurements of Phanerozoic rocks are also available from the surrounding provinces/states (Gosnold, 1999; Gosnold *et al.*, 2010; 2012; Jones *et al.*, 1984).

Measurement of thermal conductivity of rock samples did not form part of this thesis. Given the importance of thermal conductivity in geothermal studies, it had to be estimated.

Thermal conductivity estimation by net rock analysis

Thermal conductivity could be estimated based on the knowledge of lithological composition, determined through net rock analysis. This approach has been frequently utilized in geothermal studies (e.g., Beach *et al.*, 1987, Majorowicz and Jessop, 1981), if there were not enough thermal conductivity measurements available.

The first part of a net rock analysis is the division of a log into vertical intervals deemed to be of the same composition. Then the volumetric ratio of 14 major different lithological groups (Table 3.5) is determined within these intervals. Such net rock analysis of 64 lithologic logs provided by MJ Systems was undertaken. Canadian Stratigraphic Services Ltd. provided additional 74 net rock analyses with similar information.

A harmonic mean (eq. (2)) was used to calculate the thermal conductivity of these mixed-lithology intervals following the previous net rock analysis. Thermal conductivity values for the rocks were derived from literature (Table 3.5).

A harmonic mean was also used to calculate the cumulative effects of these intervals, i.e., the effective thermal conductivity of the log. Depending on what

stratigraphic intervals did the log cover, integral, Mesozoic-Cenozoic, and Paleozoic effective thermal conductivities were individually determined.

Table 3.5 The thermal conductivity values used in this study. k is thermal conductivity at 20°C. The studies referenced above under the studies part are the following: 1 Bachu, 1993; 2 Beach *et al.*, 1987; 3 Garland and Lennox, 1962; 4 Gosnold, 1990; 5 Gosnold *et al.*, 2012; 6 Issler and Jessop, 2011; 7 Jessop and Vigrass, 1989; 8 Jones *et al.*, 1984; 9 Majorowicz and Jessop, 1981; 10 Majorowicz *et al.*, 1985b; 11 McKenna and Sharp, 1998; 12 McKenna *et al.*, 1996; 13 Nathenson and Guffanti, 1988; 14 Phillips *et al.*, 1938; 15 Vasseur *et al.*, 1995; 16 Jessop *et al.*, 2005; 17 Majorowicz, 2012 pers. comm..

Lithology	K ($W \cdot m^{-1} \cdot °C^{-1}$)	Source
Shale	1.1	1,2,3,4,5,6,7, 8,9,10,11,12, 13,14,15,17
Siltstone	2.5	1,2,8,9
Sandstone	3.2	1,2,3,6,7,8,9, 11,12
Dolomite	3.3	1,2,6,7,8, 9
Limestone	3	1,2,3,6,7,8, 9,11, 12
Marl	2.3	1,2,9
Chert	3	1,2,9
Salt	6	1,2,7,9
Anhydrite	5.7	1,2,9
Gypsum	3.1	
Glacial till	1.2	1, 2
Conglomerate	2.5	2
Coal	0.5	1,2,3,9

Lithology	K ($W \cdot m^{-1} \cdot °C^{-1}$)	Source
Gabbro	2.5	16
Metadiorite	2.2	16
Metagabbro	2.8	16
Felsic gneiss	3.2	16
Granite gneiss	3.5	16
Gneiss	4.2	16
Metadacite	3.4	16
Basalt	3.5	13,16
Rhyolite	3.7	12,16
Metarhyolite	3.3	16
Quartz biotite	3.4	16
Dacite	3.5	16
Schist	5.1	16
Pegmatite	3.4	16

Although harmonic mean (eq. (2)) was used in this study to calculate the thermal conductivity of the mixed-lithology intervals, the choice of mathematical mean is somewhat controversial. Theoretically, the geometric mean (eq. (3)) is the most correct mathematical mean if the mineral components are isotropic, while harmonic mean (eq. (2)) is the most correct mathematical mean, if the components are in the series arrangement, i.e., if the material is layered or bedded perpendicular to heat flow (Fjeldskaar *et al.*, 2009; Midttømme and Roaldset, 1998).

$$\frac{1}{k_{eff_i}} = \frac{1}{\sum \frac{v_i}{k_i}} \quad (2)$$

$$k_{eff_i} = \prod k_i^{v_i} \quad (3)$$

$$\sum v_i = 1 \quad (4)$$

where Π is the mathematical operator for product, k_{effi} is the effective thermal conductivity of the interval in question, k_i and v_i are the thermal conductivity and the volumetric fraction of the rock type in question.

Brigaud and Vasseur (1989) concluded that as long as the samples are isotropic, the geometric mean is appropriate for estimating the effects of the various constituents and the pores and pore fluids on the net conductivity of the rock sample. A similar conclusion was made by Issler and Jessop (2011), who tested several methods for determining wet conductivity from dry conductivity.

Fjeldskaar *et al.,* (2009) suggested that using geometric mean is appropriate on the thin section scale, but on larger scale geologic media are layered. Therefore, they suggested that harmonic mean should be used to calculate thermal conductivity. Fjeldskaar *et al.,* (2009) also found that net conductivity calculated with harmonic mean represented better the measured thermal conductivity values.

Thermal conductivity of the intervals was calculated both ways to test the significance of using the two different mathematical means. The results of this analysis showed that thermal conductivities calculated with the two methods do not differ significantly, with maximum difference between the calculated thermal conductivities for the same wells less than 0.3 $W \cdot m^{-1} \cdot °C^{-1}$, and an average difference of less than 0.1 $W \cdot m^{-1} \cdot °C^{-1}$ (Figure 3.12). Calculation with harmonic mean resulted in lower thermal conductivity. Thus, harmonic mean was used to calculate the interval thermal conductivities to rather underestimate than overestimate heat flow.

Correcting thermal conductivity for in-situ conditions

The main factor determining thermal conductivity is the previously accounted lithology/mineral composition of a sample. However, there are several other factors, which can significantly impact the in-situ thermal conductivity of a rock sample. The following are most commonly identified: anisotropy; grain and pore size and shape; porosity and type of pore fluids; pressure; temperature; texture. [20]

From these factors the amount of porosity and temperature were incorporated in thermal conductivity calculations to make thermal conductivity estimates better represent in-situ thermal conductivity of rocks.

Effects of porosity

The porosity and pore fluids (e.g., oil, natural gas, freshwater, brine) stored in the pores impact significantly the thermal conductivity. The more porous the rock is, the lower the effective thermal conductivity is going to be, since the thermal conductivity of the pore fluids is almost always lower than that of the rocks (compare Table 3.5 and values calculated via Equation (7)).

To be able to calculate wet thermal conductivity (i.e., thermal conductivity of fluid saturated rocks) the porosity variation with depth had to be characterized. Similarly to previous studies (e.g., Athy, 1930; Schmoker and Halley, 1982; Sclater and Christie, 1980), exponential curves were used to describe the porosity-depth relationship:

$$\Phi_d = \Phi_0 * e^{-cd} \qquad (5)$$

where "Φ_d" is the porosity at "d" depth, Φ_0 is surface porosity and c is a constant determined via curve fitting. Table 3.6 shows all the parameters used for estimating the porosity of the various rock types at depth.

[20] The list is based on the parameters named by: Beach *et al.*, 1987; Fjeldskaar *et al.*, 2009; Issler and Jessop, 2011; McKenna *et al.*, 1996; Midttømme and Roaldset, 1998; Vasseur *et al.*, 1995.

The pore space calculated with the parameters of Table 3.6 and Equation (5) was assumed to be filled with water. Following the conclusion of Issler and Jessop (2011), geometric mean was used to incorporate the effects of the pore fluids.

Table 3.6 Initial porosity and c constant values for the various lithologies.
Based on: I. Values determined by curve fitting to core porosity data (Figure 3.13) II. By using the assumption of Bachu and Hitchon (1996), that evaporites are "aquicludes". Secondary porosity (e.g., fractures) not taken into account as they are local scale features. III. Φ_0 is the shallow coal porosity from Gan *et al.*, 1972, while c is by curve fitting to their measured values IV. Sclater and Christie, 1980 V. Schmoker and Halley, 1982. Marlstone and siltstone were calculated as 50% mixtures, glacial till, conglomerate, gravel was assumed to be governed by the same parameters as sand, chert was assumed to have a constant porosity of 0.1.

	Φ_0	c	Based on:
Shale	0.3614	-0.0007	I
Sand, glacial till, conglomerate, gravel	0.4095	-0.0006	I
Limestone	0.5	-0.0005	I, IV, V
Dolomite	0.3	-0.0008	I, IV, V
Evaporite	0	0	II
Marlstone	0.4307	-0.0006	Shale + limestone
Siltstone	0.38545	-0.00065	Shale + sandstone
Coal	0.23	-0.0006	III
Chert	0.1		

Effects of temperature

Temperature has a significant influence on the thermal conductivity of both the rocks and the pore fluids. While the thermal conductivity of the matrix material generally decreases with temperature, the thermal conductivity of the pore fluid increases slightly with temperature (Sekiguchi, 1984).

In order to account for the effects of temperature on the rock matrix the method of Chapman *et al.,* (1984) was used:

$$k_{eff}(T) = k_{20} * \frac{293}{273 + T} \quad (6)$$

where $k_{eff}(T)$ is the temperature dependent thermal conductivity of the interval, k_{20} is the thermal conductivity at 20 °C (Table 3.5), and T is temperature in [°C].

To account for the increase of the thermal conductivity of water with temperature, the function used by Deming and Chapman (1988) was applied:

$$k_w = a + bT + cT^2 \quad (7)$$

where T is temperature [°C], and a, b, c are temperature dependent constants (a=0.5648, b=1.878*10^{-3} and c=-7.231*10^{-6} under 137 °C. Temperatures in the study area are lower than this).

Other factors

Correction for anisotropy is not done in this study, since anisotropic effects on thermal conductivity are controversial. Some studies suggest (e.g., Vasseur *et al.*, 1995) that shale minerals are going to re-orientate with depth due to pressure and thus such corrections are important. However, Fjeldskaar *et al.*, (2009) analysed shale samples with depth and did not found signs of re-orientation. A decision in this question is beyond the scope of this thesis.

The effects of pressure on thermal conductivity are not taken into account for two reasons. First, changes in porosity account for the pressure increase for soft rocks (Sekiguchi, 1984). Second, Bachu (1993) found for hard rocks that the pressure corrections are negligible (<0.5 %) in the WCSB.

Midttømme and Roaldset (1998) showed that grain size is proportionate with the thermal conductivity of the rock sample, i.e., the smaller the grains, the smaller the thermal conductivity is going to be. However, for the lack of such data on the regional scale of this study, texture and grain size could not be accounted for.

To summarize Chapter 3.2, the lithological composition was used to estimate the thermal conductivity with corrections being made for porosity and temperature. The thermal conductivities determined in this way were used for heat flow calculations, which will be investigated in the following.

3.3 Heat flow

Heat flow density or heat flow in short, is the quantity, which characterizes the amount of thermal energy transported across a surface. Its value is independent from the material it is transported through[21]. Heat flow is a basic parameter in geothermal studies, and is used in many branches of geosciences, for example: tectonics, magnetotellurics, geochemistry, petrology, and seismology (Gosnold, 1990).

In this study heat flow was calculated with the following formula:

$$Q = k * \frac{dT}{d\boldsymbol{d}} \tag{8}$$

where Q is heat flow, k is thermal conductivity, and $\frac{dT}{d\boldsymbol{d}}$ is geothermal gradient determined via curve fitting to groups of data.

Heat flow was calculated in all wells that had thermal conductivity values. Furthermore, if the depth range of the temperature data, as well as the thermal conductivity data allowed for it, separate calculations were made both for the Cenozoic-Mesozoic and the Paleozoic rock intervals. Paleoclimate effects were accounted for according to the method of Majorowicz and Wybraniec (2011) based on the depth of the heat flow determination.

Several questions may arise with regards to the determination of heat flow. First, equation (8) is only appropriate if the system is conduction dominated (e.g., Haenel *et al.*, 1988). However, dimensional analysis indicate that the WCSB on a basin wide scale is conduction dominated (see Chapter 2.3).

Second, although a temperature transient can be often observed in the subsurface due to variable surface forcing (e.g., Majorowicz, 1993), the importance and the magnitude of heat flow corrections required for climatic effects has been debated

[21] If no heat is produced or consumed in the material.

(e.g., Mareschal *et al.*, 1999; Sass *et al.*, 1971). However, more recent studies (e.g., Gosnold *et al.*, 2011) based on more extensive datasets indicate that paleoclimate effects on heat flow are globally present and they should be accounted for to avoid systematic bias of heat flow determinations.

A correction derived for Saskatchewan would be more favourable to account for the paleoclimate effects. However, deriving a correction would require a deep, high quality temperature log in a well, where the thermal conductivities are known[22]. Since such well is not available, no site-specific correction could be derived.

Third, the above-mentioned representation of heat flow (eq. 8) does not take into account heat sources or sinks in the system (e.g., heat generated by radioactive decay). The heat contribution of the geological strata has to be assessed to determine the accuracy of such representation. The methods for this assessment will be detailed in the following.

3.4 Heat generation

The decay of radiogenic elements (U, Th, and K) in the crust is a significant contributor to terrestrial heat flow. Assessing the amount of heat generated in the basement and in the sedimentary rocks in conjunction with heat flow determinations is important for understanding the relationship between heat flow and geology (Rybach, 1988).

Basement heat generation

Radioactive heat contribution of the basement rocks was determined by using the function of Rybach (1986) (from Bücker and Rybach, 1996):

$$A = 10^{-5} * \rho * (9.52c_u + 2.56c_{th} + 3.48c_k) \quad (9)$$

[22] This is the reason, why the Regina well would be not appropriate. Jessop and Vigrass (1989) already identified the thermal conductivities in that well to be potentially erroneous.

where A is the heat generated [$\mu W \cdot m^{-3}$], ρ is rock density [$kg \cdot m^{-3}$], c_u, c_{th} and c_k are uranium [ppm], thorium [ppm] and potassium [weight %] concentrations respectively.

Radioactive element concentration data measured on Precambrian rock core samples are available for the study area (from the studies of Bachu and Burwash, 1991; Beach, 1985; Burwash and Cumming, 1976), and its surroundings (e.g., Guillo-Frottier *et al.*, 1996; Rolandone *et al.*, 2004).

An average density of 2.7 $g \cdot cm^{-3}$ was used for equation (9). This value was chosen based on the studies of Bachu and Burwash (1991) (reporting a range of 2.65 and 3.05 $g \cdot cm^{-3}$ with an average of 2.72 $g \cdot cm^{-3}$ for the province) and Burwash and Krupicka (1970) (reporting 2.744 $g \cdot cm^{-3}$ for the block covering Saskatchewan and 2.718 $g \cdot cm^{-3}$ for the whole WCSB).

Sedimentary heat generation

The heat contribution of the sedimentary strata was also estimated using digital gamma ray logs with equation (2) of Bücker and Rybach, (1996):

$$A = 0.0158 * (GR - 0.8) \quad (10)$$

where A is heat generated [$\mu W \cdot m^{-3}$] and GR is the count of the gamma-ray log [API].

3.5 Generating maps

The data processed according to the previous chapters (Chapters 3.1-3.4) were mapped (Appendix A- Appendix H) with default point kriging with linear variogram in Golden Software Surfer® 10.7.972. This gridding method is one of the most flexible gridding methods. Also, it produces good results independent from the number and distribution of data points (Golden Software, 2002). Anisotropy was not used for creating the maps, since no processes resulting in preferential directions were identified. Nugget effect was used in case of maps

with really dense data distributions to smooth contour lines by accounting for inherent errors of data.

The other different gridding methods available in Surfer® were also tested (Appendix I). The maps created with the various gridding methods were compared to the map created with kriging (Figure I.1). The Cenozoic-Mesozoic geothermal gradient map was used for testing the different gridding methods, since it has areas of variable data density: from very low data density in the north to very high data density in the Weyburn-Estevan and Lloydminster areas.

Nearest neighbour gridding method does not interpolate, it just assigns the closest measured value to the grid point (Golden Software, 2002). Therefore sharp, physically meaningless contacts occur (e.g., in T18-26W2 on Figure I.2).

Moving average assigns values to the grid by averaging data within the specified search ellipse (Golden Software, 2002). However, the radius of the search ellipse is of question. The larger the search radius, the larger area mapped, but the less the data are honoured by gridding, i.e., the more details are lost while gridding (Figure I.3 and Figure I.4). Also the circular pattern of the contour lines, especially characteristic in areas of low data density are only the artifact of the gridding method.

Triangulation with linear interpolation needs evenly distributed data. If the data are not evenly distributed, as in the case of this study area, triangulation produces similar contouring artifacts to those of the moving average method: in areas of low data density distinct triangular faces are created (e.g., in the north on Figure I.5).

Polynomial regression gridding method tries to define large scale trends in data (Golden Software, 2002). It does not honour data. No custom polynomial

functions were tested, but the other surfaces were found not to be complex enough to represent well the trends observed (compare Figure I.6[23] with Figure I.1).

High order (third order) local polynomial regression gridding (Figure I.7) does produce similar results to kriging in areas of high data density (in the south). However, in the areas of low data density, the fitted polynomial trend extrapolates unreasonable values (< 0 °C·km^{-1} and over > 50 °C·km^{-1}, northwest of T65-1W3).

Radial base function (Figure I.8) and modified Shepherd's method (Figure I.9) gridding methods are similar to the local polynomial method in a sense that they extrapolate to unreasonable values not supported by data. In addition to this, they cannot handle well areas of high data density (e.g., between T5-15W2 and T5-1W2 both on Figures I.8 and I.9).

These previously summarized seven gridding methods produce unrealistic maps prone to errors due to gridding artifacts. Therefore these methods were determined not to be useful for producing the maps of this study due to data distribution.

The other four gridding methods (kriging, Figure I.1, minimum curvature, Figure I.10, inverse distance method, Figure I.11, and natural neighbours, Figure I.12) were capable of producing physically meaningful maps from the heterogeneously distributed data.

Minimum curvature does not honour the data as closely as the other methods. Also differences exist between the results of this method (Figure I.10) and the result of the other methods (Figure I.1, I.11, and I.12). Largest differences (up to 10 °C·km^{-1}) exist north of the 1000 m basement depth line. This difference can be explained by the smoothing effect of using minimum curvature method.

The results of the other three methods are very similar. However, inverse distance gridding method is prone to creating bull's eyes (Golden Software, 2002), while

[23] Only the most complex surface tested, the cubic surface is presented here, but the others did not represent data well either.

natural neighbour gridding method does not extrapolate beyond the areas where data is available (Golden Software, 2002). Therefore, kriging was chosen to be the method for creating the maps in this study. The conformity between the results of these three gridding methods proves that kriging produces good results from the data.

In areas of high data density the potential difference between different useful gridding methods was determined to be less than <5 °C·km^{-1}, in areas of low data density it was determined to be <10 °C·km^{-1} by comparing the maps free of gridding issues in Appendix I.

In this chapter (Chapter 3) the methods used in this study were explained. First, an explanation was given how temperature data were quality controlled. Then, it was described, how temperature maps were generated and analyzed. The processed temperature data were used to calculate geothermal gradients. These were used in conjunction with the thermal conductivities estimated by net rock analysis to determine heat flow. Finally, sedimentary and basement heat generation estimations were described. The results produced with these methods will be detailed in the next chapter.

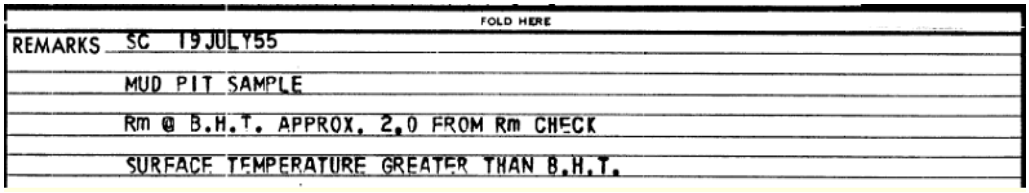
FOLD HERE

REMARKS SC 19JULY55

MUD PIT SAMPLE

Rm @ B.H.T. APPROX. 2.0 FROM Rm CHECK

SURFACE TEMPERATURE GREATER THAN B.H.T.

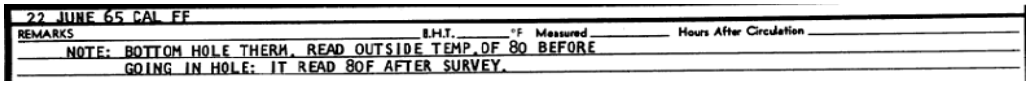
22 JUNE 65 CAL FF

REMARKS B.H.T. °F Measured Hours After Circulation

NOTE: BOTTOM HOLE THERM. READ OUTSIDE TEMP. OF 80 BEFORE GOING IN HOLE: IT READ 80F AFTER SURVEY.

Figure 3.1 Two examples from well headers, where the maximum thermometer error was identified.

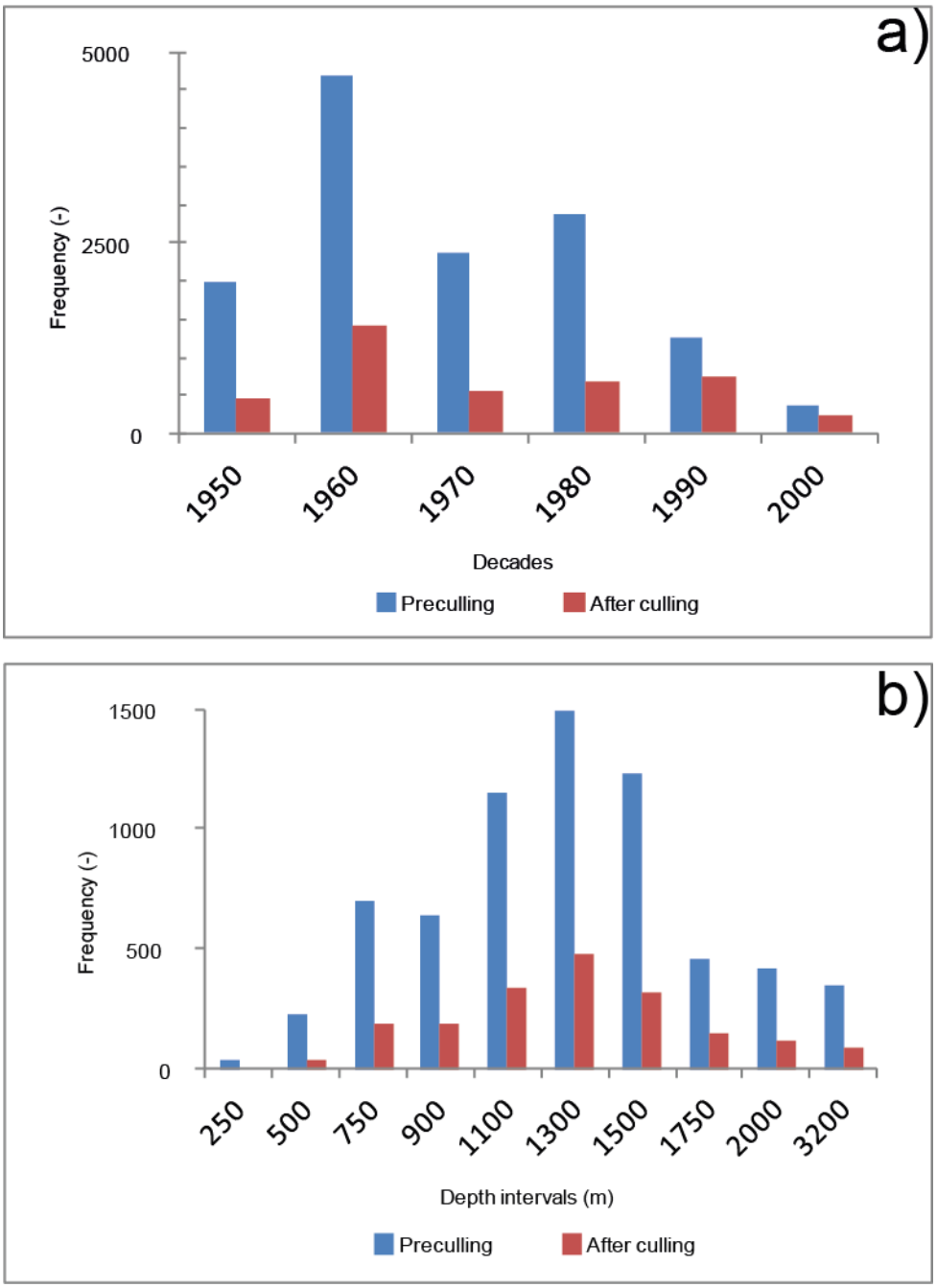

Figure 3.2 Decadal age (a) and depth distribution (b) of DSTs before and after culling. Note the different scale on a) and b).

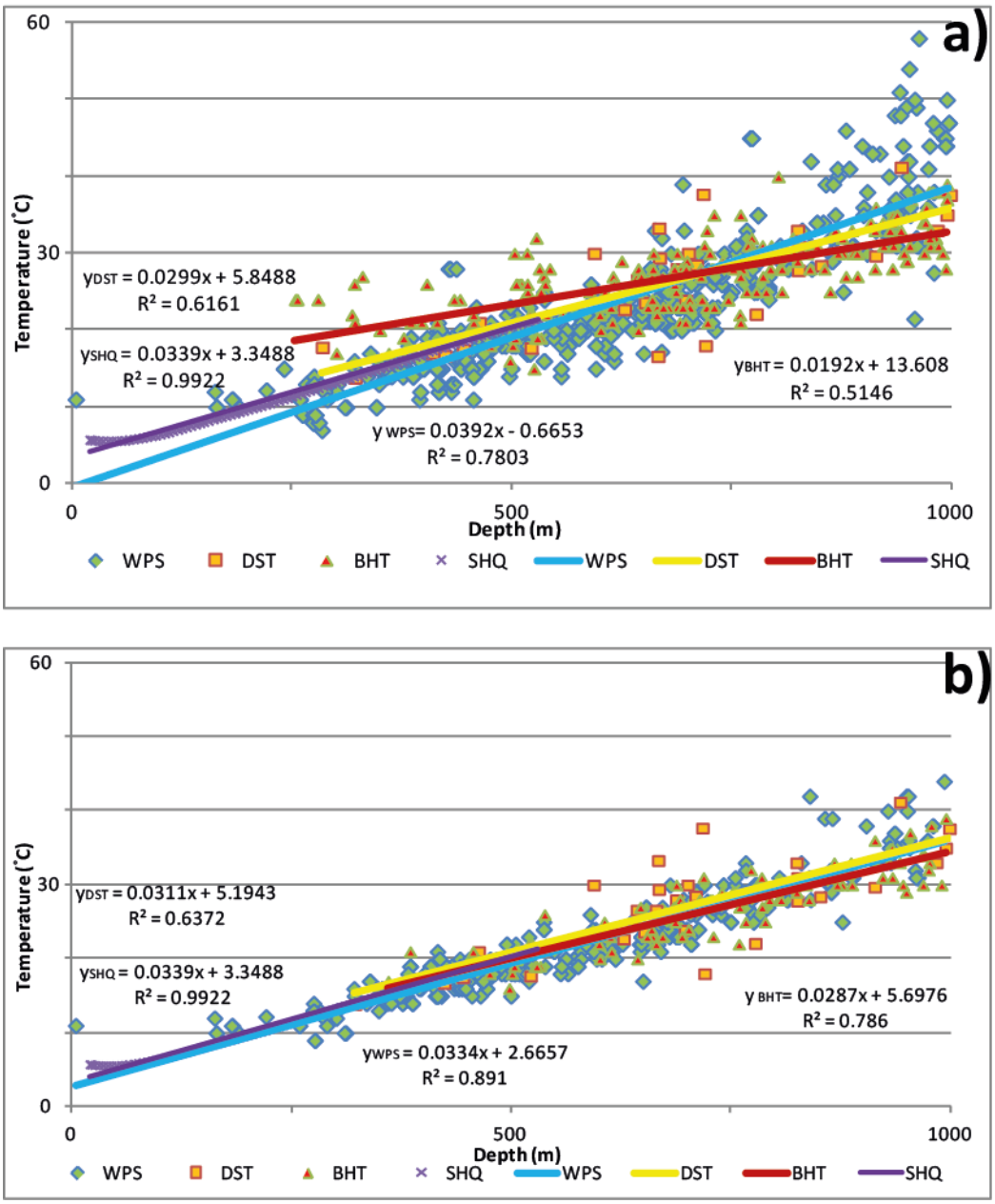

Figure 3.3 Comparison of various temperature data and their fitted linear regression trend before (a), and after culling (b). SHQ is a precise temperature log courtesy of Dr. J. Majorowicz.

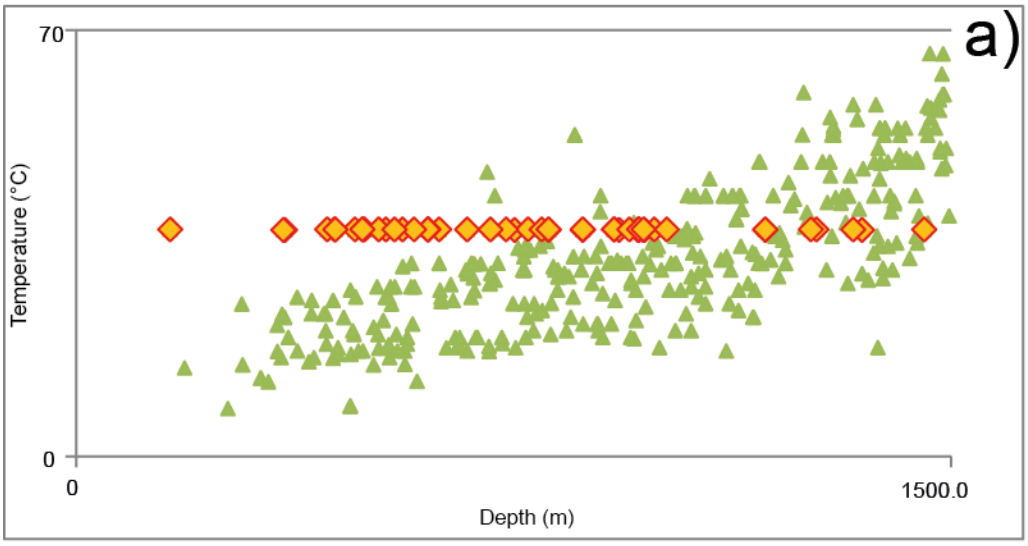

b)

K B Elevation	1420	Top Packer Depth	3190	Bottom Packer Depth	
Total Depth	3265	Casing Perforations	Top Bottom		
Interval Tested	3190 – 3265	Formation Tested	Nisku		
Casing or Hole Size	9	Liner or Rathole Size	6 1/8 x 50		
Size Surface Choke	1½	Size Bottom Choke	½	Size and Type Wall Packer	7½ E.S.
Size Drill Pipe	4½ F.H.	ID and Length Drill Collars	2 7/8 x 80.50		
Anchor Size	I.D. O.D. 4½	Amount-Type of Cushion			
Gauge Depth	~~118~~ 100 °F meas. Temp. °F est.	Mud Weight	10.3	Mud Viscosity	64
All Depths Measured From	K.B.			No. Folders Reproduced	5

Figure 3.4 100 F estimates. a) demonstrated on the initial DST database b) on a cut-out from an actual DST.

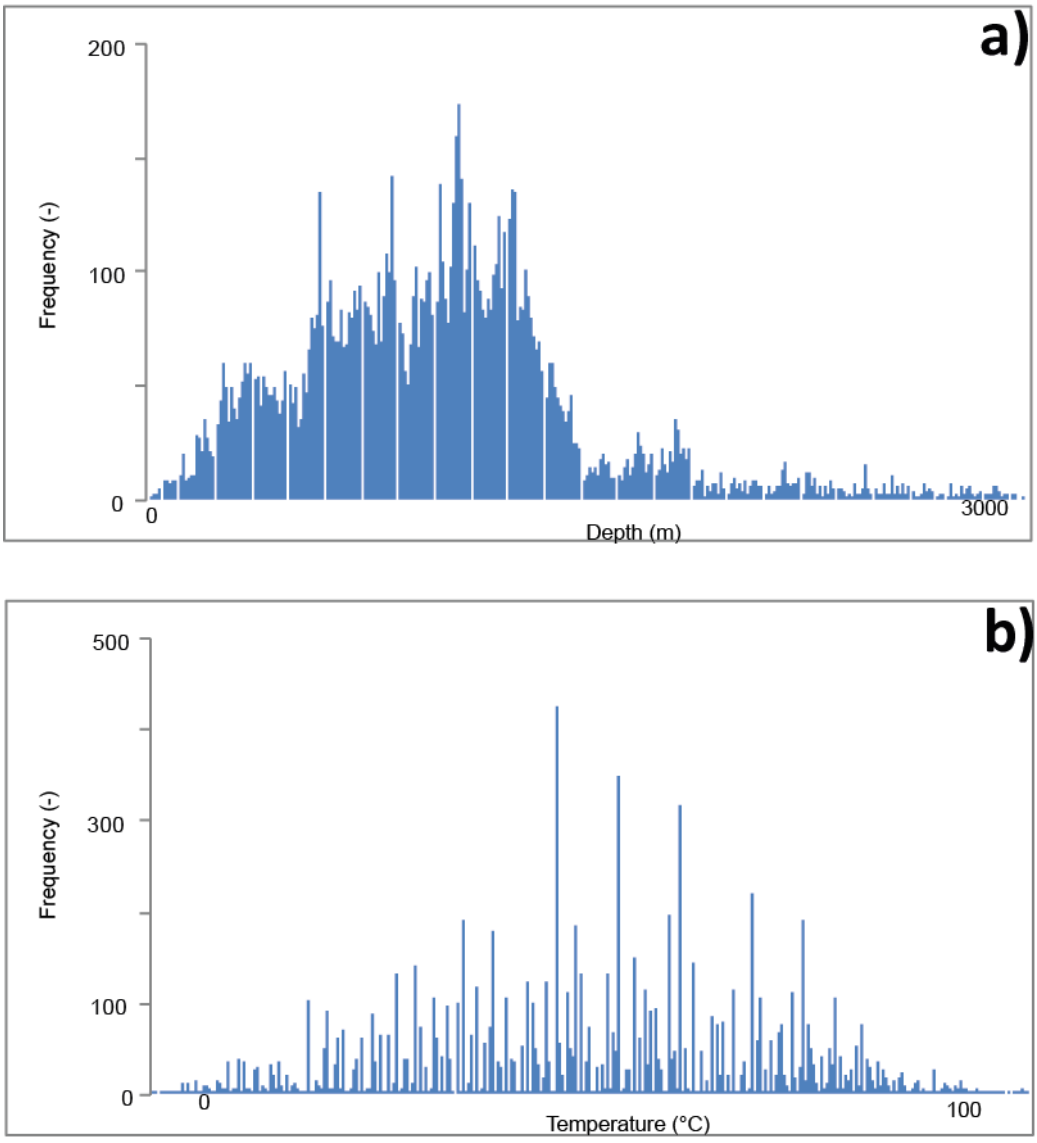

Figure 3.5 Distribution of original DST measurements with a) depth and with b) temperature. Note the different scale on a) and b).

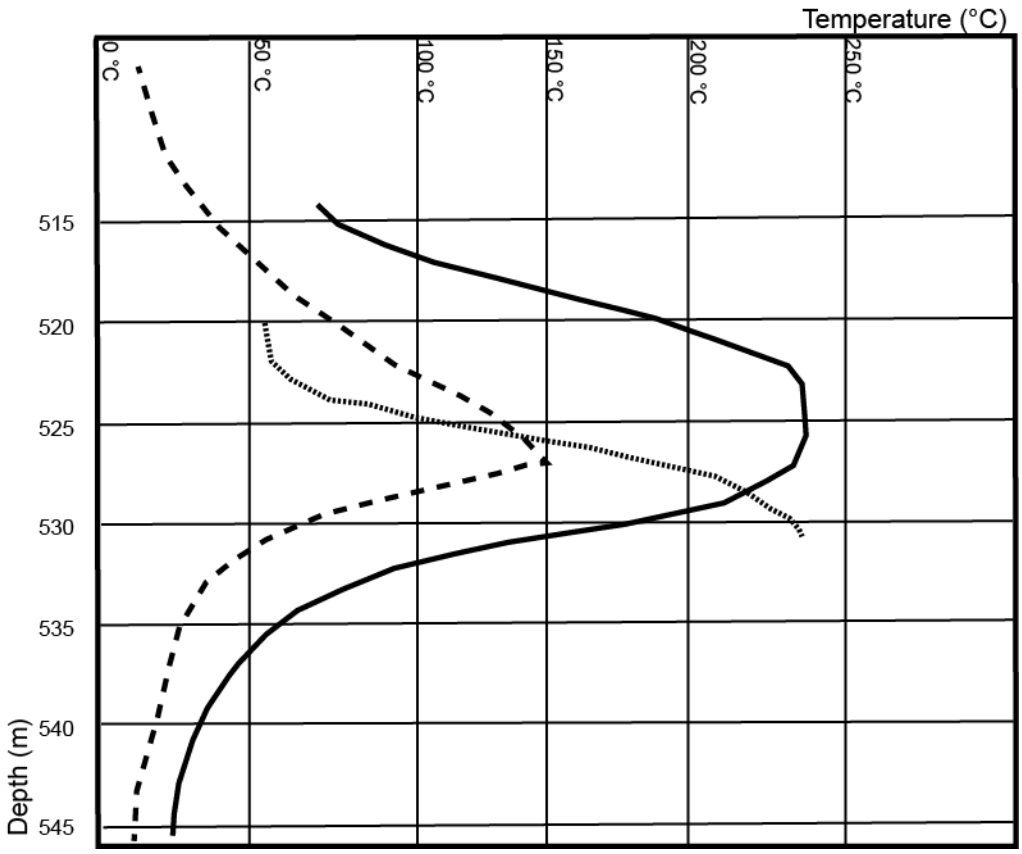

Figure 3.6 Temperature depth plot digitized from a temperature log conducted in 115/03-20-049-26W3/0 to measure the effects of steaming. No information available on steaming schedule. Different lines measured at different dates: solid - 1981.09.20, dotted - 1981.05.13, dashed - 1981.04.04.

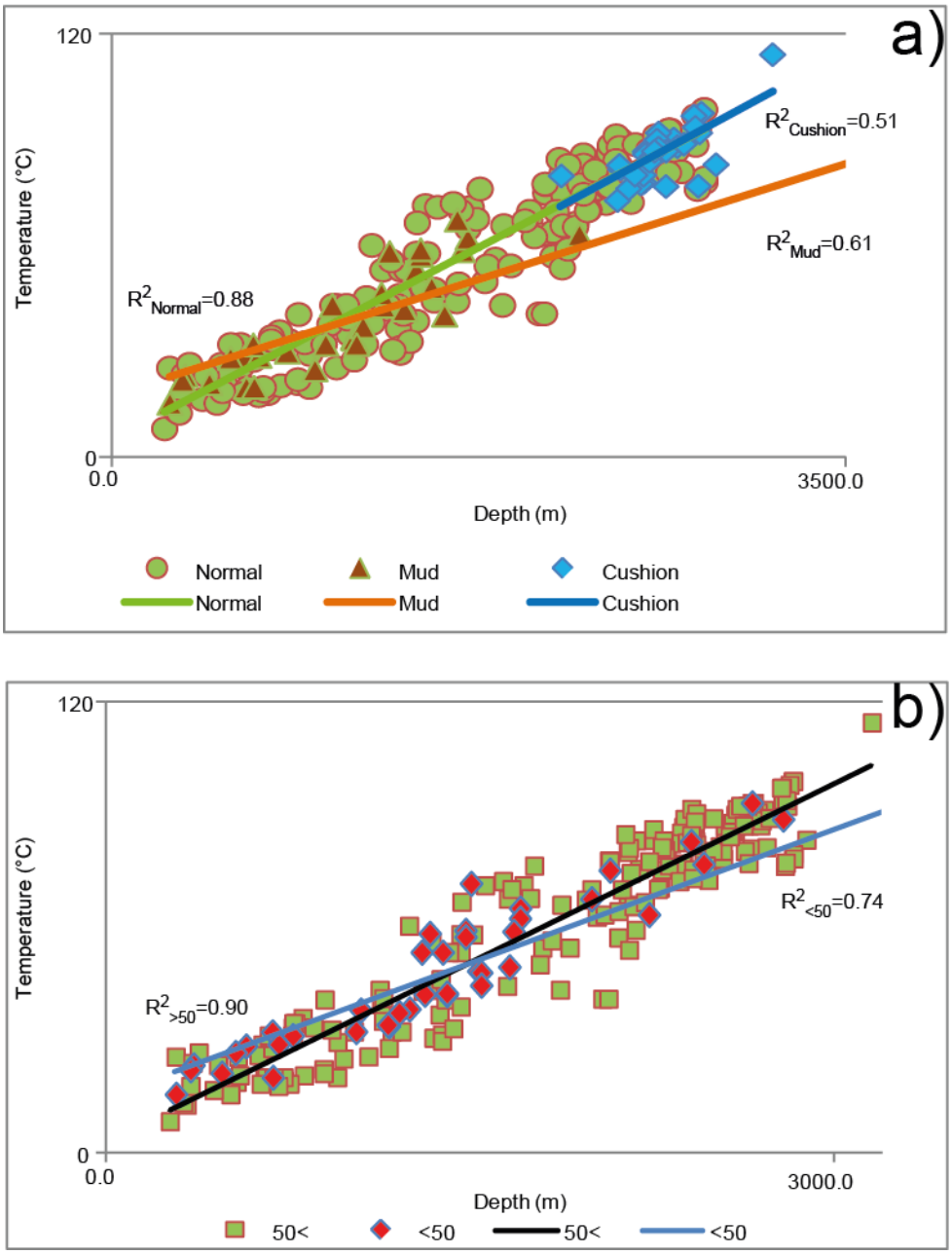

Figure 3.7 Temperature depth plot for the DSTs of the database of Figure 3.3 sorted according to the material (a) and the amount (b) of recovery.

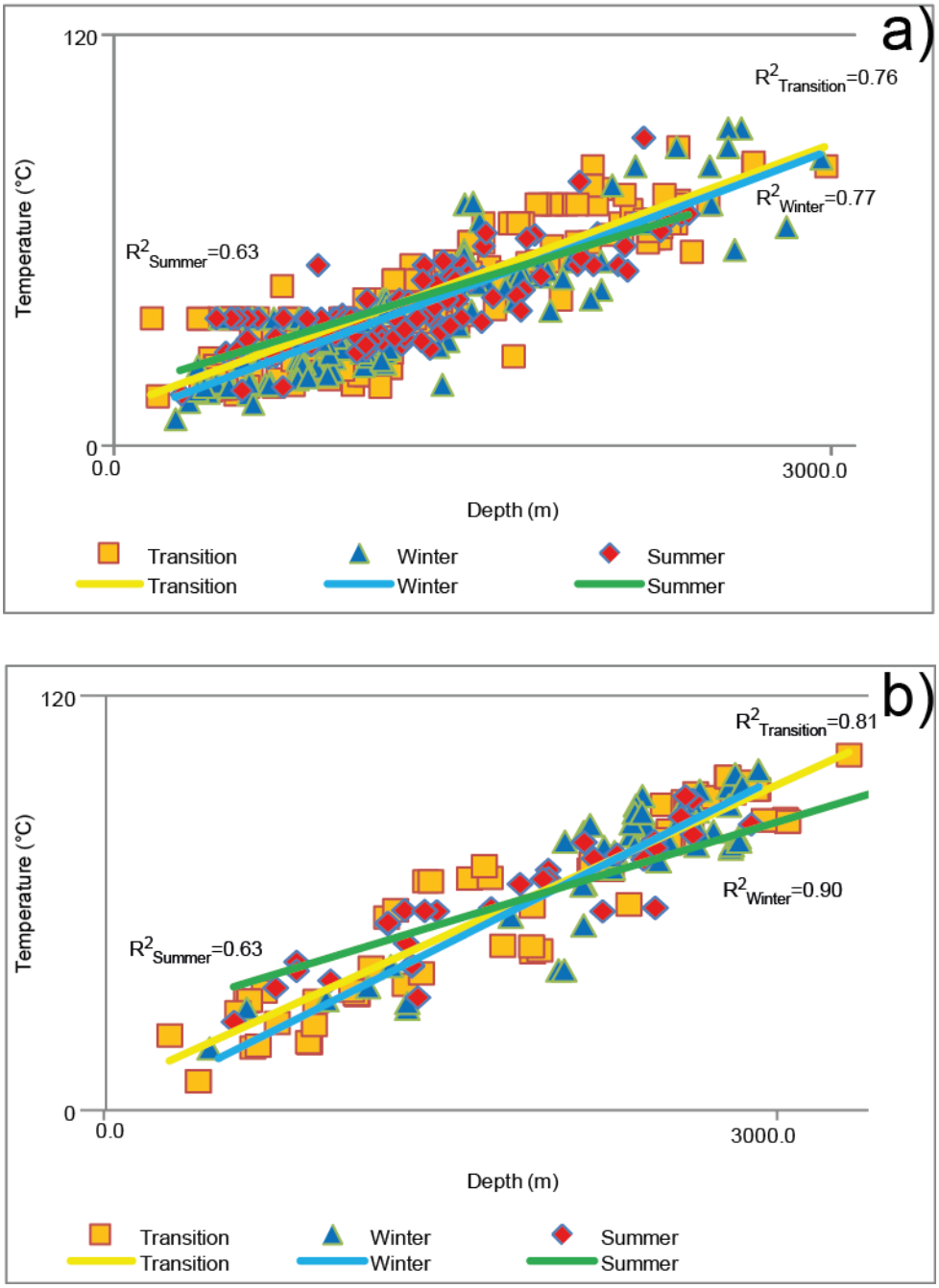

Figure 3.8 Temperature depth plot for the DSTs measured prior to (a) and after (b) 1980 for the database of Figure 3.3 sorted according to season of the measurements. Seasons: Winter: November to February; Summer: June-August; Transitional season: March-May, September-October.

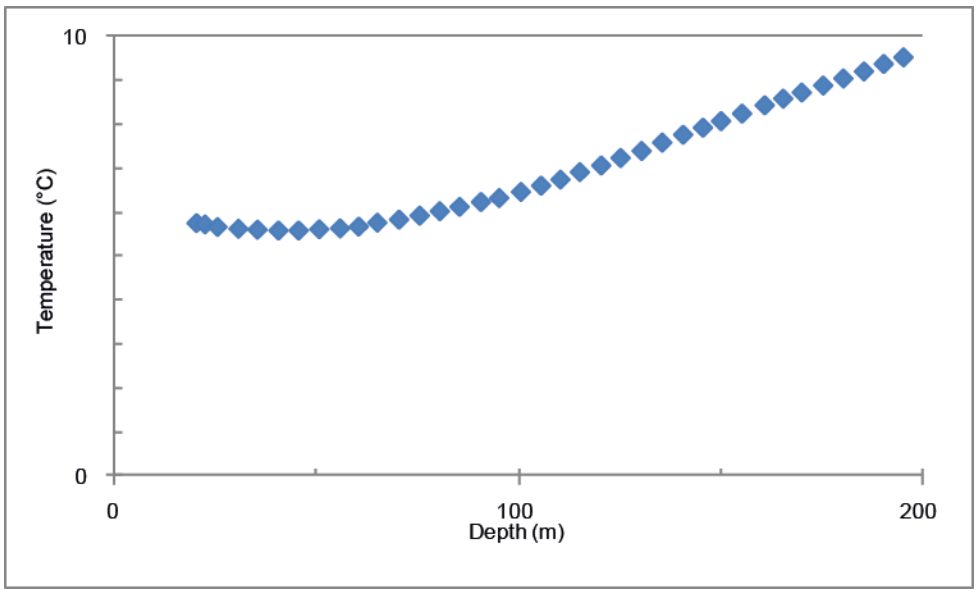

Figure 3.9 Temperature reversal and shallow temperature transient illustrated by the part of log CA-JM-A. Log, courtesy of Dr. J. Majorowicz and archived in the World Data Center for Paleoclimatology. URL<http://www.ncdc.noaa.gov/paleo/wdc-paleo.html >, [Last accessed: 2011.12.13].

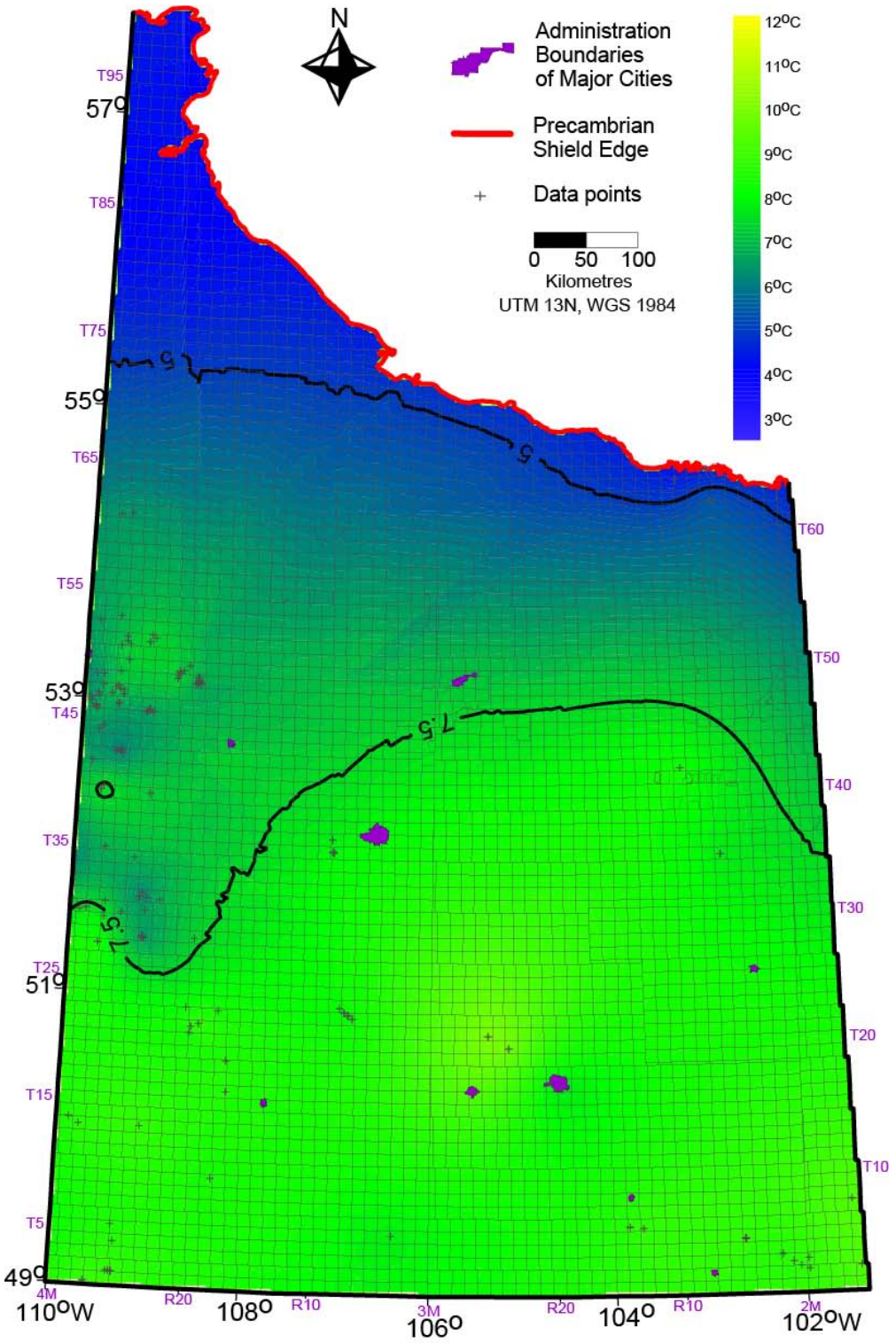

Figure 3.10 Temperature map for the 100 m depth surface utilized for the surface boundary for geothermal gradient calculations. R, M, T marks location (Range, Meridian, Township) defined in the Dominion Land Survey system (in the grid). CI: 2.5 °C. Nugget effect: 1(°C)^2.

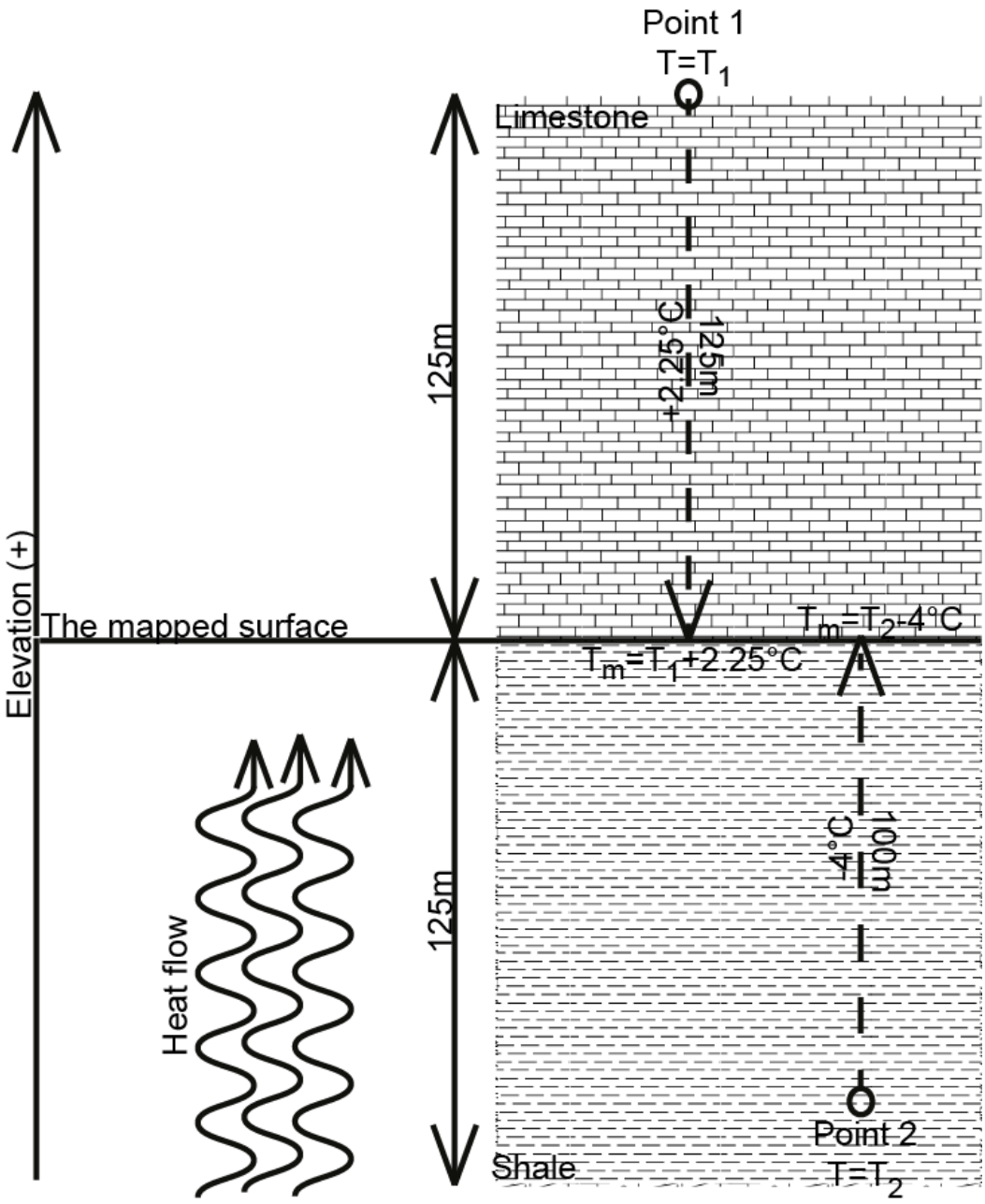

Figure 3.11 Correction for interval thickness. Maximum distance for data collection: was ±125 m from the mapped surface. A correction was applied to project the measured temperatures on the mapped surface based on lithology (if known), and distance from the mapped surface. Point 1 is located at 125 m higher than the mapped surface in limestone. Therefore the mapped temperature (T_m) is, $T_m=T_1+2.25$ °C. Point 2 is 100 m deeper in shale then the mapped surface. Therefore the mapped temperature for this point is $T_m=T_2-(100m/125m)*5°C=T_2-4$ °C. Values used for corrections are illustrated in Chapter 3.1.3.1.

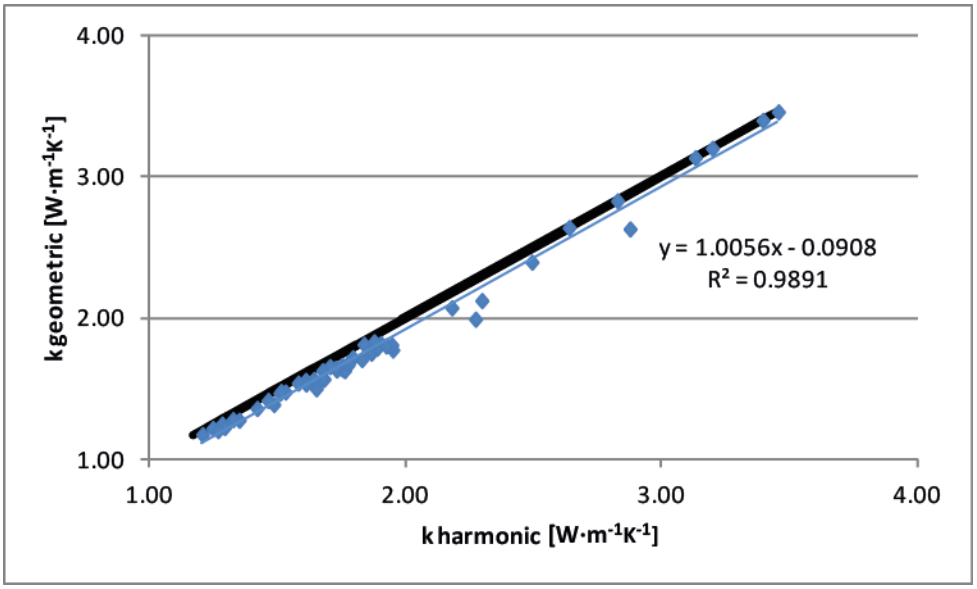

Figure 3.12 Comparison of thermal conductivities calculated within an interval via the harmonic and geometric means. Black line represents the 1:1 slope.

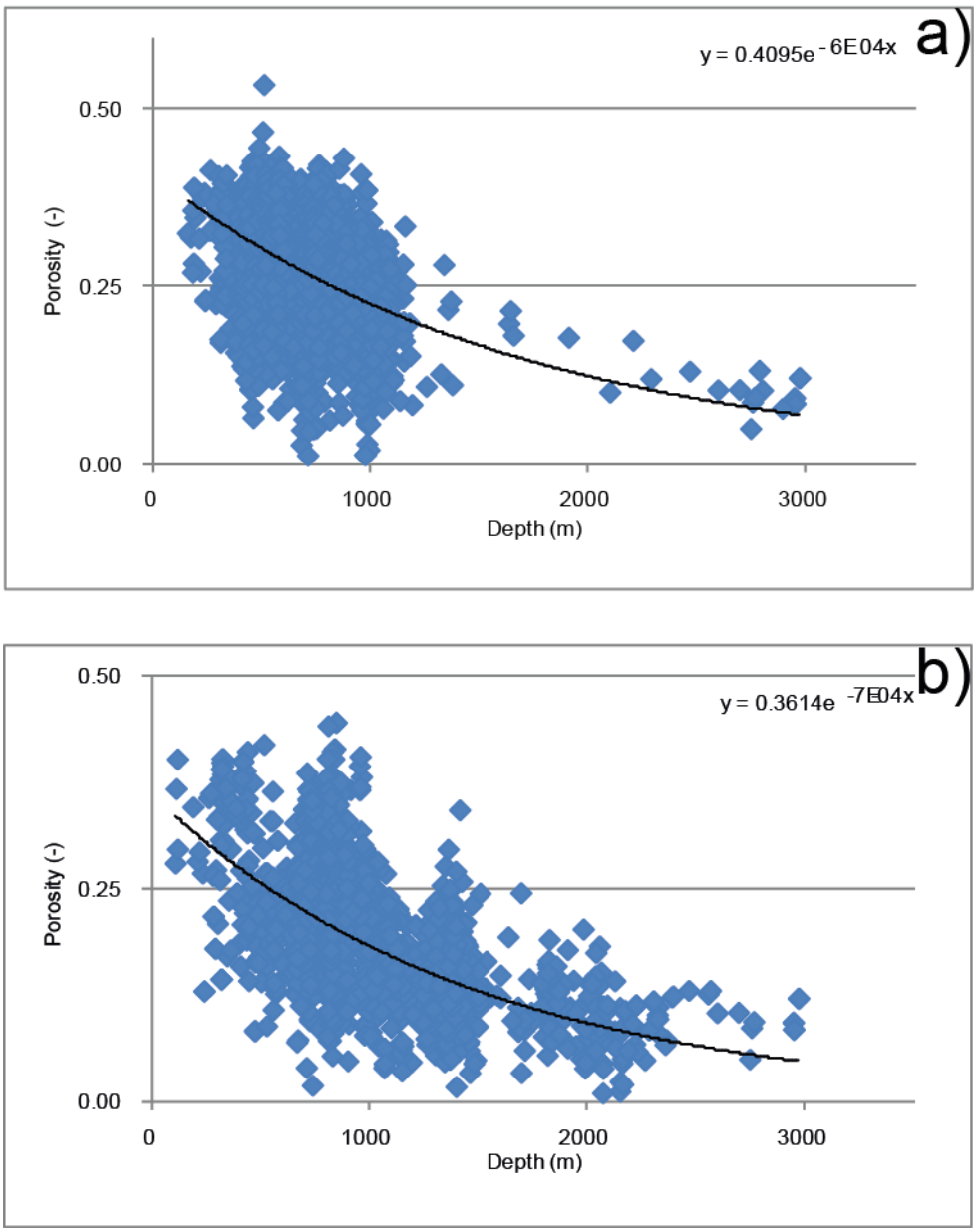

Figure 3.13 Porosity depth trends for a) sandstones b) shale

4 Results

The results of the analysis of the geothermal conditions of Saskatchewan will be described in this chapter. First, the temperature field was determined by analysing quality-controlled temperature data. Temperatures were mapped horizontally for selected depths; elevations; and formation tops. Next, geothermal gradients were used to characterize the vertical distribution of temperature. Finally, heat flows were calculated via estimating the thermal conductivity of the rock formations.

4.1 Horizontal temperature distribution

The strata, depth and elevation specific temperature maps and the isothermal depth maps (Chapter 3.1.3.1) characterize the horizontal distribution of temperature. Their analysis was undertaken according to Chapter 3.1.3.2. The key trends and regionally characteristic anomalies (Figure 4.1) identified will be described in the following.

General trends

Temperatures range from <5 °C (Figure 3.10) to >120 °C (Townships T1-8W2 to T1-12W2 on Figure 4.3) in the subsurface of Saskatchewan. Temperatures increase with depth. Therefore the highest temperature values are located in areas where the basin is the deepest: i.e., in the southeast, next to the Canada-US border (Figure 4.4)[24]. This trend can be observed on all sets of temperature maps (see Appendix A - Appendix D).

Temperatures generally decrease from south to north. In the case of the strata specific maps (Appendix A) this pattern can be explained by the structure of the

[24] The Deadwood temperature map (Figure 4.3) is hotter in parts of this deep area than the deeper Precambrian temperature map (Figure 4.2). This is because the Precambrian map is almost exclusively based on BHTs since only such measurements were available close to the basement. This illustrates one of the issues of using only BHTs for mapping geothermal conditions.

basin (Figure 4.4), i.e., the further north a location is, the closer to the surface, and the cooler the same formations will be.

On the elevation specific temperatures maps (Appendix B) temperatures generally decrease from southwest to northeast. On some shallow elevation specific maps the lateral temperature difference between the hottest and coldest points is as much as 20- 25 °C (e.g., Figures B.4, and B.5).

However, this trend of temperatures decreasing towards the northeast becomes less important and less visible with depth. For example, the temperature map created for 1250 mbsl (Figure B.9) is the shallowest elevation specific map, where the highest temperature values are located not in the Cypress Hills area, but north of it, near Swift Current (T16-14W3), and also, in the southeastern corner of the province, west of Estevan (T1-10W2)[25].

This distortion of the north-south trend can be explained by the effects of topography: the highest temperature values are located in the SW corner of the province on the elevation specific maps between 750 masl and 250 mbsl (Figures B.1- B.5). This area coincides with the Cypress Hills, the most elevated topographic feature of the study area (Figure 1.2).

The depth specific maps (Appendix C) also prove that topography significantly impacts the geothermal conditions of Saskatchewan. On these maps topographic effects are minimized as the mapped surfaces are parallel to the ground surface. Temperatures are higher on some of the depth specific maps under the Cypress Hills than the background temperature (e.g., >50 °C on Figure C.7, while background is 40- 50 °C). However, the magnitude and the extent of these anomalies is significantly reduced compared to the anomalies on the elevation specific maps. Therefore the hot anomaly observed under the Cypress Hills is deemed to be caused largely by the effect of topography.

[25] However, it should be noted, that the amount of data available in the southwest corner decreases the deeper the map is, and this might also contribute to the disappearance of this high temperature anomaly from the maps.

The isotherm lines of the strata specific maps (Appendix A) more or less conform to the isopachs (for these, see Marsh and Love, 2013) in the area between the highest temperature values in the south and coldest temperature values in the north. This observation confirms the conclusions drawn from Peclet numbers, i.e., that heat conduction is the dominant heat transfer method in the basin.

Anomalous regions

Three hot and six relatively cold anomalies were identified on these maps according to the methods described in Chapter 3.1.3.2. Figure 4.1 illustrates all of these anomalous regions. These anomalies will be described in the following.

The highest temperature values on all strata specific maps were located in the southeast part of the study area, generally between T1-5W2 and T1-15W2. This is also the deepest part of the basin (Figure 4.4). However, elevation and depth specific maps (e.g., Figures B.8-B.14 and C.5-C.14) also show that this area and its surroundings have significantly higher temperature values than the background temperature of the respective maps. For example, Figure B.10 shows that the background temperature is 60-70 °C, but significant portion of this area near Estevan has values >80 °C (as far north as Township T8-5W2 - T8-11W2).

The second regionally characteristic high temperature anomaly is located in the southwest part of the study area (e.g., on Figure 4.4., temperatures are >75 °C in the area of T5-25W3 - T25-15W3). It is one of the most prominent high temperature regions of the temperature maps (e.g., on Figure C.4, the highest values, up to 40 °C, of the map are located in this area).

Although the southwest portion of the anomaly was in part related to the effects of topography by comparing the elevation and the depth specific temperature maps, topography alone cannot explain the existence of this anomaly. First, it extends further north from the area of the Cypress Hills. Second, highest temperature values of the anomaly are located close to Swift Current (T17-16W3 – T19-14W3), north from the topographically elevated area. For example, on the 2250 m KB map (Figure C.10) temperature values in the northeast portion of the anomaly

(between T14-16W3 and T22-16W3) are >80 °C, while the background temperature is <70 °C.

This anomaly breaks up into a northern anomaly near Swift Current, and a southern anomaly in the Cypress Hills area on some shallower temperature maps (e.g., Figure A.17). Also its northeast portion is not continuous vertically due to lack of data (e.g., it does not show up on Figures C.7 and C.8).

The third regionally characteristic high anomaly can be less readily observed than the other two. This high temperature anomaly extends west to north of Yorkton. It is most obvious on the Precambrian temperature map (Figure 4.4, here it extends from T15-25W2 to T35-5W2). However this anomaly does not show up as a continuous feature on all other temperature maps, although some parts of it are traceable. For example, it can be observed on the 500 mbsl temperature map (Figure B.6) as a trend of values of close to 40 °C.

The cold anomaly located in the area of Saskatoon is the easiest to notice. Coldest temperature values are often located here. For example, it is the coldest area on the 1000 mbsl map (Figure B.8), where temperatures at Saskatoon are <40 °C, while the background is 50-60 °C (coldest also e.g., on Figures B.5-B.12, C.7, and C.8). This anomaly is often part of a larger anomaly, which on some maps extends as far south as Moose Jaw (e.g., colder values are protruding into a warmer region as far south as T17-29W2 on Figure A.5)

On several maps (e.g., Figures B.8, C.6 and C.7) the cold region near Saskatoon is linked to another regionally characteristic cold area: the cold anomaly located along the Alberta border. It restricts the Swift Current high temperature anomaly from the northwest. However, its extent varies widely from map to map. For example, on the Precambrian temperature map (Figure 4.2) it is present between Township T57-27W3 and T35-28W3, while on the Shaunavon temperature map (Figure A.15) it covers the area between the subcrop edge of the Shaunavon Formation and Township T10-30W3.

Three smaller relatively cold anomalies exist in the eastern half of the province. The northernmost of these, is a cold anomaly close to Regina (e.g., Figure 4.2). It is most often not as readily identifiable as the previous two cold anomalies, but rather just an area, where cold temperatures are protruding into a region of hotter temperatures (e.g., the 45 and 50 °C isothermal lines on Figures A.6., and A.7).

There is a very pronounced relatively cold anomaly south of the Regina anomaly at T1-20W2 bisecting the southeastern high temperature region. This second anomaly, is present on almost all deeper temperature maps (e.g., from Figures A.2 to A.13, or from Figures B.8 to B.13). It is usually 5-10 °C colder than the areas to the east and the west of it and extends as north as Township T7-22W2 (e.g., Figure B.10). It potentially also shows up on the Viking Formation temperature map (Figure A.17) as the boundary of the higher temperature region of the southeast.

The third small relative cold anomaly of the east is also located within the heart of the high temperature region of the southeast. Generally it covers an area between T4-12W2, T4-16W2, T10-12W2, and T10-16W2. It often acts as the northern boundary of the highest temperatures in the anomaly. It is more similar to the Regina anomaly that it is less pronounced than the anomaly at Saskatoon. Also, this anomaly is often just a an extension of colder temperature values from the north protruding into the south. Its location varies slightly. For example, colder temperature values protrude into the higher temperature regions as south as T5-4W2 on Figure B.6 (<45 °C) and as south as T3-13W2 on Figure B.10 (<75 °C).

The sixth cold anomaly observed is located between the high temperature anomalies of the southwest and the southeast. For example, values <75 °C cover a significant area located between the two high temperature regions on Figure 4.2, between T1-13W3 and T17-26W2. This anomaly was examined on the elevation specific temperature maps as well. However, on these maps it was identified that this cold anomaly has approximately the same temperatures as the background

temperature (e.g., values of 45- 50 °C on Figure B.7., where the background value is 40- 50 °C)[26]. Therefore, this cold anomaly is deemed to be only apparent, and its existence is explained by an area of normal geothermal conditions intersecting two areas of hotter than average geothermal conditions.

4.2 Vertical temperature distribution

The previously described temperature maps characterize the lateral change of temperatures along selected depth, elevation and strata specific surfaces. However, it is hard to determine the vertical rate of change of temperatures based on only those maps. Therefore, to characterize the vertical change, geothermal gradient values were calculated (Chapter 3.1.4) and mapped.

Three geothermal gradient maps were generated to represent the vertical change of temperatures: an integral geothermal gradient map for the entire sedimentary package, and two interval geothermal gradient maps for the sub-Mesozoic formations, and for the Mesozoic-Cenozoic formations. It was necessary to distinguish between the Paleozoic and the younger formations since they are of very different lithologies and thermal conductivities (see Chapter 2.1), and thermal conductivities have an impact on the geothermal gradients.

4.2.1 Integral geothermal gradient map

Temperature data used for the Precambrian temperature map and the temperature map of 100 m depth were used to calculate the integral geothermal gradient. To facilitate identification of shallow regions, both the 1000 m and the 200 m basement depth lines are shown on this geothermal gradient map (Figure 4.5).

Geothermal gradients in the study area range from <20 °C·km^{-1} to >40 °C·km^{-1} (Figure 4.5). The interval of 25- 30 °C·km^{-1} covers most of the province, i.e., this

[26] This is true for the shallower maps, but not for the very deep elevation specific temperature maps, i.e., the 1500 mbsl and 1750 mbsl, on which this area is the coldest. However, on these maps the background temperature cannot be determined, since there is only a little area not covered by the identified hot anomalies.

is the representative integral geothermal gradient for the Phanerozoic strata of Saskatchewan.

Major areas of higher than average geothermal gradient values (>30 °C·km^{-1}) exist in the north-northwest part of the province (T55-1W3 to T65-1W3 linked with T60-25W3 to T65-25W3), in the southwest, near Swift Current (T15-15W3 to T20-15W3), and in the southeast, in the Estevan-Weyburn area (in an area marked by T1-5W2, T1-20W2, T19-20W2 and T19-6W2). Other minor anomalies covering much smaller areas are substantiated by only one or two data points, thus they are not discussed here further.

Both of the high geothermal gradients anomalies identified in the south correspond to high temperature regions identified on the temperature maps. They are located in an area, where depth to the basement is over 2000 m (Figure 4.4), and the temperatures are over 70 °C (as illustrated by Figure 4.2). The geothermal anomaly in the north does not correspond to the previously determined high temperature anomalies.

Major areas, where the integral geothermal gradients are relatively cold (<25 °C·km^{-1}) are located at Saskatoon and west of it (along an axis of Saskatoon and T35-28W3), southeast of Prince Albert (T35-10W2 to T45-10W2), and along the Precambrian outcrop edge.

Colder than average geothermal conditions at Saskatoon and along the Alberta border correspond to cold temperature areas on the temperature maps. The colder than average values in the northeast are also reliable, as the temperature measurements for these gradients were taken from scientific temperature log data from boreholes (published in Jessop *et al.*, 2005). The colder than average area southeast of Prince Albert does not correspond to previously identified temperature anomalies.

4.2.2 Interval geothermal gradient maps

While the integral geothermal gradient map averages out the change of temperature over the entire sedimentary package, the interval geothermal gradient maps are more representative of the gradients within smaller rock packages.

Sub-Mesozoic formations, are dominated by carbonate-evaporite rocks, while in the younger strata clastic sediments with thick shale packages prevail (Chapter 2.1). Therefore geothermal gradients were determined between the sub-Mesozoic unconformity and the temperature at 100 m depth (for the Mesozoic and Cenozoic formations, Figure 4.6); and between the sub-Mesozoic unconformity and the Precambrian basement (for the Paleozoic formations, Figure 4.7).

Geothermal gradient in the younger strata varies over the range of <20 °C·km^{-1} to >40 °C·km^{-1} (Figure 4.6). The geothermal gradient of 30- 35 °C·km^{-1} was determined to be representative for the Cenozoic-Mesozoic strata by examining the geothermal gradient map.

Areas where the geothermal gradient is higher than 35 °C·km^{-1} exist parallel to the 1000 m basement depth line (between Townships T30-30W1 and township T27-60W3), in a large patch near Swift Current (between T1-25W3 and T20-15W3), in the southeast (between T1-1W2 and T10-20W2), and in the north-central part of the study area (T55-3W3 to T70-3W3).

The highest geothermal gradient values in the younger strata occur in the north central area coinciding with the highest values of the integral geothermal gradients map (Figure 4.5). While the southeastern anomaly has values above 40 °C·km^{-1}, the southwestern anomaly (near Swift Current) does not reach this value.

Areas where the Cenozoic-Mesozoic geothermal gradients are low, exist along a T-shape, with its tips being located at T30-8W3, T20-30W1, and between the two high geothermal gradient anomalies of the south, at T1-5W3.

The sub-Mesozoic geothermal gradient (Figure 4.7) map has a gradient range similar to that of the shallower strata: <20 °C·km^{-1} to >40 °C·km^{-1}. However, the distribution of gradients is very different. 20- 30 °C·km^{-1} interval covers most of the study area. Therefore the representative geothermal gradient of the sub-Mesozoic formations is ~25 °C·km^{-1}. This is lower than the gradient determined for the younger formations.

Major high geothermal gradient (>30 °C·km^{-1}) areas are present in the northwest, shallower part of the basin (between T55-1W3 and T75-25W3) and in the southwest, near Swift Current (T10-15W3 to T20-15W3). Several other high anomalies also exist north of the Moose Jaw and Regina (e.g., T23-20W2 to T23-28W2), and north of Yorkton (T35-3W2).

When comparing the Weyburn-Estevan high geothermal gradient anomaly observed on the Cenozoic-Mesozoic geothermal gradient map (Figure 4.6) to the area on this map (Figure 4.7), the anomaly found on the Paleozoic map is much less pronounced. However, the Cypress Hills-Swift Current anomaly shows about the same values (30- 40 °C·km^{-1}) on both maps.

The high geothermal gradient anomalies of the southwest, the southeast, and north of Yorkton correspond to areas of previously observed high temperature anomalies.

The areas with the coldest geothermal gradients (<20 °C·km^{-1}) are located at Saskatoon and west of it along the Alberta border, and also in the northeastern part of the province (T65-9W2 to T58-30W1). The Saskatoon and Alberta border areas have been previously recognized as cold temperature anomalies.

The two interval geothermal gradient maps were compared. The geothermal gradients are significantly higher in the Cenozoic- Mesozoic rocks. However, the anomalous regions occur in the same areas, with hottest temperature values being located in the north central portion of the study area.

It is important to note that BHT data are almost twice as frequent in this database as all other types of temperature measurements (111 vs. 67 data points). Most of the shallow measurements are BHTs. Therefore, shallow gradients should be used with precaution for temperature extrapolations, as shallow temperature values are prone to the maximum thermometer error described in Chapter 3.1.2.1.

The geothermal gradient anomaly in the shallow, north-central portion of the basin is substantiated only by BHT data. The only measurements in the extreme north of the study area, which are not BHTs, are the high precision temperature logs published by Jessop *et al.*, (2005). These indicate colder than average geothermal gradients (<20 °C·km^{-1}) in the northeast. Therefore temperature measurements, other than BHTs are recommended to be taken in the north-central portion of the basin to verify the high geothermal gradients observed there.

4.3 Heat flow

Heat flow is the basic parameter characterizing the amount of heat transported through the strata. Heat flow is independent from changes in lithology, i.e., it does not vary vertically. Thus, its understanding is desired for a proper geothermal characterization of an area.

However, to be able to calculate heat flow the knowledge of thermal conductivity is required. Therefore, first thermal conductivity will be analysed. Then the heat generated by the basement and the heat generated by the Phanerozoic sediments will be described to investigate the potential sources of heat. And finally the results of the heat flow calculations will be presented.

4.3.1 Thermal conductivity

Thermal conductivity values were calculated based on net rock analysis as detailed in Chapter 3.2. Thermal conductivity maps (Figure 4.8- Figure 4.10) were generated for the entire sedimentary package, the Paleozoic strata, and the Cenozoic-Mesozoic interval.

Since thermal conductivity values measured in the scientific wells located in extreme northeast part of the study area (T62-1W2 to T65-10W2, from Jessop *et al.*, 2005) were measured on mostly rocks of non-sedimentary origin, thus their values were not incorporated in thermal conductivity maps.

Integral thermal conductivity

The calculated thermal conductivity of the entire sedimentary package (Figure 4.8) varies between 1.1 $W \cdot m^{-1} \cdot °C^{-1}$and values >2 $W \cdot m^{-1} \cdot °C^{-1}$. Values generally increase towards the north and the east. Values above 2 $W \cdot m^{-1} \cdot °C^{-1}$ are constrained to the edges of the study area, with the exception of well 101/06-24-030-28W2/0. This well has a calculated thermal conductivity of 2.05 $W \cdot m^{-1} \cdot °C^{-1}$. However, this conductivity anomaly in the central parts of the province is constrained in space by other measurements.

The lowest thermal conductivity values are located in the south, southwest part of the basin. There is a major insulating blanket of low conductivity rocks extending from the US border north to Saskatoon (<1.5 $W \cdot m^{-1} \cdot °C^{-1}$). A second, smaller low conductivity blanket also exists in the southeastern corner of the province.

It is expected that the thermal conductivity values will be the lowest, where the amount of shale within the rock column is the highest. This parameter was estimated in the current study by comparing the thickness of the Cenozoic-Mesozoic strata, to the thickness of the entire Phanerozoic interval (Figure 4.11). Although the lowest thermal conductivities are found in the southwestern part of the study area, the correlation between the amount of shale and thermal conductivity is not everywhere clear.

Paleozoic thermal conductivity

Paleozoic thermal conductivities (Figure 4.10) vary from 1.5 to 2.9 $W \cdot m^{-1} \cdot °C^{-1}$. Since the rocks in the Paleozoic strata are more conductive than the younger formations, the thermal conductivity of this map shows the highest values among the three thermal conductivity maps.

The general pattern of thermal conductivity is different from that observed in the case of integral thermal conductivity. A major thermal conductivity high (>2 $W \cdot m^{-1} \cdot °C^{-1}$) extends between T26-30W1 and T30-29W3. This highly conductive anomaly also branches to the south partially coinciding in area with the Estevan-Weyburn temperature high.

One similarity exists between the integral (Figure 4.8) and the Paleozoic thermal conductivity map (Figure 4.10): there is a low conductivity anomaly in the southwest. However, the major insulating blanket observed in the southwest on Figure 4.10 is broken up into two pieces by the highly conductive zone in the central part of the province in the Paleozoic strata.

Cenozoic-Mesozoic thermal conductivity

Cenozoic-Mesozoic thermal conductivities (Figure 4.9) in the province vary between 0.9 $W \cdot m^{-1} \cdot °C^{-1}$ and 1.7 $W \cdot m^{-1} \cdot °C^{-1}$. These values are the lowest among the three maps. This can be explained by the abundance of low conductivity shale in the younger strata. As these lower thermal conductivity strata are located on top, they can potentially insulate the heat at depths.

The lowest thermal conductivity values have a north-south trending anomaly from the US border to Saskatoon similar to that of the integral thermal conductivity map. However, this thermal conductivity anomaly is offset to the east compared to the other one, and the northern parts of the anomaly extend more to the east-west directions.

The relationship between the maps matches the overall lithology, that is the Paleozoic formations have only minor amounts of shale (Winnipeg and Deadwood formations) with rocks dominantly made up of carbonates and evaporite. These rock types generally have a high thermal conductivity, as outlined previously (Chapter 3.2). Meanwhile, the thermal conductivity of the clastic sediments, especially that of shale is much lower than the thermal conductivity of carbonates and evaporite.

The difference in the calculated thermal conductivity between the two rock packages can explain the difference in observed interval geothermal gradients: the geothermal gradients in the Cenozoic-Mesozoic package are larger due to the lower thermal conductivity of the rocks than the geothermal gradients in the Paleozoic strata.

Formation thermal conductivities

Besides mapping the thermal conductivities for the Paleozoic and Cenozoic-Mesozoic intervals, they were also calculated for selected formations to compare with the most relevant and most recent thermal conductivity measurements from the US portion of the Williston Basin (Table 4.1).

Table 4.1 Comparison of formation thermal conductivity calculated in Saskatchewan (k_i – surface thermal conductivity, k_f – in-situ thermal conductivity) and measured in North Dakota by Gosnold *et al.*, (2010). Formation name after the "/" corresponds to the name reported by Gosnold, *et al* (2010). Ls – Limestone, Do – dolomite, Sh – shale, Ss – sandstone. $k_{prev.}$ – value based on just lithology, used before measurements/net rock analysis have been undertaken.

	Saskatchewan			North Dakota		
Formation	Rock type	k_i ($W \cdot m^{-1} \cdot °C^{-1}$)	k_f ($W \cdot m^{-1} \cdot °C^{-1}$)	Rock type	k ($W \cdot m^{-1} \cdot °C^{-1}$)	$k_{prev.}$ ($W \cdot m^{-1} \cdot °C^{-1}$)
Mississippian/ Madison	Ls/Do	2.65	2.04	Ls	2.49±0.48	3.5
Duperow	Do/Ls	3.12	2.43	Ls	3.03±0.34	3.5
Ashern	Sh	2.83	2.22	Ls/Do	2.97±0.24	3.5
Interlake	Do/Ls	3.06	2.37	Do/Ls	3.6±0.64	3.5
Red River	Ls/Do	2.82	2.17	Ls/Do	3.28±0.94	3.5
Winnipeg/ Black Island	Ss/Sh	2.28	1.72	Do-SS	4.16±0.52	3.5
Deadwood	Ss/Sh	2.23	1.68	Do-SS	3.26±1.02	2.4

The calculated surface thermal conductivity (i.e., thermal conductivity void of the effects of temperature and pore fluids) of three formations (Mississippian, Duperow, and Ashern) were close to the values measured by Gosnold *et al.*, (2010, Table 4.1). The calculated in-situ thermal conductivities, were significantly lower than the measured thermal conductivities of the respective formations (0.4-0.8 $W \cdot m^{-1} \cdot °C^{-1}$).

In the case of the other four formations (Interlake, Red River, Winnipeg, Deadwood) there was a more significant difference between the thermal conductivities measured on the US side of the Williston Basin and the values used in this study (1.1- 2.4 $W \cdot m^{-1} \cdot °C^{-1}$).

The largest difference exists in the case of the Winnipeg-Black Island comparison. However, there is a lithological difference between the two investigated units (Winnipeg Formation is a mixture of sandstone and shale in the study area, while Gosnold *et al.,* (2010) reported the Black Island Member to be dolomite-sandstone).

The differences in thermal conductivity could be the result of the lateral variation of lithology within the formations in the Williston Basin. In addition to this the same formations are generally located deeper in the US portion of the basin due to the basement structure, thus some of the parameters influencing thermal conductivity are going to be different (e.g., lower porosity, higher temperature) resulting in different measured thermal conductivities.

The thermal conductivity values calculated for the study area are lower than those measured in the US portion of the Williston Basin. However, the range of values conforms previously determined values for these lithologies.

4.3.2 Heat generation

4.3.2.1 Sedimentary heat generation

Heat generated by the sediments has been estimated based on gamma ray logs in 10 wells. These wells were chosen based on the spatial distribution (to cover a large, representative area of the province, see Figure 4.12), the interval the log covered (i.e., wells covering most of the Phanerozoic strata were chosen) and availability of digital logs[27].

[27] Digital Well Database of Saskatchewan, http://www.dwd.gov.sk.ca/ [Last accessed: 2012.12.31]

Heat generation in the sediments of these wells varies between 0.01 $\mu W \cdot m^{-3}$ and over 10 $\mu W \cdot m^{-3}$. However, heat generation values over 10 $\mu W \cdot m^{-3}$ occur only in the upper and lower shale members of the Bakken Formation in the Devonian Three Forks Group, which Martiniuk (1988) described to be highly radioactive (also Figure 4.13).

Furthermore, heat generation in the Paleozoic strata is on average significantly lower than in the younger strata with the exception of the Devonian Three Forks Group. Heat generation becomes significant again in the Winnipeg, Deadwood formations corresponding to the lithological change from the younger Paleozoic carbonates, to the older Paleozoic shale and sandstones.

Table 4.2 Heat generated in the Phanerozoic sediments of selected wells. Crt/Qrt. - Cretaceous/Quarter, Undiff. - undifferentiated.

UWI	Top (m)	Bottom (m)	Top Formation	Bottom Formation	Estimated Heat Generation ($mW \cdot m^{-2}$)
141/10-10-002-15W2/0	322.00	2991.13	Crt/Qrt	Interlake	2.66
101/04-31-006-01W2/0	400.51	2492.65	Crt/Qrt	Deadwood	1.85
132/11-32-006-11W2/0	243.40	2824.70	Crt/Qrt	Precambrian	2.29
131/15-20-008-08W2/0	208.63	2588.63	Crt/Qrt	Deadwood	2.14
101/08-20-011-17W2/0	302.00	2569.80	Crt/Qrt	Precambrian	2.12
141/07-19-051-06W2/0	85.00	349.60	Undiff.	Precambrian	0.12
141/02-09-017-14W3/0	187.50	2070.70	Crt/Qrt	Deadwood	2.15
131/16-10-034-22W3/0	217.00	2023.80	Crt/Qrt	Precambrian	1.83
122/15-36-037-18W3/0	0.00	1918.40	Crt/Qrt	Precambrian	2.00
131/01-03-074-24W3/0	12.00	816.00	Crt/Qrt	Deadwood	0.52
122/15-36-037-18W3/0	0.00	1918.40	Crt/Qrt	Deadwood	2.00
131/01-03-074-24W3/0	12.00	816.00	Crt/Qrt	Deadwood	0.52

After calculating the total heat generation of the Phanerozoic sediments in the wells (Table 4.2), it can be determined, that the heat generated by the sedimentary strata is not a major contributor to the surface heat flow in Saskatchewan.

4.3.2.2 Basement heat generation

Heat generation at the top of the basement was also calculated from radioactive element concentration data measured on cores (Chapter 3.4) to see the potential contribution of the basement to the heat flow. Figure 4.14 depicts the heat generation values of the basement rocks. Values north from the Precambrian outcrop edge were also included for mapping (but not shown on Figure 4.14).

There has been only very few new data generated since the latest study of heat generation in the basement, thus the features of this current map and the map of Bachu and Burwash (1994) are very similar. One of the most prominent feature of the map is that the anomalies trend SW-NE.

There are two major positive anomalies on the map representing excessive basement heat generation. The northwestern anomaly (>6 $\mu W \cdot m^{-3}$, at T75-25W3) is probably related to the Edmonton anomaly detailed by Bachu and Burwash (1994). Also its area approximately corresponds to the area of the Virgin River Sheer Zone (e.g., Figure 5.1 in Burwash *et al.*, 1994).

The southwestern anomaly is located near Swift Current (heat generation >3 $\mu W \cdot m^{-3}$, between T7-23W3 and T17-16W3). It was previously tied to magmatic rocks enriched in uranium, thorium and potassium, which are considered to be the source rocks for the helium commercially produced in the area (Burwash and Cumming, 1976). Its northeast portion (T15-17W3) has significantly higher heat generation than its southeast portion (T6-22W3). Furthermore, its area coincides with a basement block inferred to be separated from the remainder of the basement by faults (see Figure 5.1 in Burwash *et al.*, 1994).

A low generation (<2 $\mu W \cdot m^{-3}$) anomaly covers a large area extending from Township T40-28W3 towards T68-15W2 (Figure 4.14).

However, the lowest heat generation values do not occur in this part of the basin, but in the extreme southwest, along the Alberta border (<1 $\mu W \cdot m^{-3}$, T1-30W3 and

T18-29W3). These low values could be related to the low heat generation of the northern extension of the ancient Wyoming craton (Bachu and Burwash, 1994).

A third low basement heat generation anomaly is located in the Weyburn-Estevan area substantiated by a single point (<1 $\mu W \cdot m^{-3}$, T8-8W2). However, its areal extent is more restricted than in the work of Bachu and Burwash (1994). A data point just off the border in Manitoba (T37-28W1) constrains the low generation anomaly from the north.

The general southwest-northeast trend of structural features (Figure 5.1 of Burwash *et al.,* 1994) is similar to the trend observed on the basement heat generation map. This indicates that structural movement along the regional faults may have influenced the distribution of radioactive elements of basement rocks.

Thus, basement heat flow, based on the calculated values might be a significant contributor to heat flow in the Swift Current area, where it coincides in area with a previously identified geothermal high.

4.3.3 Heat flow

Integral heat flow

Integral heat flow (Figure 4.15) varies on the range of 38- 76 $mW \cdot m^{-2}$. An average heat flow of 50- 60 $mW \cdot m^{-2}$ covers most of Saskatchewan. Lower than average heat flows are located mostly in the southwest. Especially low values coincide with cold temperature (and geothermal gradient) anomalies: i.e., heat flow values considerably less than 50 $mW \cdot m^{-2}$ exist at Saskatoon, south of it (T27-1W3), in the west along the Alberta border (T25-29W3 to T35-28W3), and between T1-30W2 and T9-22W2. The area south-southwest of Swift Current also has slightly lower heat flow than 50 $mW \cdot m^{-2}$ (i.e., 48.5 $mW \cdot m^{-2}$ 10-25-003-27W3; 46.2 $mW \cdot m^{-2}$ 11-20-013-13W3).

Highest heat flow values of the study area are located in the northeast (T65-9W2), and in the eastern part of the province next to the Manitoba border (T25-30W1 to

T35-32W1). A continuous high heat flow trend is present between these two high regions (Figure 4.15). Higher than average heat flow values (>60 $mW \cdot m^{-2}$) coincide with areas of high temperature anomalies near Swift Current and east of Estevan but are much more constrained in space. High heat flows were also identified southeast and southwest of Saskatoon (T30-28W2, T32-8W3), and northwest of North Battleford (T62-25W3).

No high heat flow anomaly (>100 $mW \cdot m^{-2}$) was identified west and southwest of Weyburn, where Majorowicz *et al.*, (1986) previously identified one to exist. This can be explained by the use of shale thermal conductivity values for estimating thermal conductivity measured in more recent studies (e.g., Gosnold, 1990).

Heat flow is constant vertically in a purely conductive case, if no heat sources or sinks are present. However, vertical heat flow differences were observed previously in the WCSB. Therefore an analysis of the heat flow in the sub-Mesozoic, and in the Cenozoic-Mesozoic strata had to be undertaken, to test these previous observations with the new data.

Heat flow in the Cenozoic-Mesozoic strata

The heat flow in the Cenozoic-Mesozoic (Figure 4.16) strata varies on the same range as the heat flow calculated for the integral rock package, i.e., 34 and 76 $mW \cdot m^{-2}$. However, the values less than 50 $mW \cdot m^{-2}$ are more prevalent, covering more than half of the study area. Lowest heat flow values (<40 $mW \cdot m^{-2}$) are located near Saskatoon (T37-3W3), west of it along the Alberta border (T20-29W3 and T40-28W3), and west of Estevan (T4-21W2). Higher values are constricted in the southeast (Estevan-Weyburn area, delineated by T1-8W2, T1-15W2, T12-15W2 and T12-8W2, and between Regina and Moose Jaw, T17-19W2 to T15-26W2), southwest (near Swift Current, T18-10W3- T18-14W3), and in the northern half of the province.

Heat flow in the Paleozoic strata

Heat flow in the Paleozoic layers (Figure 4.17) is higher than the heat flow calculated for the other two intervals. Lower heat flows (<50 $mW \cdot m^{-2}$) are restricted to the areas at Saskatoon (T37-3W3), west of it, along the Alberta border (T35-28W3 to T45-27W3), and west of Estevan (T2-20W2 to T18-20W2). These areas coincide with areas, where low temperature anomalies have been identified on the previously analysed set of temperature maps. Two smaller high anomalies are present in the southwest, near Swift Current (T18-14W3), and in the southeast, just north of Estevan (T4-7W2) also corresponding to the previously identified temperature anomalies.

However, several heat flow anomalies were determined in areas were temperature anomalies could not be observed: Two low (T66-13W3, and T10-32W1) and several high heat flow anomalies (>70 $mW \cdot m^{-2}$, T30-28W2, T32-8W3, and T65-9W2) were not indicated previously by temperature maps.

Match with previous measurement

Jessop and Vigrass (1989) calculated heat flow for the University of Regina well based on measured thermal conductivity and high precision temperature logs. This is the only heat flow determination in the Phanerozoic strata of the province, which can be used as a constraint of the current calculations. They determined heat flow in the Regina well to be 51 $mW \cdot m^{-2}$. The heat flows calculated in this study for the entire sedimentary package (49 $mW \cdot m^{-2}$) and for the Cenozoic-Mesozoic interval (54 $mW \cdot m^{-2}$) are close to those values calculated by Jessop and Vigrass (1989).

A few published heat flow and thermal conductivity values are also available at the northeast edge of the study area (Table 4.3). The published and the calculated geothermal gradient and thermal conductivity values were compared.

Previously published uncorrected heat flow values and those calculated in this study show a very good match for three out of the four sites. Significant discrepancy (>5 $mW \cdot m^{-2}$) between the calculated uncorrected heat flow values exists only in the case of the McIlvenna Bay wells. The published corrected heat flow values are more different from those determined in this study. However, this larger discrepancy is explained by applying a different, more recent paleoclimatic correction in this study (the correction of Majorowicz and Wybraniec, 2011).

Table 4.3 Heat flow in the northern wells - comparison of previously published values and those calculated in this study (References: a- Rolandone *et al.*, 2004; b- Guillo-Frottier *et al.*, 1996). *dT/d**d*** is geothermal gradient, *k* is thermal conductivity, $Q_{uncorrected}$ is heat flow before correcting for the paleoclimatic effects, while $Q_{corrected}$ is heat flow after correction for the paleoclimatic effects. Rolandone *et al.*, (2004) determined 60 $mW \cdot m^{-2}$ as pre-correction heat flow for the Bigstone Lake site from the deep data of Bigstone Lake B. However, using his values an uncorrected heat flow of 71.24 $mW \cdot m^{-2}$ can be calculated for Bigstone Lake A.

This study	*dT/d**d*** ($°C \cdot km^{-1}$)	$k_{In\text{-}situ}$ ($W \cdot m^{-1} \cdot {}^{o}C^{-1}$)	$Q_{Uncorrected}$ ($mW \cdot m^{-2}$)	$Q_{Corrected}$ ($mW \cdot m^{-2}$)	Reference
Bigstone Lake A	19.4	3.45	67.00	81.25	a
Bigstone Lake B	17	3.39	57.69	70.85	a
McIlvenna Bay A	16.7	2.83	47.18	59.11	a
McIlvenna Bay B	15.3	3.13	47.88	60.68	a
Reed Lake	14.4	2.64	37.96	51.69	b
Suggi Lake	14.9	3.20	47.62	61.36	a
Published values	*dT/d**d*** ($°C \cdot km^{-1}$)	*k* ($W \cdot m^{-1} \cdot {}^{o}C^{-1}$)	$Q_{Uncorrected}$ ($mW \cdot m^{-2}$)	$Q_{Corrected}$ ($mW \cdot m^{-2}$)	Reference
Bigstone Lake A	19.9	3.58	*71.24*		a
Bigstone Lake B	17.4	3.45	60	63.3	a
McIlvenna Bay A	15.7	2.49	39.2	41.9	a
McIlvenna Bay B	14.6	2.49	36.5	39.8	a
Reed Lake	13.7	2.74	37.8	40	b
Suggi Lake	14.1	3.31	46.7	53.7	a

Rolandone *et al.*, (2004) do not specify the interval for determining the thermal conductivity of the McIlvenna Bay wells. However, using the published values[28] for determining the thermal conductivity of total length of these wells results in higher thermal conductivities than those published. Therefore, the values

[28] Published by Jessop *et al.*, (2005).

calculated here are retained for consistency. The good match between the published heat flow values and the values determined in this study supports that the values determined in this study are reliable.

Vertical heat flow difference

Although the previous paragraphs provide a description of the Cenozoic-Mesozoic and the Paleozoic heat flows, the potential vertical difference in heat flow is not obvious. In order to enhance the visibility of the differences between the two intervals, a heat flow difference map was also produced (Figure 4.18). On this map the Cenozoic-Mesozoic heat flow was subtracted from the Paleozoic heat flow wherever both are available:

$$\Delta Q = Q_{pz} - Q_{mz} \quad (11)$$

where Q_{pz} and Q_{mz} are Paleozoic and Mesozoic heat flows respectively. The differences were plotted (similar to the map of Majorowicz *et al.*, 1986). Previously maps similar to this difference map were one of the qualitative arguments used to prove the significance of regional groundwater flow in the determination of the geothermal regime.

This map (Figure 4.18) shows that heat flow in the Paleozoic strata is almost everywhere significantly higher (>10 $mW \cdot m^{-2}$) than heat flow in the Mesozoic and Cenozoic strata. However, no significant, systematic heat flow difference exist in the potential recharge area (i.e., in the Cypress Hills), and the discharge areas (along the basin outcrop edge) between the shallow and the deep layers, as the difference in these areas is mostly less than 5 $mW \cdot m^{-2}$. Thus, the previous theory that groundwater flow is responsible for the basin wide redistribution of heat is not supported by this work (Figure 4.5 and Figure 4.18).

Paleozoic heat flow is systematically higher in this study than Cenozoic-Mesozoic heat flow (Figure 4.18) in almost all of Saskatchewan. Thermal conductivity could be potentially responsible for this bias. The heat flow difference map

(Figure 4.18) suggests that the thermal conductivity calculated for the Paleozoic strata are too high.

However, the opposite conclusions were drawn from comparing the calculated formation thermal conductivities to the data measured in North Dakota and Manitoba (Chapter 4.3.1), i.e., the thermal conductivities were found to be too low. Also, the calculated Paleozoic heat flow in Regina (37.4 $mW \cdot m^{-2}$) is much lower than the heat flow of Jessop and Vigrass (1989). This also suggests that thermal conductivities estimated for the Paleozoic strata are too low. In order to resolve this controversy, actual thermal conductivity measurements in Saskatchewan are required.

Thus, it cannot be answered without further measurements, what is the reason that heat flow is higher in a large area in the Paleozoic strata than in the Cenozoic-Mesozoic strata. However, heat flow maps show the same trends as temperature and geothermal gradient maps and high and low heat flow areas coincide with temperature anomalies (e.g., highs near Swift Current and in the southeast, lows west of Estevan, near Saskatoon, or west of it, along the border with Alberta).

Horizontal and vertical temperature distribution in the subsurface of Saskatchewan were described in this chapter based on the temperature and geothermal gradient maps. Several anomalous regions were identified, where temperature is warmer, or relatively colder than in the adjacent areas. Although thermal conductivity, heat generation and heat flow patterns were also described individually, no attempt was made in this chapter to explain the existence of the anomalous regions. Therefore, the next chapter will attempt to interpret the observed patterns.

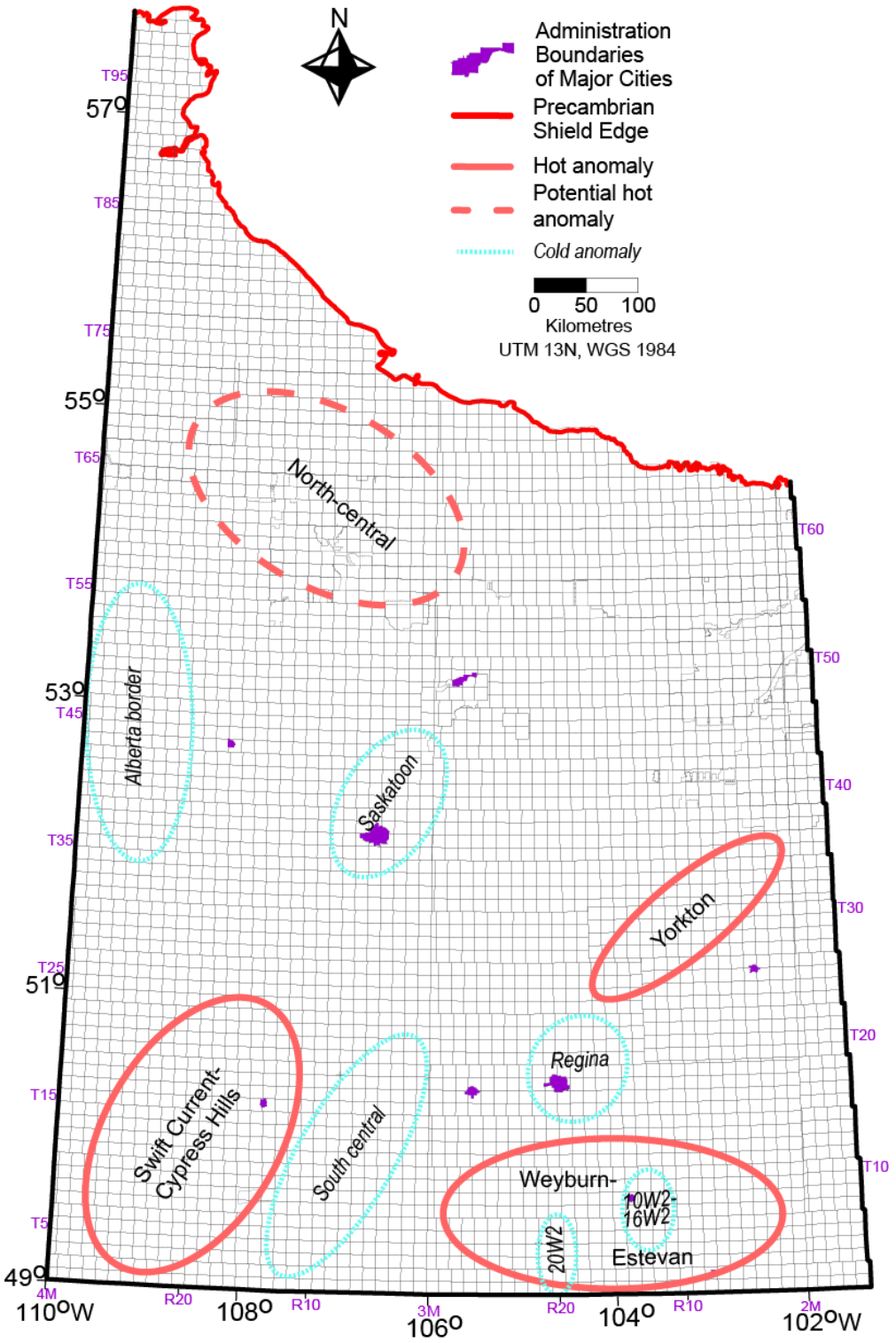

Figure 4.1 Map of the study area with the approximate locations of the identified anomalies, relatively colder/warmer than their surroundings. R, M, T marks location (Range, Meridian, Township) defined in the Dominion Land Survey system (in the grid).

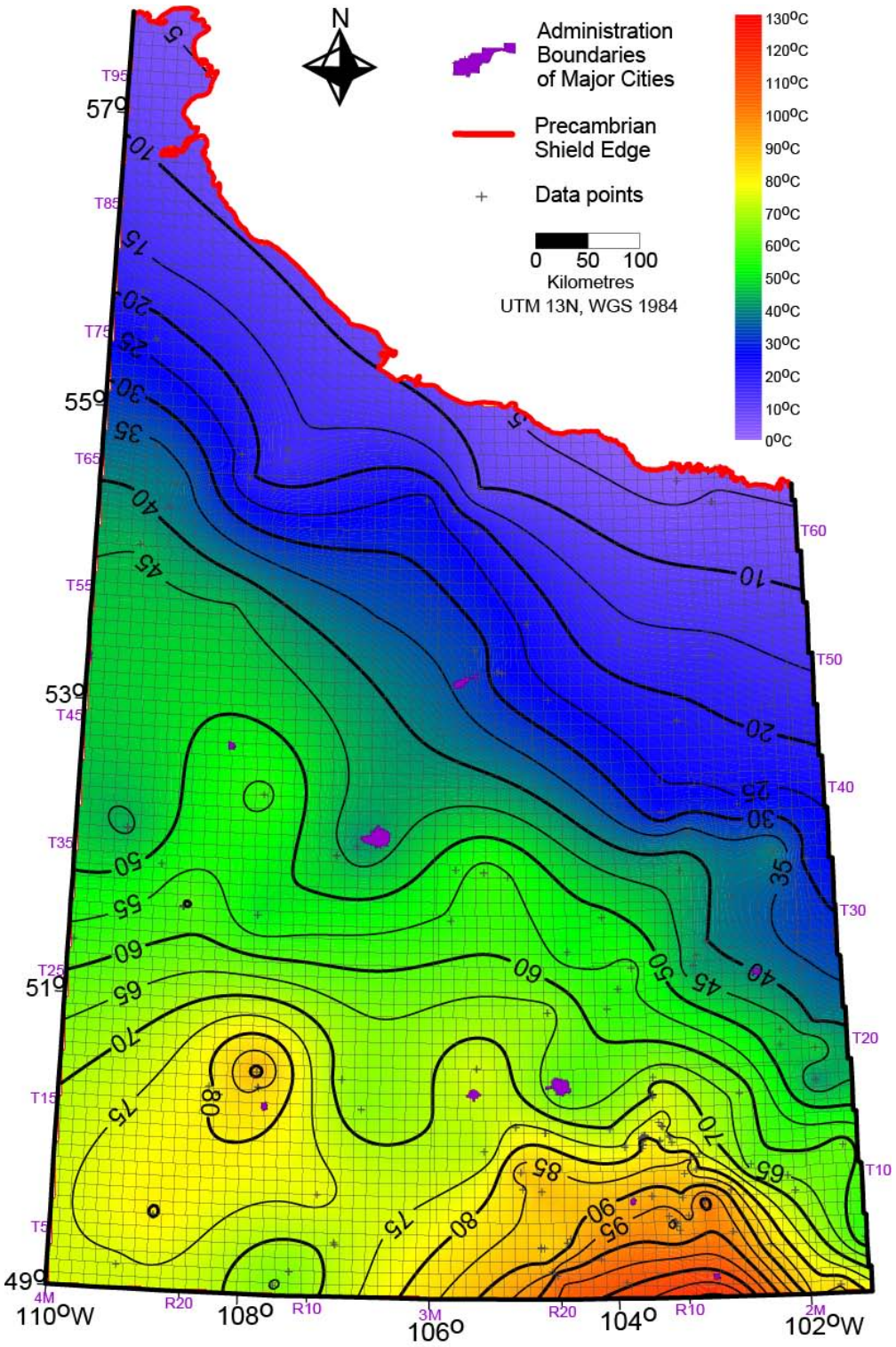

Figure 4.2 Precambrian temperature map. Contour interval (CI): 5 °C.

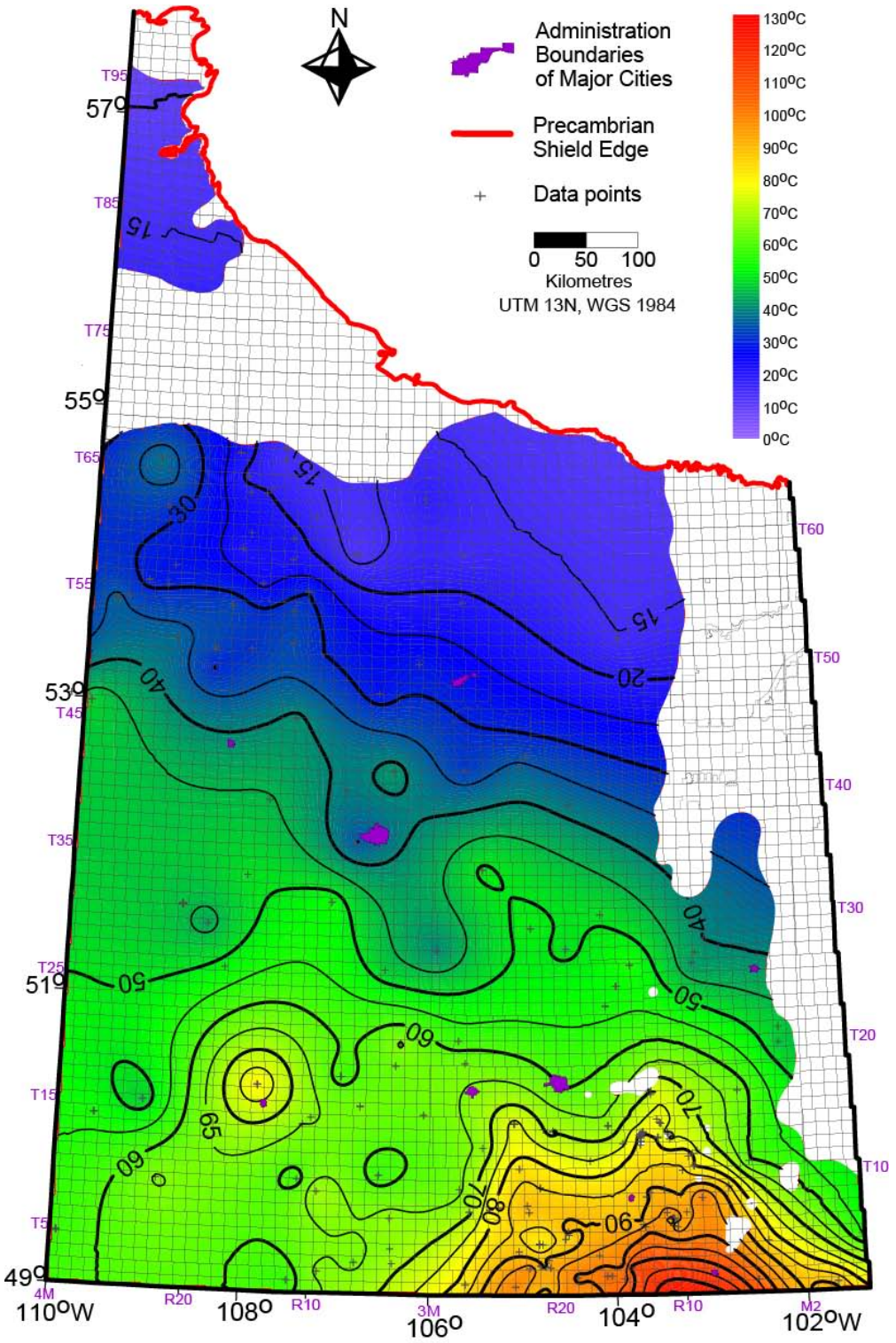

Figure 4.3 Deadwood temperature map. CI: 5 °C. Blank areas represent areas where the formation is not present.

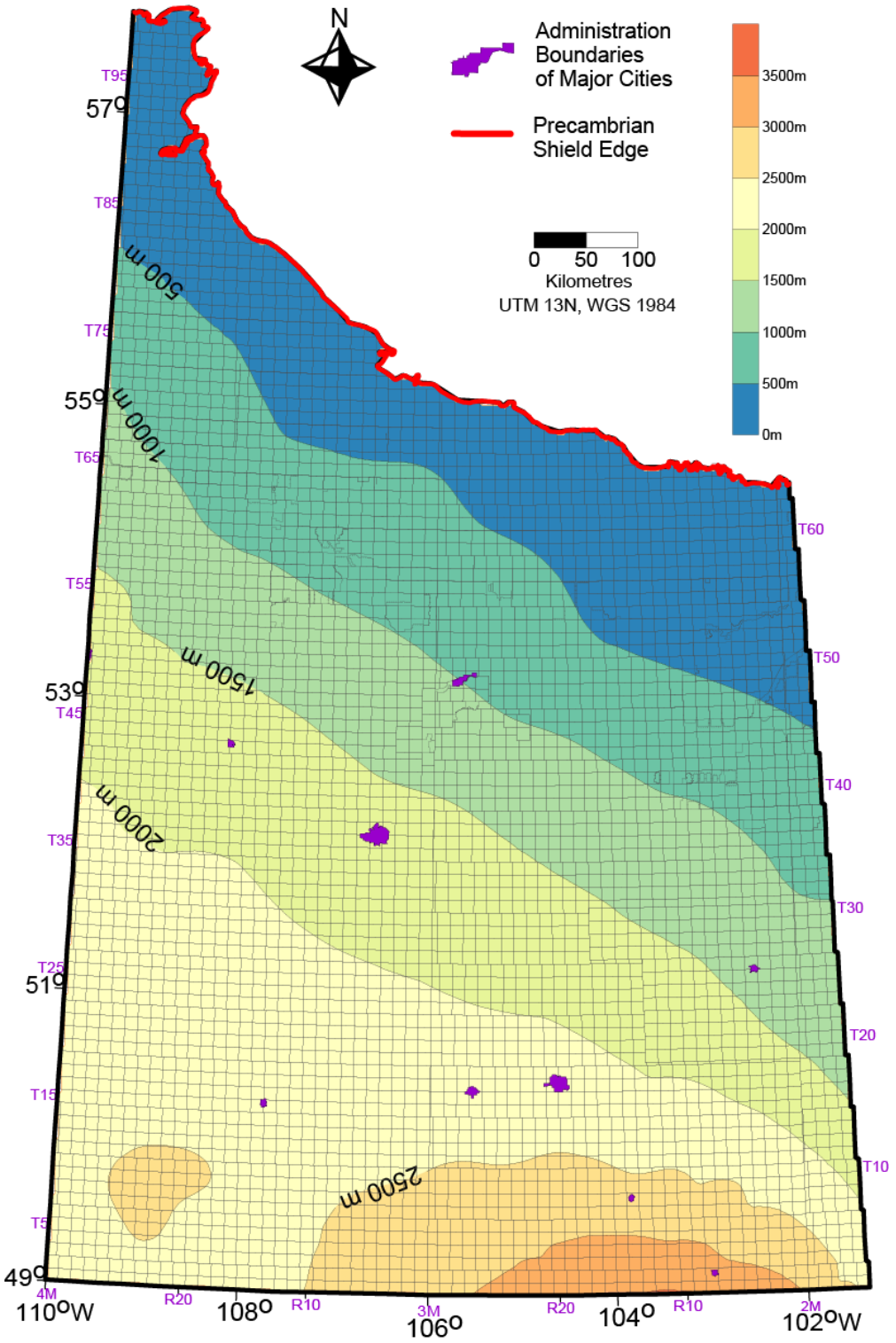

Figure 4.4 Precambrian basement depth map (from Marsh and Love, 2013). R, M, T marks location (Range, Meridian, Township) defined in the Dominion Land Survey system (in the grid).

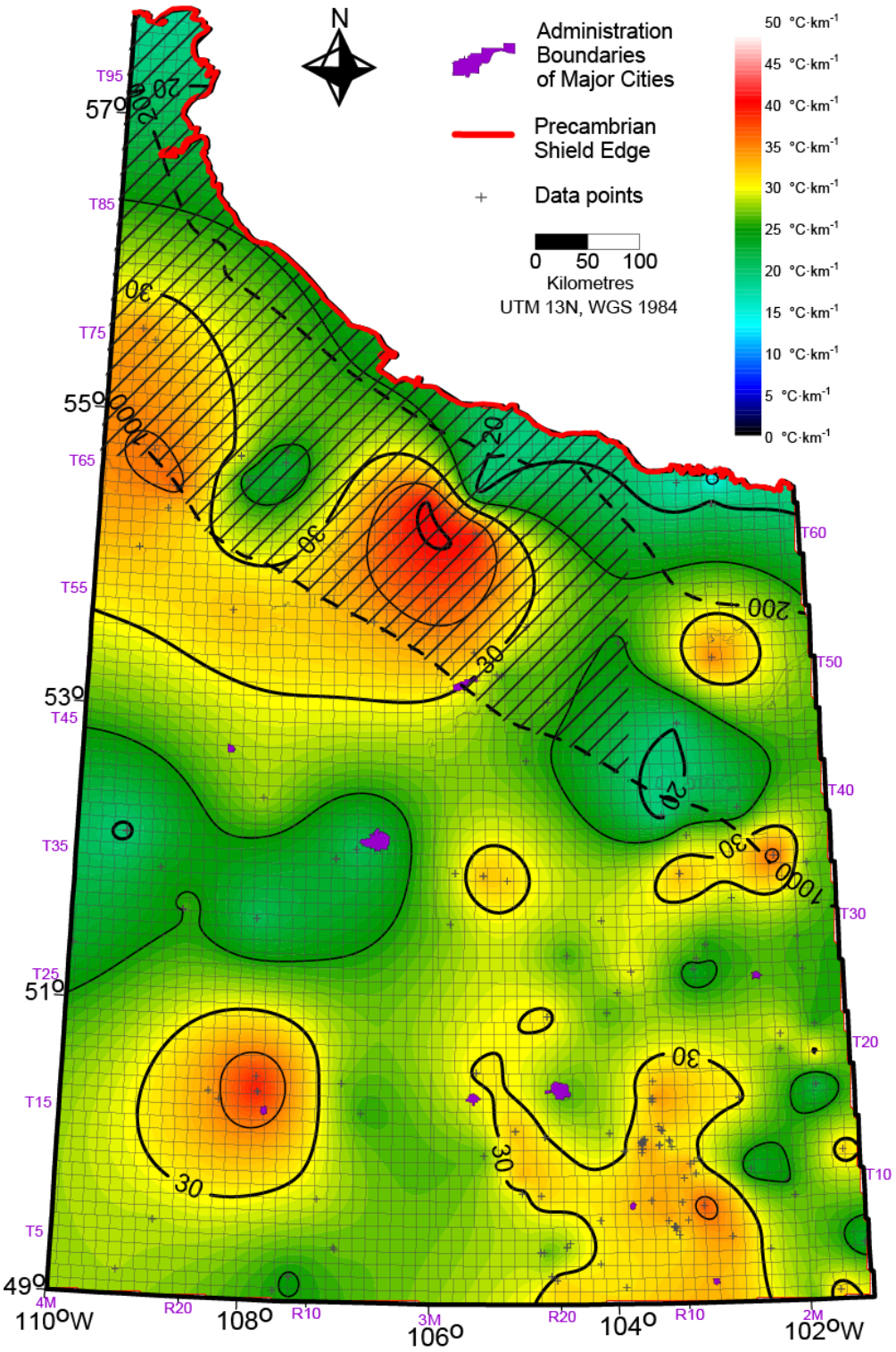

Figure 4.5 Integral geothermal gradient map. CI: 5 °C·km^{-1}. Hatched area identifies shallow region supported by few, Quality B measurements.

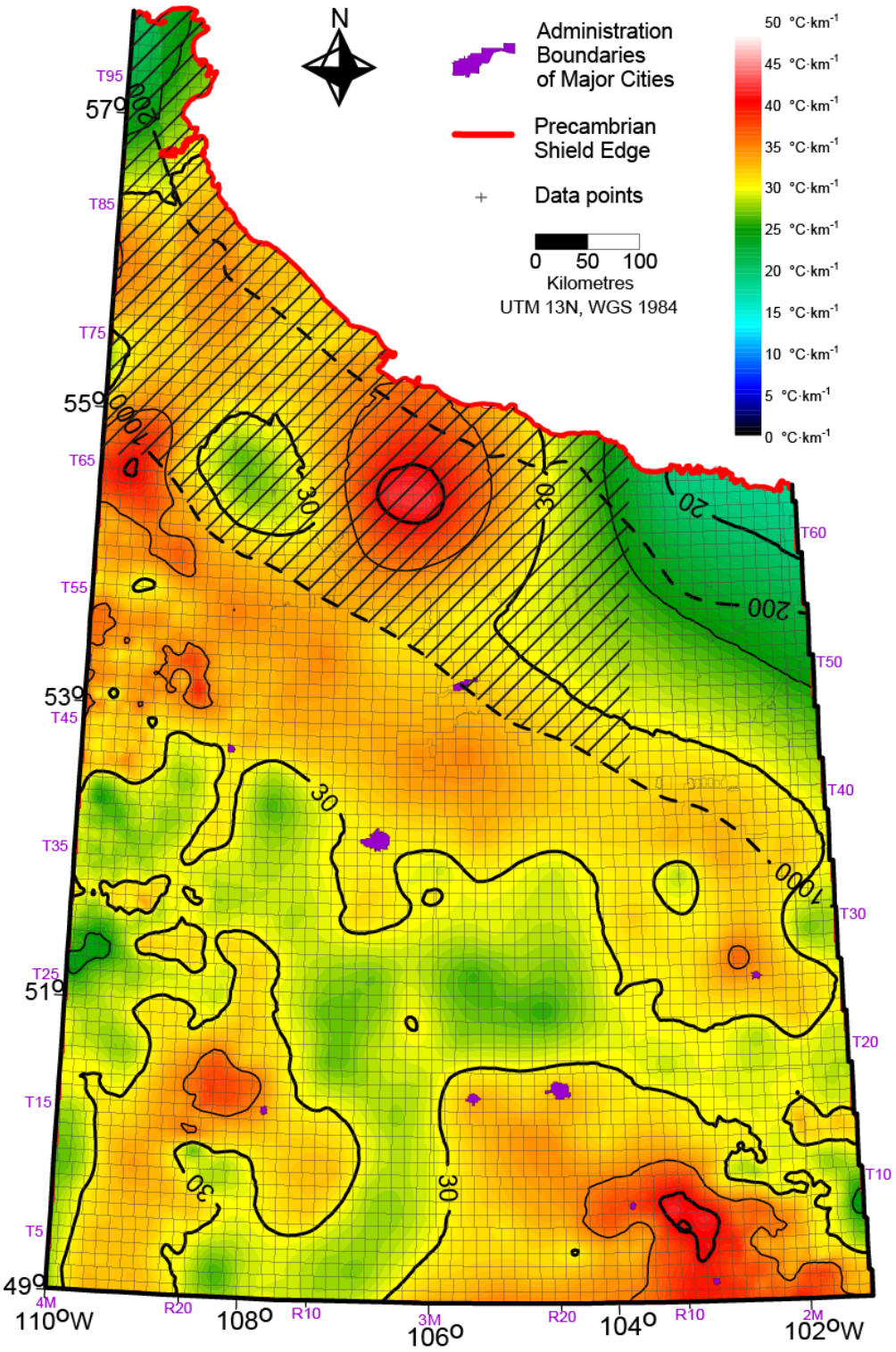

Figure 4.6 Mesozoic-Cenozoic interval geothermal gradient map. Data distribution is the same as A.13.b. CI: 5 °C·km^{-1}. Nugget effect: 1 (°C)^2·km^{-2}. Hatched area identifies shallow region supported by few, Quality B measurements.

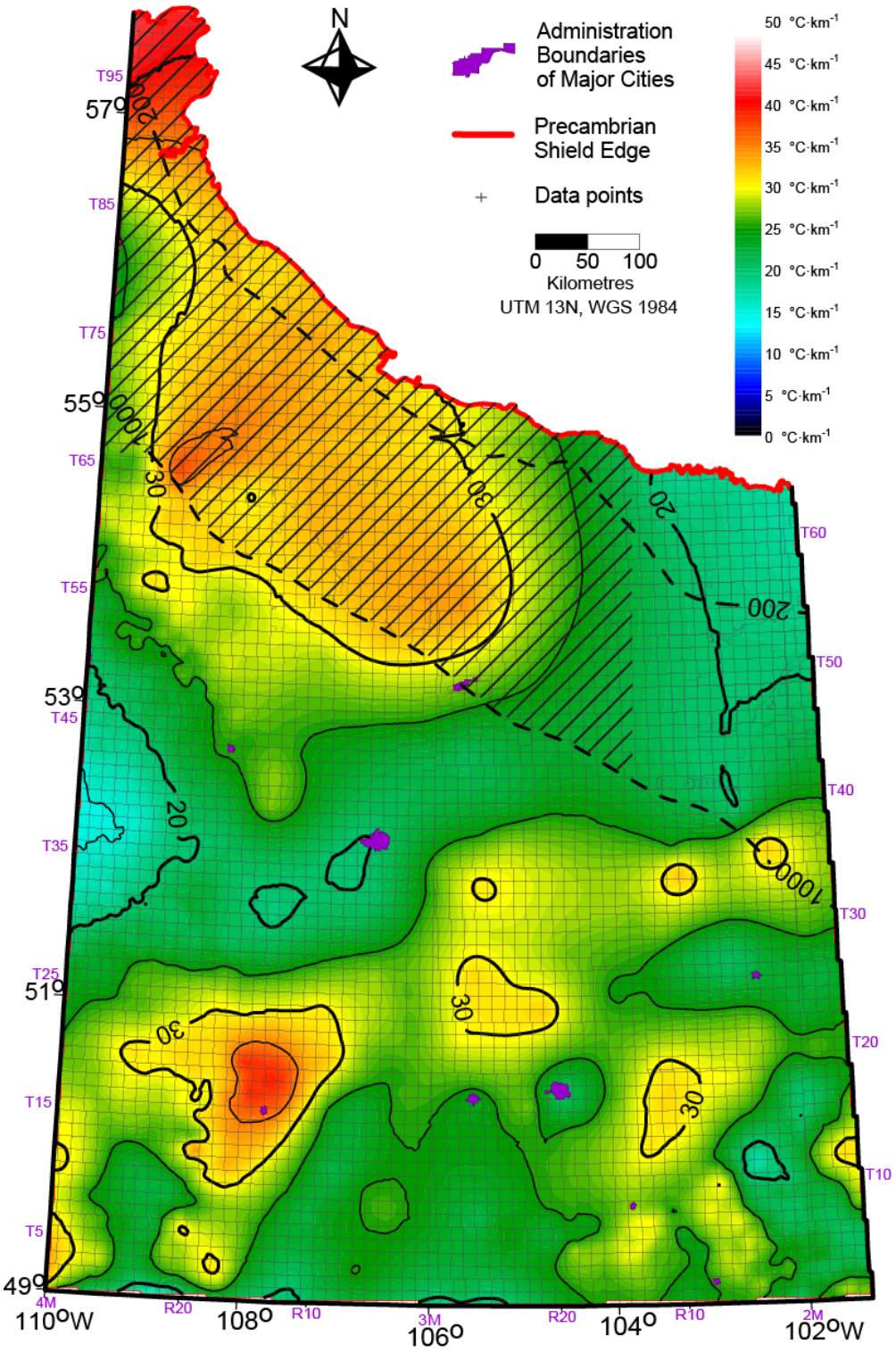

Figure 4.7 Paleozoic interval geothermal gradient map. Data distribution is the same as A.13.b. CI: 5 °C·km^{-1}.Nugget effect: 1 (°C)^2·km^{-2}. Hatched area identifies shallow region supported by few, Quality B measurements.

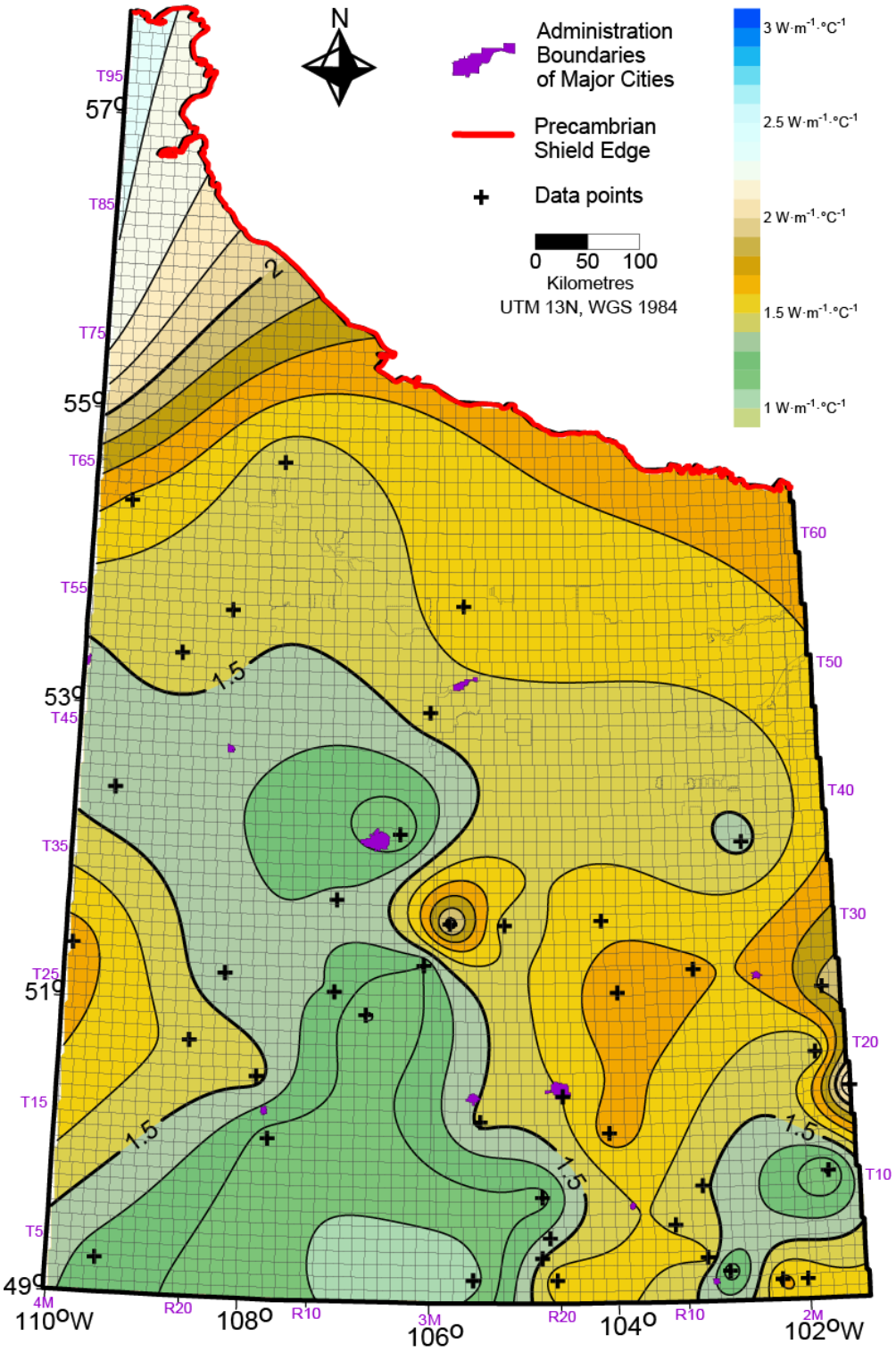

Figure 4.8 Integral thermal conductivity map. CI: 0.1 $W \cdot m^{-1} \cdot °C^{-1}$.

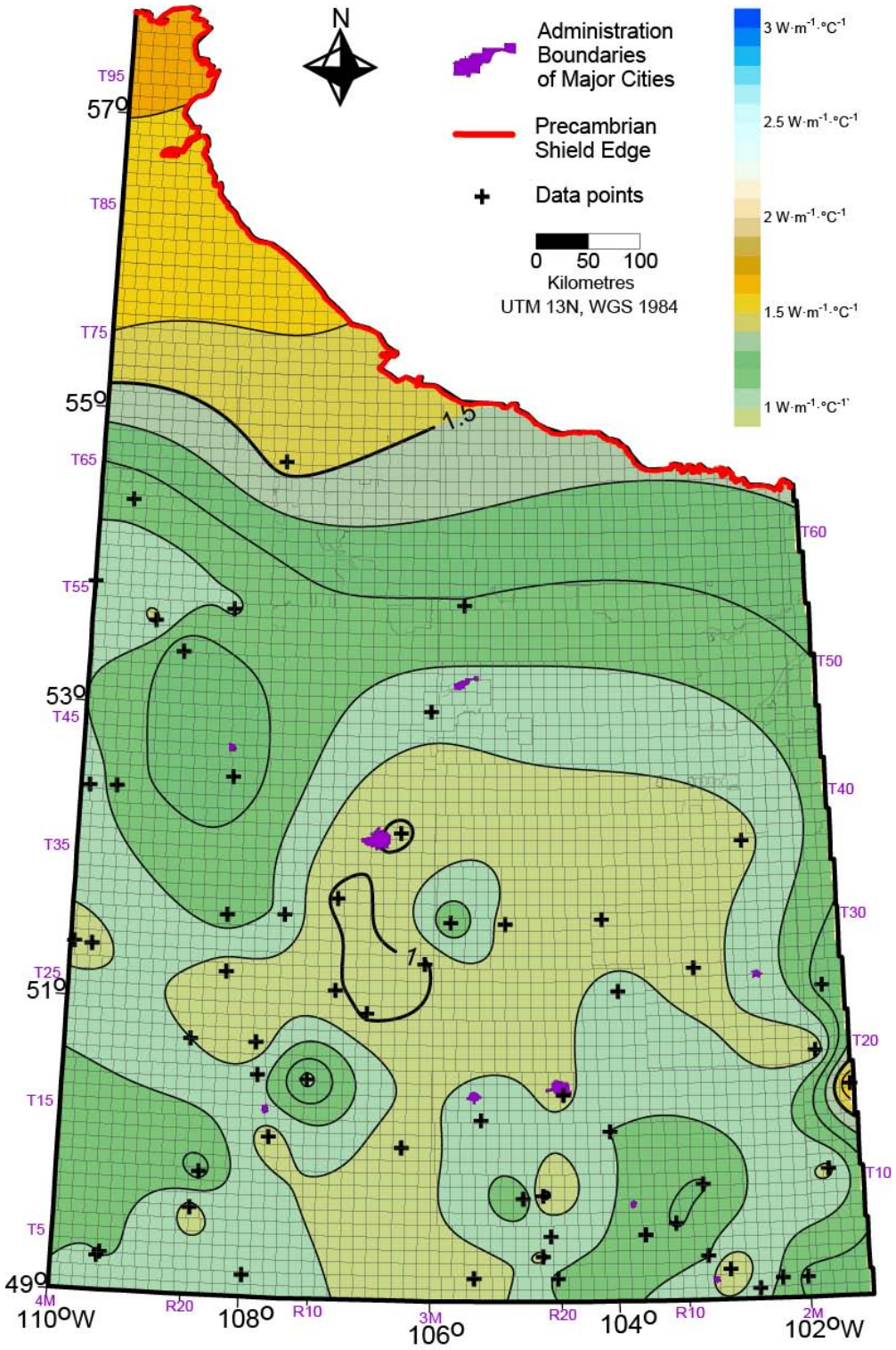

Figure 4.9 Mesozoic-Cenozoic interval thermal conductivity map. CI: 0.1 $W \cdot m^{-1} \cdot °C^{-1}$.

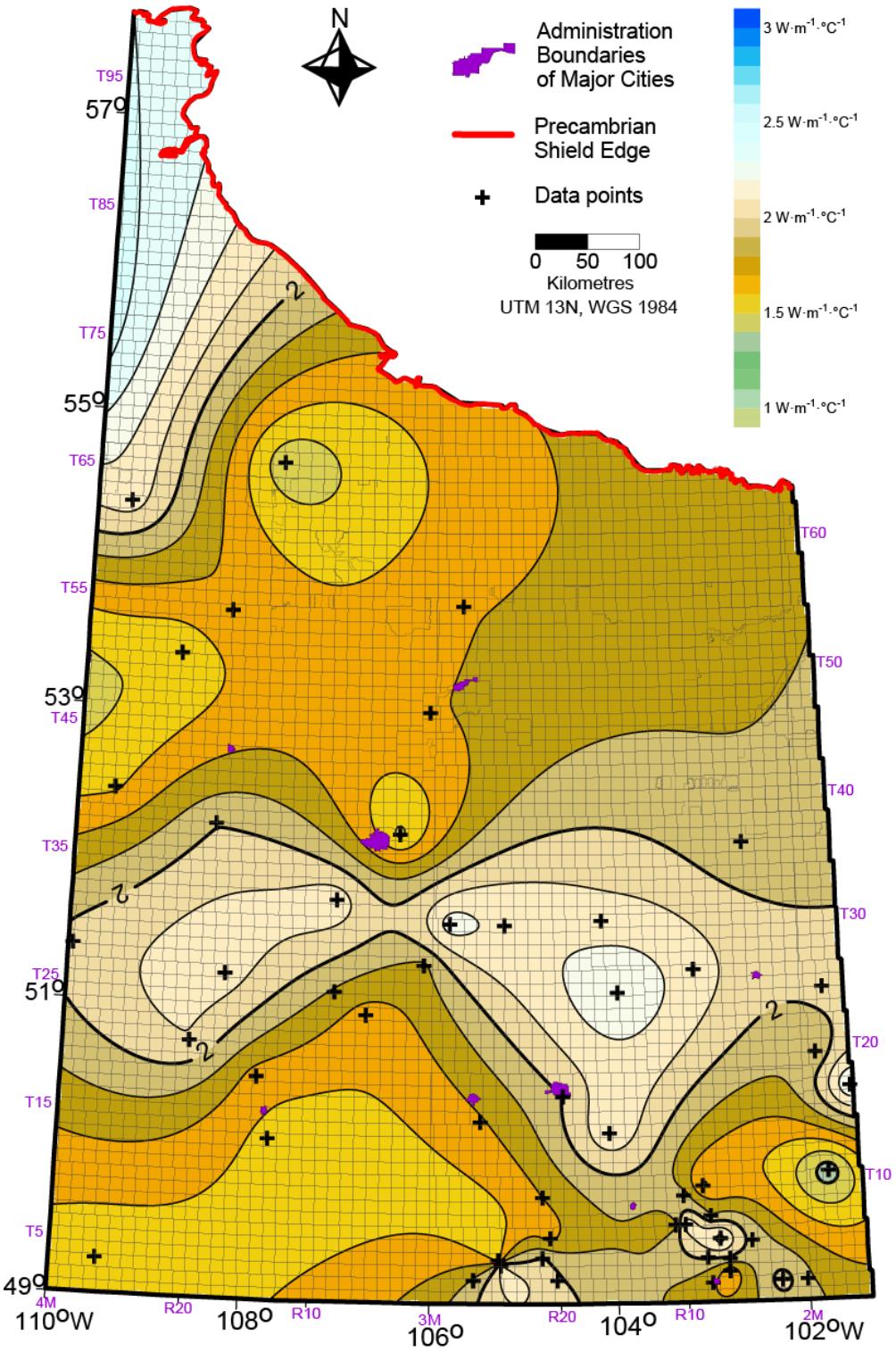

Figure 4.10 Paleozoic interval thermal conductivity map. CI: 0.1 $W \cdot m^{-1} \cdot °C^{-1}$.

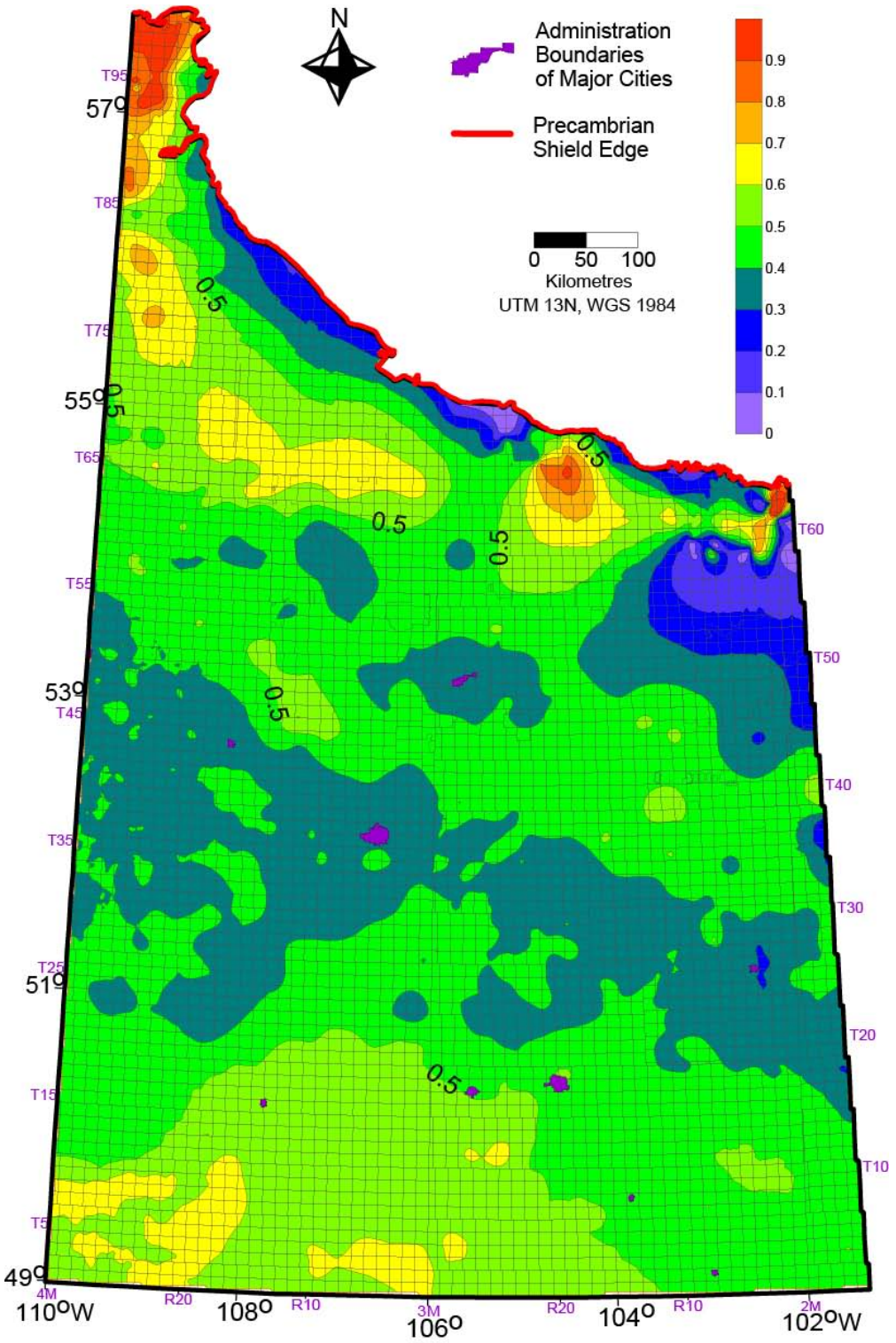

Figure 4.11 Illustration of the ratio of the thickness of the Cenozoic-Mesozoic strata to the entire thickness of the Phanerozoic sediments. CI: 0.1.

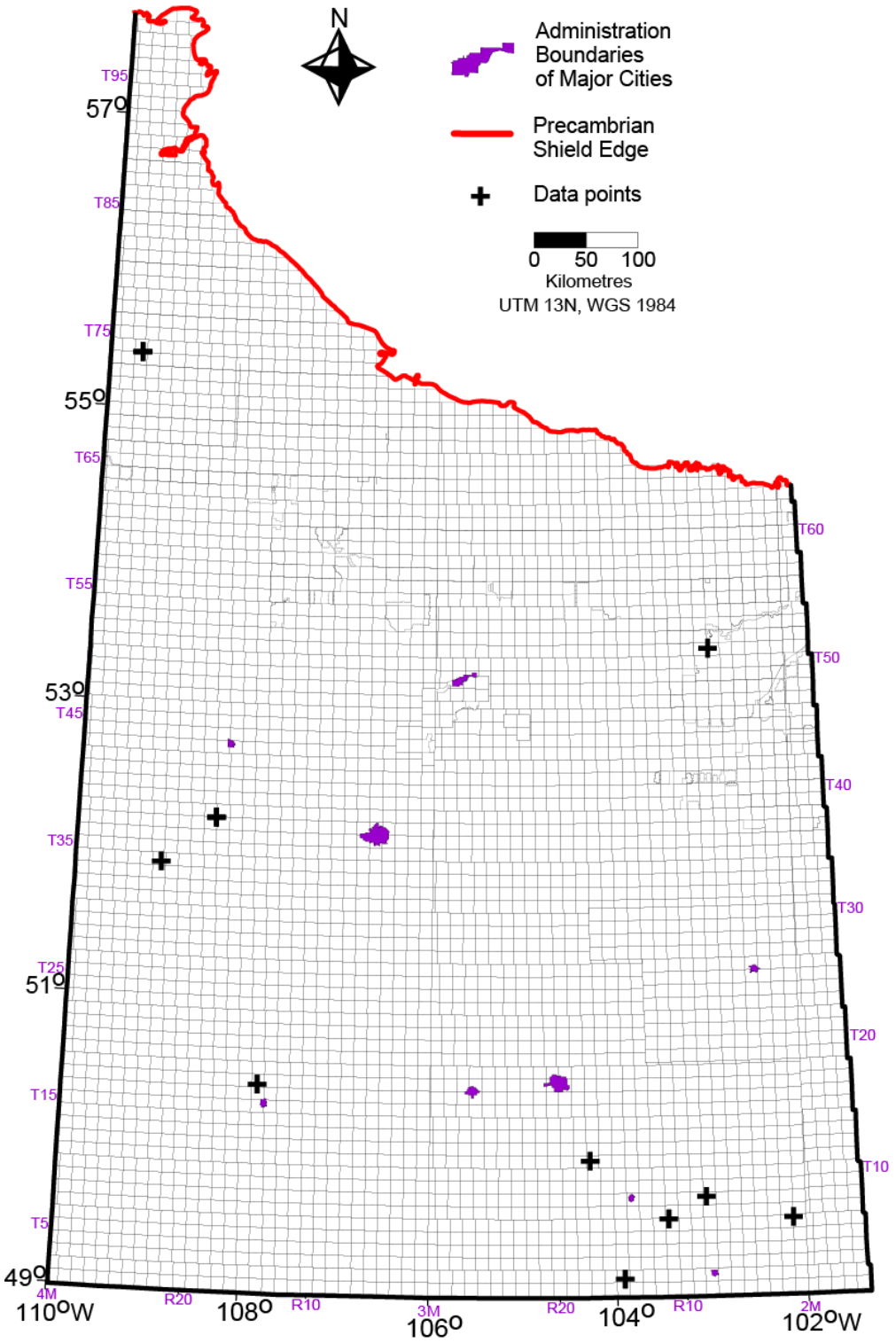

Figure 4.12 Distribution of wells with sedimentary heat generation estimates.

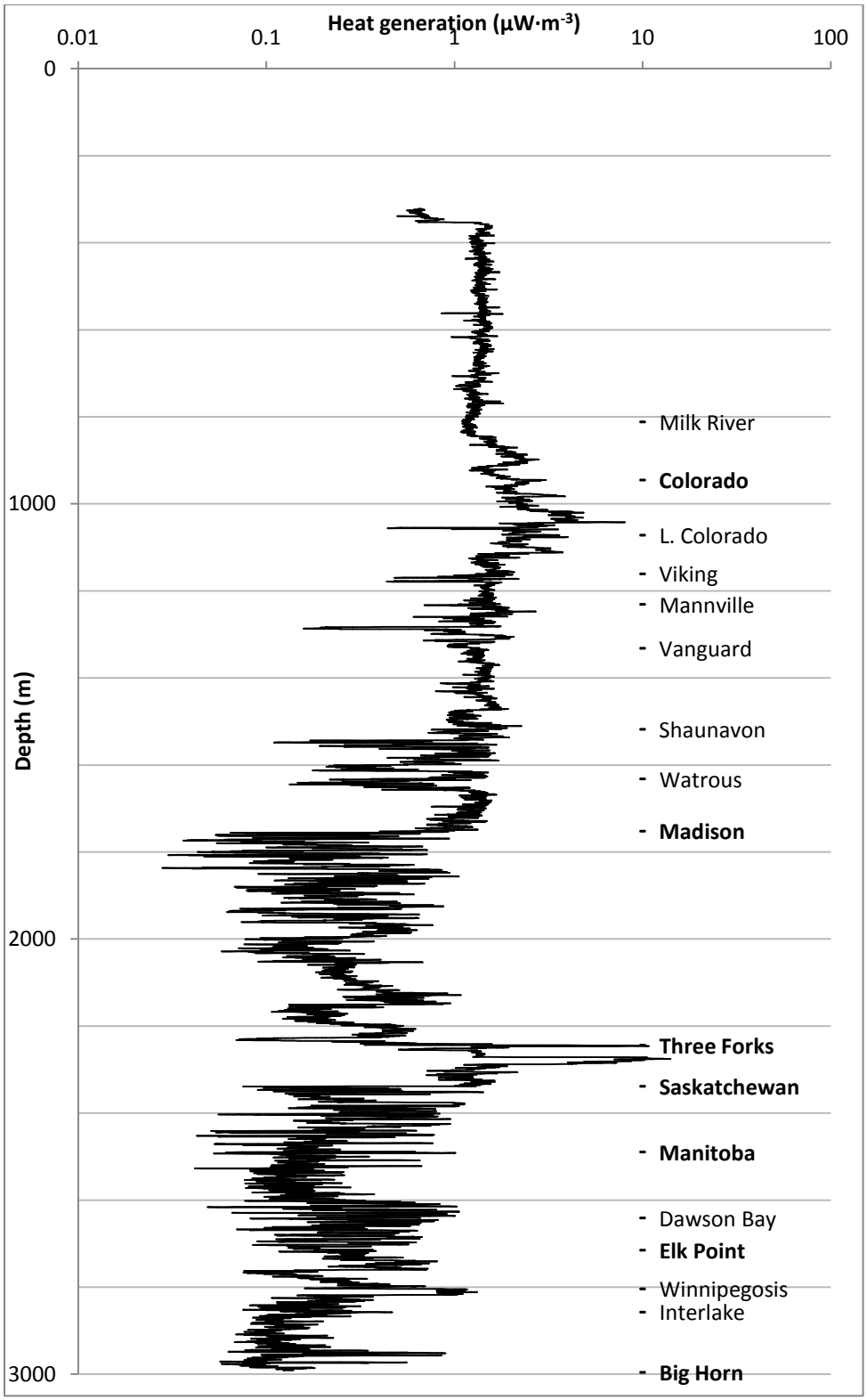

Figure 4.13 An example heat generation log for well: 141/10-10-002-15W2/0.

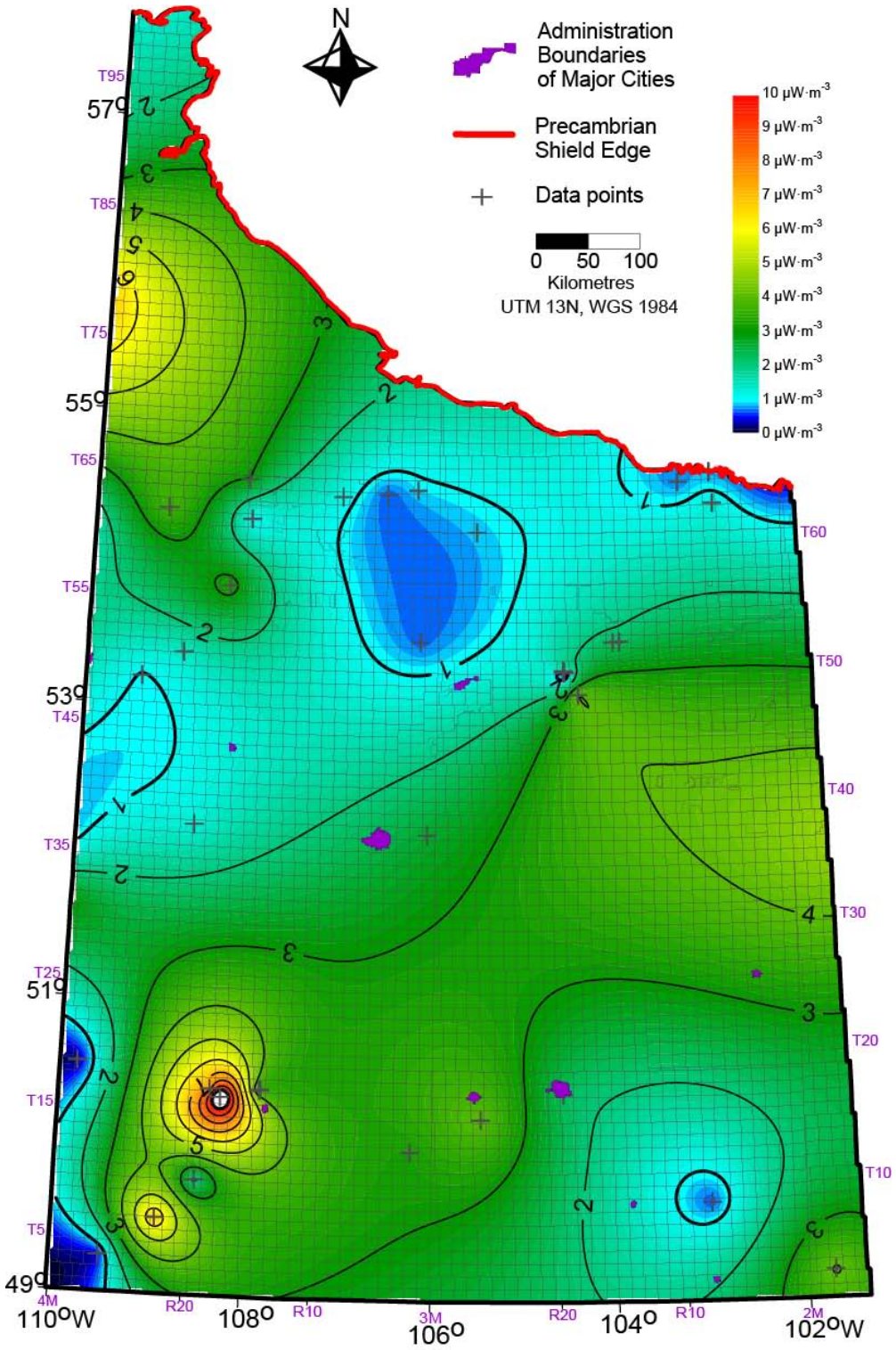

Figure 4.14 Top of basement heat generation map. CI: 1 μW·m^{-3}.

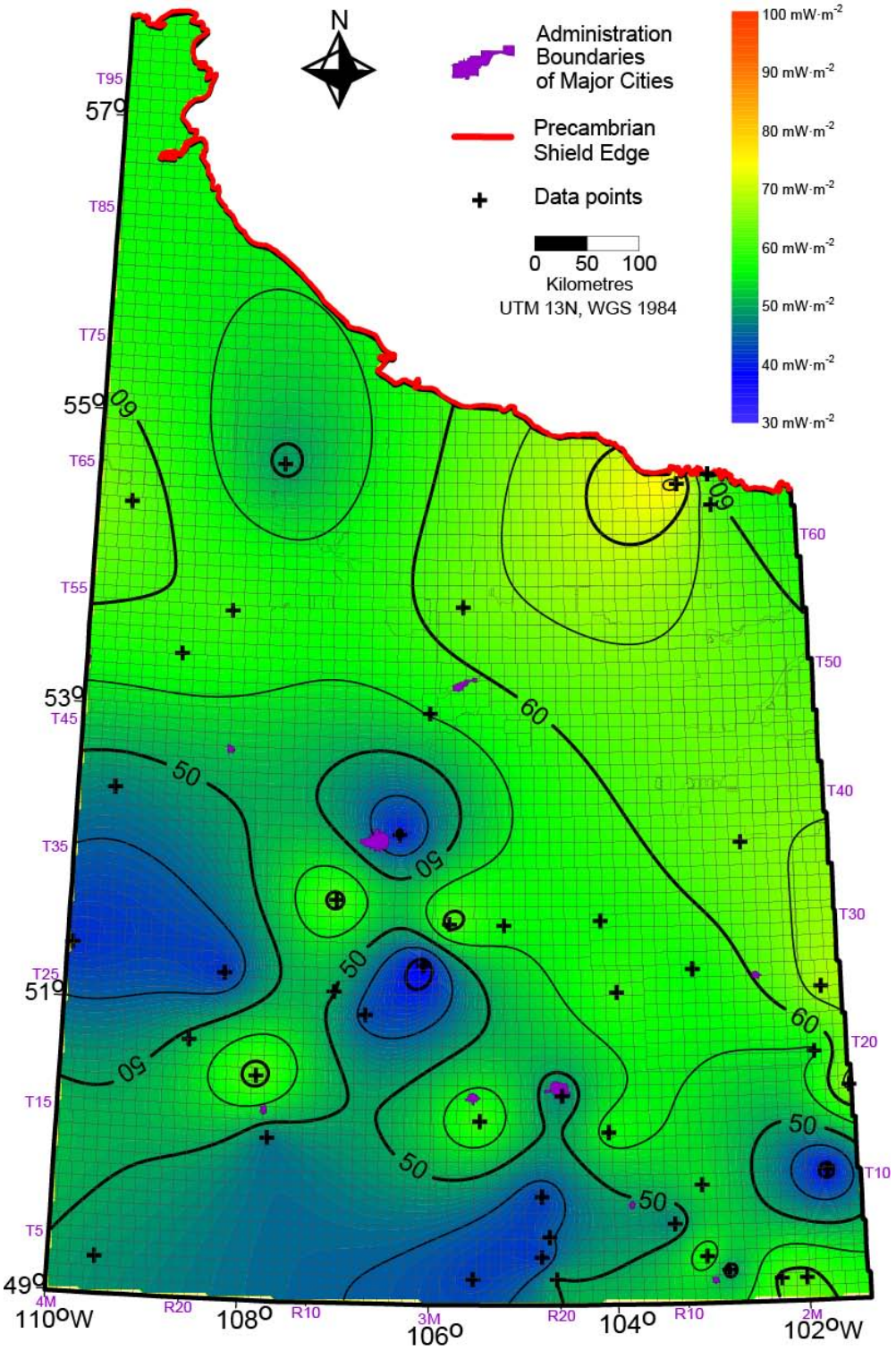

Figure 4.15 Integral heat flow map. CI: 5 mW·m^{-2}.

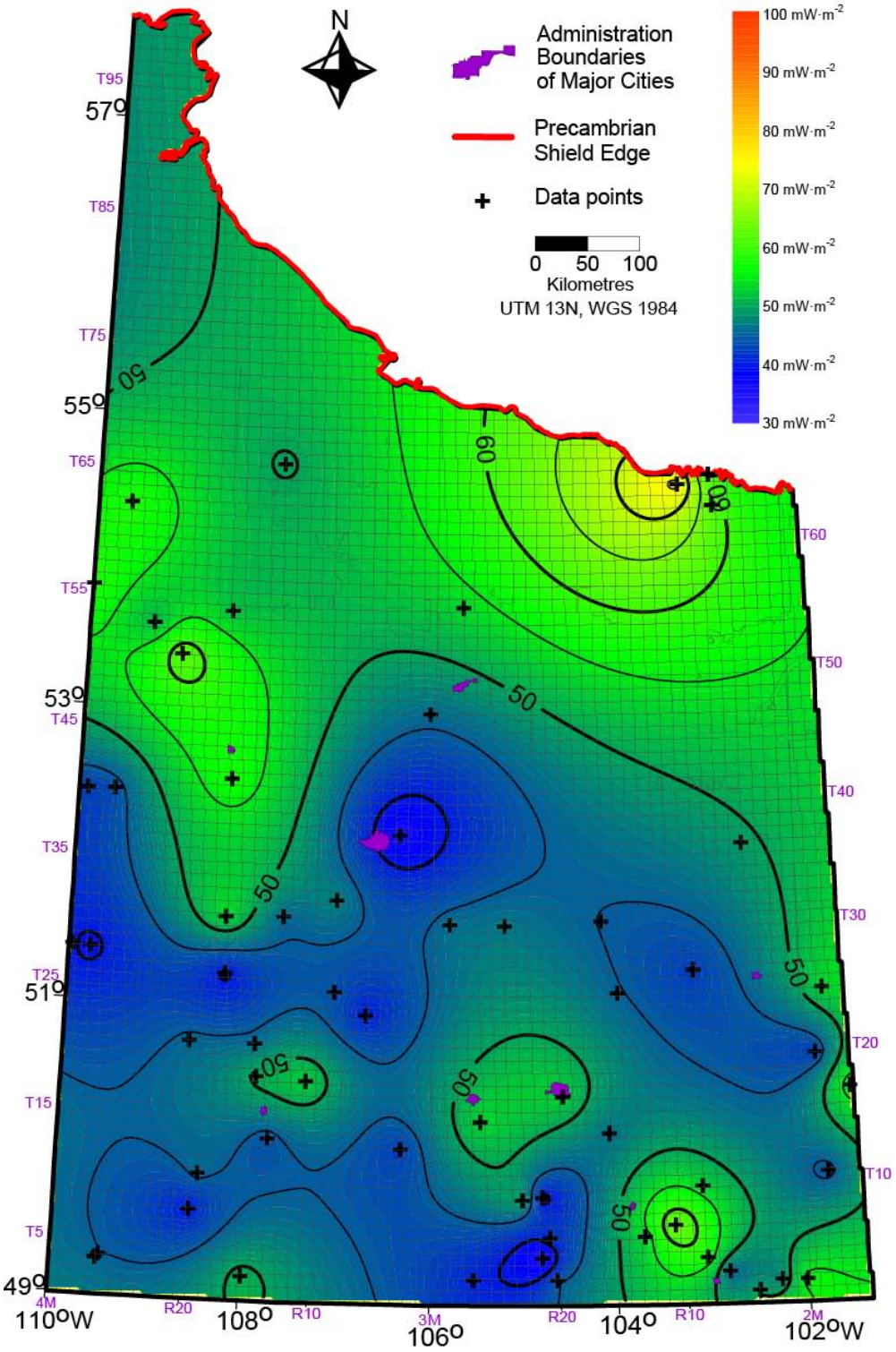

Figure 4.16 Mesozoic-Cenozoic interval heat flow map. CI: 5 mW·m^{-2}.

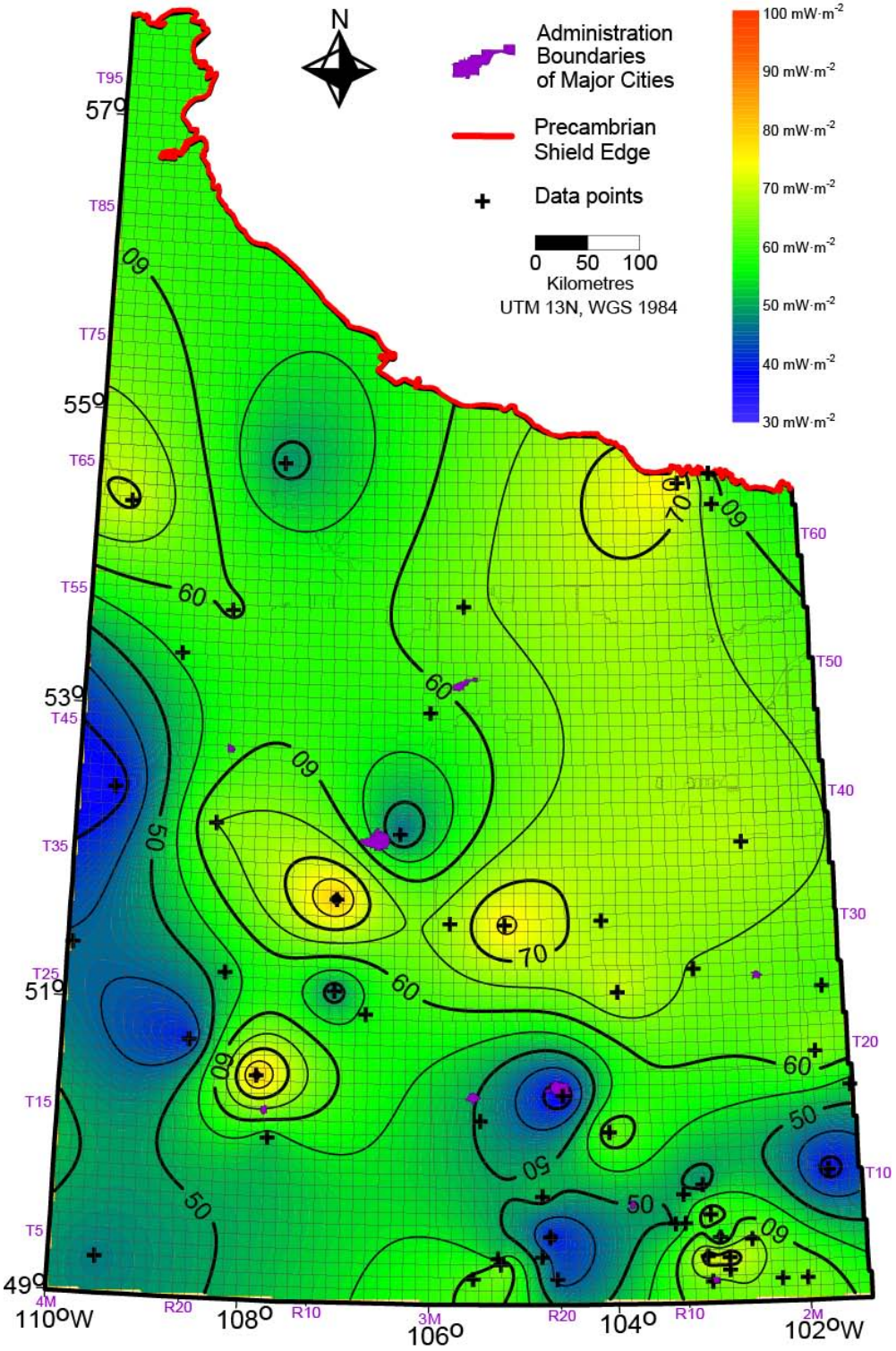

Figure 4.17 Paleozoic interval heat flow map. CI: 5 mW·m^{-2}.

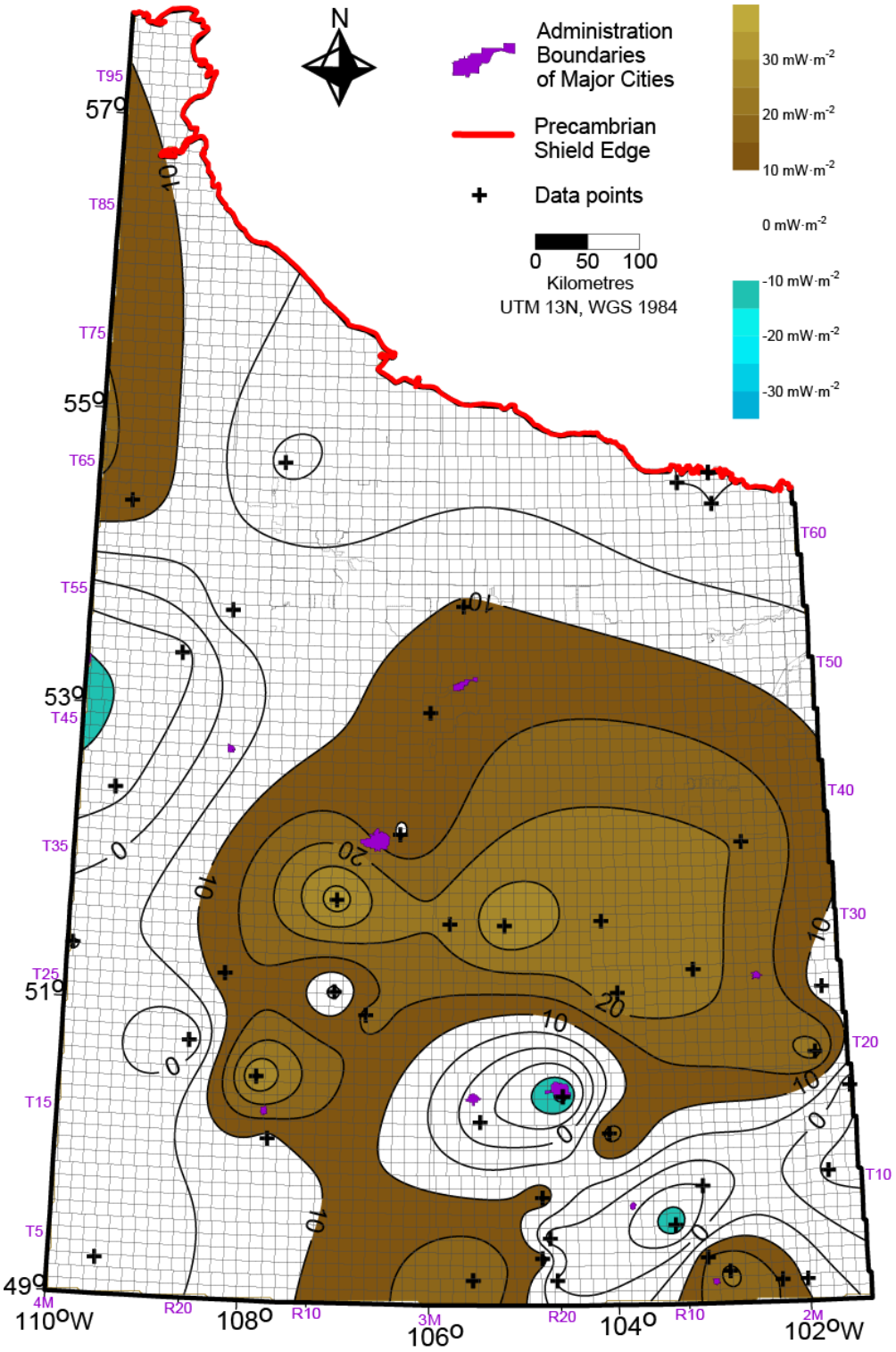

Figure 4.18 Heat flow difference map. It was generated via subtracting the Mesozoic-Cenozoic heat flow from the Paleozoic heat flow. CI: 5 mW·m^{-2}.

5 Regional synthesis

Several temperature anomalies were identified in Saskatchewan (Figure 4.1). In the previous chapter these anomalies were described but not interpreted. This chapter attempts to interpret and explain the observed patterns.

Temperatures in Saskatchewan increase with depth. Temperature values range between 5 °C at 100 m and >120 °C in the deepest parts of the basin. At 100 m depth (Figure 3.10) temperature distribution largely follows the surface temperature distribution, i.e., temperatures are decreasing towards the north from temperatures as high as 10 °C in the south to temperatures <5 °C in the north.

Highest temperatures are illustrated by the deepest temperature maps (including those of the deepest formations, e.g., Figure 4.2 and Figure 4.3). The Deadwood temperature map (Figure 4.3) illustrates that the area with temperature values >120 °C is largely constrained to a few townships at the international border (T1-7W2 to T1-11W2).

Temperatures on the strata specific temperature maps increase towards the north. However, this increase can be explained by the structure of the basin, i.e., the same formations are located shallower the further north in the basin they are observed. On the elevation specific temperature maps an increase of temperatures from the southwest towards the northeast is present. This is in part present due to topographic effects impacting the geothermal conditions as indicated by the depth specific temperature maps.

The rate of the vertical increase of temperatures is not the same in the whole study area, therefore temperatures are not the same at any given depth or elevation. Three high temperature anomalies were identified on several maps:

- In the southeast, in the area of Weyburn and Estevan;
- in the southwest, between the Cypress Hills and Swift Current; and
- near Yorkton.

Weyburn-Estevan anomaly

The Weyburn-Estevan anomaly (Figure 4.1) coincides with the area, where the basin is the deepest (Figure 4.4). Temperatures in this area are significantly higher than at the same depths or elevations in other parts of the study area (e.g., Figures B.10 and C.6).

This temperature anomaly also corresponds to above average geothermal gradient values (Figure 4.5). The geothermal gradient of this anomaly in the Cenozoic-Mesozoic formations (Figure 4.6) is significantly higher than its surroundings. However, only a minor geothermal gradient high exists in the Paleozoic formations in this area (Figure 4.7).

The integral thermal conductivity in the area reflects a low conductivity, insulating blanket partially overlapping the geothermal high identified (Figure 4.8). A similar very low conductivity area can be identified in the same area in the Cenozoic-Mesozoic formations (Figure 4.9). The calculated heat flow in the area of the anomaly is average on the various heat flow maps. Also, low heat generation is indicated east of Weyburn.

Majorowicz *et al.*, (1986) proposed previously this temperature anomaly to be caused by the insulating effect of the large amount of overlying shale. In order to test this, the relative amount of shale was calculated by calculating the ratio of the thickness of the Cenozoic-Mesozoic strata to the thickness of the Phanerozoic sediments (Figure 4.11). This ratio is 40-50 % in the area of the anomaly and even higher to the west.

However, the distribution of geothermal gradients above and below the sub-Mesozoic unconformity indicates that the difference in lithology is the cause of this anomaly. Geothermal gradients in the Cenozoic-Mesozoic strata in the area of this anomaly are the highest on Figure 4.6. Meanwhile, the Paleozoic geothermal gradients of the area are much more constrained in magnitude and in size (Figure 4.7). Therefore, the Estevan-Weyburn high temperature anomaly is thought to be caused by the insulating effect of low conductivity rocks.

Swift Current anomaly

The second major high temperature anomaly, the Swift Current anomaly is located in the southwest part of the province largely between Swift Current and the Cypress Hills. Parts of this high temperature anomaly can be observed on several shallow and deep maps (e.g., Figures B.9-B.10, C.5-C.7).

Geothermal gradients in the various intervals are consistently high in the area of this anomaly (>35 °C·km^{-1} on all geothermal gradient maps). However, it shall be noted that the gradients are very high north of Swift Current, but they are not as significant in the Cypress Hills area. For example, Figure 4.6 shows that geothermal gradient is >35 °C·km^{-1} north of Swift Current at T18-14W3, but 30-35 °C·km^{-1} under the Cypress Hills.

Thermal conductivities in this area are among the lowest in the study area, i.e., this is the area, where a major low conductivity blanket extends into Saskatchewan from the US on the thermal conductivity maps (Figure 4.8- Figure 4.10). This low thermal conductivity also corresponds well to the ratio of the Cenozoic-Mesozoic strata to the Phanerozoic strata (Figure 4.11), i.e., this area, especially the area under the Cypress Hills, has the highest ratio of younger sediments in the south (as high as 65%). Corresponding heat flows are average, or above average in the Paleozoic interval for the Swift Current area (>70 mW·m^{-2}), but are lower than average under the Cypress Hills (<50 mW·m^{-2}, Figure 4.17).

The basement is generating the most heat just west of Swift Current (>10 μW·m^{-3}, Figure 4.14). This observation led previous researchers identifying the same geothermal anomaly to consider the higher basement heat flow the source of this anomaly. This is thought to be in part causing the observed anomaly.

The basement under the Cypress Hills also generates high amounts of heat (>6 μW·m^{-3}, Figure 4.14). However, less heat is generated here than north of Swift Current. Therefore, two other sources are considered to be causing the observed anomaly in the south: the effects of topography (as explained in Chapter 4.1); and the significant amount of overburden shale insulating the subsurface

temperatures. This insulation is indicated by the very low thermal conductivity of the area (Figure 4.8- Figure 4.10) and the high ratio of younger Cenozoic-Mesozoic sediments (Figure 4.11).

In addition to the above, a fourth potential reason might play a role in the existence of the Swift Current anomaly. Higher temperatures in the southwest could also be present due to heat transported by groundwater flow in the basement.

Groundwater circulation in the basement would require open faults in the basement allowing flow to occur in the area. Faults in the basement likely exist in the area, as several Precambrian basement anomalies have been identified on the Swift Current platform (see Figure 27.8 in Kent and Christopher, 1994). According to Kent and Christopher (1994) some of these anomalies are probably reactivated fault blocks indicating the existence of fault surfaces.

Weathering could also make such deep groundwater circulation possible. For example, Melnik (2012) also indicated that the Precambrian aquitard might become an aquifer due to weathering. However, fluid flow in the basement cannot be proven due to lack of data.

Yorkton anomaly

The third high temperature anomaly, the Yorkton anomaly has a SW-NE trend (Figure 4.1). Limited amount of data are available in this area. Probably in part because of this data scarcity, the anomaly near Yorkton is much less prominent than the previously investigated two anomalies. Only parts of the anomaly can be identified on some of the temperature maps (e.g., north end Figure A.4 with isothermal line of 35 °C, or only the south end, Figure B.4, values >25 °C).

A geothermal gradient high can also be observed along the trend in all intervals. The values are higher than the respective background gradient (30- 35 °C·km^{-1} on all geothermal gradient maps, Figure 4.5- Figure 4.7), but are generally not as high as the geothermal gradients of the other two hot anomalies.

The relative amount of Cenozoic-Mesozoic sediments increases along the anomaly towards the northeast (Figure 4.11). This increasing ratio is reflected by the decreasing integral thermal conductivities along the trend in the same direction (Figure 4.8). The thermal conductivity of the area is about average, it is almost everywhere above 1.5 $W \cdot m^{-1} \cdot °C^{-1}$.

Paleozoic heat flows in the area of the anomaly are slightly above average (>65 $mW \cdot m^{-2}$, Figure 4.17), but the Mesozoic and the integral heat flows are not higher than the respective background values (<65 $mW \cdot m^{-2}$ and<50 $mW \cdot m^{-2}$, Figure 4.16 and Figure 4.15). No radioactive element concentrations have been measured on basement rock samples in this area (Figure 4.14). Due to the lack of data it cannot be determined what is the possible source of this hot anomaly.

Cold anomalies

Cold anomalies have not been analysed previously in the province, since areas warmer than the surroundings are more interesting for geothermal research (i.e., these are more likely to be utilized than colder areas).

Six relatively cold regions were identified on the temperature maps. However, the one separating the two high areas is most likely only apparent, since it is located between two high anomalies and on most elevation and depth specific temperature maps the temperature values in the area are about the same as the background temperature of the selected surface (e.g. Figure B.5-B.7). The rest of the anomalies were located at the following locations (see also Figure 4.1):

- along the Alberta border;
- at Saskatoon;
- at Regina;
- at T1-20W2 toT5-20W2 (*20W2*); and
- between T10-10W2, T10-16W2, T4-16W2 and T4-10W2 (*10W2-16W2*).

Only the first two anomalies are present consistently on all geothermal gradient maps as regions of colder geothermal gradients than the background gradient. However, on the sub-Mesozoic geothermal gradient map the anomalies near Regina and (A) can also be observed (areas <25 °C·km^{-1} on Figure 4.7). Anomaly (B) does not show up very much on the geothermal gradient maps.

Saskatoon has the lowest thermal conductivity (<1.3 W·m^{-1}·°C^{-1}) among these cold temperature anomalies. It is also the most prominent anomaly (e.g., coldest on several maps, like Figures B.7, and B.8). The other cold anomalies lie in regions of average thermal conductivities (1.5- 1.7 W·m^{-1}·°C^{-1}).

Heat flow in the area of these cold anomalies is lower than average on all heat flow maps (<50 mW·m^{-2}, Figure 4.15- Figure 4.17), except for (B). There is only few radioactive element concentration data measured near these areas, but according to them there is only limited amount of heat generated along the Alberta border, and in the area of (B).

The anomaly at Regina, and anomalies (A), (B) are protruding into regions of high geothermal gradients and temperatures, unlike the other two anomalies. The existence of these anomalies might be explained simply by the lack of the process creating the adjacent high anomaly.

The anomalies at Saskatoon and west of it, along the Alberta border are slightly harder to explain. Decreased mantle heat flow, or lower than average upper-crustal heat production are the most likely explanations for their existence. It shall be noted though, that heat generation at the top of the basement is not exceptionally low in the area, so this option would necessitate much lower heat generation at depths.

Heat transfer in the basin

The horizontal temperature distribution corresponds well to the depth of the measurement. The isotherms (Appendix A) and the depth of the formations

(Marsh and Love, 2013) conform to each other indicating that there are few, if any lateral disturbances in the heat flow field.

Extremely high geothermal gradients (>60 °C·km^{-1}) were previously noted along the edges of the basin (e.g., Bachu and Burwash, 1994) and were considered to be potentially the result of the lateral heat redistribution by regional groundwater flow. In this study, significant portion of the shallow measurements close to the edges of the basin were found to be affected by the maximum thermometer error. High geothermal gradients can be still observed along the Precambrian outcrop edges in Saskatchewan (Figure 4.5- Figure 4.7), but their magnitude significantly decreased (<45 °C·km^{-1}). Therefore, this evidence of convective heat flow regime is also questioned by this work.

Finally, the distribution of heat flow was also used previously as an argument for the importance of heat convection in the basin (e.g., Majorowicz *et al.*, 1986). A vertical heat flow difference map was generated for Saskatchewan (Figure 4.18). This map does not indicate systematic differences in vertical heat flow distribution in recharge and discharge areas. Indeed, it shows a difference of <10 mW·m^{-2} both in the potential regional recharge (Cypress Hills) and discharge areas (along the Precambrian outcrop edge). Therefore, heat conduction is considered to be the dominant heat transfer method in the basin.

Implications for geothermal energy utilization

The two maps of particular interest for geothermal energy utilization are the 75 °C and the 100 °C isothermal depth maps (Figure D.3, and D.4). The 75 °C is of special interest, since this is the lowest temperature currently used for economic geothermal electricity production[29], while 100 °C is the atmospheric boiling point of water.

[29] Chena Hot Springs, http://www.yourownpower.com/Power/ [Last accessed: 2012.12.31]

For reaching 75 °C depths (Figure D.3) from >2500 m to less than <2000 m are required. 100 °C (Figure D.4) can be reached from >3000 m to about 2500 m. Both temperatures can be reached with the least amount of drilling in the area of the Weyburn-Estevan anomaly.

Conclusions

- Temperature increases with depth in Saskatchewan, it ranges from 5 °C to >120 °C in the deepest part of the basin.
- On average, the integral geothermal gradient is 25- 30 °C·km^{-1}. However, it changes vertically. In the Cenozoic-Mesozoic formations the average geothermal gradient is higher (30- 35 °C·km^{-1}), while in the Paleozoic strata the average geothermal gradient is lower (25 °C·km^{-1}) than the average integral geothermal gradient.
- Geothermal gradients also vary horizontally; three hot and six relatively cold temperature anomalies could be delineated based on the horizontal variation of geothermal gradients and the temperature maps. The hot anomalies are:
    - the Weyburn-Estevan;
    - the Swift Current-Cypress Hills; and
    - the Yorkton anomalies.
- The cold anomalies are:
    - the Saskatoon;
    - the Alberta border;
    - the Regina;
    - the 20W2; and
    - the 10W2-16W2 anomalies.
- The sixth cold anomaly is located between the Weyburn-Estevan and Swift Current-Cypress Hills hot anomalies. This is most likely just an apparent anomaly.
- The Saskatchewan portion of the Williston Basin is seriously void of actual thermal conductivity measurements, thus more are recommended to be taken. Thermal conductivity was estimated via net rock analysis to overcome this gap in knowledge. Thermal conductivities range from 1 to ~2 W·m^{-1}·°C^{-1}. A major low-conductivity (<1.5 W·m^{-1}·°C^{-1}) thermal

blanket was identified in the southeast portion of the province extending as far north as Saskatoon.

- Calculated integral heat flow varies between 35 $mW \cdot m^{-2}$ and 75 $mW \cdot m^{-2}$. The region with highest heat flow is in the northeast close to the Precambrian outcrop edge. These values are lower than previous calculations. Previously identified heat flow anomaly near Weyburn could not be reproduced
- The sedimentary heat generation provides only a minor contribution to surface heat flow (<3 $mW \cdot m^{-2}$).
- Basement heat generation ranges <1 $\mu W \cdot m^{-3}$ to >10 $\mu W \cdot m^{-3}$. This conforms to previous observations. Highest heat generation occurs in the southwest corner of the province.
- The Weyburn-Estevan anomaly is potentially caused by the insulating effect of the thick overlying shale package.
- The Swift Current-Cypress Hills anomaly is caused by multiple effects; the three causes identified here are topographic effects, the insulating effect of thick overlying shale packages and the high basement heat production.
- The major vertical lithological differences are the cause of the variation in geothermal gradients with depth.
- Previously observed very high geothermal gradients in the shallow basement are an artifact of BHTs.
- Vertical differences in heat flow, as well, as the conformity of temperatures mapped for the strata tops to the strata depths indicate that heat conduction is the dominant heat transfer method in the study area, i.e., groundwater flow does not impact the geothermal conditions of the recharge and discharge areas of Saskatchewan to a great extent.
- Temperatures required for geothermal electricity production are available in the subsurface of Saskatchewan. These temperatures are located at shallowest depths in the area of the Weyburn-Estevan anomaly (75 °C and 100 °C at <2000 m and ~2500 m)

Recommendations for future work

The following areas would require more data: reliable temperature data other than BHTs are required in the north-central, northwest portion of the basin, where the geothermal gradient anomaly was determined to verify high geothermal gradients.

Second, high precision temperature data and radioactive element concentration measurements of basement rock samples from the area of the Yorkton anomaly are required to allow for a more detailed description of the anomaly.

Third, reliable thermal conductivity measurements of the Phanerozoic sediments are required to determine thermal conductivity of the sediments. These would facilitate reliable heat flow determinations.

Fourth, flow rates also influence the feasibility of geothermal projects in addition to temperatures. Therefore flow parameters should be integrated with the geothermal conditions determined in this study to determine, which aquifers are most economic for potential geothermal electricity production.

References

Al-Kalali, A. (2002): Petroleum hydrogeology of the Nisku Aquifer: Unpubl. M.Sc. thesis, University of Alberta, Edmonton, Alberta, Canada, 152p.

Anglin, F. M. and Beck, A.E. (1965): Regional heat flow pattern in Western Canada. Can. J. of Earth Sci., v2, p176-182.

ASME Committee (2004): Drilling fluids processing handbook. Elsevier Science and Technology, 693p.

Athy, L. F. (1930): Density, porosity, and compaction of sedimentary rocks. AAPG Bulletin, v14, no. 1, p1-24

Bachu, S. (1985): Influence of lithology and fluid flow on the temperature distribution in a sedimentary basin: A case study from the Cold Lake area, Alberta, Canada. Tectonophys., v120, p257-284.

Bachu, S. (1988): Analysis of heat transfer processes and geothermal pattern in the Alberta Basin, Canada. J. of Geophys. Res., v93, no. B7, p7767-7781.

Bachu S. (1993): Basement heat flow in the Western Canada Sedimentary Basin. Tectonophys., v222, p119-133.

Bachu, S. (1995): Flow of variable-density formation water in deep sloping aquifers: review of methods of representation with case studies. J. Hydrology, v164, p19-38.

Bachu (1999): Regional-scale geothermal and hydrodynamic regimes in the Alberta Basin: A synthesis. *In*: Förster., A. and Merriam., D. F. (eds.): Geothermics in basin analysis, Kluwer Academic/Plenum Publishers, 1999, p81-98.

Bachu, S. and Burwash. R. A. (1991): Regional-scale analysis of the geothermal regime in the Western Canada Sedimentary Basin. Geothermics, v20, no. 5/6, p387-407.

Bachu, S. and Burwash, R. A. (1994): Chapter 30 - Geothermal regime in the Western Canada Sedimentary Basin. *In*: Mossop, G. and Shetsen, I. (comps.), Geological atlas of the Western Canada Sedimentary Basin, Can. Soc. Petrol. Geol./Alberta Res. Counc., p.447-454.

Bachu, S. and Hitchon, B. (1996): Regional-scale flow of formation waters in the Williston Basin. AAPG Bulletin, v80, no. 2, p248-264.

Beach, R. D. W. (1985): Sedimentary heat flow in the ΔQ=0 region of Alberta. Unpubl. M.Sc. thesis, University of Alberta, Edmonton, Alberta, Canada, p128.

Beach, R. D. W., Jones, F. W. and Majorowicz, J. A. (1987): Heat flow and heat generation estimates for the Churchill basement of the Western Canadian Basin in Alberta, Canada. Geothermics, v16, no. 1, p1-16.

Beardsmore, G. R. and Cull, J. P. (2001): Crustal heat flow: a guide to measurement and modelling. Cambridge Univ. Press., 324p.

Beck, A. E. and Balling, N. (1988): Determination of virgin rock temperatures. *In*: Haenel, R., Rybach, L. and Stegena, L. A. (eds.): Handbook of terrestrial heat-flow density determination. Kluwer Academic Publishing, Dordrecht, Netherlands, 1988, p59-85.

Ben Dhia, H. (1988): Tunisian geothermal data from oil wells. Geophysics, v53, no. 11, p1479-1487.

Black, W. M. (1956): A review of drill stem testing techniques and analysis. J. of Petroleum Technology. v8, no. 6, p21-30.

Boberg, T. C. (1988): Thermal methods of oil recovery. John Wiley and Sons Inc., New York, 412p.

Brigaud, F. and Vasseur, G. (1989): Mineralogy, porosity and fluid control on thermal conductivity of sedimentary rocks. Geophysical Journal, v98, p525-542.

Burgess, P. M. (2008): Phanerozoic evolution of the sedimentary cover of the North American craton. Sedimentary Basins of the World, v5, p31-63.

Burwash, R. A. and Cumming, G. L. (1976): Uranium and thorium in the Precambrian basement of Western Canada. Can. J. of Earth Sci., v13, p284-293.

Burwash, R. A. and Krupicka, J. (1970): Cratonic reactivation in the Precambrian basement of western Canada. Part II. Metasomatism and isostasy. Can. J. of Earth. Sci., v7, p1275-1294.

Burwash, R. A., McGregor, C. R. and Wilson, J. A. (1994) Chapter 5 - Precambrian basement beneath the Western Canada Sedimentary Basin. *In*: Mossop, G. and Shetsen, I. (comps.), Geological atlas of the Western Canada Sedimentary Basin, Can. Soc. Petrol. Geol./Alberta Res. Counc., p49-56.

Bücker, C. and Rybach, L. (1996): A simple method to determine heat production from gamma-ray logs. Marine and Petrol. Geol., v13, no. 4, p373-375.

Carlson, C. G. and Anderson, S. B. (1965): Sedimentary and tectonic history of North Dakota part of Williston Basin. AAPG Bulletin, v49, no. 11, p1833-1846.

Čermák, V. and Haenel, R. (1988): Geothermal maps. *In*: Haenel, R., Rybach, L. and Stegena, L. A. (eds.): Handbook of terrestrial heat-flow density determination. Kluwer Academic Publishing, Dordrecht, Netherlands, 1988, p261-300.

Chapman, D. S., Keho, T. H., Bauer, M. S. and Picard, M. D. (1984): Heat flow in the Uinta Basin determined from bottom hole temperature (BHT) data. Geophysics, v49, no. 4, p453-466.

Crowell, A. M., Klenner, R. and Gosnold, W.D (2011): GIS analysis for the volumes, and available energy of selected reservoirs: Williston Basin, North Dakota. GRC Transactions, v35, p1557-1562.

Deming, D. (1989): Application of bottom-hole temperature corrections in geothermal studies. Geothermics, v18, no. 5/6, p775-786.

Deming, D. and Chapman, D. S. (1988): Heat flow in the Utah-Wyoming thrust belt from analysis of bottom-hole temperature data measured in oil and gas wells. J. of Geophys. Res., v93, no. B11, p13657-13672.

Deming, D., Sass, J. H., Lachenbruch, A. H. and De Rito, R. F. (1992): Heat flow and subsurface temperature as evidence for basin-scale ground-water flow, North Slope of Alaska. GSA Bulletin, v104, p528-542.

DeMis, W.D. (1995): Effect of cross-basinal hydrodynamic flow on oil accumulations and oil migration history of the Bakken–Madison petroleum system; Williston Basin, North America. *In:* Hunter, L. D. V., and Schalla, R. A. (eds.): Seventh International Williston Basin Symposium. Montana Geological Society, Billings, Montana, p291–301.

Domenico, P. A. and Palciauskas, V. V. (1973): Theoretical analysis of forced convective heat transfer in regional ground-water flow. GSA Bulletin, v84, p3803-3814.

Erdlac R. J. Jr. (2006): A resource assessment of geothermal energy resources for converting deep gas wells in carbonate strata into geothermal extraction wells: A Permian Basin evaluation. URL. <http://dx.doi.org/10.2172/893183> [Last accessed: 2012.05.14].

Fjeldskaar, W., Christie, O. H. J, Midttømme, K., Virnovsky, G., Jensen, N. B., Lohne, A., Eide, G. I. and Balling, N. (2009): On the determination of thermal conductivity of sedimentary rocks and the significance for basin temperature history. Petrol. Geosci., v15, p367-380.

Förster, A (2001): Analysis of borehole temperature data in the Northeast German Basin. Continuous logs versus bottom-hole temperatures. Petrol. Geosci., v7, p241-254.

Gan, H., Nandi, S. P. and Walker, P. L., Jr. (1972): Nature of porosity in American coals. Abstract in Fuel, v51, no. 4, 272-277.

Garland, G. D. and Lennox, D. H. (1962): Heat flow in Western Canada. Geophys. J. of the Royal Astr. Soc., v6, no. 2, p245-262.

Gerhard, L. C., Anderson, S. B., LeFever, J. A. and Carlson, C. G. (1982): Geological development, origin, and energy mineral resources of Williston Basin, North Dakota. AAPG Bulletin, v66, no. 8, p989-1020.

Golden Software (2002): Surfer® 8 - User's Guide - Contouring and 3D Surface Mapping for Scientists and Engineers. Golden Software Inc., Golden, Colorado, 640p.

Gosnold, W. D. (1990): Heat flow in the Great Plains of the United States. J. of Geophys. Res., v95, no. B1, p353-374.

Gosnold W. D. (1999): Basin scale groundwater flow and advective heat flow: An example from the northern Great Plains. *In*: Förster., A. and Merriam., D. F., Geothermics in basin analysis, Kluwer Academic/Plenum Publishers, 1999, p99-116.

Gosnold, W. D., LeFever, R., Mann, M., Klenner, R. and Salehfar, H. (2010): EGS potential in the northern midcontinent of North America. GRC Transactions, v34, p355-358.

Gosnold, W. D., Majorowicz, J. A., Klenner, R. and Hauck, S. (2011): Implications of post-glacial warming for northern hemisphere heat flow. GRC Transactions, v35, p795-800.

Gosnold, W. D. McDonald, M. R., Klenner, R. and Merriam, D. (2012): Thermostratigraphy of the Williston Basin. GRC Transactions, v36, p663-670.

Grasby, S. E. and Betcher, R. (2000): Pleistocene recharge and flow reversal in the Williston Basin, central North America. J. of Geochem. Expl., v69-70, p403-407.

Grasby, S.E., Allen, D.M., Bell, S., Chen, Z., Ferguson, G., Jessop, A. M., Kelman, M., Ko, M., Majorowicz, J. A., Moore, M., Raymond, J. and Therrien, R., (2012): Geothermal Energy Resource Potential of Canada, Geological Survey of Canada, Open File 6914, 322p.

Gray, A.D., Majorowicz, J. A. and Unsworth, M (2012): Investigation of the geothermal state of sedimentary basins using oil industry thermal data: case study from Northern Alberta exhibiting the need to systematically remove biased data. J. Geophys. and Eng., v9, p534-548.

Guillo-Frottier, L., Jaupart, C., Mareschal, J. C, Gariépy, C., Bienfait, G., Cheng, L. Z. and Lapointe, R. (1996): High heat flow in the Trans-Hudson Orogen, central Canadian Shield. Geophys. Res. Lett., v23, no. 21, p3027-3030.

Haenel, R., Rybach, L. and Stegena, L. A. (1988): Fundamentals of geothermics. *In*: Haenel, R., Rybach, L. and Stegena, L. A. (eds.): Handbook of terrestrial heat-flow density determination. Kluwer Academic Publishing, Dordrecht, Netherlands, 1988, p9-57.

Haidl, F.M., Kreis, L. K. and Dancsok, E. F. R (1996): New oil discoveries in Ordovician Red River strata, southeastern Saskatchewan. *In*: Summary of Investigations 1996, Sask. Geological Survey, Sask. Energy Mines, Misc. Rep. 96-4, p136-144.

Hannon, N. (1987): Subsurface water flow patterns in the Canadian sector of the Williston Basin. *In:* Peterson, J. A., Kent, D. M. , Anderson, S. B., Pilatzke, R. H., and Longman, M. W. (eds.): Williston Basin: Anatomy of a Cratonic Oil Province. Rocky Mountain Association of Geologists, Denver, CO, p313–322.

Hermanrud, C., Cao, S. and Lerche, I (1990): Estimates of virgin rock temperature derived from BHT measurements: Bias and error. Geophysics, v55, no. 7, p924-931.

Hermanrud, C., Lerche, I. and Meisingset, K. K. (1991): Determination of virgin rock temperature from drillstem tests. J. of Petrol. Techn., v43, no. 9, p1126-1131.

Hitchon, B. (1984): Geothermal gradients, hydrodynamics, and hydrocarbon occurrences, Alberta, Canada. AAPG Bulletin, v68, no. 6, p713-743.

Horner, D. R. (1951): Pressure build-up in wells. Proc. Third World Petroleum Congress, p503-521.

Iampen, H. T. (2003): The Genesis and Evolution of Pre-Mississippian Brines in the Williston Basin, Canada-U.S.A.: Unpubl. M.Sc. thesis, University of Alberta, Edmonton, Alberta, Canada, 124p.

Issler, D.R. and Jessop, A. M. (2011): Thermal conductivity analysis of Cenozoic, Mesozoic and Paleozoic core samples, Beaufort-Mackenzie Basin, northern Canada. Geological Survey of Canada, Open File 6734, 128p.

Jessop, A. M. (1989): Hydrological distortion of heat flow in sedimentary basins. Tectonophys., v164, p211-218.

Jessop, A. M. (1990): Comparison of industrial and high-resolution thermal data in a sedimentary basin. Pure and Applied Geophysics, v133, no. 2, p251-267.

Jessop, A. M. and Vigrass, L. W. (1989): Geothermal measurements in a deep well at Regina, Saskatchewan. J. of Volcanology and Geothermal Res., v37, p151-166.

Jessop, A. M., Allen, V. S., Bentkowski, W., Burgess, M., Drury, M. J, Judge, A. S., Lewis, T., Majorowicz, J. A., Mareschal, J. C. and Taylor, A. E. (2005): The Canadian geothermal data compilation. Geological Survey of Canada, Open File 4887, one CD.

Jones, F. W. and Majorowicz, J. A (1987): Regional trends in radiogenic heat generation in the Precambrian basement of the Western Canadian Basin. Geophys. Res. Lett., v14, no. 3, p268-271.

Jones, F. W., Kushigbor, C., Lam, H. L., Majorowicz, J. A. and Rahman, M. (1984): Estimates of terrestrial thermal gradients and heat flow variations with depth in the Hinton-Edson area of the Alberta Basin derived from petroleum bottom-hole temperature data.. Geophys. Prosp., v32, p1111-1130.

Jones, F. W., Lam, H. L. and Majorowicz, J. A. (1985): Temperature distributions at the Paleozoic and Precambrian surfaces and their implications for geothermal energy recovery in Alberta. Can. J. of Earth Sci., v22, p1774-1780.

Khan, D. K. (2006): Hydrogeological characterization of the Weyburn CO2 project area and gradient-free inverse conditioning of heterogeneous aquifer models to hydraulic head data: Unpubl. Ph.D. thesis, University of Alberta, Edmonton, Alberta, Canada, 238p.

Kent, D. M. (1987): Paleotectonic controls on sedimentation in the northern Williston Basin, Saskatchewan. *In:* Peterson, J. A., Kent, D. M. , Anderson, S. B., Pilatzke, R. H., and Longman, M. W. (eds.): Williston Basin: Anatomy of a Cratonic Oil Province. Rocky Mountain Association of Geologists, Denver, CO, p45-56.

Kent, D. M. and Christopher, J. E. (1994): Chapter 27 - Geological History of the Williston Basin and Sweetgrass Arch. *In*: Mossop, G. and Shetsen, I. (comps.), Geological atlas of the Western Canada Sedimentary Basin, Can. Soc. Petrol. Geol./Alberta Res. Counc., p421-429.

Kreis, L.K., Haidl, F. M., Nimegeers, A. R., Ashton, K. E., Maxeiner, R. O. and Coolican, J. (2004): Lower Paleozoic Map Series – Saskatchewan. Saskatchewan Industry Resources, Misc. Rep., 2004-8, CD-ROM.

Kushigbor, C. A. (1984): Detailed heat flow studies in the west central Alberta sedimentary basin from bottom-hole temperature values. Unpubl. M.Sc. thesis, University of Alberta, Edmonton, Alberta, Canada, 115p.

Kutasov, I. M. and Eppelbaum, L. V. (2005): Determination of formation temperature from bottom-hole temperature logs – a generalized Horner method. J. of Geophys. and Eng., v2, p90-96.

Lachenbruch, A.H. and Brewer, M.C. (1959): Dissipation of the temperature effect of drilling a well in arctic Alaska. Bull. U.S. Geol. Surv., v1083-C, p73-109.

Lam, H. L. and Jones, F. W. (1984): Geothermal gradients of Albert in western Canada. Geothermics, v13, no. 3, p181-192.

Majorowicz, J. A. (1993): Climate change inferred from analysis of borehole temperatures: First results from Alberta Basin, Canada. Pure and Applied Geophysics, v140, no. 4, p655-666.

Majorowicz, J.A. and Jessop, A.M. (1981): Regional heat flow patterns in the Western Canadian Sedimentary Basin. Tectonophys., v74, p209-238.

Majorowicz, J. A and Safanda, J. (1998): Ground surface temperature history from inversions of underground temperatures - a case study of the Western Canadian Sedimentary Basin. Tectonophys., v291, p287-298.

Majorowicz, J. A. and Safanda, J. (2001): Composite surface temperature history from simultaneous inversion of borehole temperatures in western Canadian plains. Global and Planetary Change, v29, p231-239.

Majorowicz, J. A. and Skinner, W. R. (2001): Reconstruction of the surface warming history of western interior Canada from borehole temperature profiles and other climate information. Climate Res., v16, p157-167.

Majorowicz, J. A. and Grasby, S. E. (2010): Heat flow, depth-temperature variations and stored thermal energy for enhanced geothermal systems in Canada. J. Geophys. Eng., v7, p232-241.

Majorowicz, J. A. and Wybraniec, S. (2011): New terrestrial heat flow map of Europe after regional paleoclimatic correction application. Int. J. of Earth. Sci., v100, p881-887.

Majorowicz, J. A., Jones, F. W., Lam, H. L. and Jessop, A. M. (1984): The variability of heat flow both regional and with depth in southern Alberta, Canada: Effect of groundwater flow? Tectonophys., v106, p1-29.

Majorowicz, J. A., Jones, F. W., Lam, H. L. and Jessop, A. M. (1985)a: Regional variations of heat flow differences with depth in Alberta, Canada. Geophys. J. of the Royal. Astron. Soc., v81, p479-487.

Majorowicz, J. A., Jones, F. W., Lam, H. L. and Jessop, A. M. (1985)b: Terrestrial heat flow and geothermal gradients in relation to hydrodynamics in the Alberta Basin, Canada. J. of Geodynamics, v4, p265-283.

Majorowicz, J. A., Jones, F.W. and Jessop, A.M. (1986): Geothermics of the Williston basin in Canada in relation to hydrodynamics and hydrocarbon occurrences. Geophysics, v51, no. 3, p767-779.

Majorowicz J. A., Garven, G., Jessop, A. M. and Jessop, C. (1999): Present heat flow along a profile across the Western Canada Sedimentary Basin: The extent of hydrodynamic influence. *In*: Förster., A. and Merriam., D. F., Geothermics in basin analysis, Kluwer Academic/Plenum Publishers, 1999, p61-79.

Majorowicz, J. A., Safanda, J. and Skinner, W. R. (2002): East to west retardation in the onset of the recent warming across Canada inferred from inversions of temperature logs. J. of Geophys. Res., v107, no. B10, 12p.

Majorowicz, J. A., Skinner, W. R. and Safanda, J. (2005): Ground surface warming history in northern Canada inferred from inversions of temperature logs and comparison with other proxy climate reconstructions. Pure and Applied Geophysics, v162, p109-128.

Majorowicz, J. A., Skinner, W. R., Safanda, J. and Gosnold, W. D. (2006): Differences between repeated borehole temperature logs in the southern Canadian Prairies – validating borehole climatology. Clim. Past. Discuss., v2, p1075-1104.

Majorowicz, J. A., Gosnold, W. D., Gray, A., Safanda, J., Klenner, R. and Unsworth, M. (2012). Implications of post-glacial warming for northern Alberta heat flow- correcting for the underestimate of the geothermal potential. GRC Transactions, v36, p693-698.

Mann, M. E. and Schmidt, G. A. (2003): Ground vs. surface air temperature trends: Implications for borehole surface temperature reconstructions. Geophys. Res. Lett., v30, no. 12, 4p.

Mareschal J. C., Rolandone, F. and Bienfait, G. (1999): Heat flow variations in a deep borehole near Sept-Iles, Québec, Canada: Paleoclimatic interpretation and implications for regional heat flow estimates. Geophys. Res. Lett., v26, no. 14, p2049-2052.

Margitai, Zs. (2002): Hydrogeological characterization of the Red River Formation, Williston Basin, Canada–USA. Unpubl. M.Sc. thesis, University of Alberta, Edmonton, Alberta, Canada, 92p.

Marsh, A. and Love, M. (2013): Saskatchewan Phanerozoic fluids and petroleum systems regional stratigraphic framework. *In* Summary of Investigations 2012, Volume 1, Saskatchewan Geological Survey, Sask. Ministry of the Economy, Misc. Rep. 2012-4.1, Paper A-7, 7p, URL < http://economy.gov.sk.ca/adx/aspx/adxGetMedia.aspx?DocID=12440,12438,11458,11455,11228,3385,5460,2936,Documents&MediaID=92a5b3ad-0e78-4c0b-b0b2-4f5a13d38746&Filename=A-7+Marsh+and+Love.pdf>.

Martiniuk, C. D. (1988): Regional geology and petroleum potential of Bakken Formation, southwestern Manitoba. (Abstract). URL<http://www.searchanddiscovery.com/abstracts/html/1988/rocky/abstracts/0877.htm> [Last accessed: 2012.12.14]

McKenna, T. E. and Sharp, J. M. Jr. (1998): Radiogenic heat production in sedimentary rock of the Gulf of Mexico Basin, south Texas. AAPG Bulletin, v82, no. 3, p484-496.

McKenna, T.E., Sharp, J.M. and Lynch, F.L. (1996): Thermal conductivity of Wilcox and Frio sandstones in south Texas; AAPG Bull., v80, no. 8, p1203-1215.

Melnik, A. (2012): Regional hydrogeology of southwestern Saskatchewan. Unpubl. M.Sc. thesis, University of Alberta, Edmonton, Alberta, Canada, 142p.

Middleton, M.F. (1979): A model for bottom-hole temperature stabilization. Geophysics, v44, p1458-1462.

Middleton, M.F. (1982) Bottom-hole temperature stabilization with continued circulation of drilling mud. Geophysics, v47, no. 12, p1716-1723.

Midttømme, K. and Roaldset, E. (1998): The effect of grain size on thermal conductivity of quartz sands and silts. Petrol. Geosci., v4, p165-172.

Mossop, G. and Shetsen, I. (comps.) (1994): Geological atlas of the Western Canada Sedimentary Basin. Can. Soc. Petrol. Geol./Alberta Res. Counc., 510p.

National Energy Board (2012): Energy Briefing Note – Canadian energy overview 2011. URL <http://www.neb-one.gc.ca/clf-nsi/rnrgynfmtn/nrgyrprt/nrgyvrvw/cndnnrgyvrvw2011/cndnnrgyvrvw2011-eng.html> [Last accessed: 2012.11.13].

Nathenson, M. and Guffanti, M. (1988): Geothermal gradients in the conterminous United States. J. Geophys. Research, v93, no. B6, p6347-6450.

Nativ, R. (1990): A supplementary method for assessing the reliability of fluids sampled from deep aquifers. Ground Water Monitoring and Remediation, v10, no. 2, p83-88.

Palombi, D. D. (2008): Regional hydrogeological characterization of the Northeastern margin in the Williston Basin. Unpubl. M.Sc. thesis, University of Alberta, Edmonton, Alberta, Canada, 196p.

Peters, K. E. and Nelson, P. H. (2009): Criteria to determine borehole formation temperatures for calibration of basin and petroleum system models. AAPG Search and Discovery Article #40463. URL <http://www.searchanddiscovery.com/documents/2009/40463peters/ndx_peters.pdf> [Last accessed: 2012.12.31].

Peterson, J. A. and MacCary, L. M. (1987): Regional stratigraphy and general petroleum geology of the U.S. Portion of the Williston Basin and adjacent areas. *In:* Peterson, J. A., Kent, D. M. , Anderson, S. B., Pilatzke, R. H., and Longman, M. W. (eds.): Williston Basin: Anatomy of a Cratonic Oil Province. Rocky Mountain Association of Geologists, Denver, CO, p9-44.

Phillips, D.W, Bullard, E.C., Jeffreys, H, Anderson, E.M., Fearnsides, W.G., Hickling, G., Holmes, A. and Poole, H. J. H. (1938): Thermal conductivities of rocks. *In*: Report of the Annual Meeting of the British Association for the Advancement of Science, 1938, p217-277.

Rolandone, F., Jaupart, C., Mareschal, J. C., Gariépy, C., Bienfait, G., Carbonne. C. and Lapointe, R. (2004): Surface heat flow, crustal temperatures and mantle heat flow in the Proterozoic Trans-Hudson Orogen, Canadian Shield. J. of Geophys. Res., v107, no. B12, 20p.

Rollin, K. E. (1995): A simple heat-flow quality function and appraisal of heat-flow measurements and heat flow estimates from the UK Geothermal Catalogue. Tectonophys., v244, p185-196.

Rybach, L. (1986): Amount and significance of radioactive heat sources in sediments. *In*: Thermal Burrus, J. (Ed.) Modelling in Sedimentary Basins, Collection Colloques et Seminaires 44, Editions Technip, Paris, p311-322.

Rybach, L. (1988): Determination of heat production rate. *In*: Haenel, R., Rybach, L. and Stegena, L. A. (eds.): Handbook of terrestrial heat-flow density determination. Kluwer Academic Publishing, Dordrecht, Netherlands, 1988, p125-142.

Sass, J. H., Lachenbruch, A. H. and Jessop, A. M. (1971): Uniform heat flow in a deep hole in the Canadian Shield and its paleoclimatic implications. J. of Geophys. Res., v76, no. 35, p8586-8596.

Schmoker, J. W. and Halley, R. B. (1982): Carbonate porosity versus depth: A predictable relation for South Florida. AAPG Bulletin, v66, no. 12, p2561-2570.

Sclater, J. G. and Christie, P. A. F. (1980): Continental stretching: An explanation of the post-mid-Cretaceous subsidence of the central North Sea Basin. J. of Geophys. Res., v85, no. B7, p3711-3739.

Sekiguchi, K. (1984): A method for determining terrestrial heat flow in oil basinal areas. Tectonophys., v103, p67-79.

Shen, P. Y. and Beck, A. E. (1986): Stabilization of bottom hole temperature with finite circulation time and fluid flow. Geophys. J. of the Royal Astr. Soc., v86, no. 1, p63-90.

Smith, L. and Chapman, D. S. (1982): On the thermal effects of groundwater flow 1. Regional scale systems. J. of Geophys. Res., v88, no. B1, p593-608.

Stewart. G. (2011): Well test design and analysis. PennWell., USA, 1081p.

Vasseur, G., Gable, R., Feugra, B. and Bienfait, G. (1991): Groundwater flow and heat flow in an area of mineral springs. Geothermics, v20, no. 3, p99-117.

Vasseur, G., Brigaud, F. and Demongodin, L. (1995): Thermal conductivity estimation in sedimentary basins. Tectonophys., v244, p167-174.

Vaught, T. L. (1980): Temperature gradients in a portion of Michigan: A review of the usefulness of data from the AAPG geothermal survey of North America. US Department of Energy Report DOE/NV/10072-1, 39p.

Whittaker, S.G., Marsh, A., Bend, S. and Rostron, B.J. (2009): Saskatchewan Phanerozoic fluids and petroleum systems assessment project. *In*: Summary of Investigations 2009, Volume 1, Saskatchewan Geological Survey, Sask. Ministry of Energy and Resources, Misc. Rep. 2009-4.1, Paper A-1, 3p, URL <http://er.gov.sk.ca/adx/aspx/adxGetMedia.aspx?DocID=11859,11858,11458,11455,11228,3385,5460,2936,Documents&MediaID=36780&Filename=whittaker.pdf>.

Wright, G. N., McMechan, M. E. and Potter, D. E. G. (1994): Chapter 3 - Structure and architecture of the Western Canada sedimentary basin. *In*: Mossop, G. and Shetsen, I. (comps.), Geological atlas of the Western Canada Sedimentary Basin, Can. Soc. Petrol. Geol./Alberta Res. Counc., p25-40.

Appendix A. Strata specific temperature maps

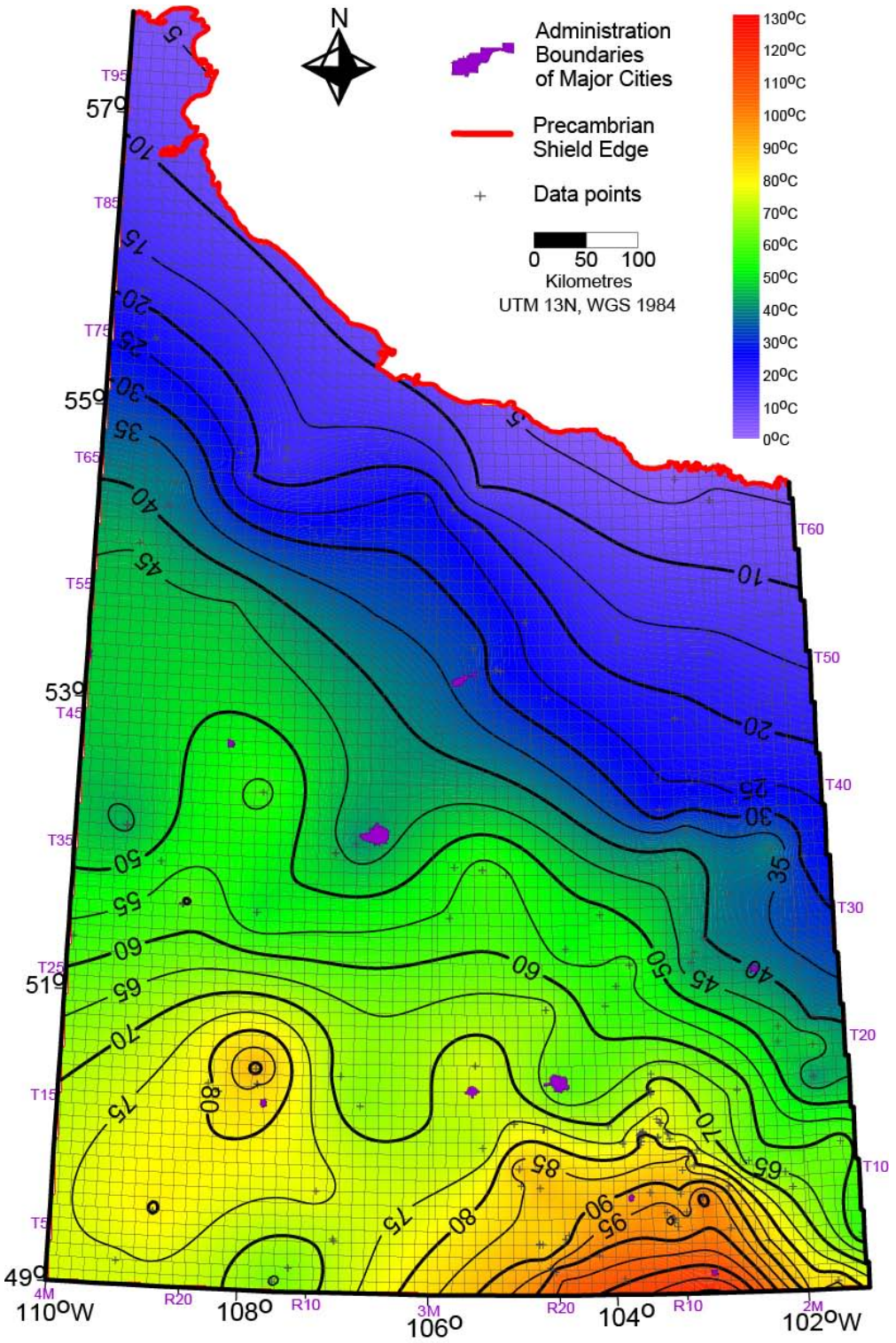

Figure A.1. Precambrian temperature map. R, M, T marks location (Range, Meridian, Township) defined in the Dominion Land Survey system (in the grid). Contour interval (CI): 5 °C.

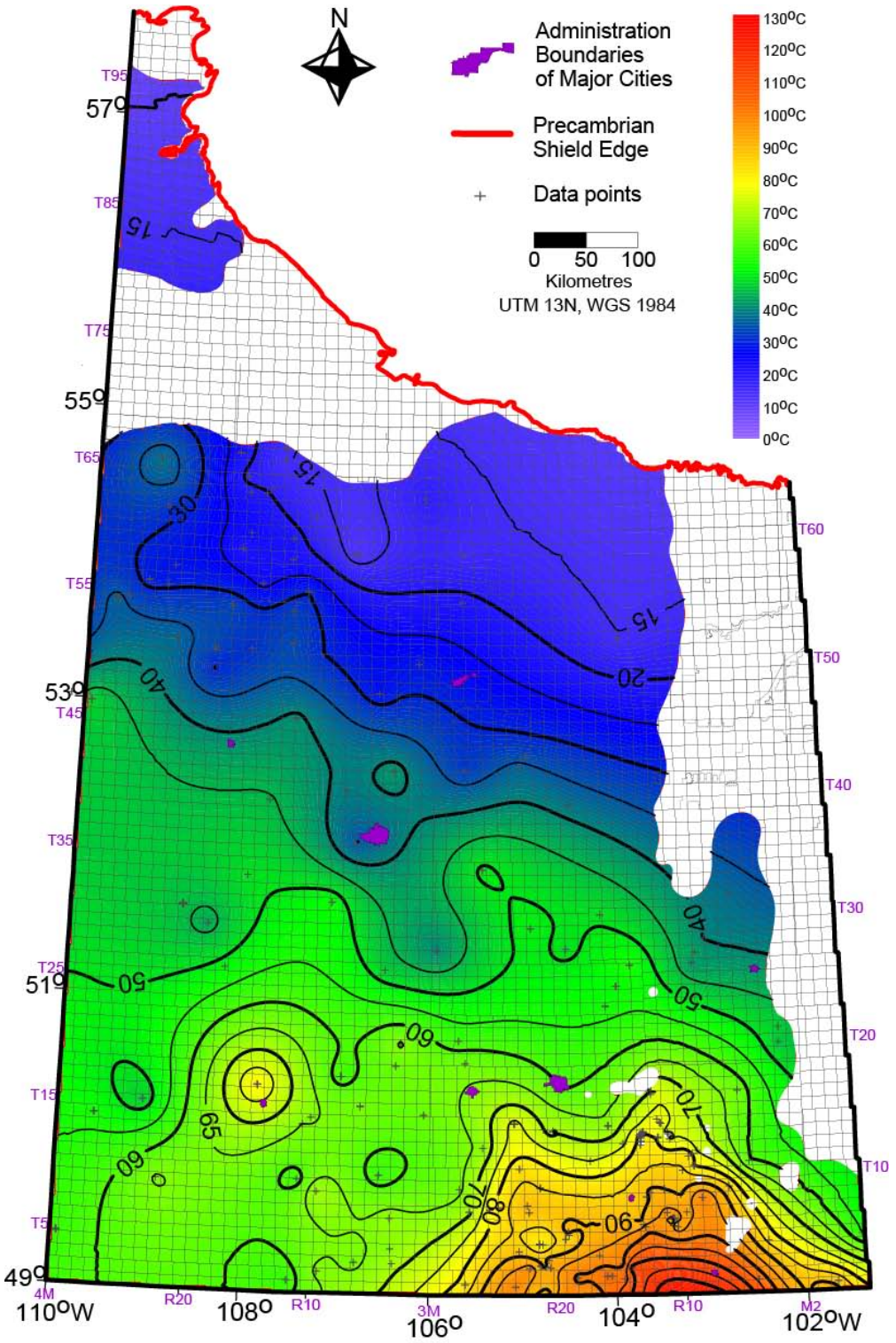

Figure A.2. Deadwood temperature map. CI: 5 °C. Blank areas represent areas where the formation is not present.

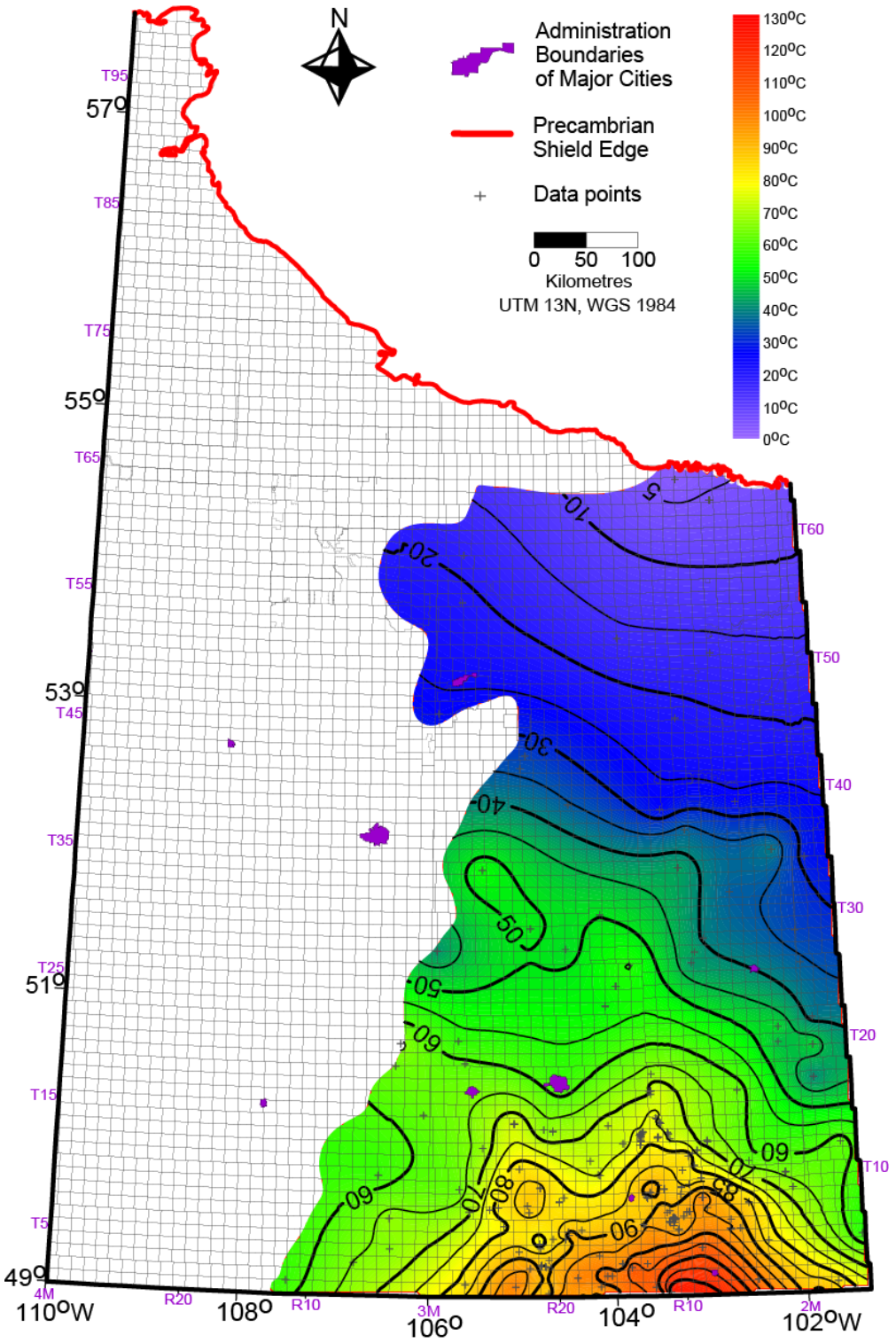

Figure A.3 Winnipeg temperature map. CI: 5 °C. Blank areas represent areas where the formation is not present.

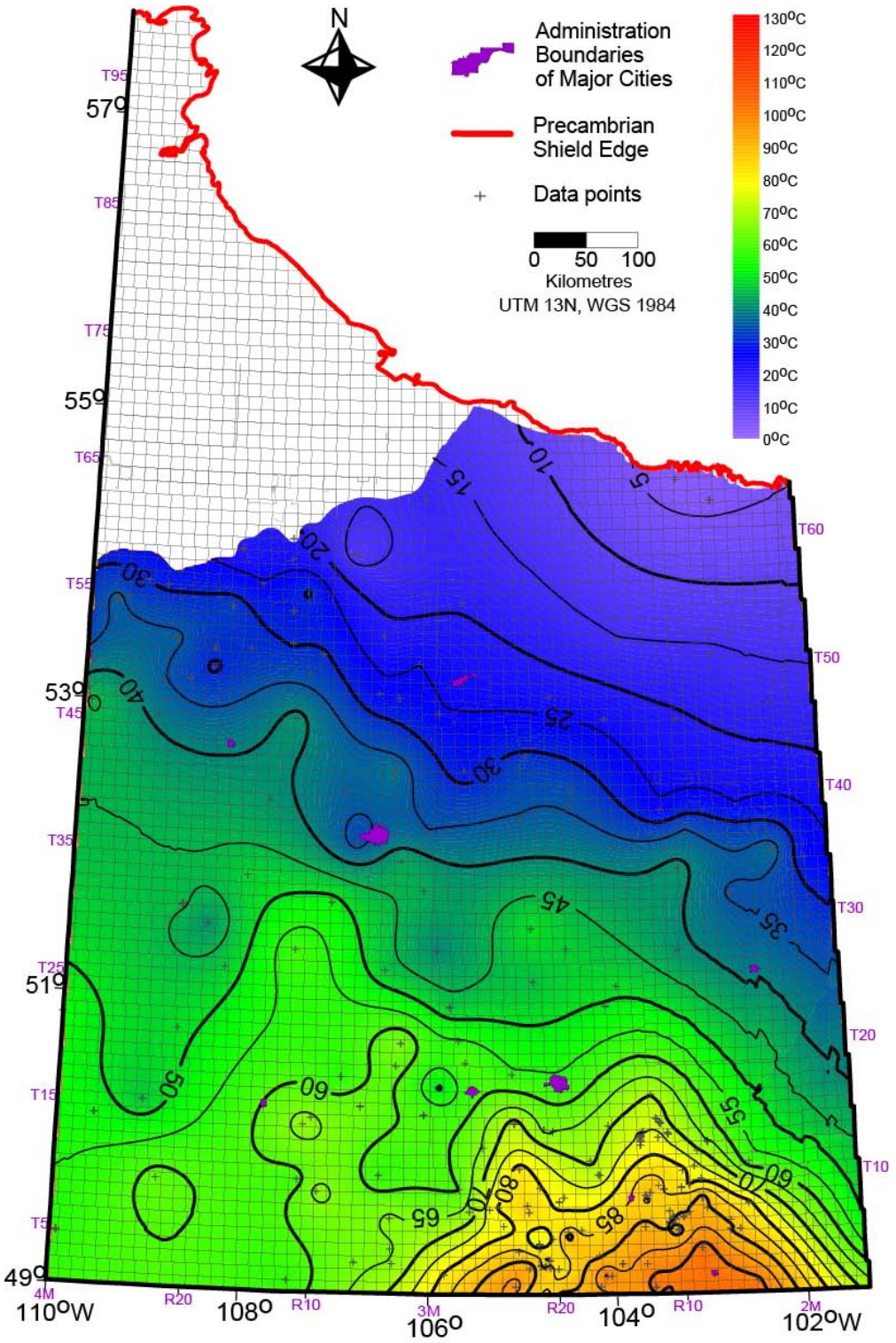

Figure A.4. Red River temperature map. CI: 5 °C. Blank areas represent areas where the formation is not present.

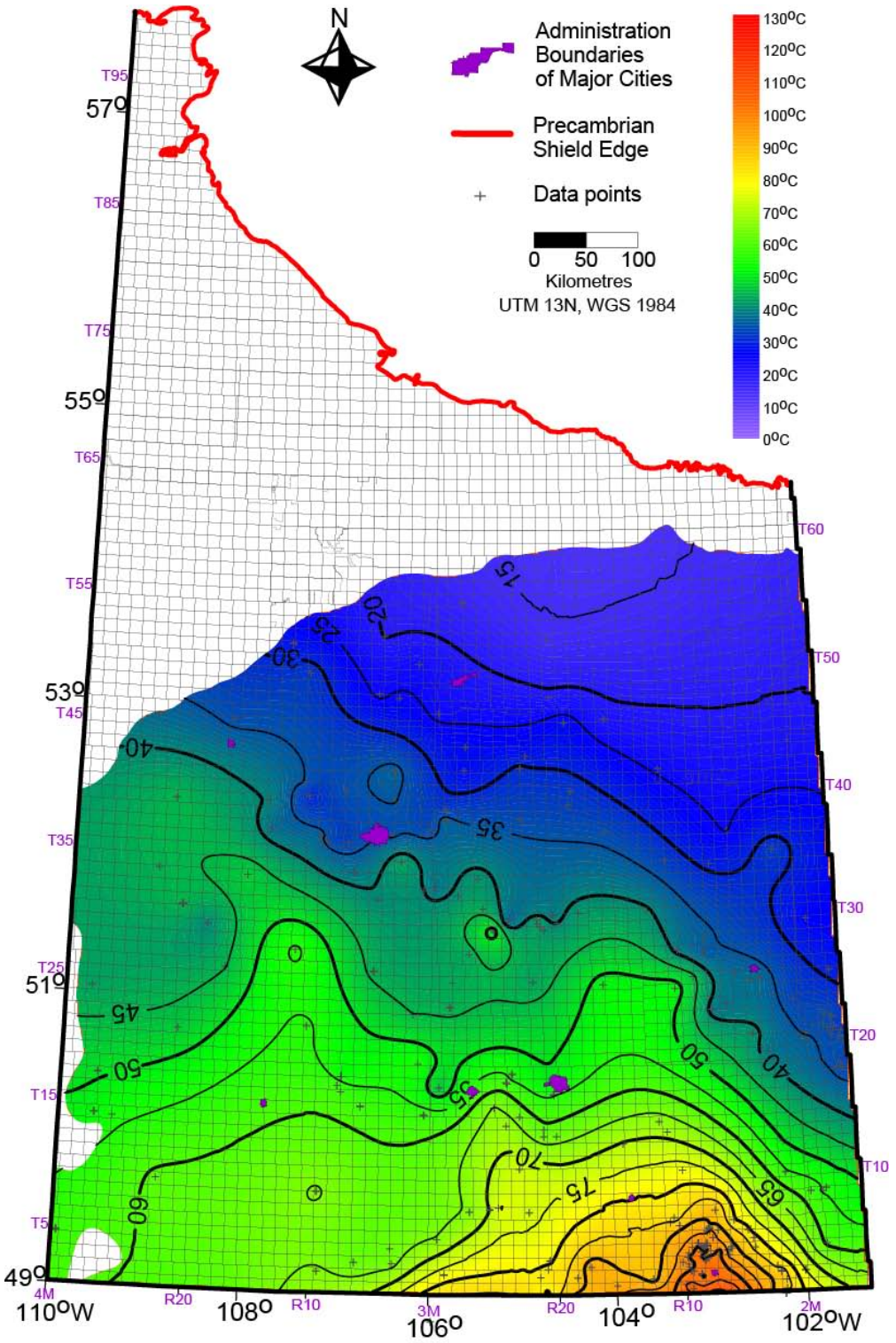

Figure A.5. Interlake temperature map. CI: 5 °C. Blank areas represent areas where the formation is not present.

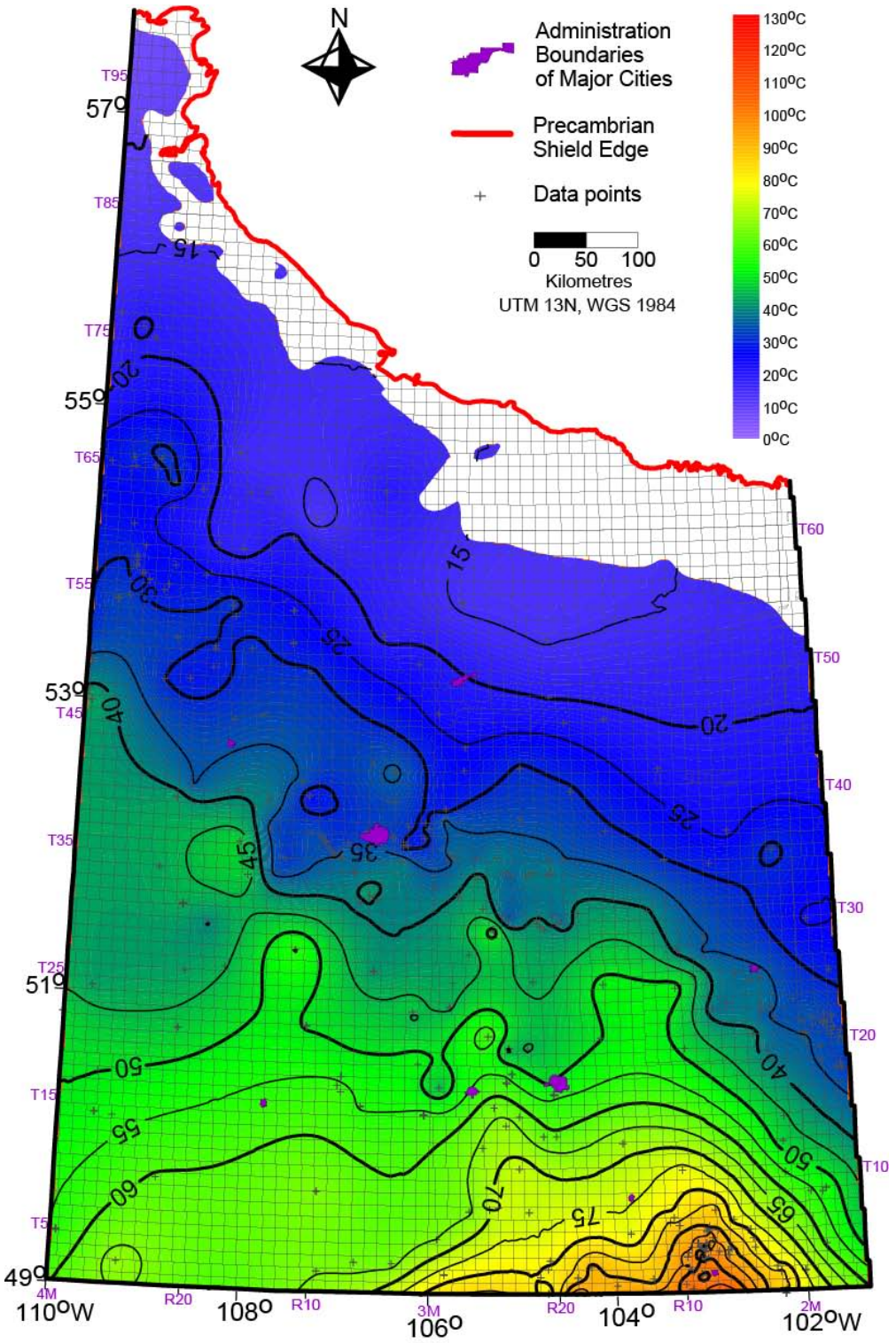

Figure A.6. Winnipegosis temperature map. CI: 5 °C. Blank areas represent areas where the formation is not present.

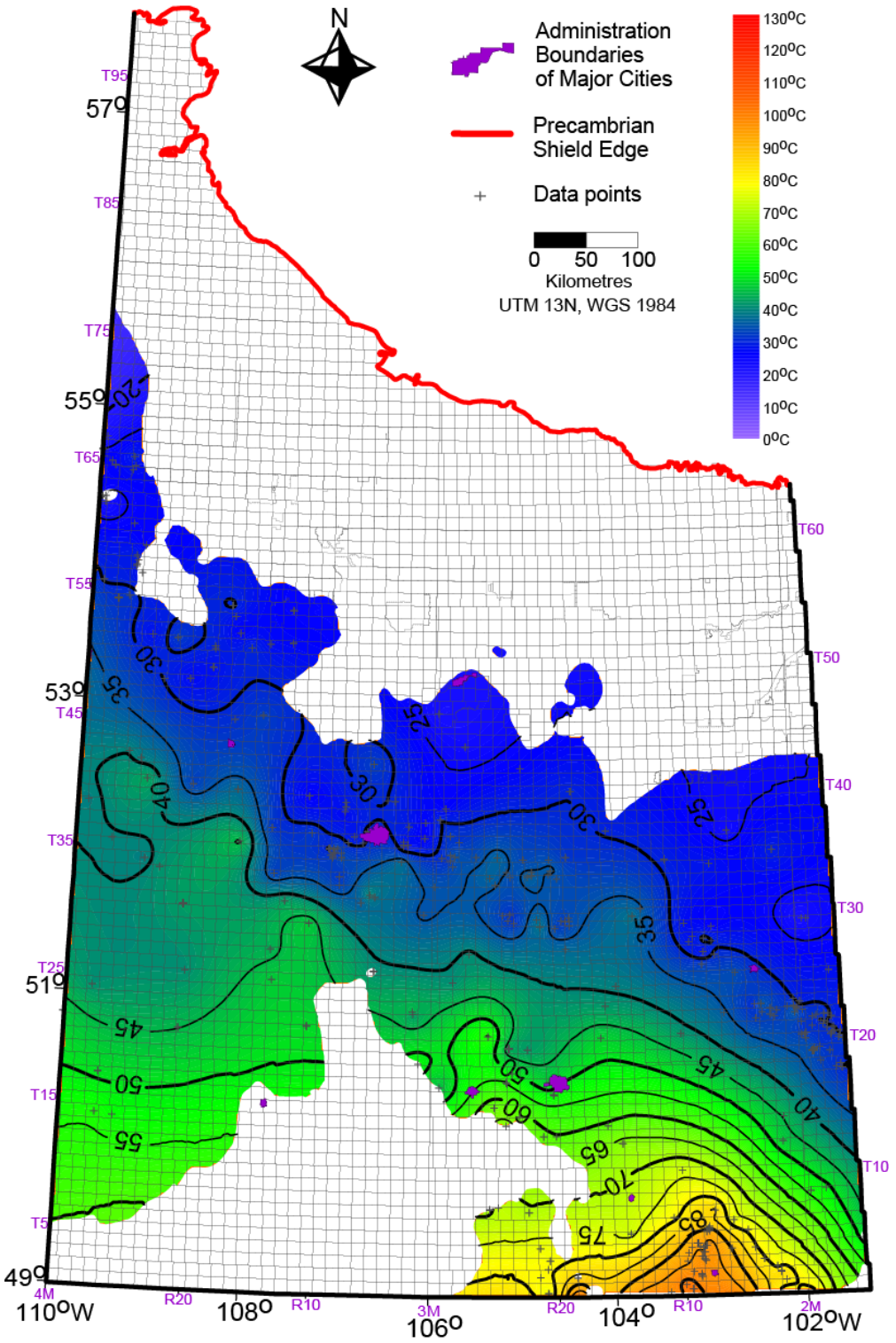

Figure A.7. Prairie temperature map. CI: 5 °C. Blank areas represent areas where the formation is not present.

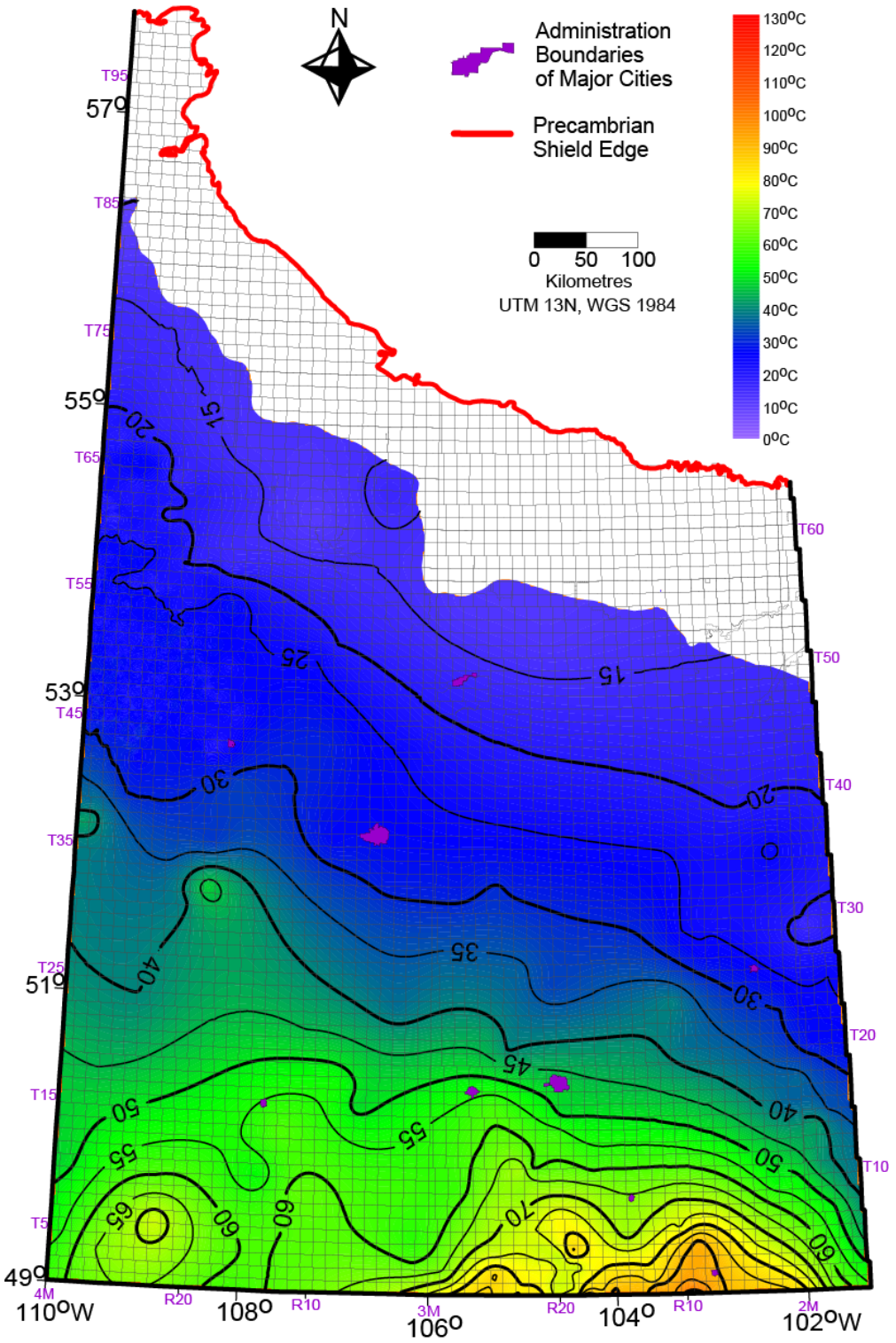

Figure A.8.a Souris River temperature map. Data distribution would obscure features thus shown on a separate map, following this. CI: 5 °C. Blank areas represent areas where the formation is not present.

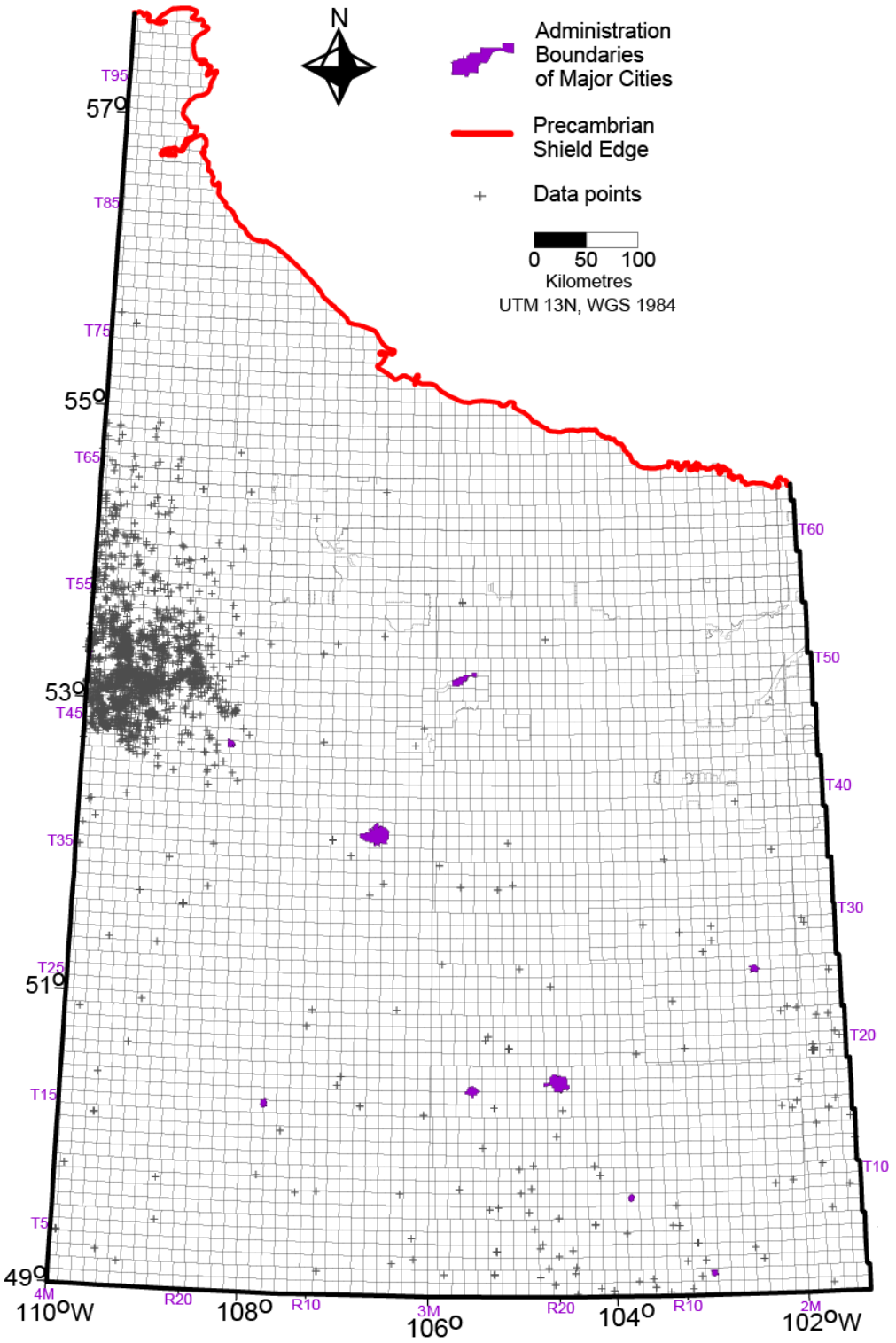

Figure A.8.b Souris River data distribution map.

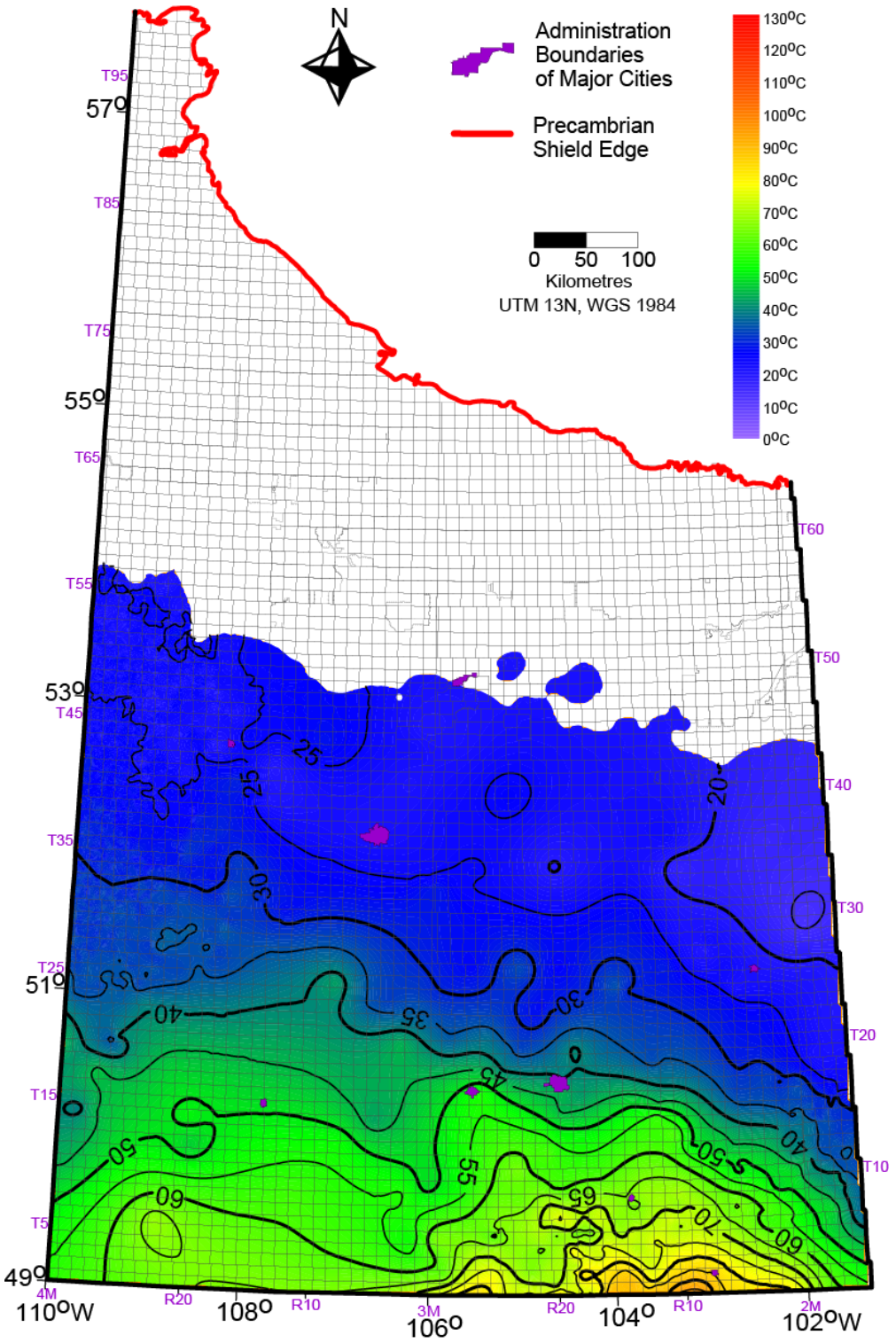

Figure A.9.a Duperow temperature map. Data distribution would obscure features thus shown on a separate map, following this. CI: 5 °C. Blank areas represent areas where the formation is not present.

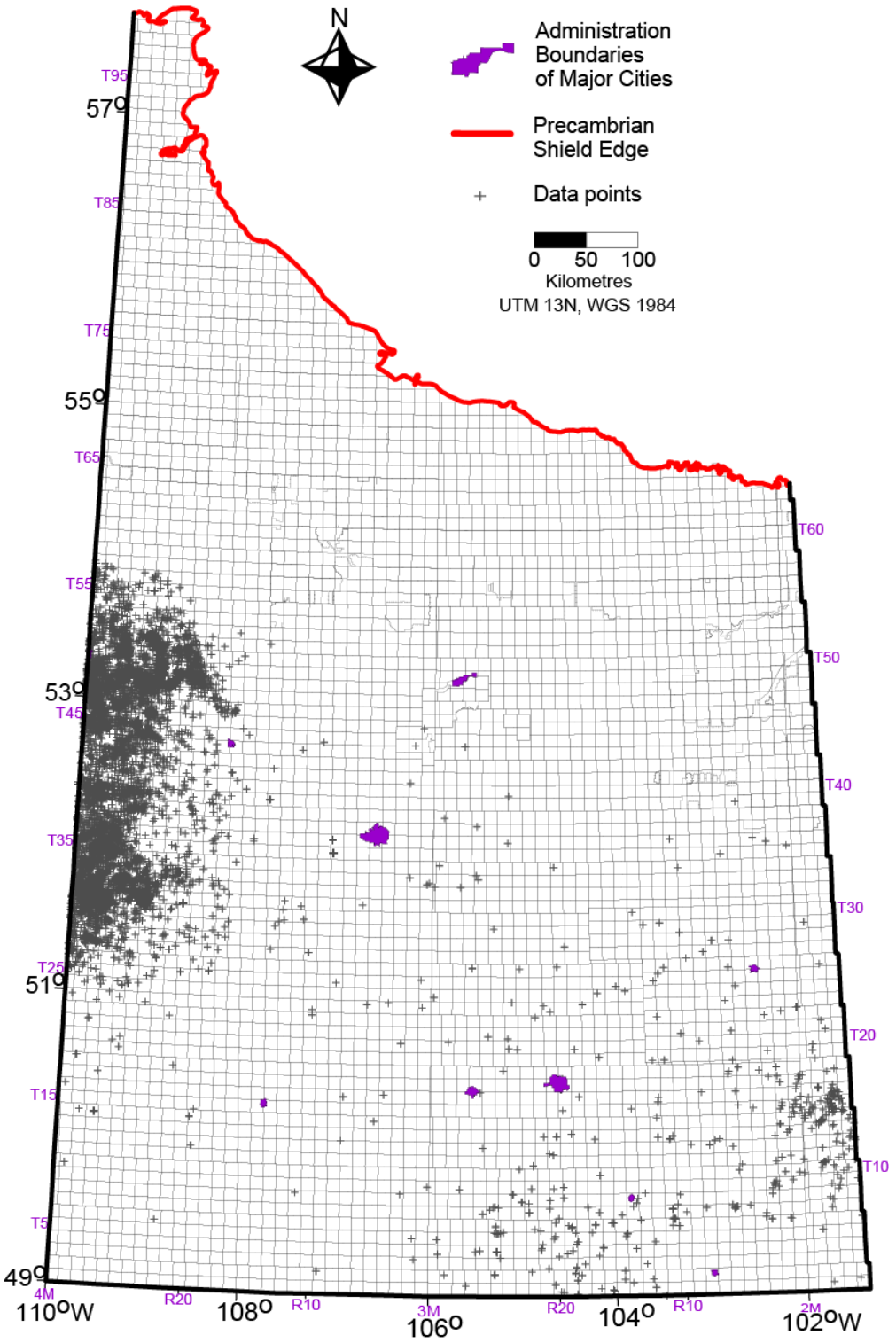

Figure A.9.b Duperow data distribution map.

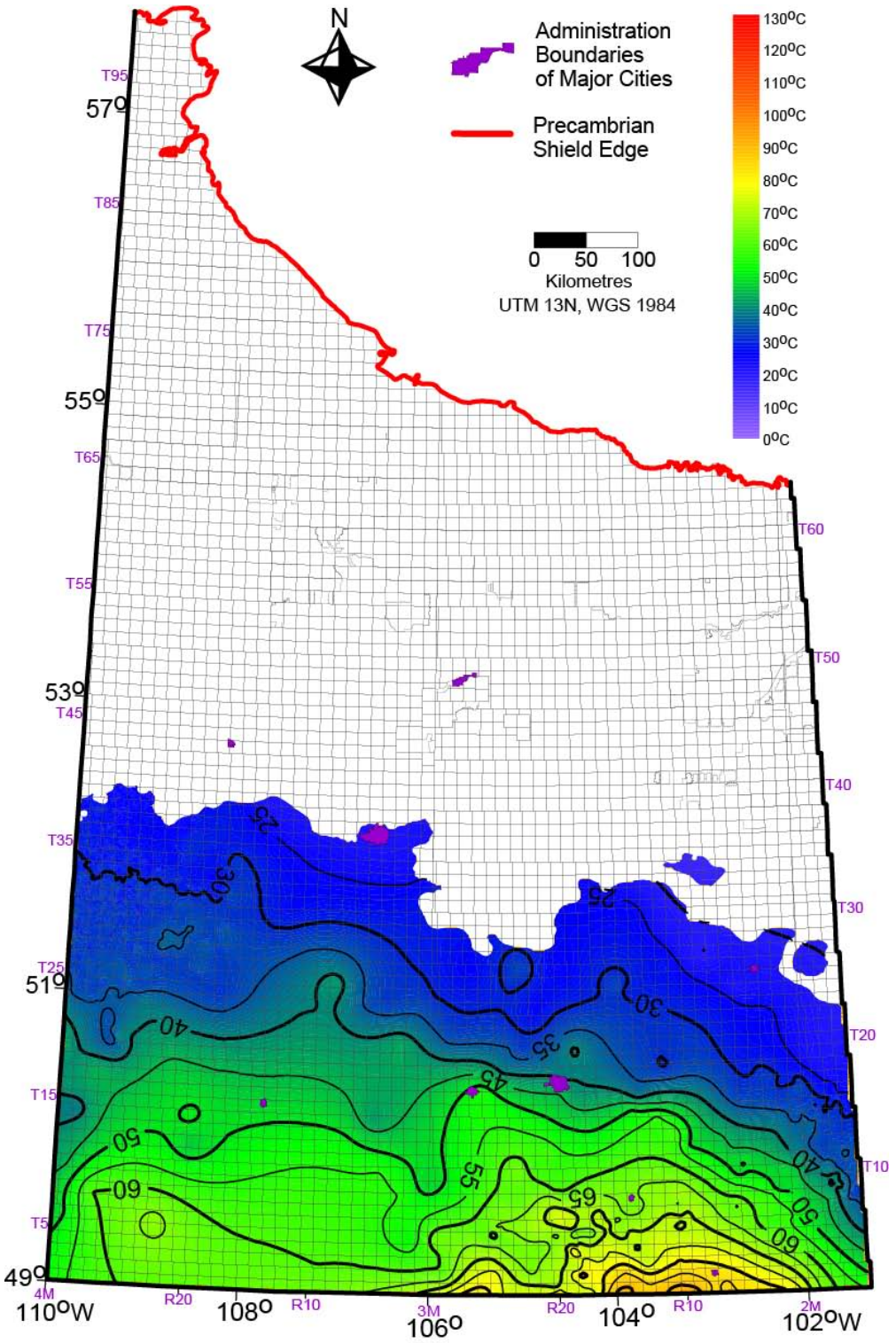

Figure A.10.a Birdbear temperature map. Data distribution would obscure features thus shown on a separate map, following this. CI: 5 °C. Blank areas represent areas where the formation is not present.

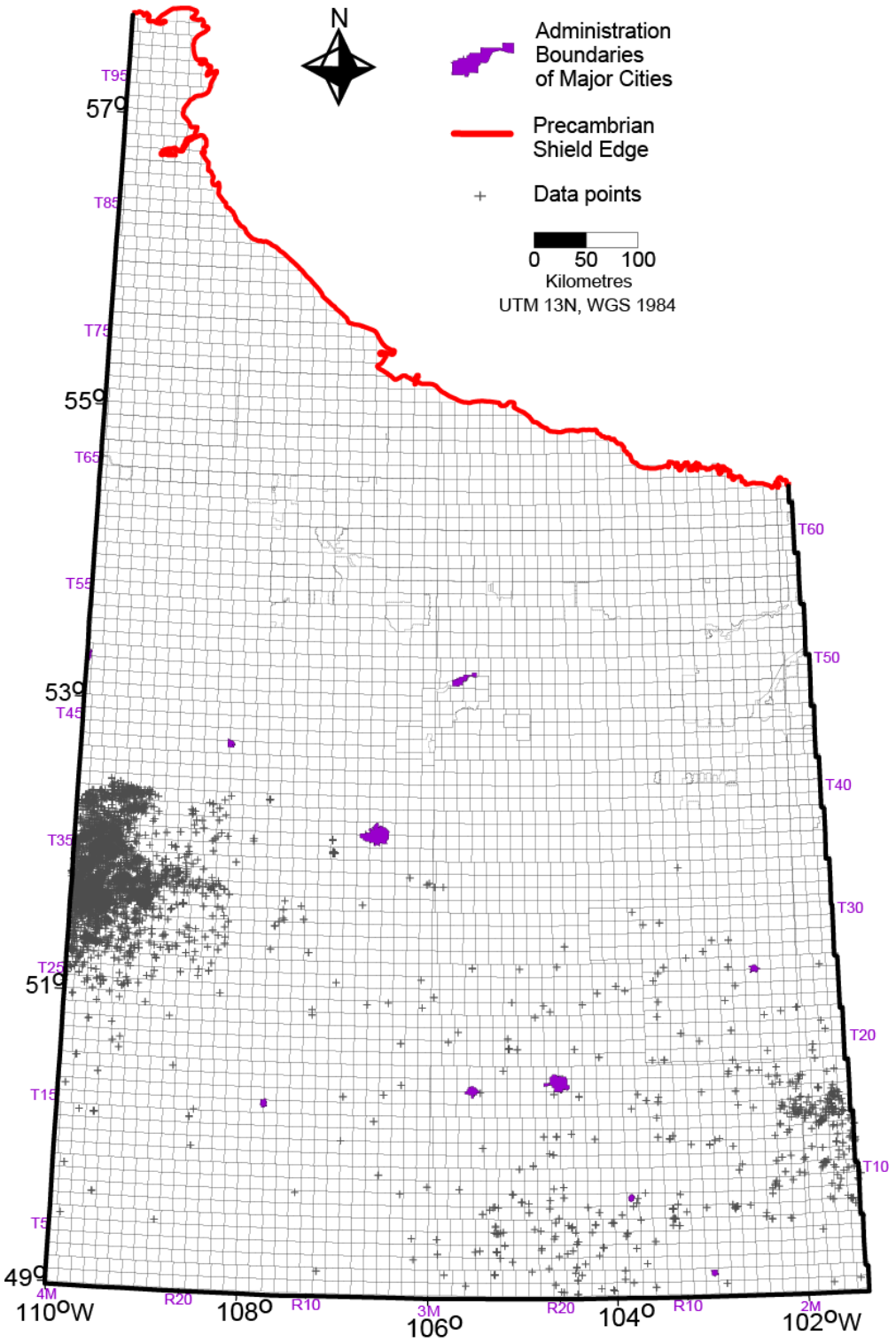

Figure A.10.b Birdbear data distribution map.

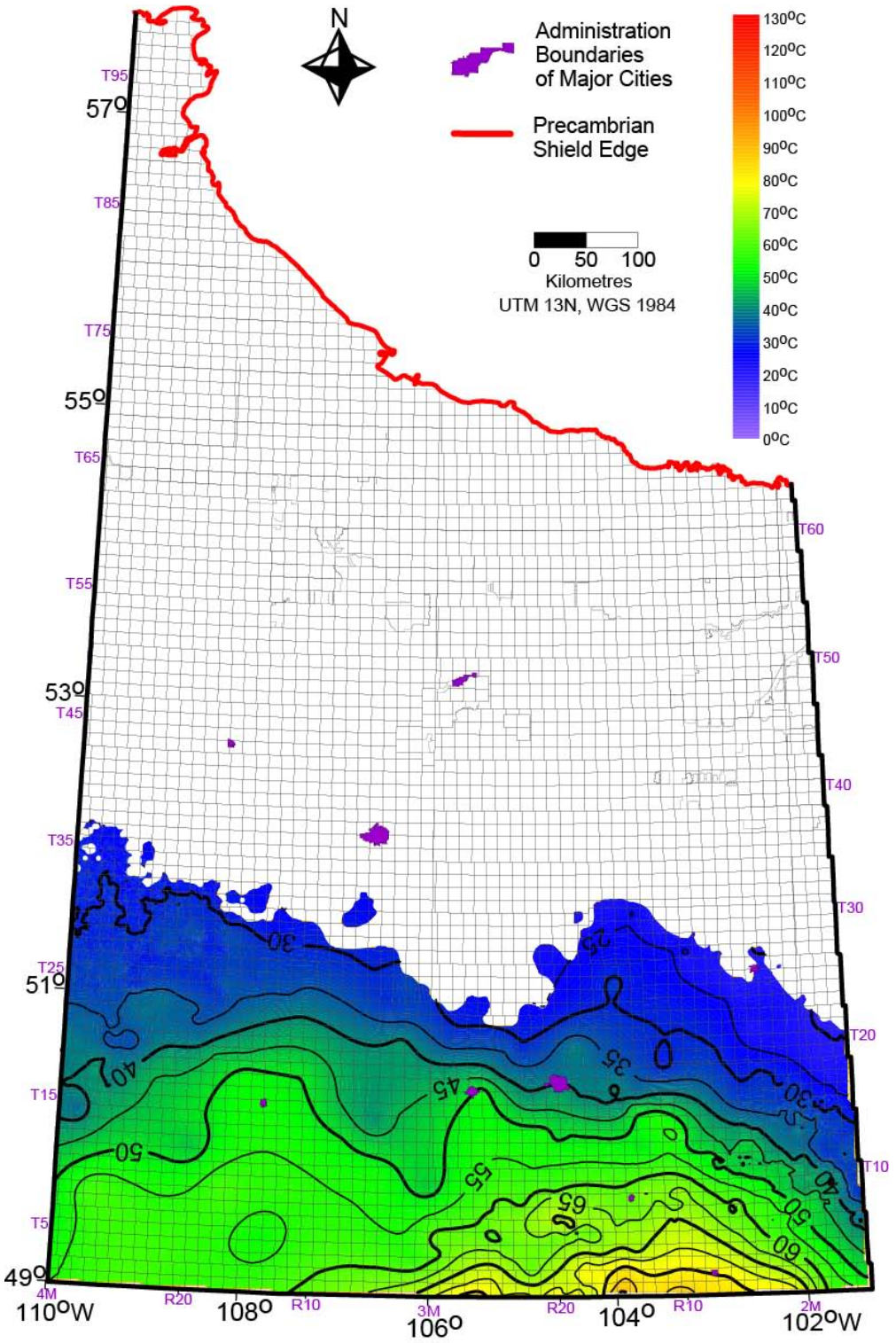

Figure A.11.a Bakken temperature map. Data distribution would obscure features thus shown on a separate map, following this. CI: 5 °C. Blank areas represent areas where the formation is not present.

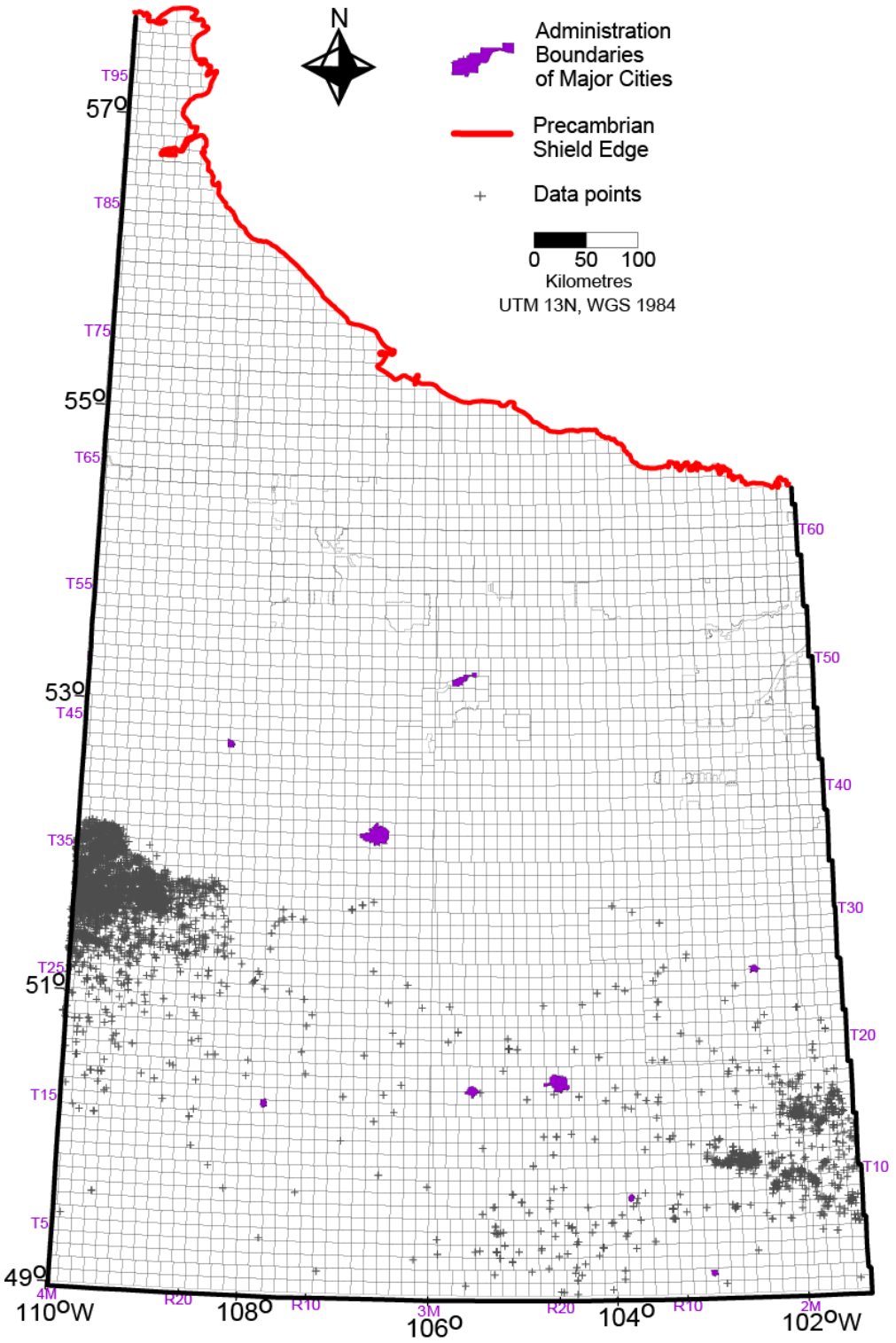

Figure A.11.b Bakken data distribution map.

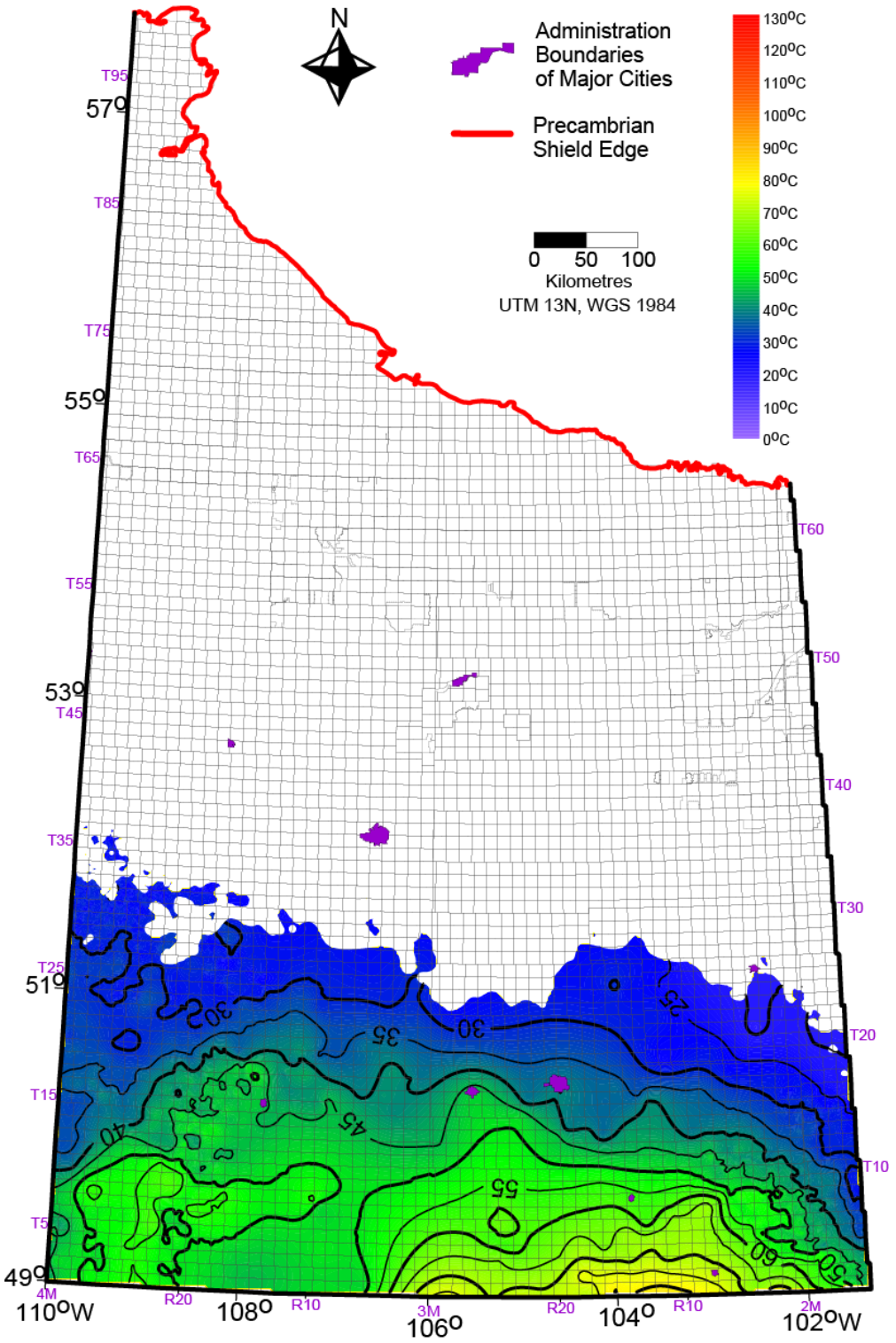

Figure A.12.a Lodgepole temperature map. Data distribution would obscure features thus shown on a separate map, following this. CI: 5 °C. Blank areas represent areas where the formation is not present.

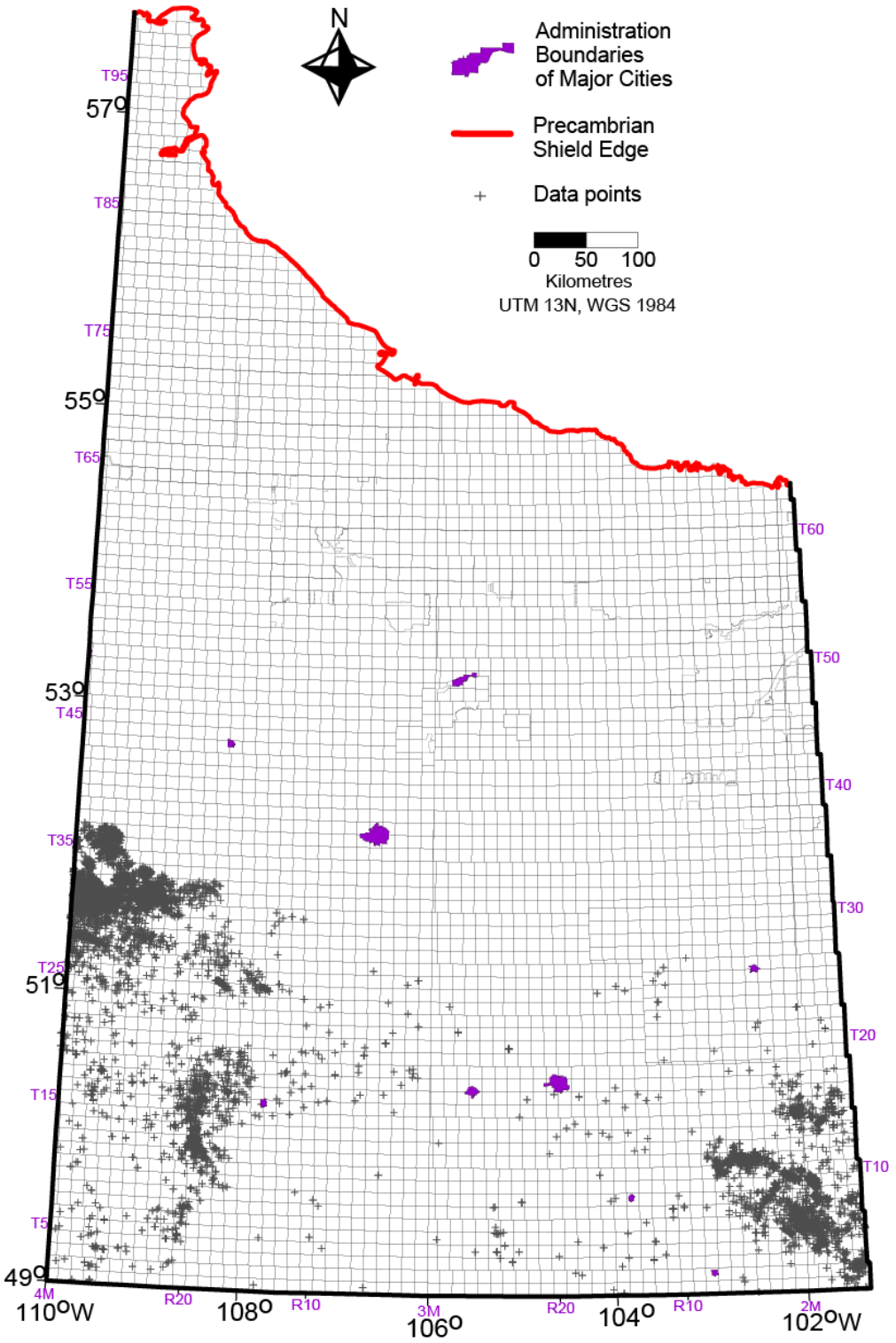

Figure A.12.b Lodgepole data distribution map.

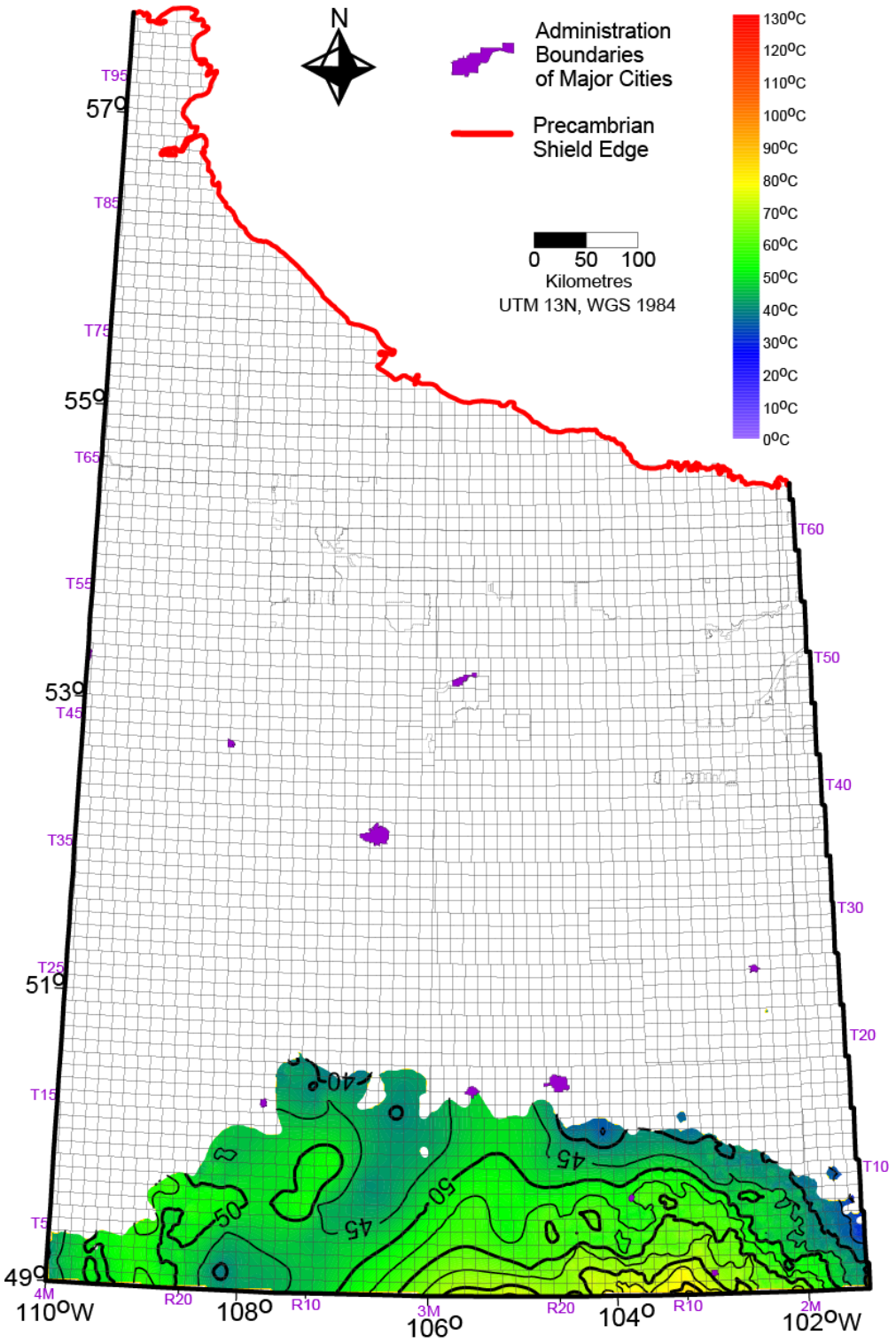

Figure A.13.a Mission Canyon temperature map. Data distribution would obscure features thus shown on a separate map, following this. CI: 5 °C. Blank areas represent areas where the formation is not present.

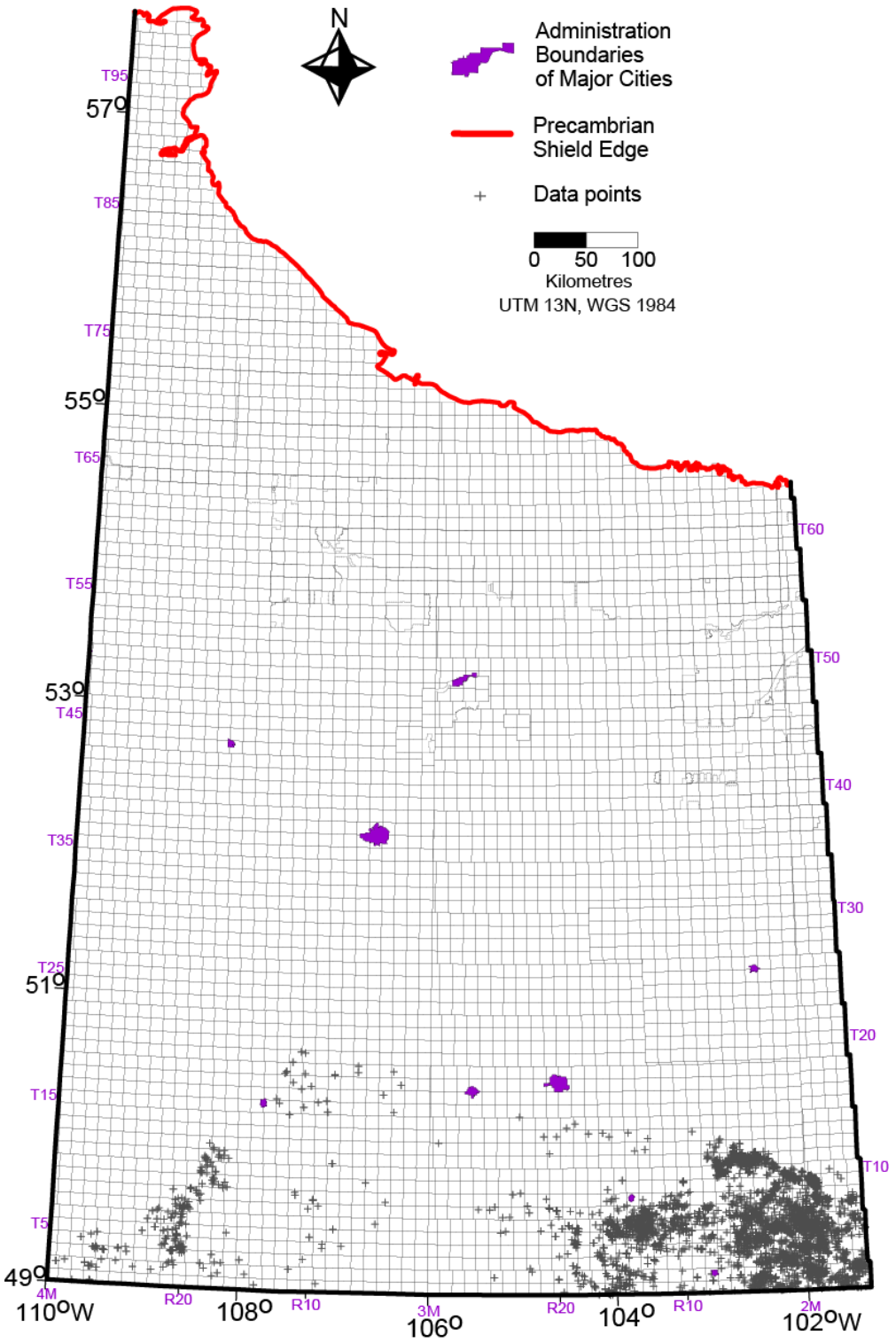

Figure A.13.b Mission Canyon data distribution map.

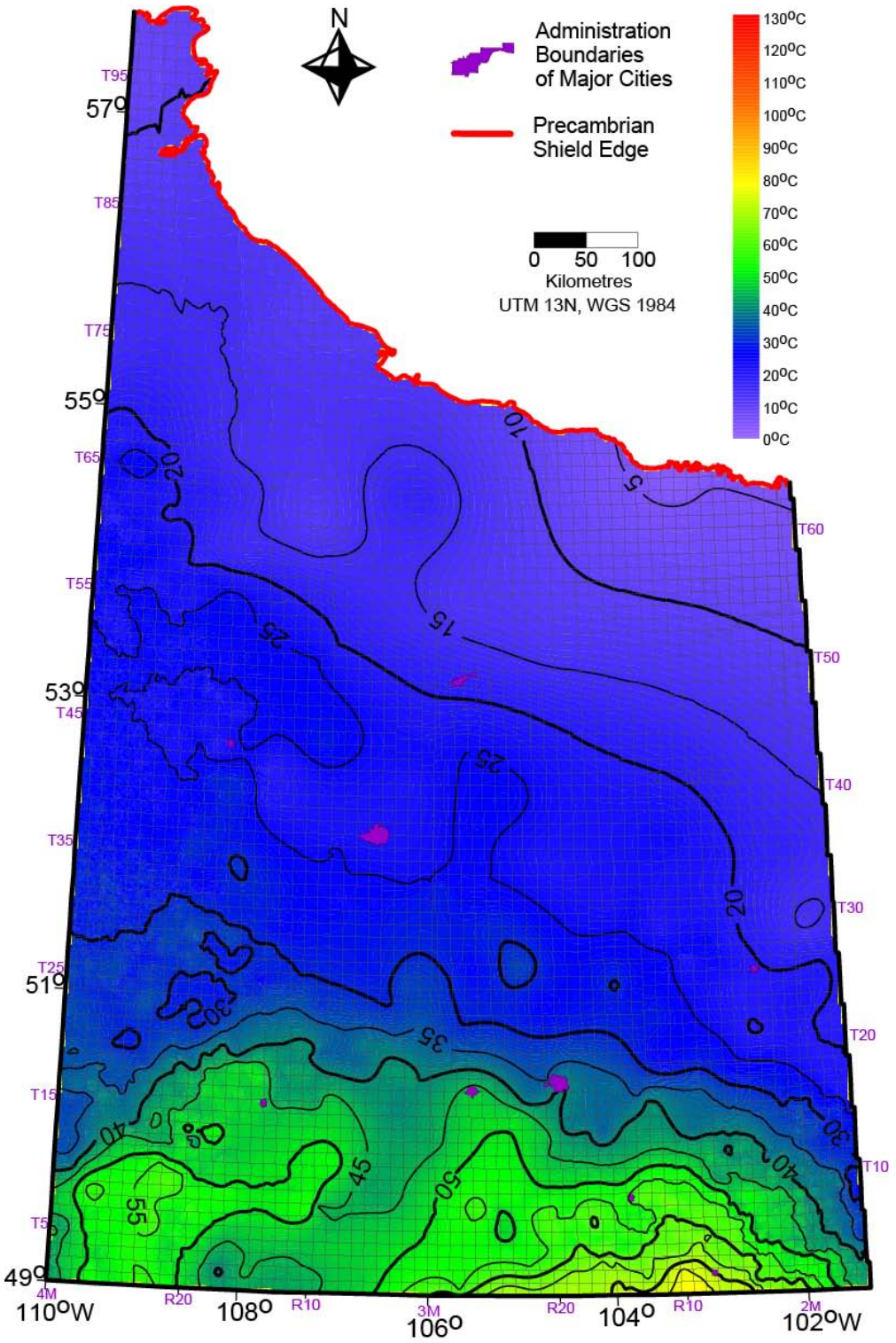

Figure A.14.a Sub-Mesozoic unconformity temperature map. Data distribution would obscure features thus shown on a separate map, following this. CI: 5 °C.

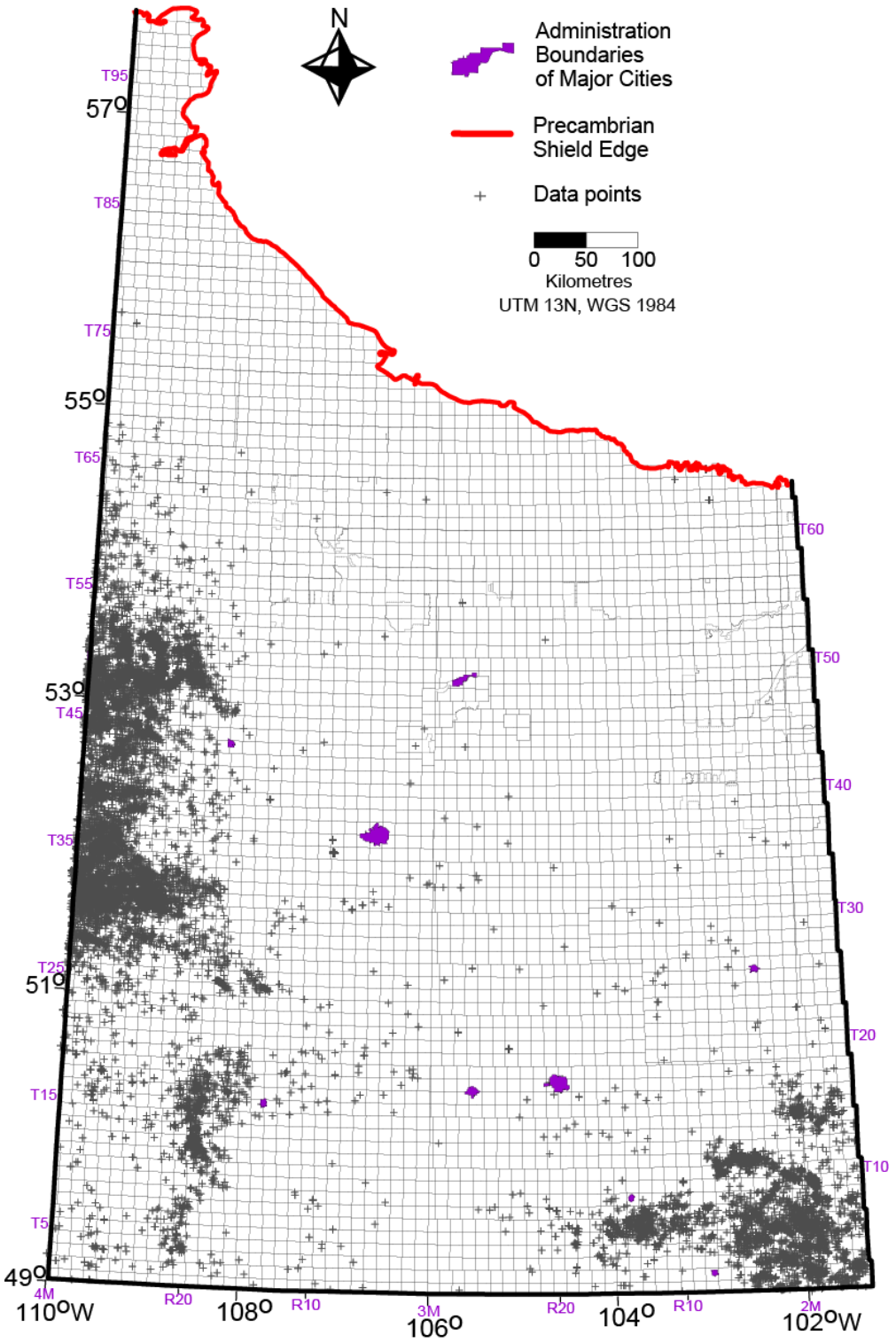

Figure A.14.b Sub-Mesozoic unconformity data distribution map.

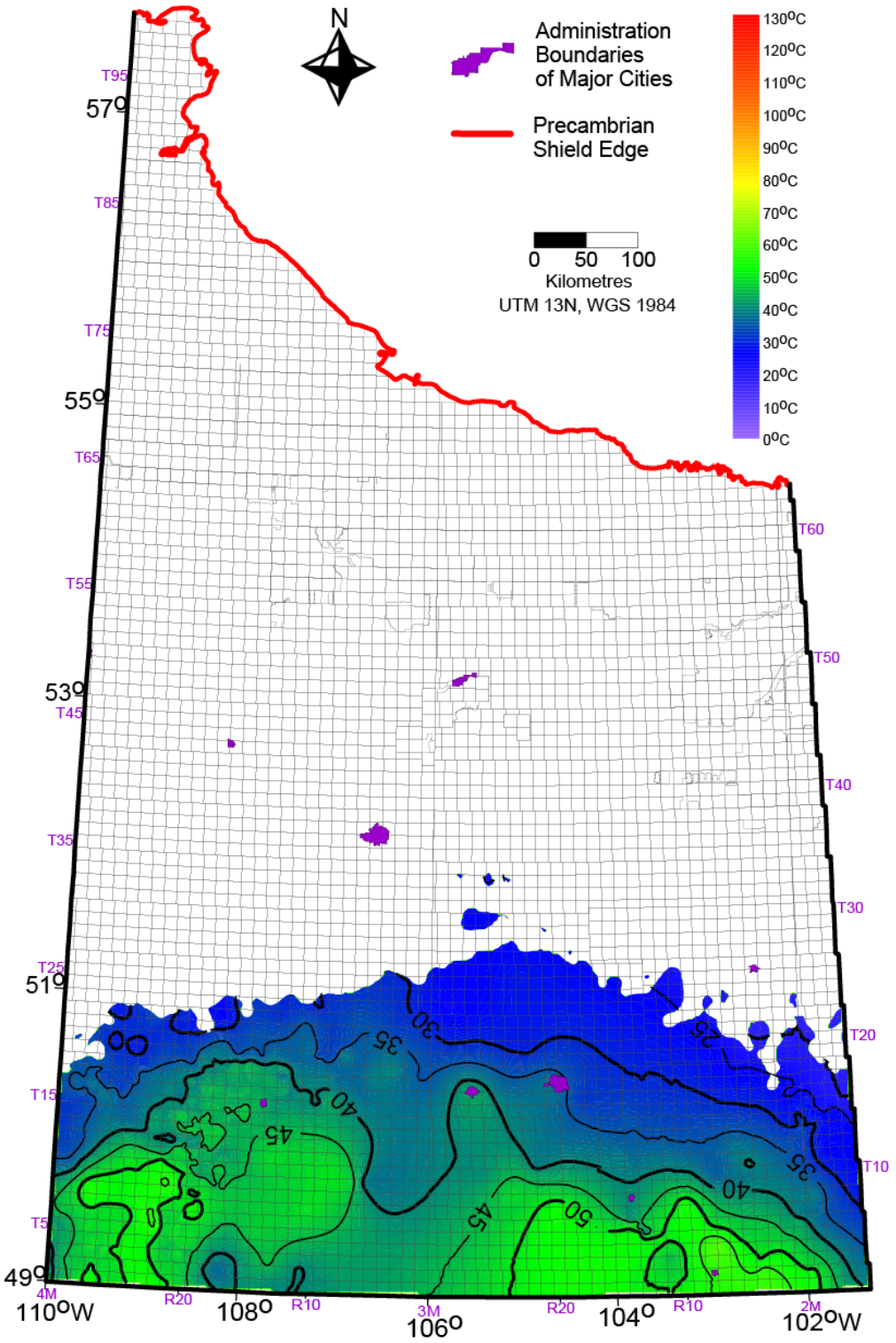

Figure A.15.a Shaunavon temperature map. Data distribution would obscure features thus shown on a separate map, following this. CI: 5 °C. Blank areas represent areas where the formation is not present.

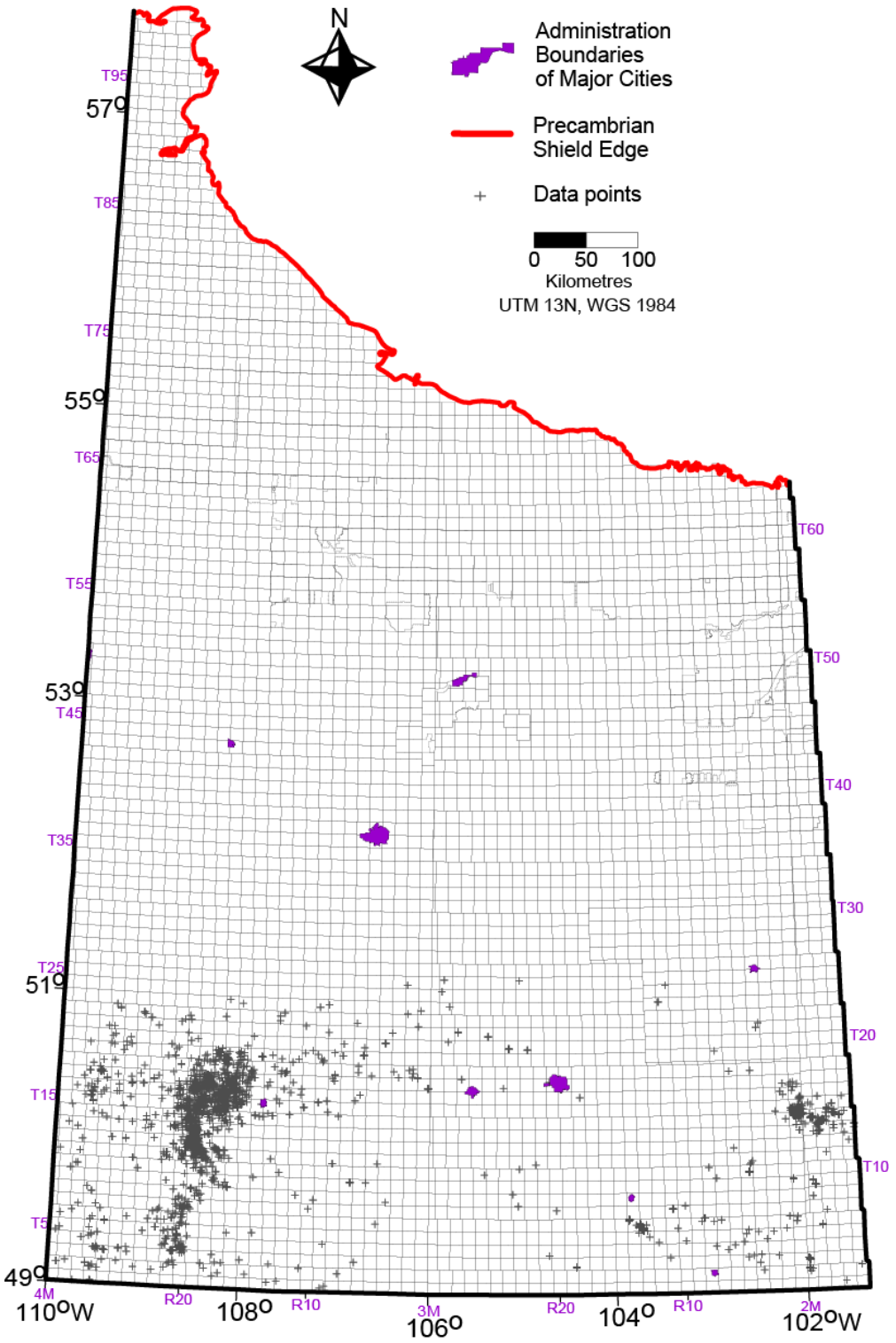

Figure A.15.b Shaunavon data distribution map.

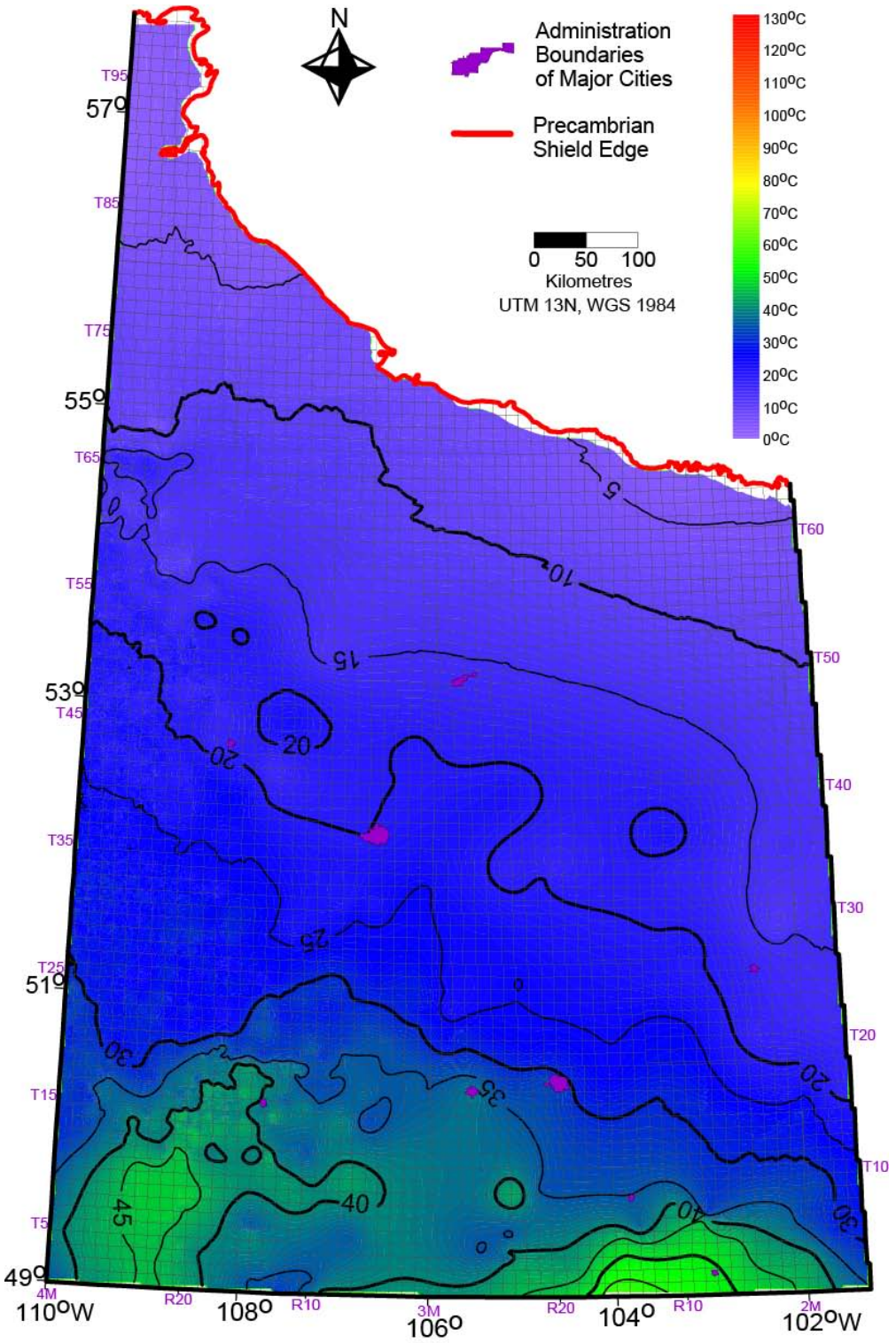

Figure A.16.a Mannville temperature map. Data distribution would obscure features thus shown on a separate map, following this. CI: 5 °C. Blank areas represent areas where the formation is not present.

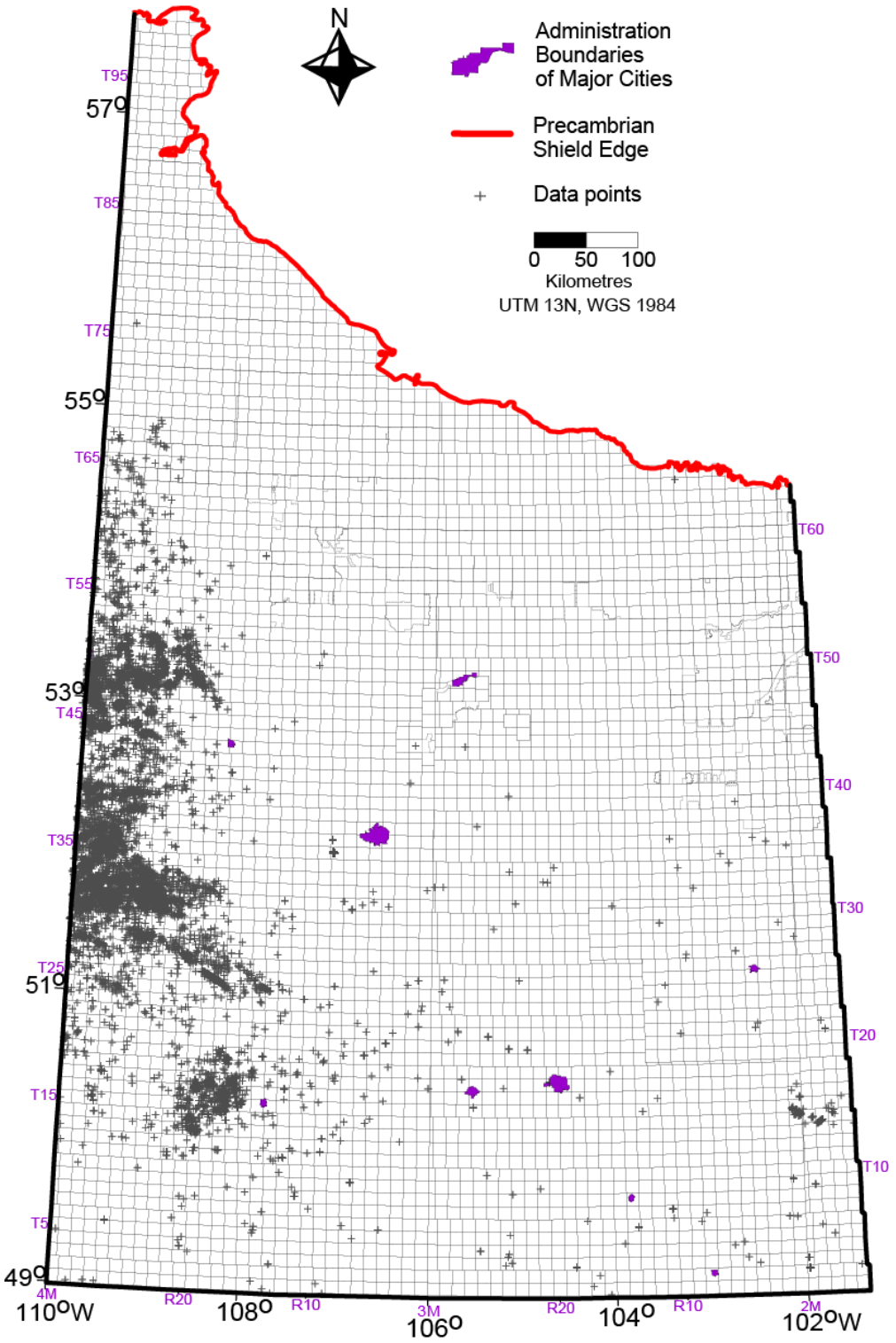

Figure A.16.b Mannville data distribution map.

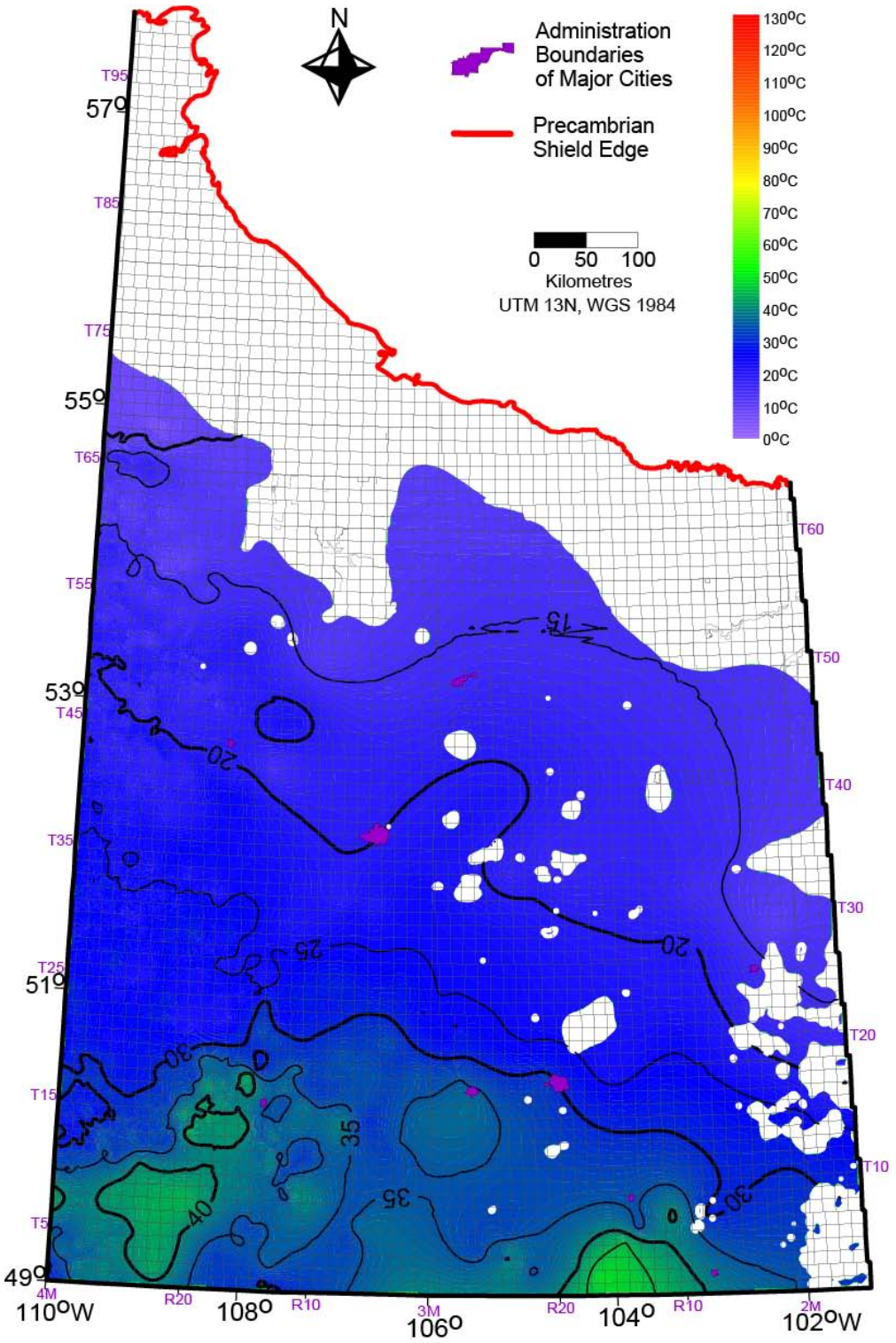

Figure A.17.a Viking temperature map. Data distribution would obscure features thus shown on a separate map, following this. CI: 5 °C. Blank areas represent areas where the formation is not present.

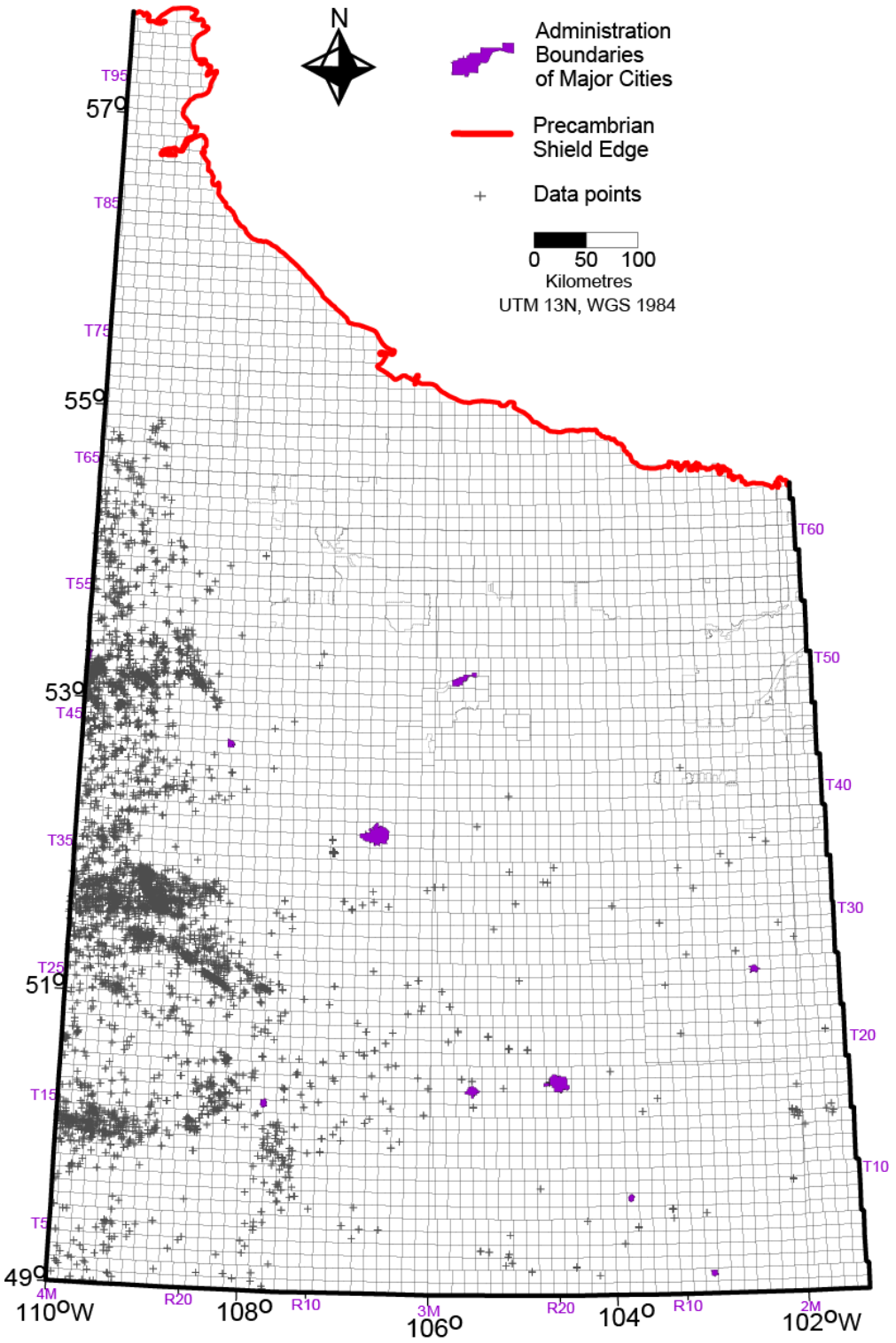

Figure A.17.b Viking data distribution map.

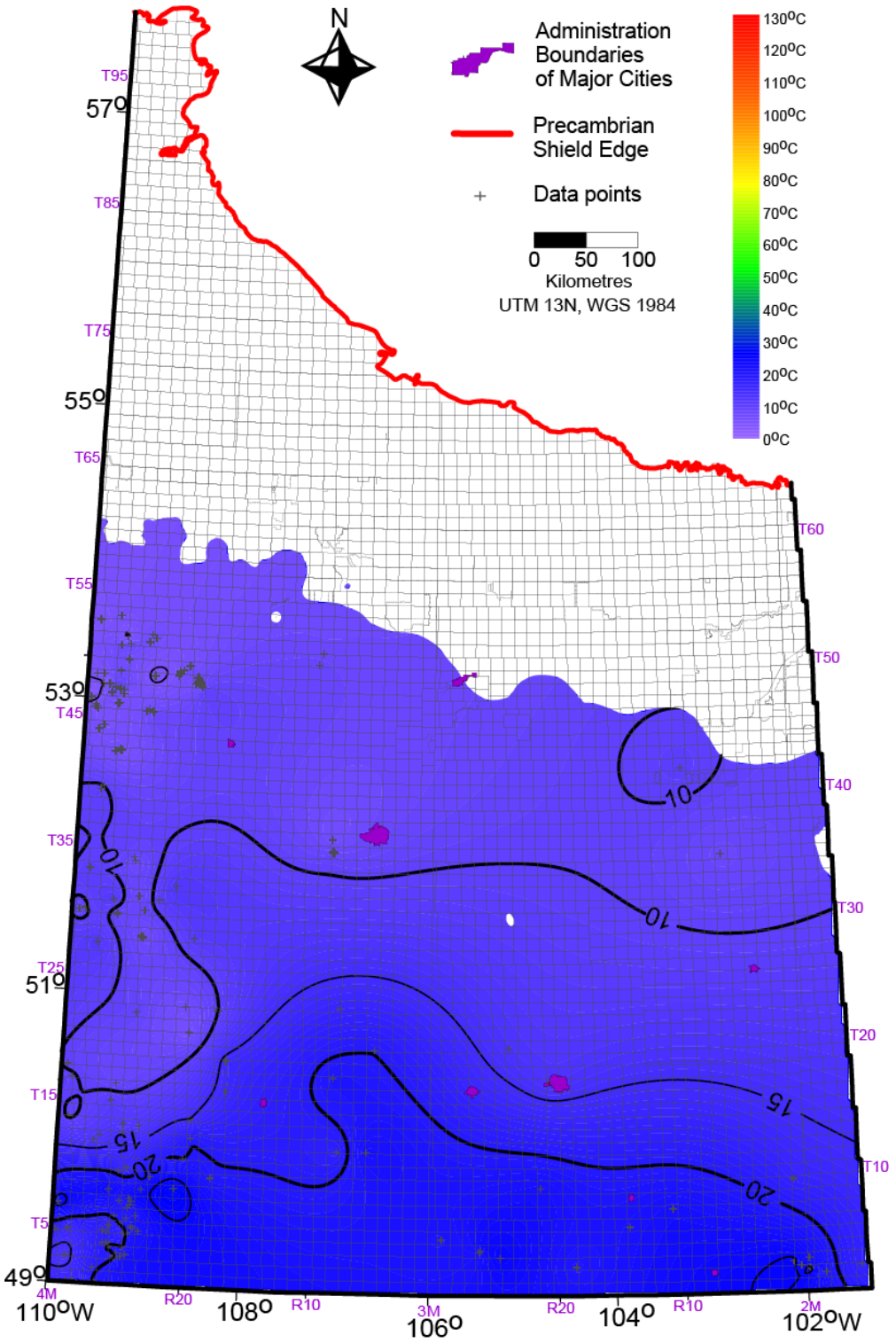

Figure A.18. Lea Park temperature map. CI: 5 °C. Blank areas represent areas where the formation is not present.

Appendix B. Elevation specific temperature maps

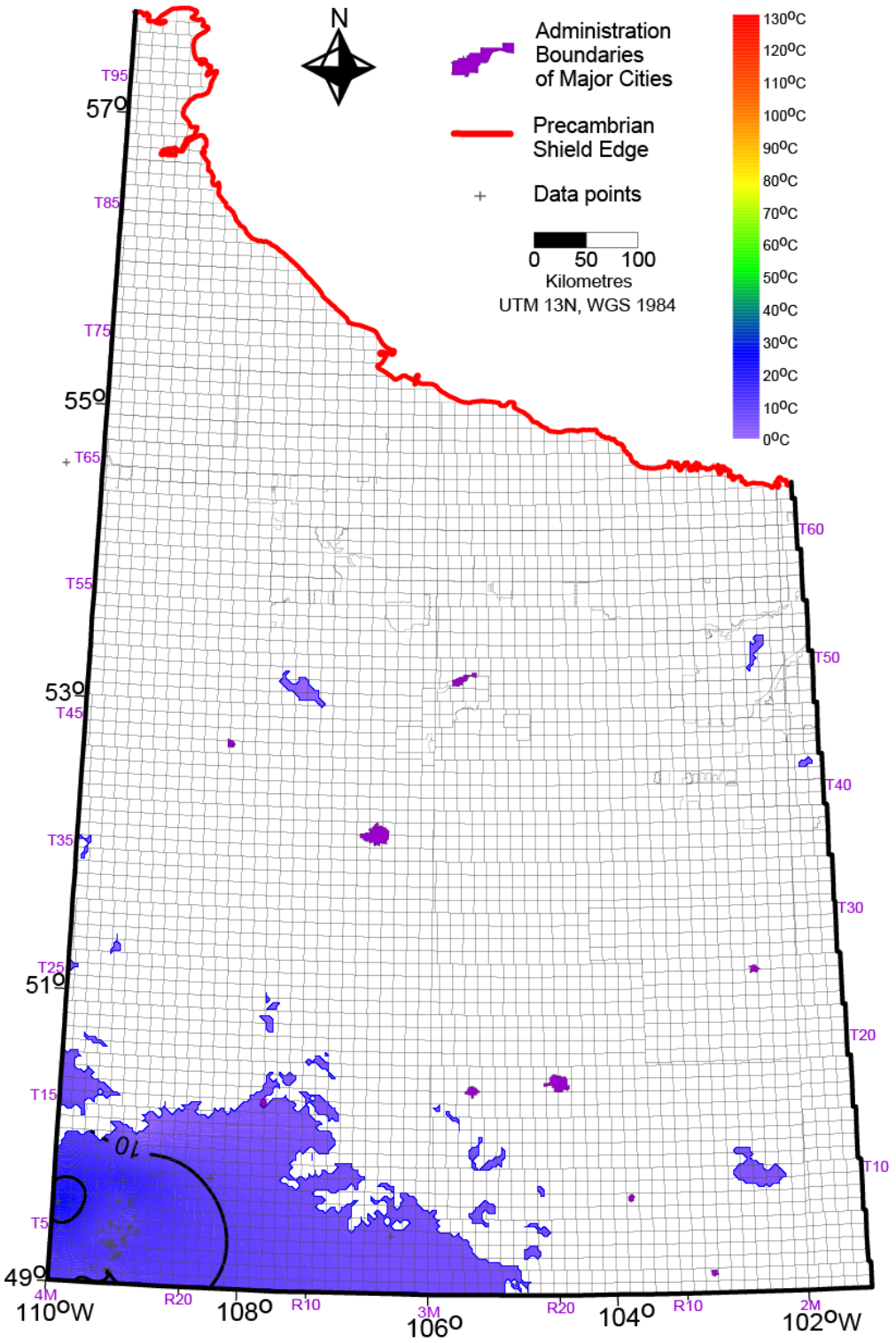

Figure B.1 Temperature at 750 masl (metres above sea level). Area bounded by the topographic contour line 750 masl. CI: 5 °C.

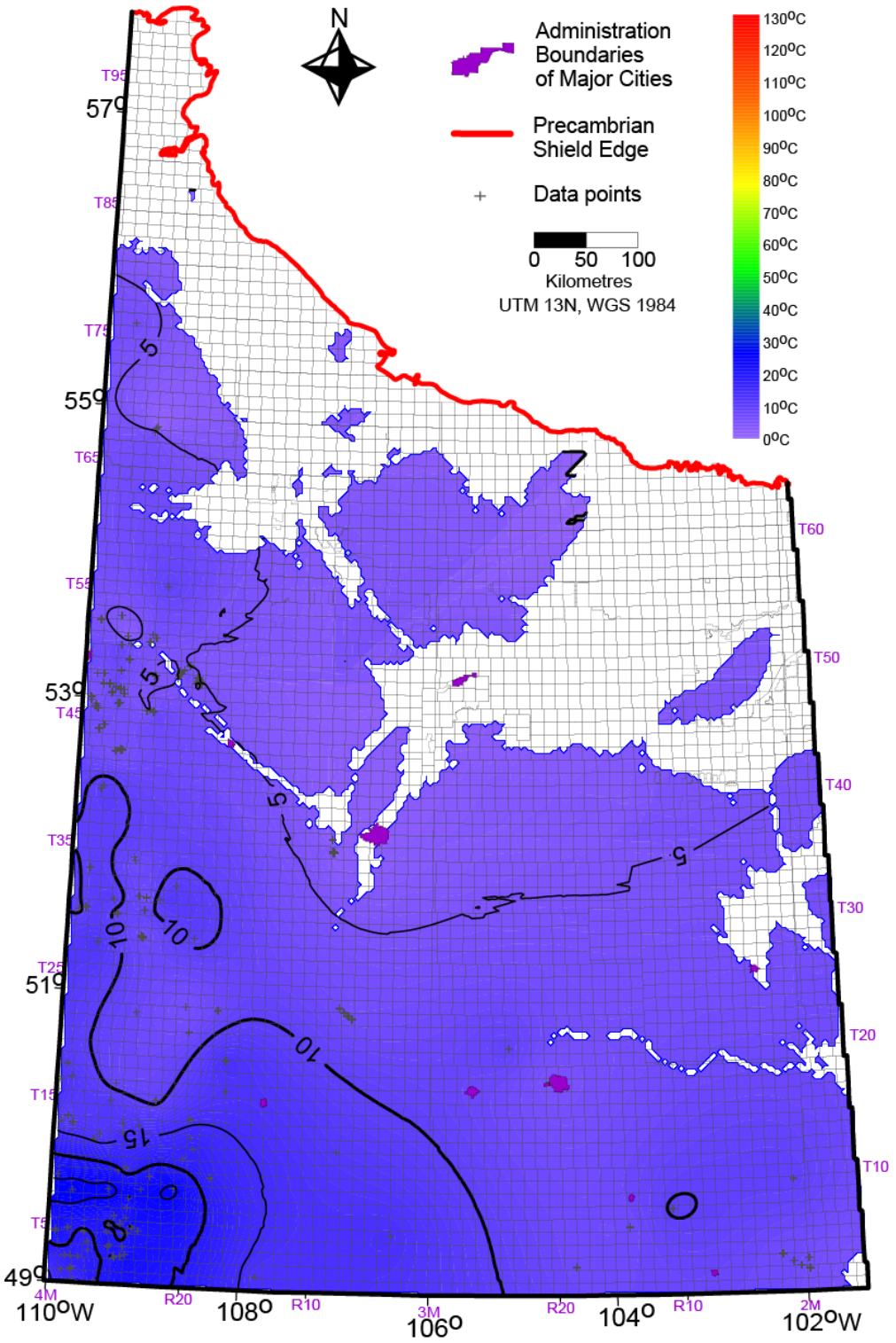

Figure B.2 Temperature at 500 masl. Area bounded by the topographic contour 500 m above sea level. CI: 5 °C.

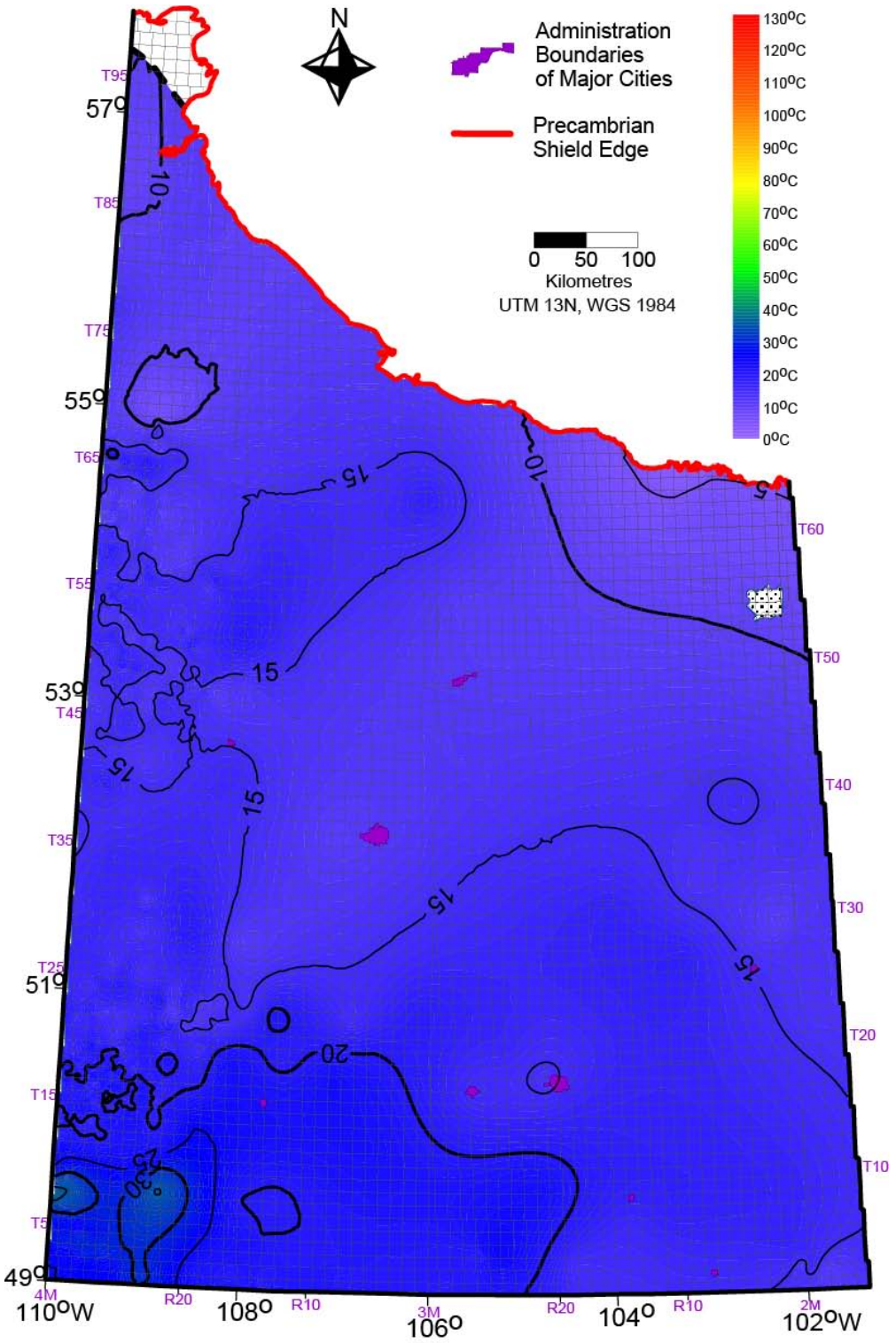

Figure B.3.a Temperature at 250 masl. Data distribution would obscure features thus shown on a separate map, following this. Area bounded in the NW by the basement elevation. The dotted area in the NE represents an area, where the surface is less than 250 masl. CI: 5 °C.

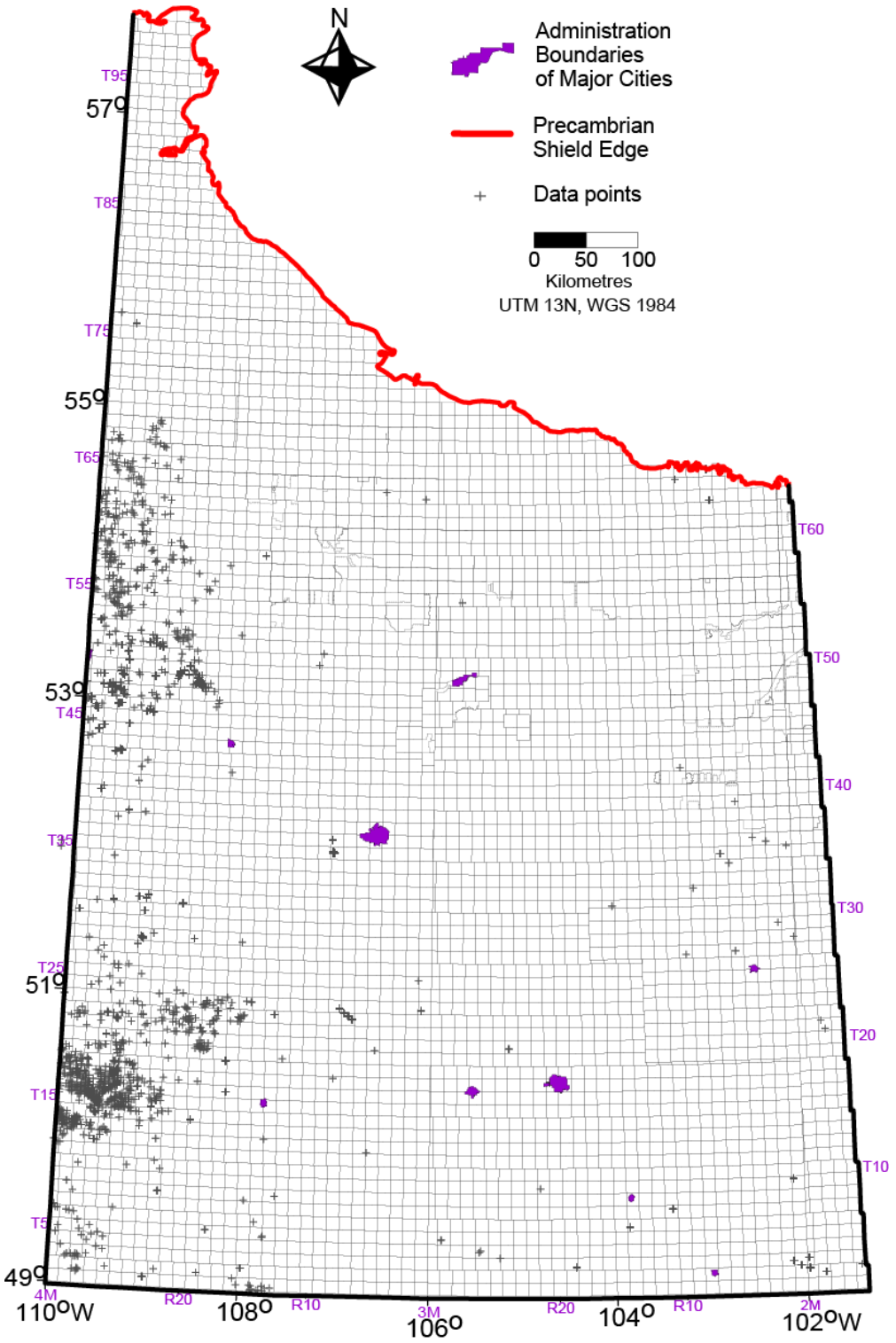

Figure B.3.b Data distribution at 250 masl.

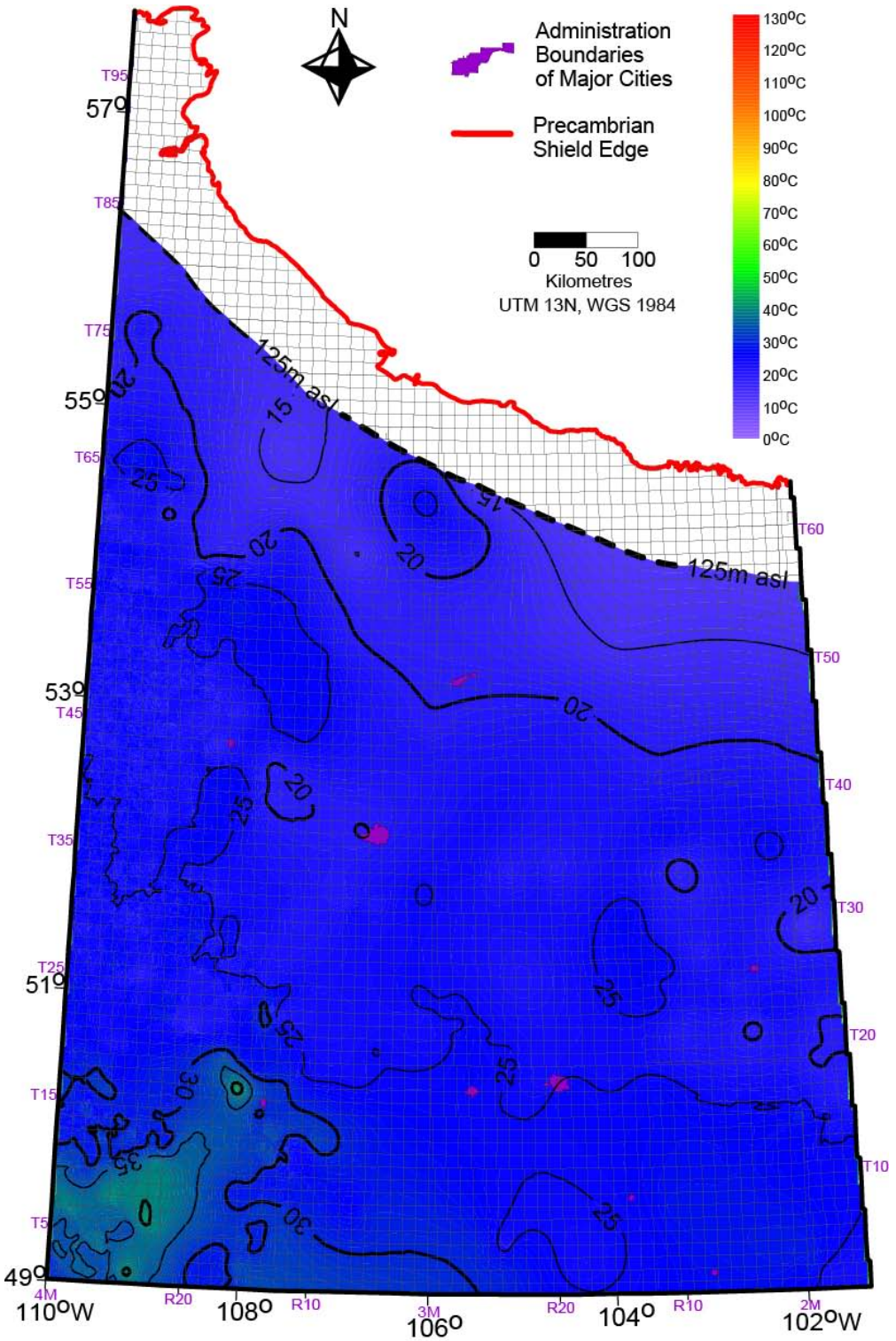

Figure B.4.a Temperature at sea level. Data distribution would obscure features thus shown on a separate map, following this. CI: 5 °C.

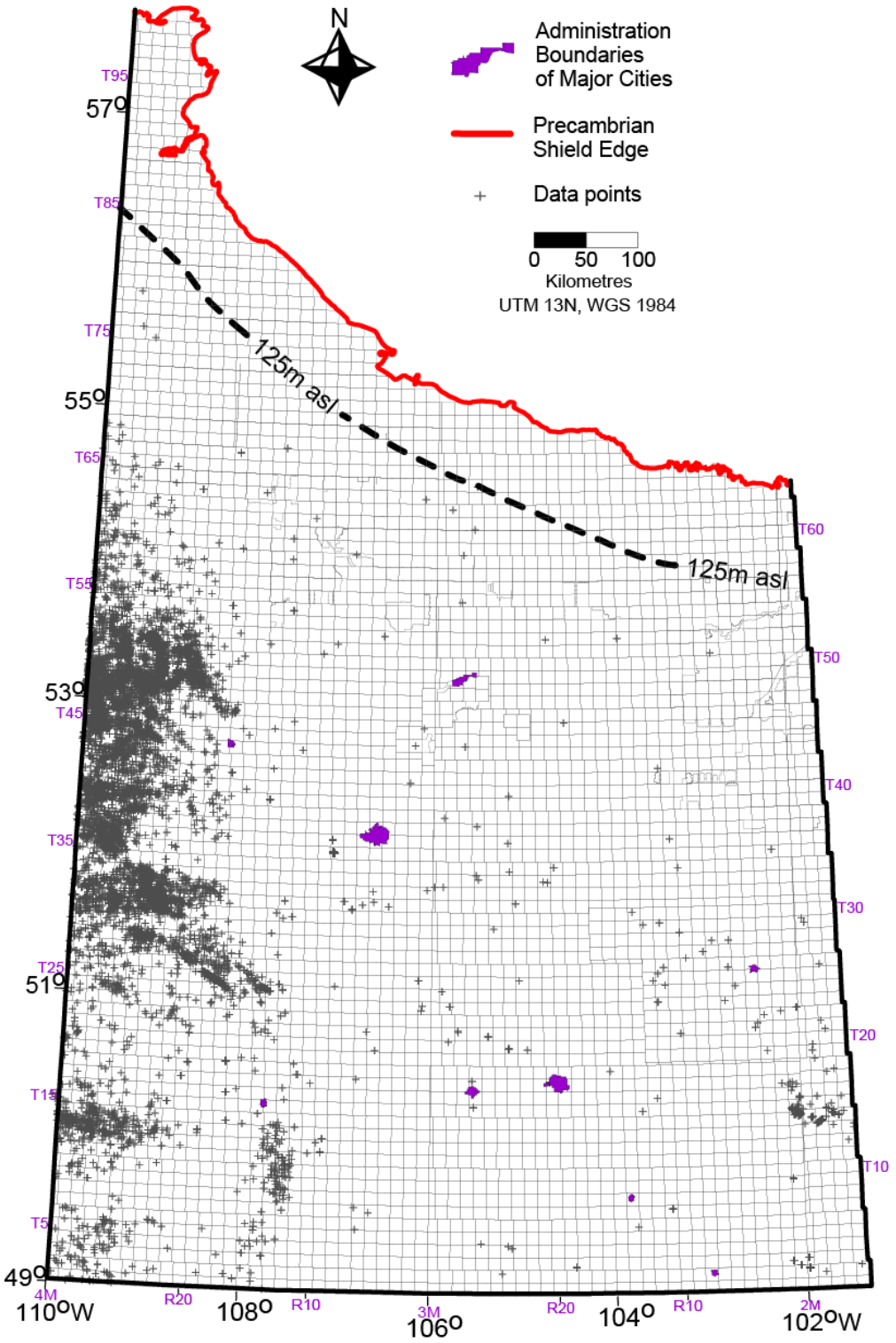

Figure B.4.b. Data distribution at sea level.

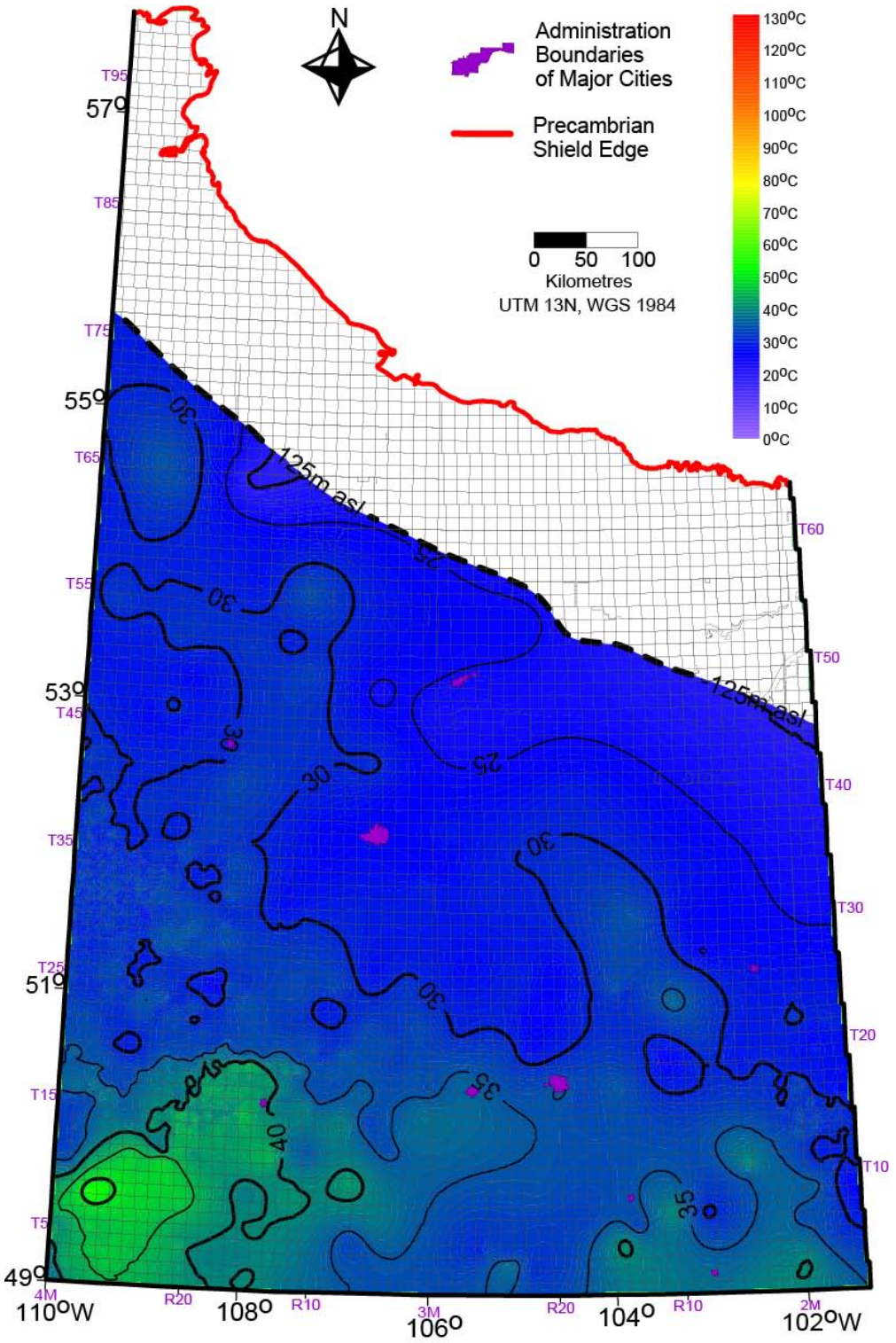

Figure B.5.a. Temperature at 250 mbsl (metres below sea level). Data distribution would obscure features thus shown on a separate map, following this. CI: 5 °C.

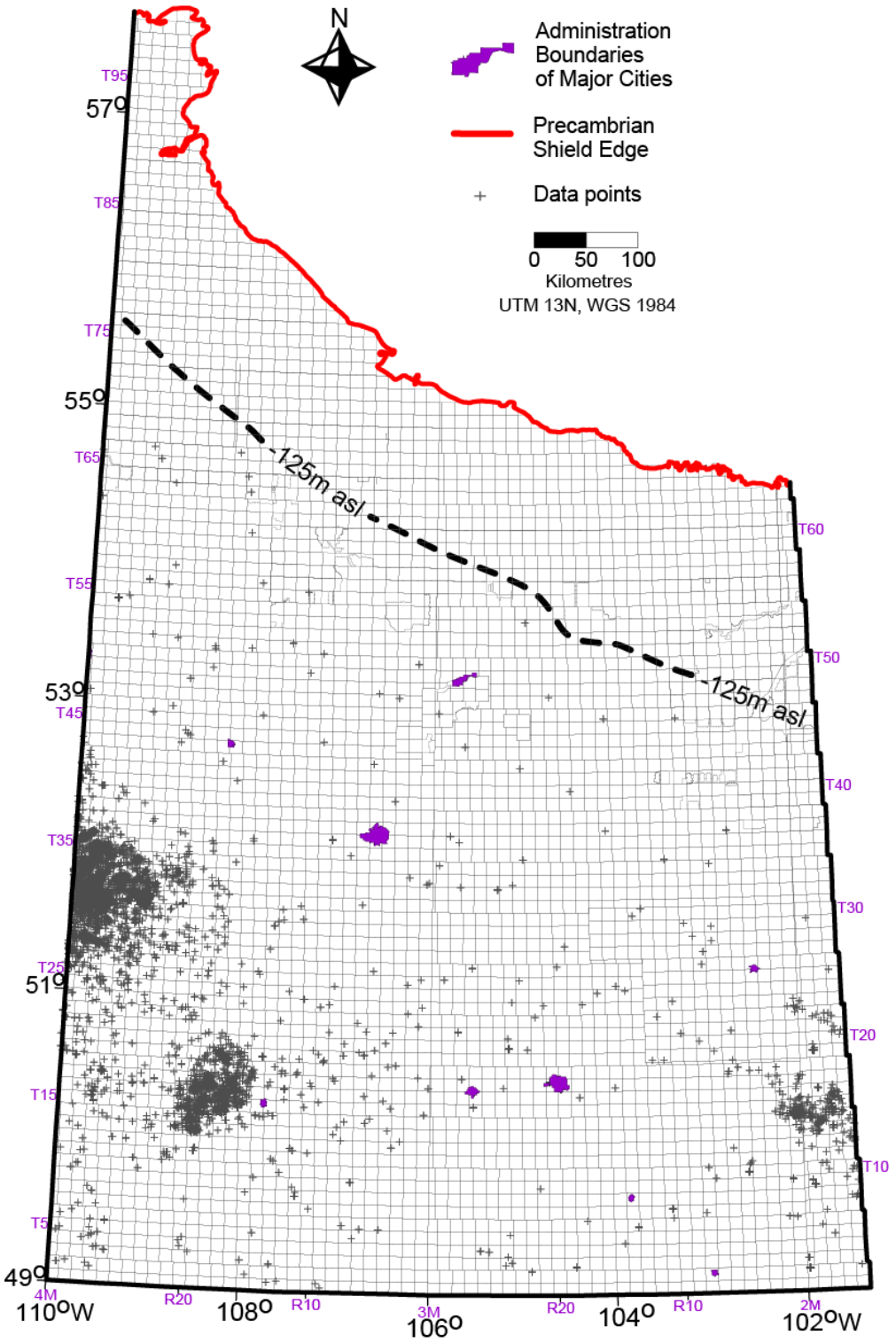

Figure B.5.b. Data distribution at 250 mbsl.

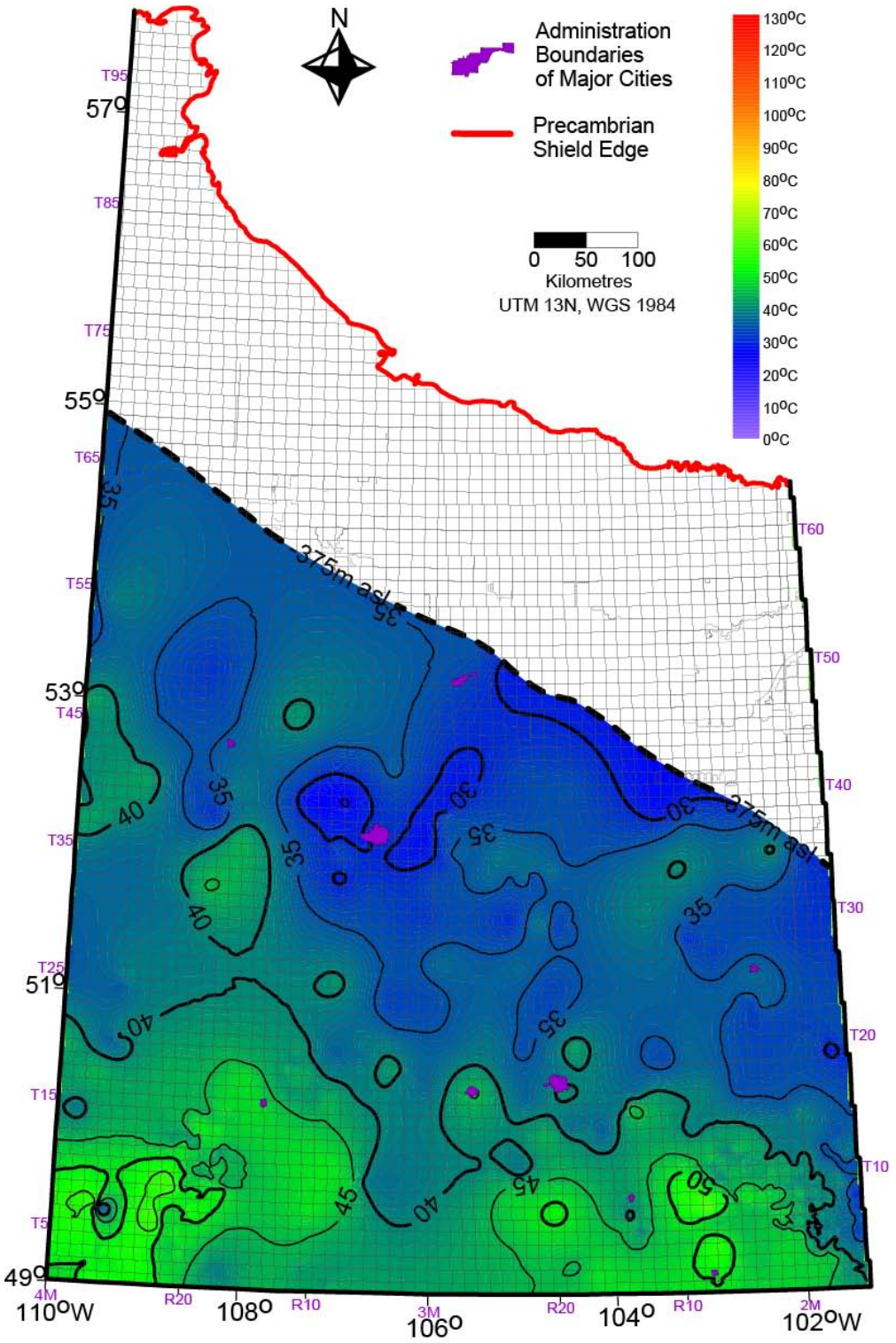

Figure B.6.a Temperature at 500 mbsl. Data distribution would obscure features thus shown on a separate map, following this. CI: 5 °C.

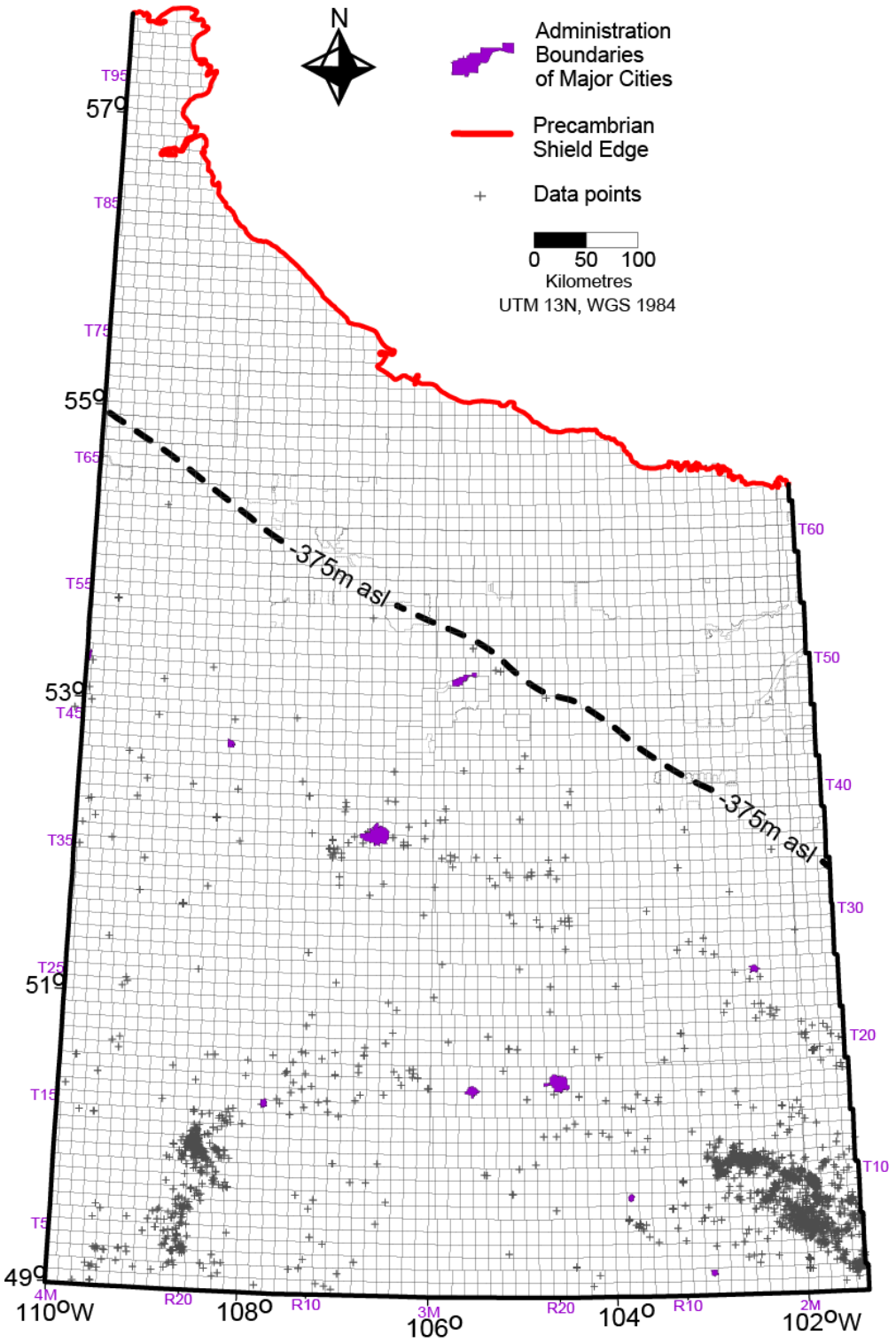

Figure B.6.b. Data distribution at 500 mbsl.

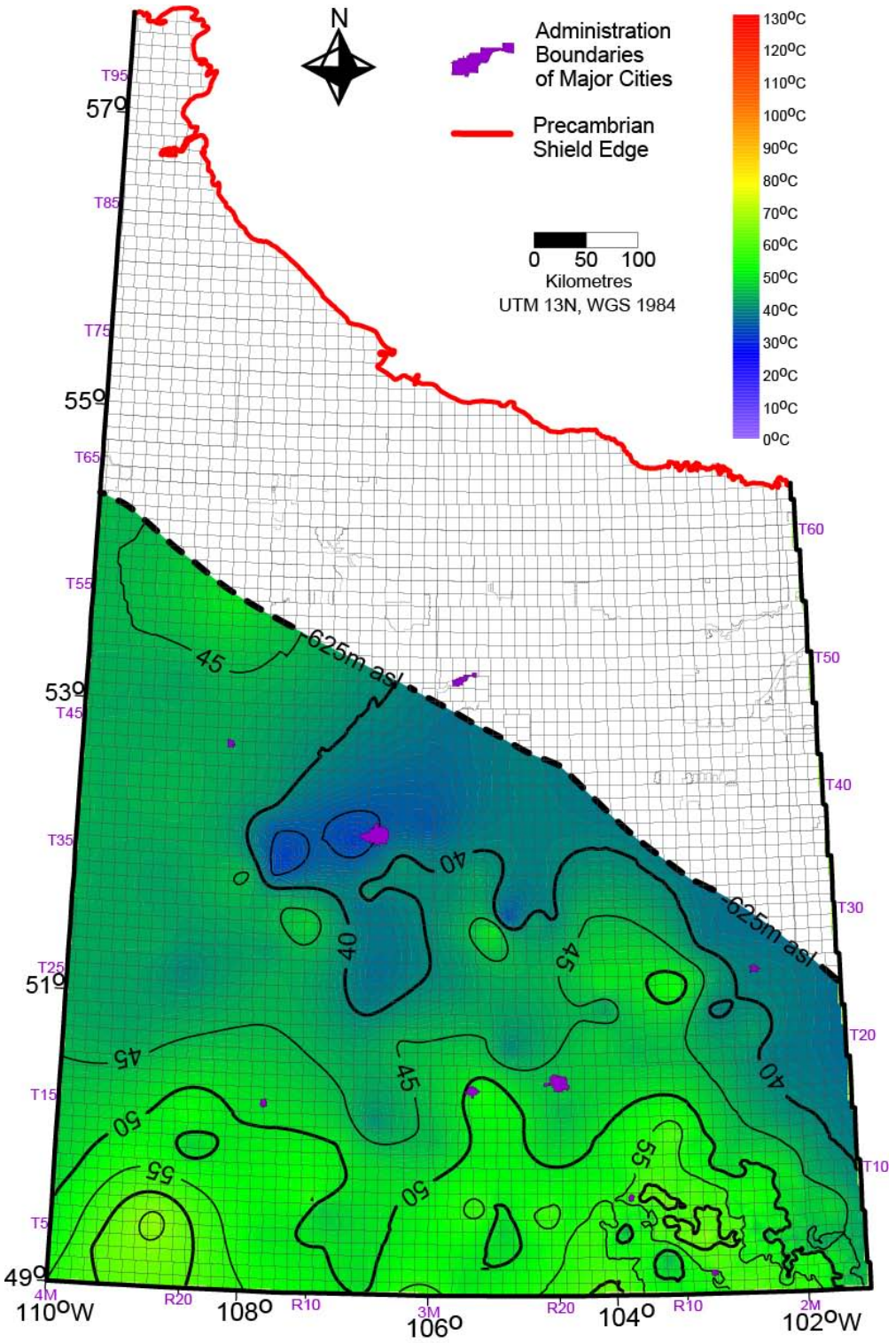

Figure B.7.a. Temperature at 750 mbsl. Data distribution would obscure features thus shown on a separate map, following this. CI: 5 °C.

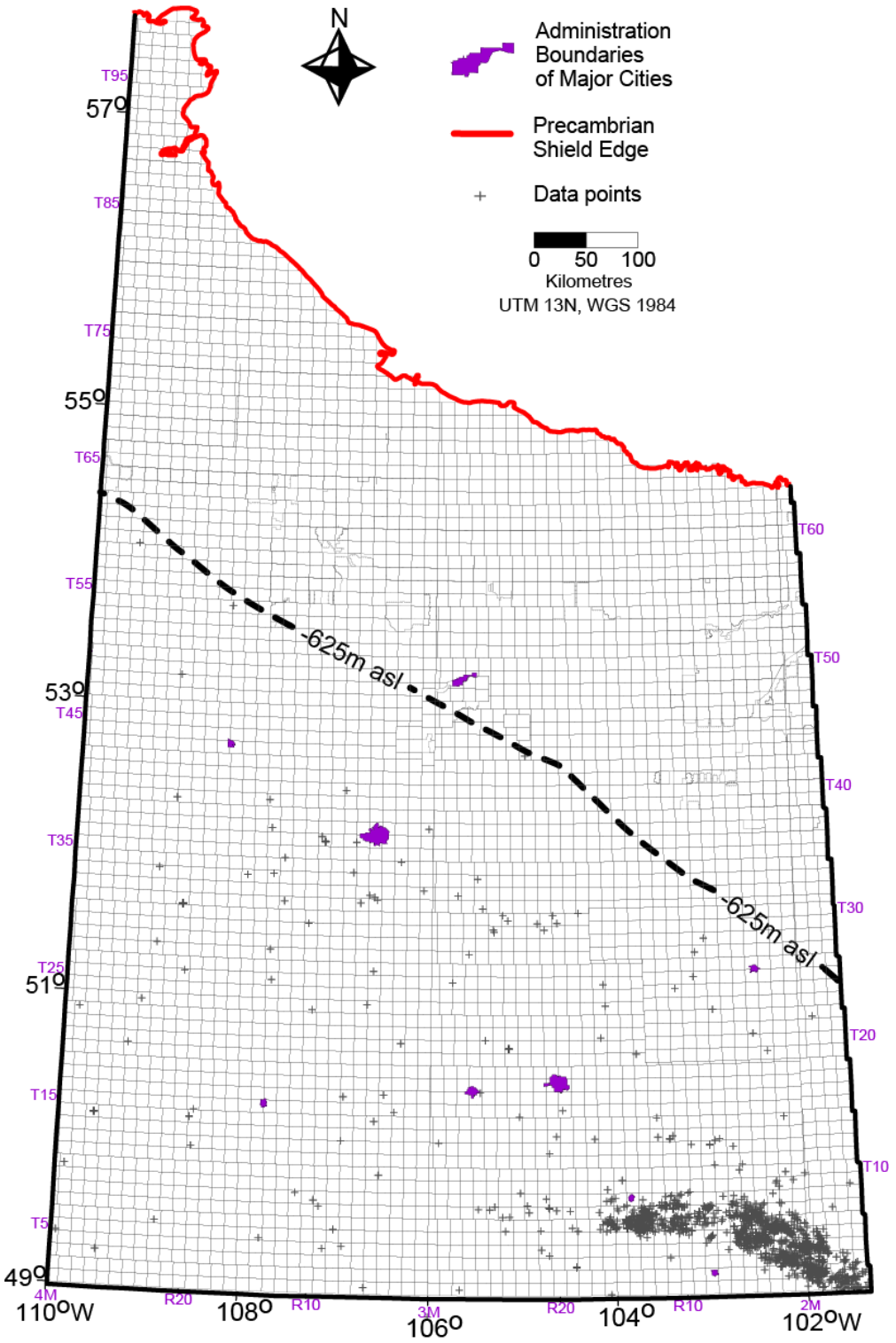

Figure B.7.b. Data distribution at 750 mbsl.

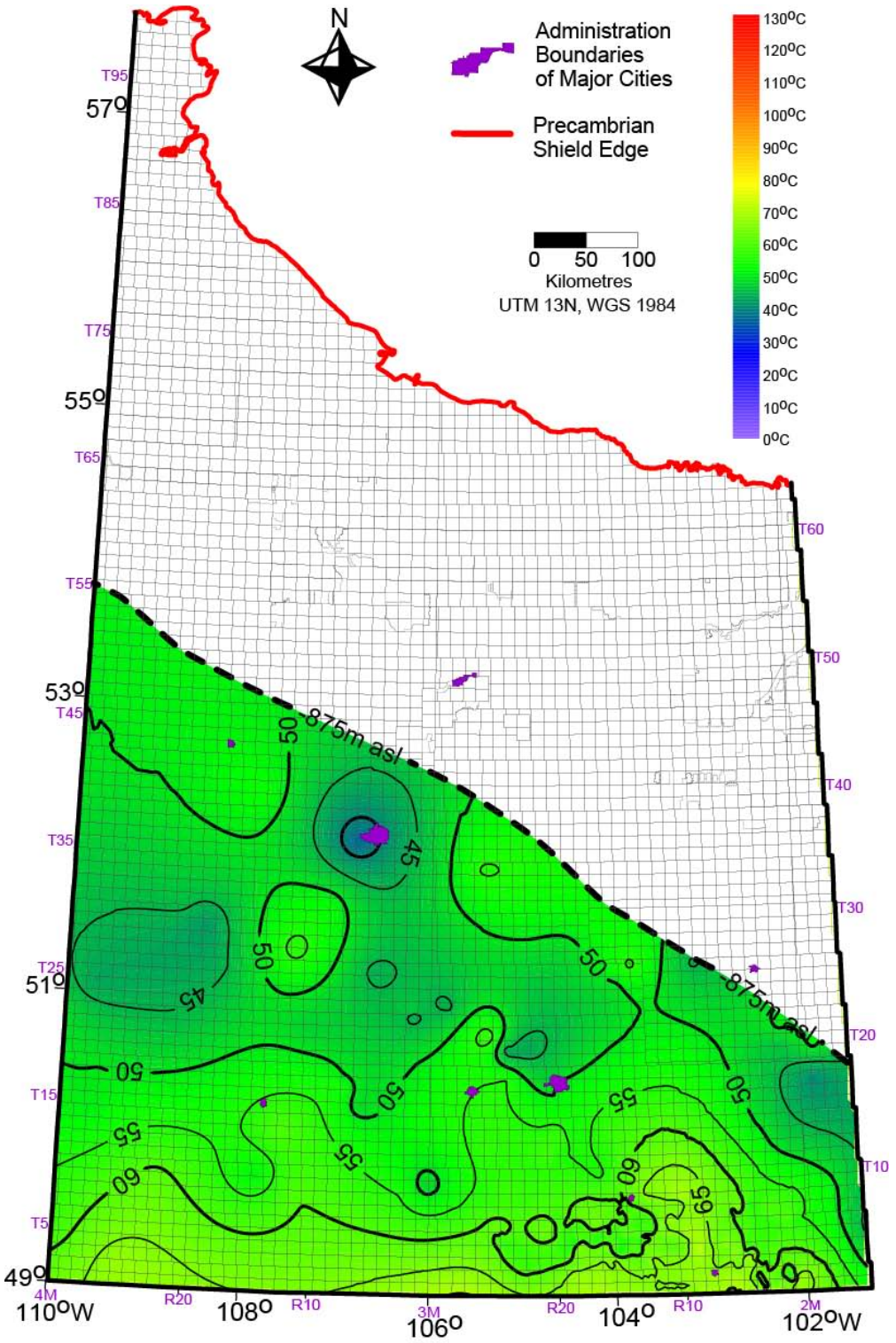

Figure B.8.a. Temperature at 1000 mbsl. Data distribution would obscure features thus shown on a separate map, following this. CI: 5 °C.

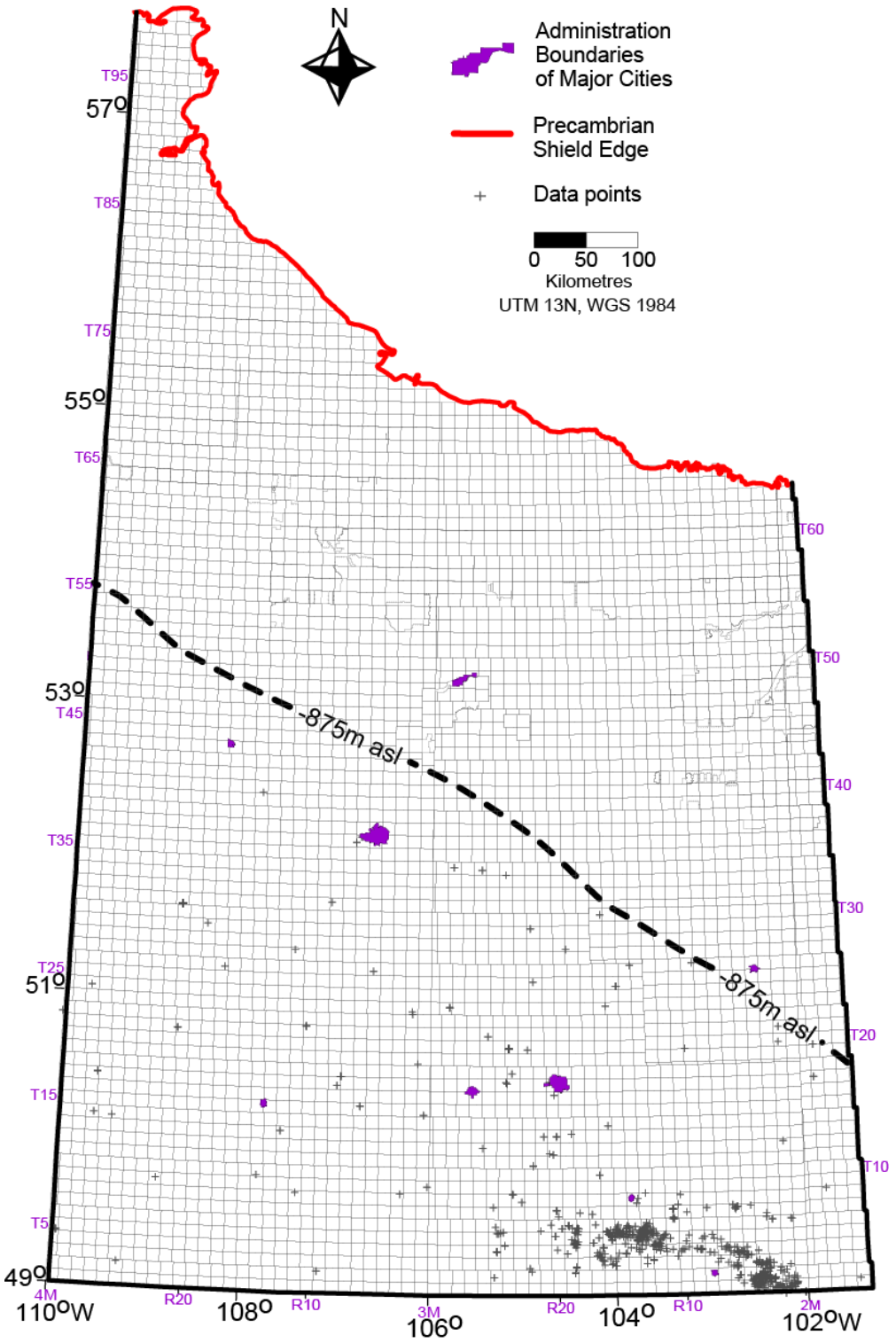

Figure B.8.b. Data distribution at 1000 mbsl.

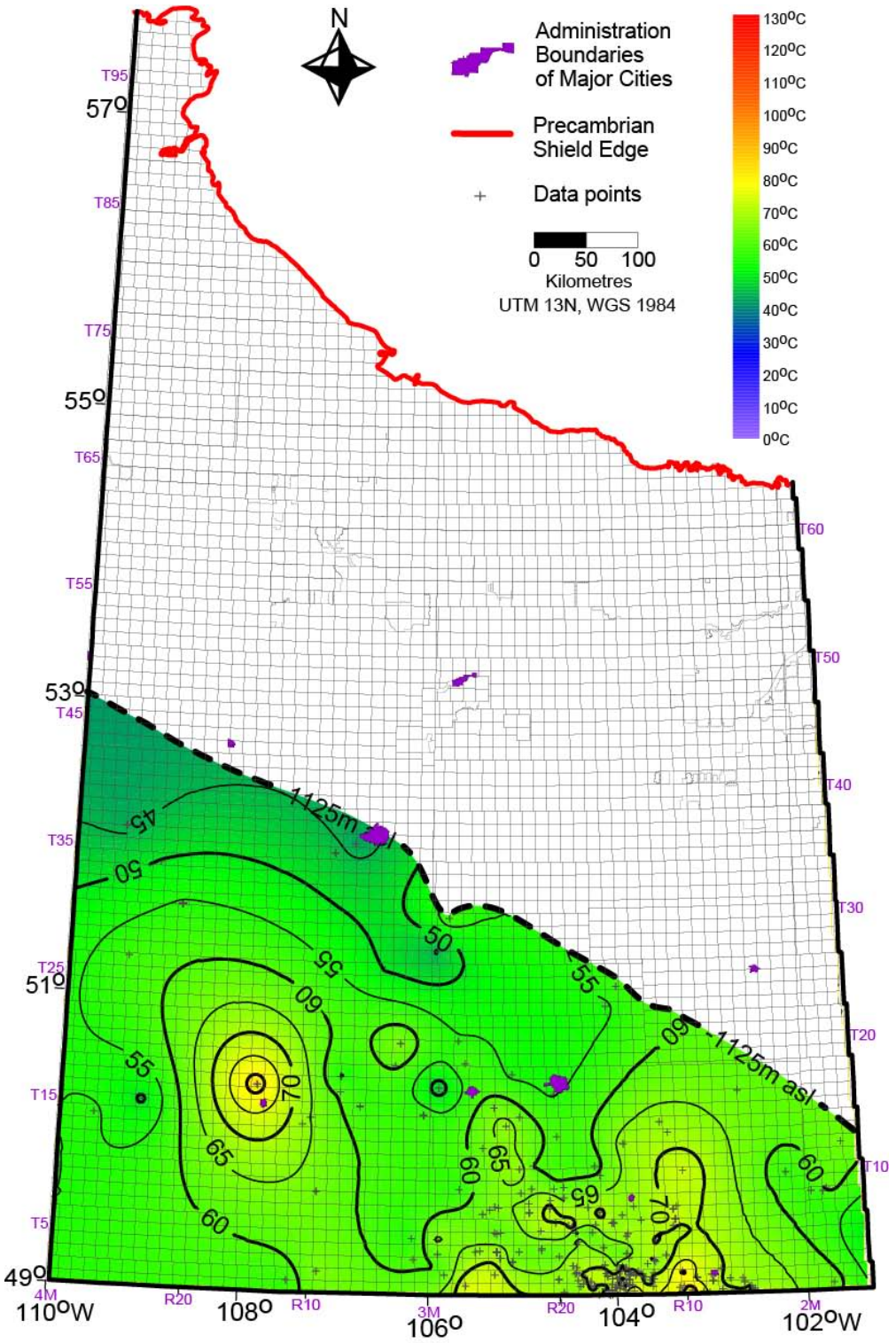

Figure B.9. Temperature at 1250 mbsl. CI: 5 °C.

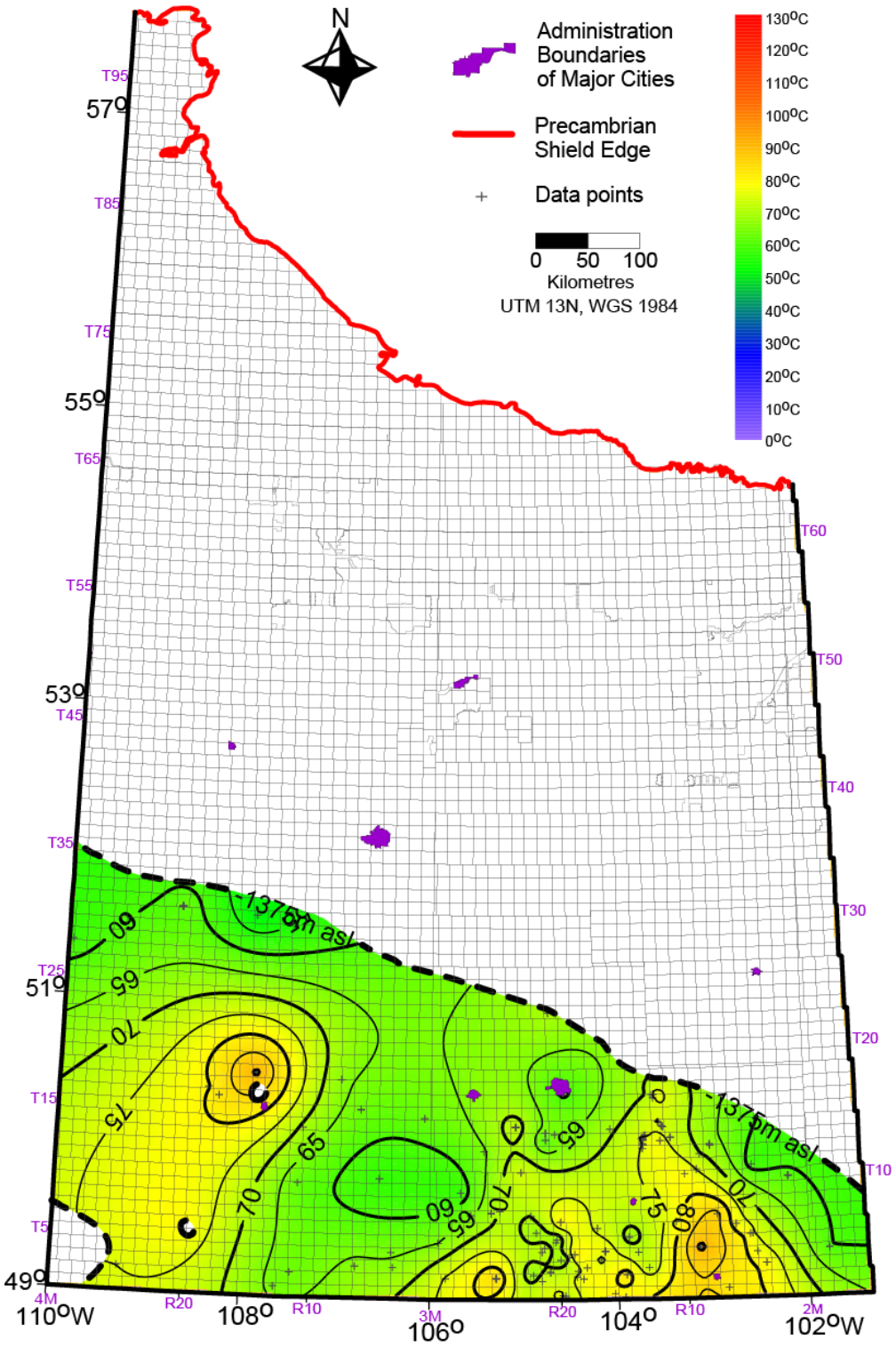

Figure B.10. Temperature at 1500 mbsl. CI: 5 °C.

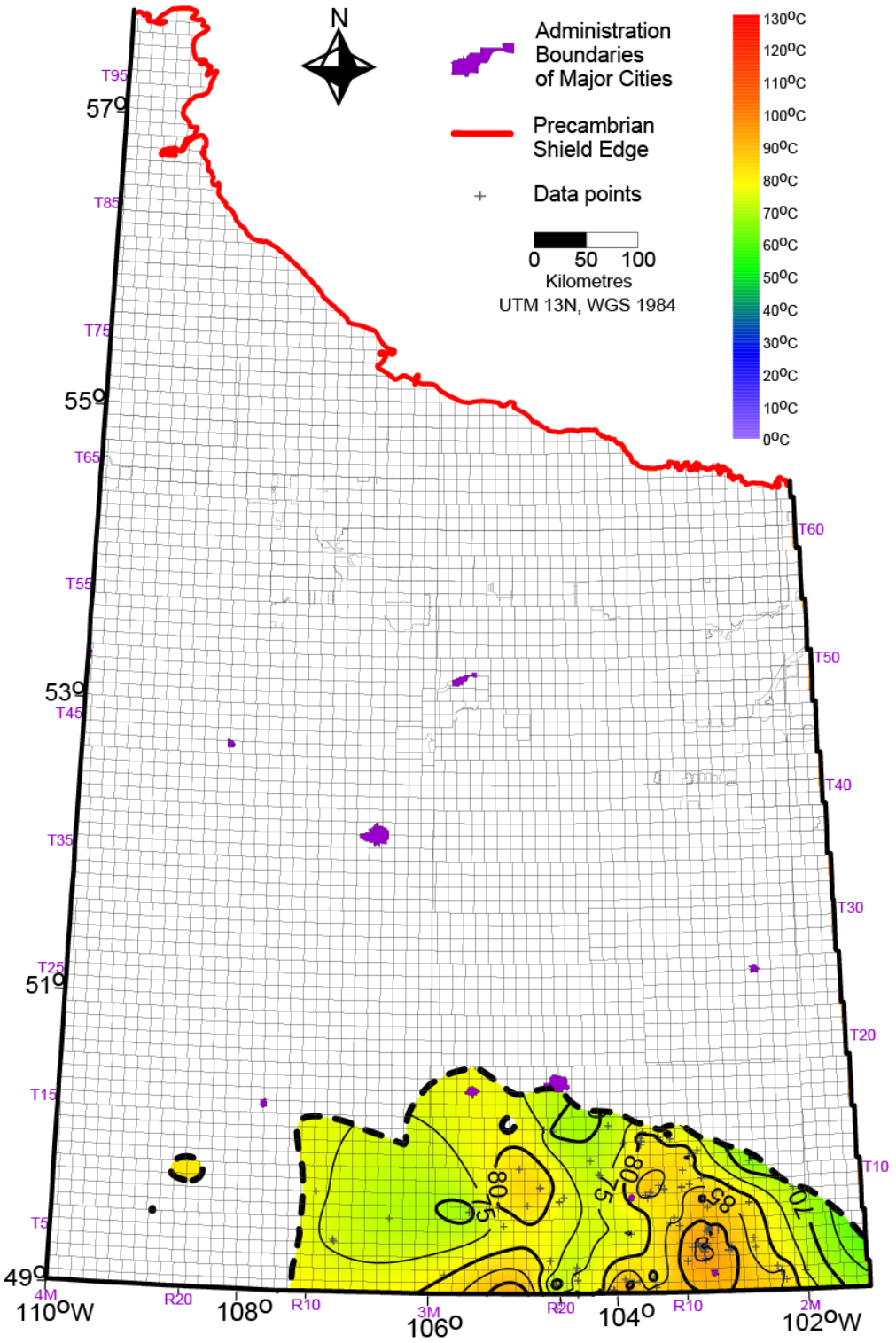

Figure B.11. Temperature at 1750 mbsl. CI: 5 °C.

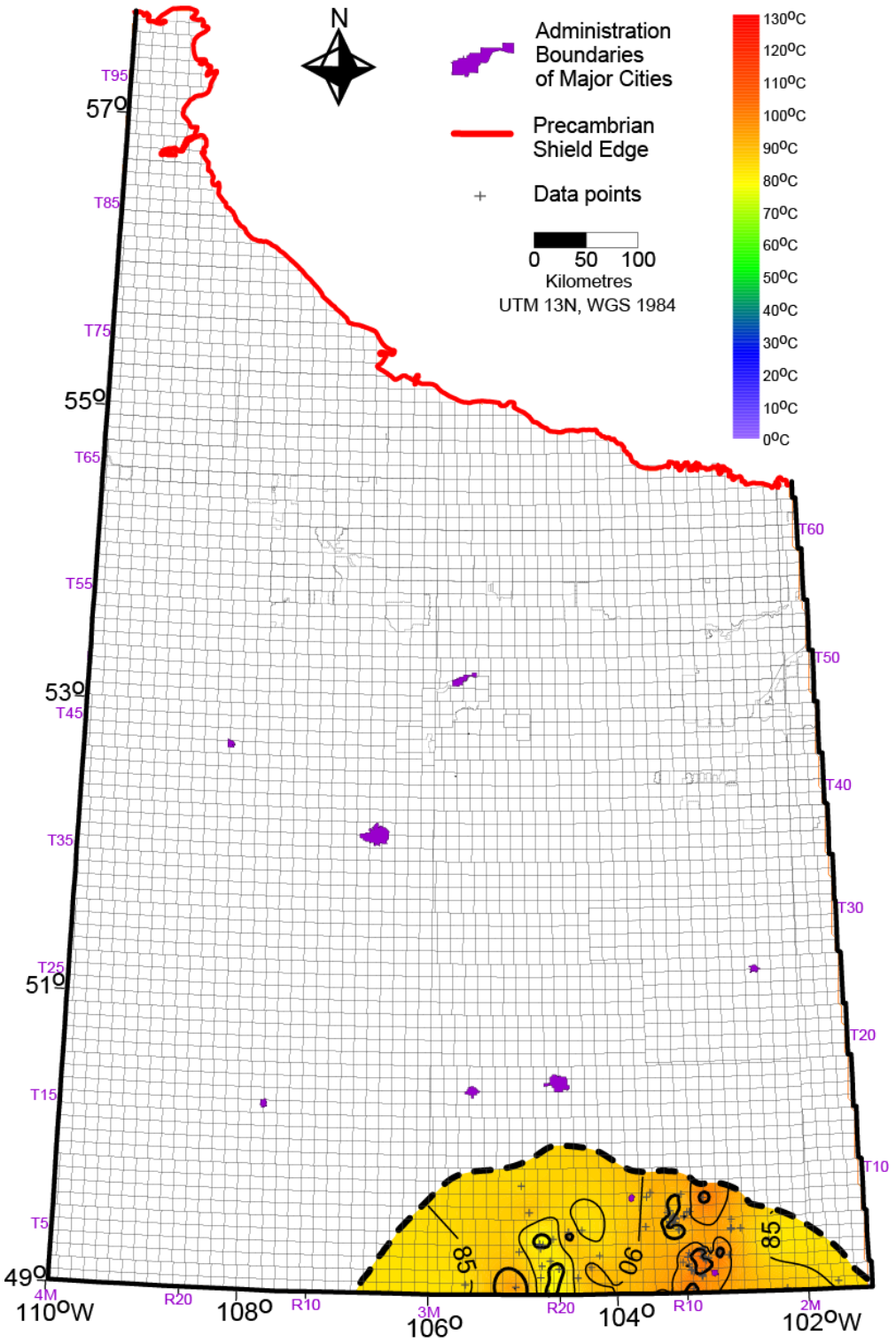

Figure B.12. Temperature at 2000 mbsl. CI: 5 °C.

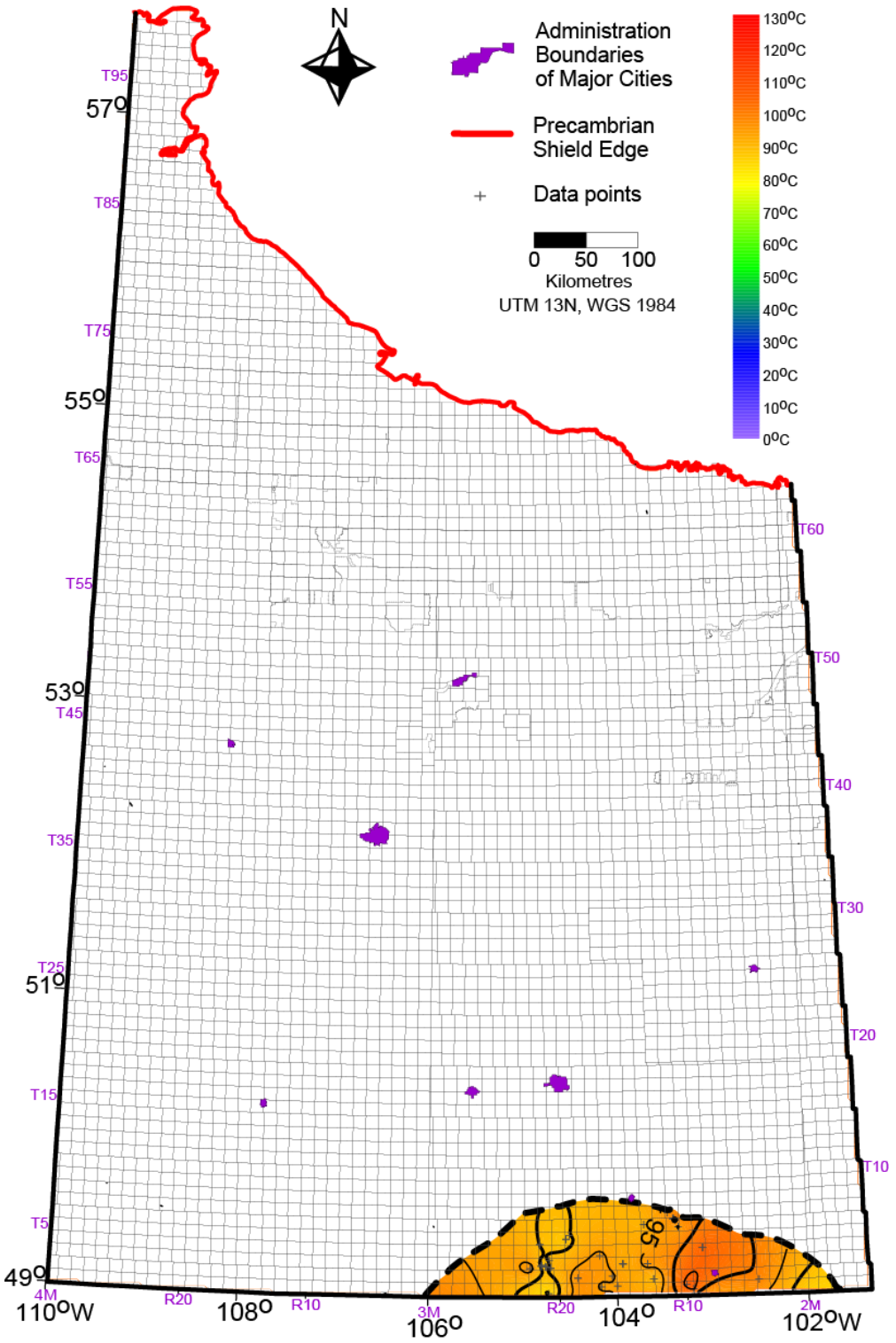

Figure B.13. Temperature at 2250 mbsl. CI: 5 °C.

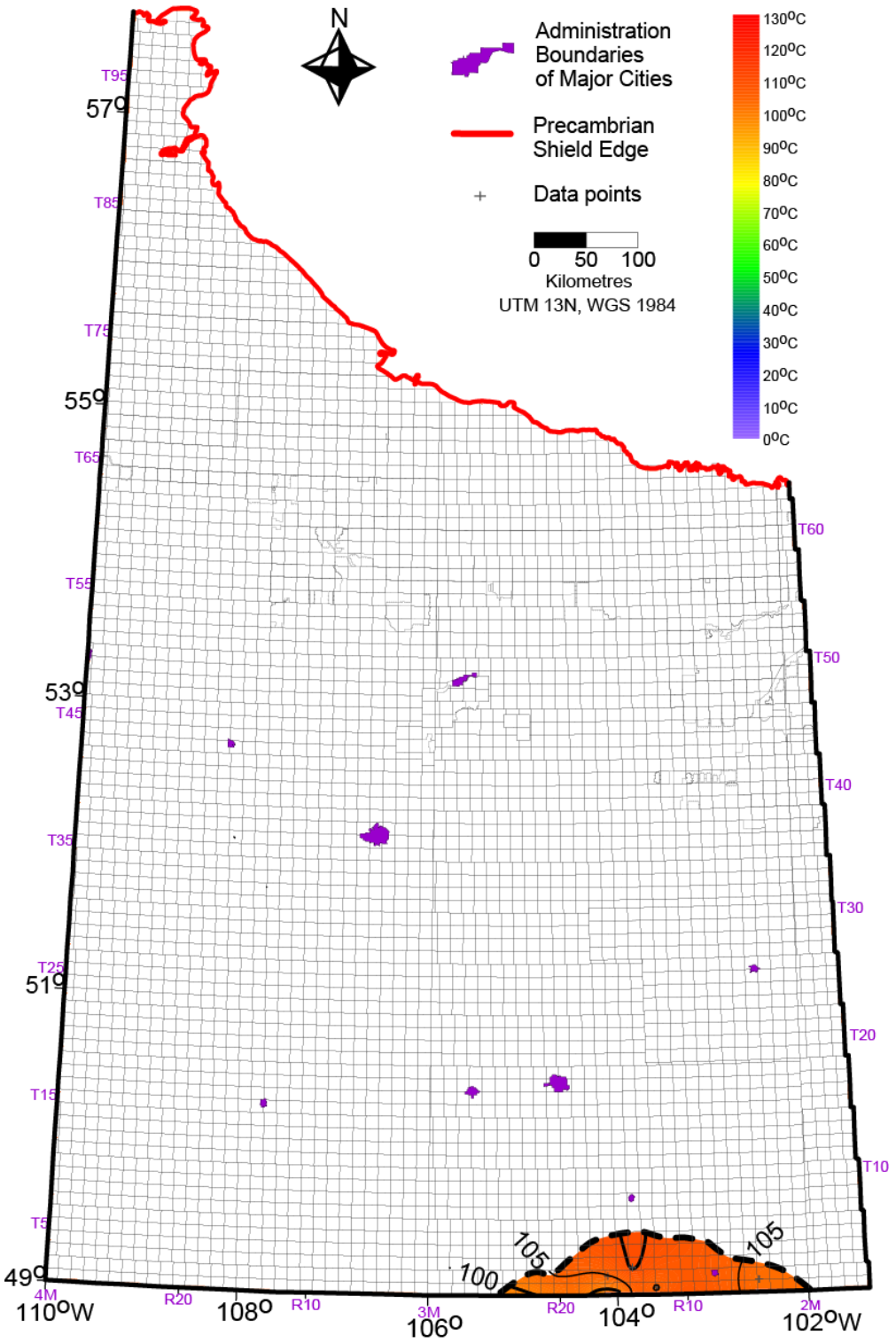

Figure B.14. Temperature at 2500 mbsl. CI: 5 °C.

Appendix C. Depth specific temperature maps

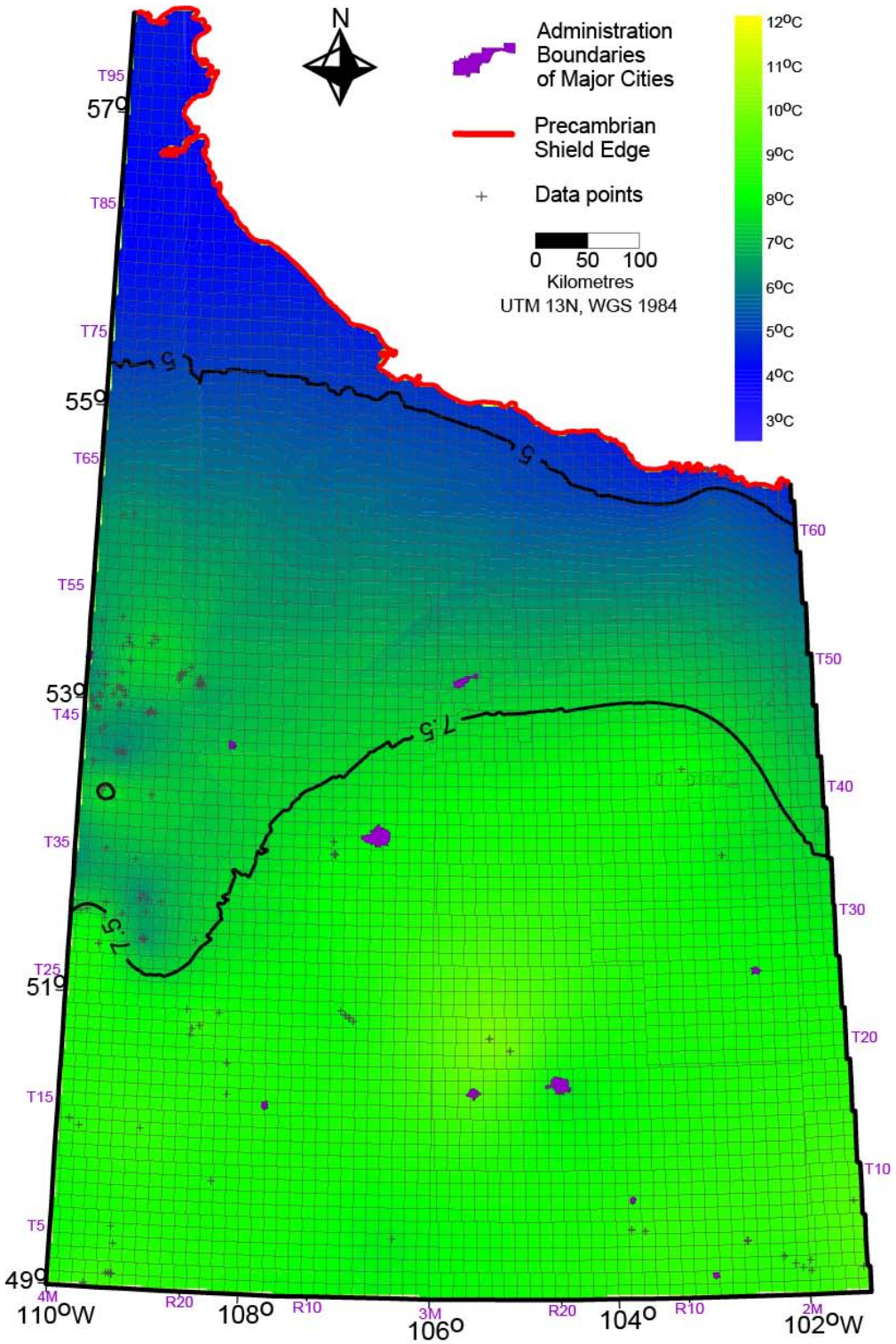

Figure C.1 Temperature at 100 m depth. CI: 2.5 °C. Nugget effect: 1(°C)^2.

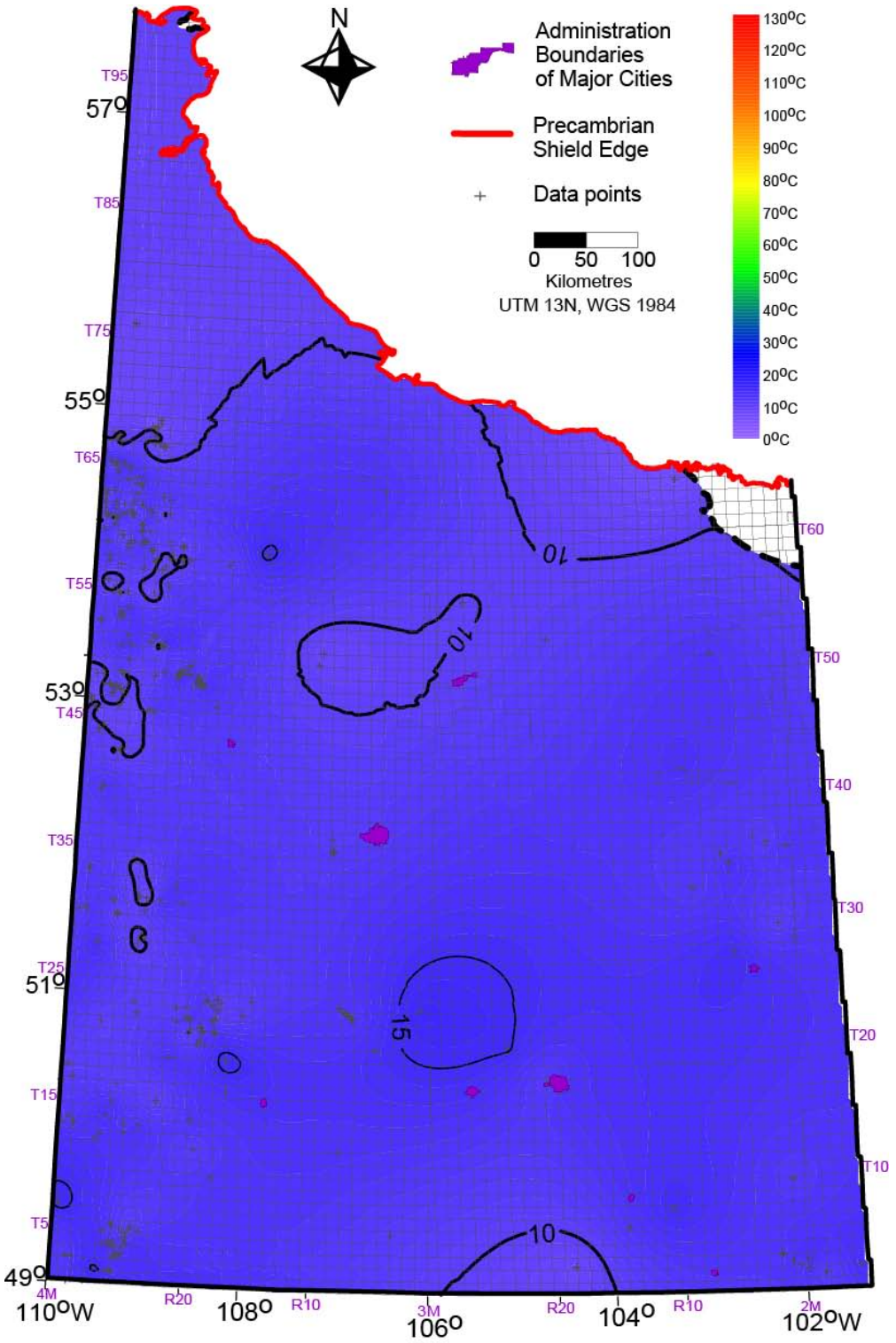

Figure C.2. Temperature at 250 m KB (metres below kelly bushing). CI: 5 °C.

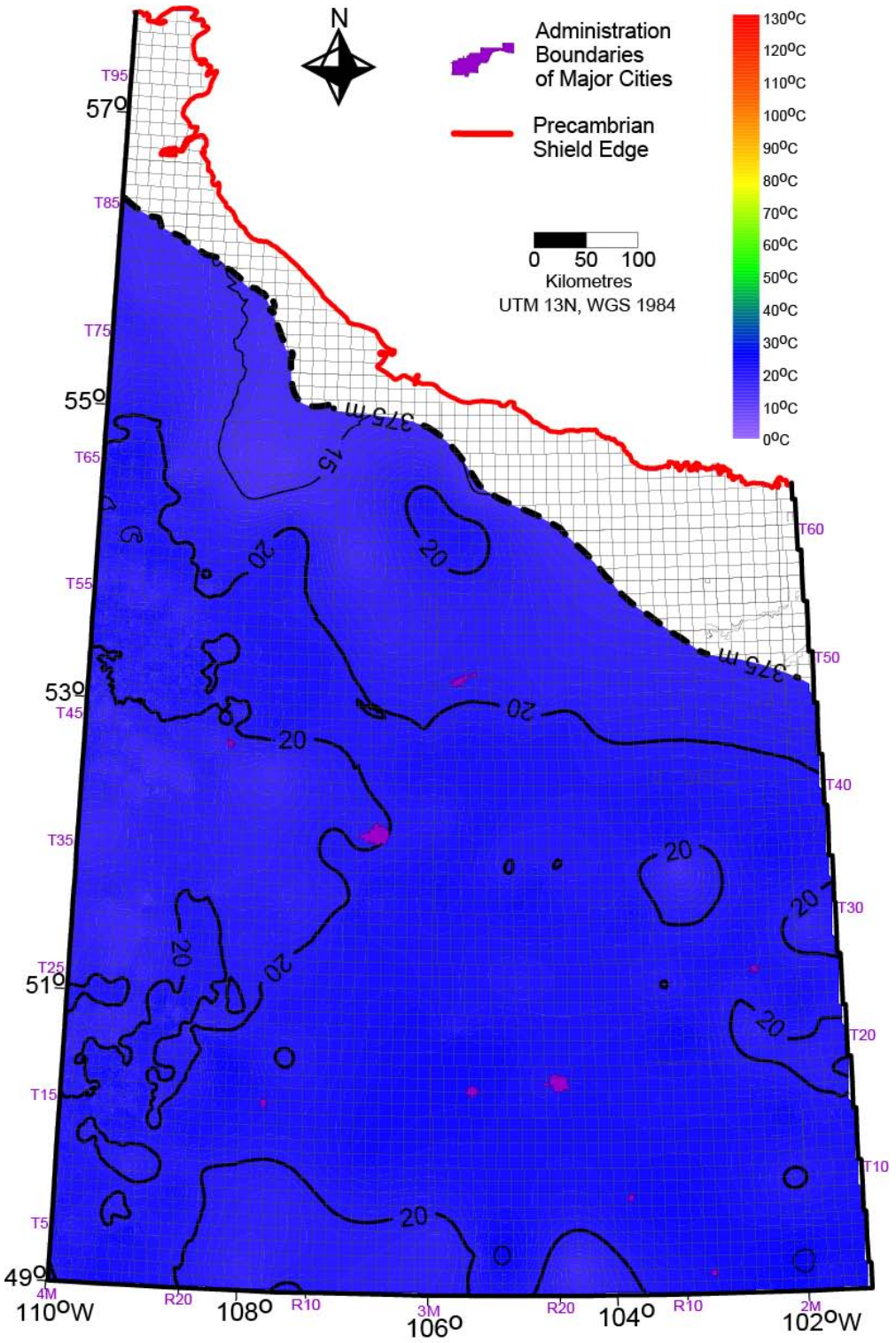

Figure C.3.a. Temperature at 500 m KB. Data distribution would obscure features thus shown on a separate map, following this. CI: 5 °C.

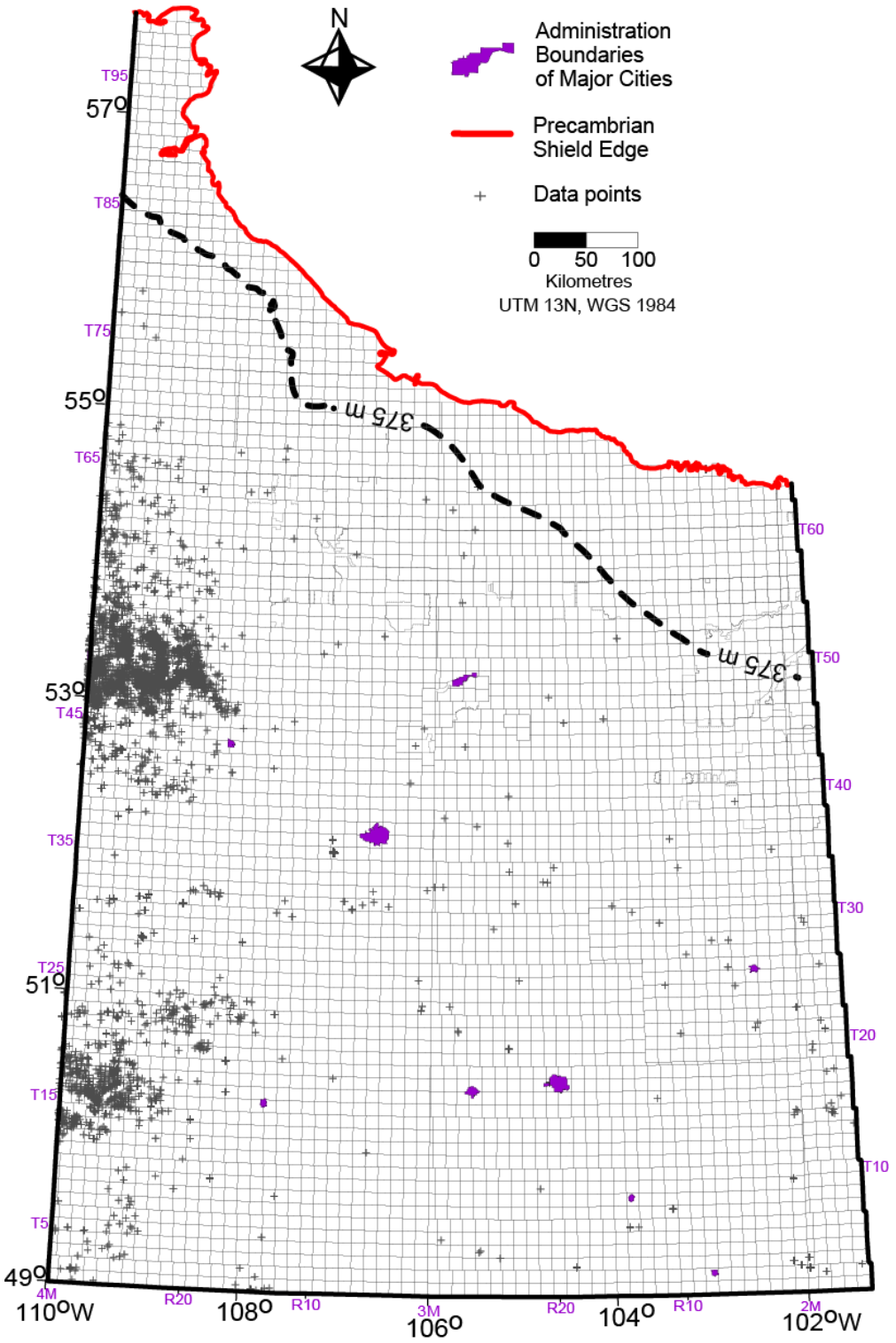

Figure C.3.b. Data distribution at 500 m KB.

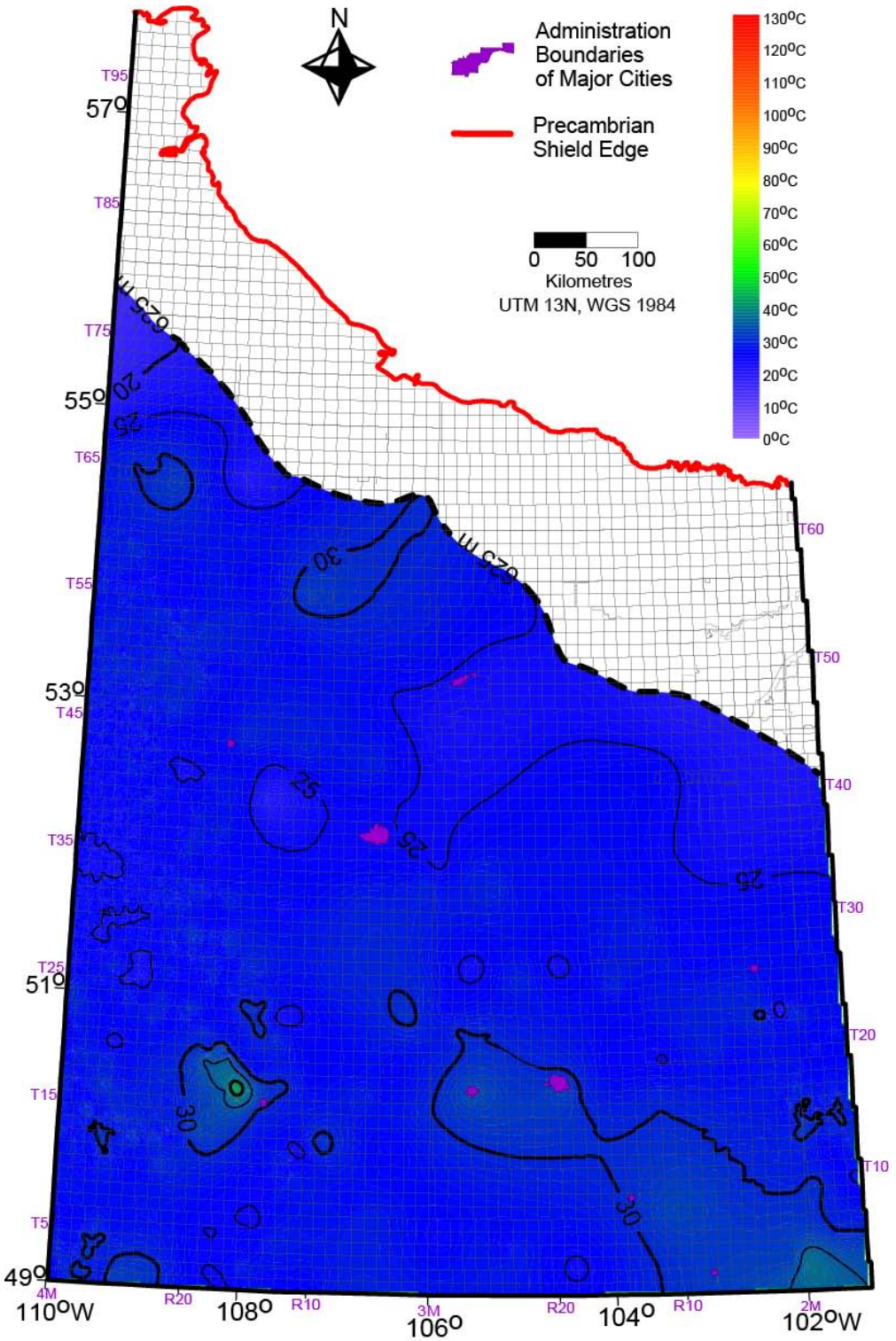

Figure C.4.a.. Temperature at 750 m KB. Data distribution would obscure features thus shown on a separate map, following this. CI: 5 °C.

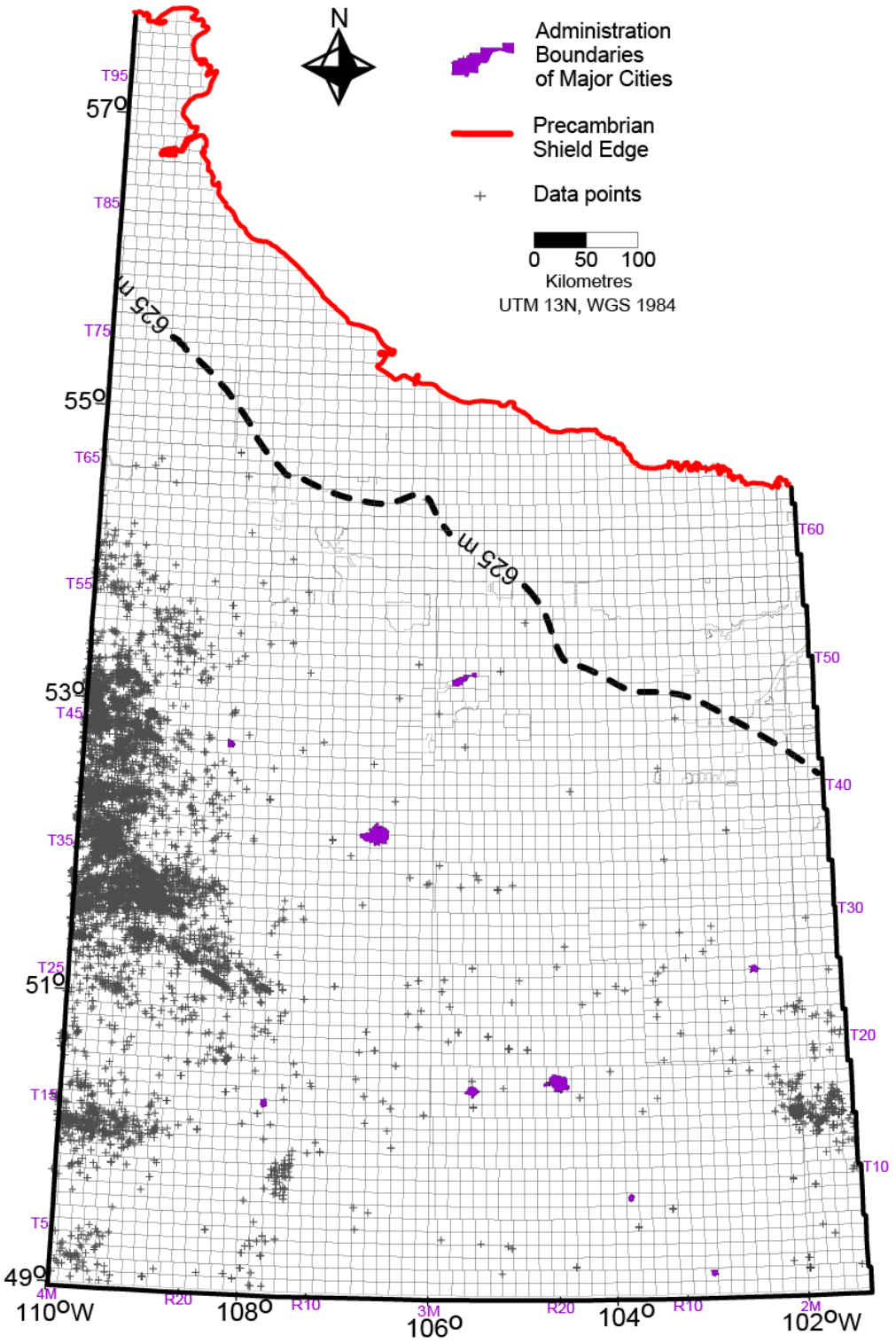

Figure C.4.b. Data distribution at 750 m KB.

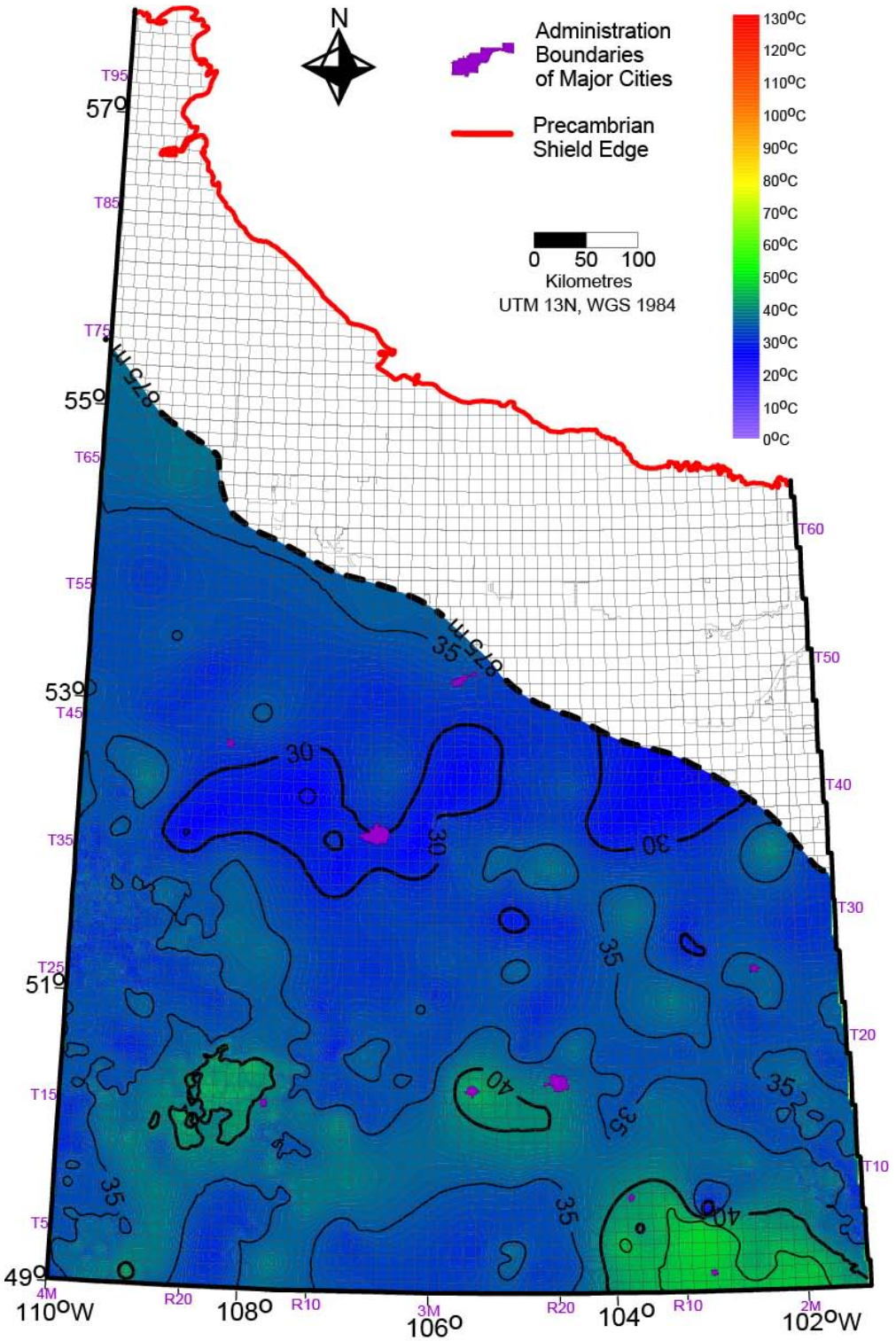

Figure C.5.a. Temperature at 1000 m KB. Data distribution would obscure features thus shown on a separate map, following this. CI: 5 °C.

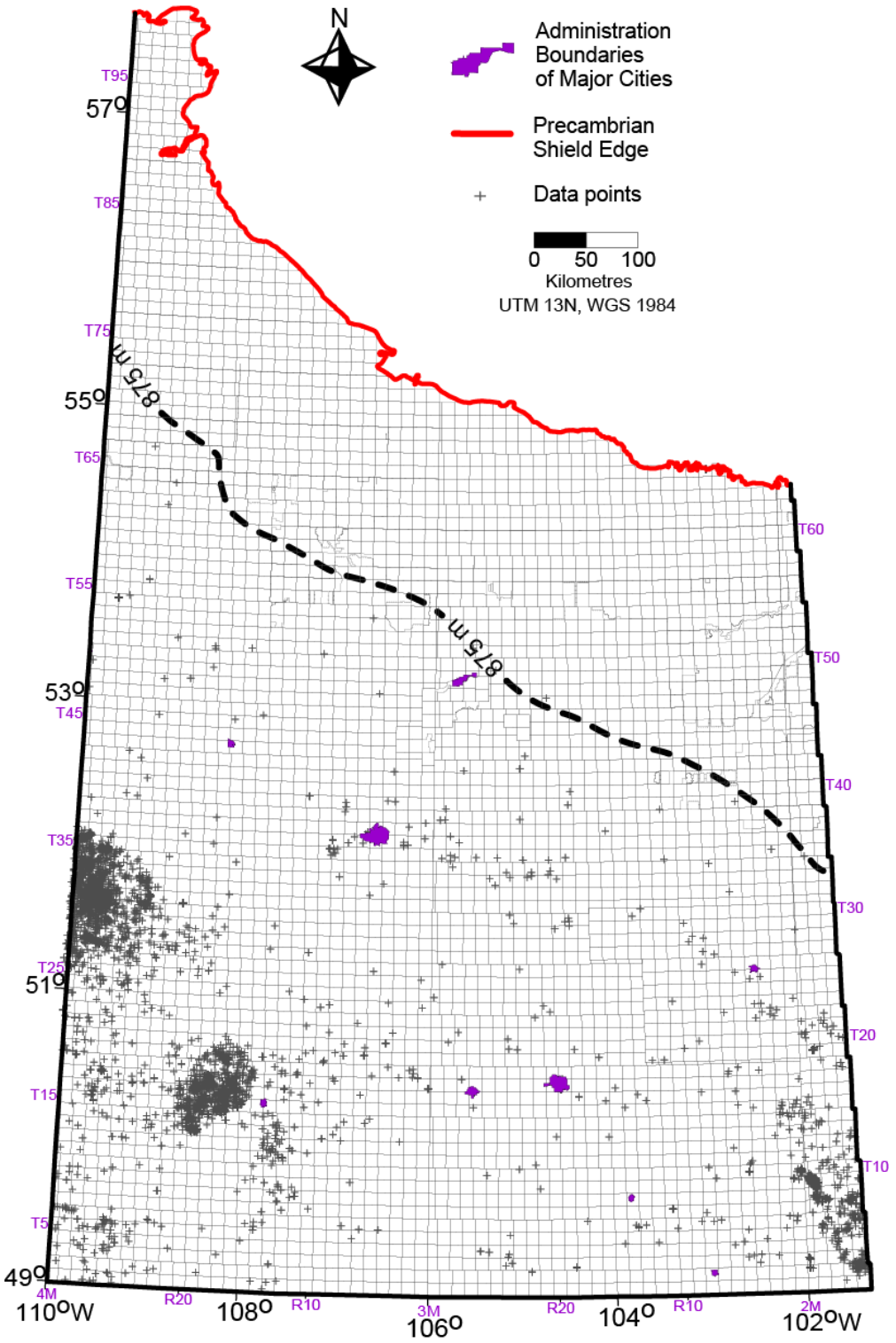

Figure C.5. b. Data distribution at 1000 m KB.

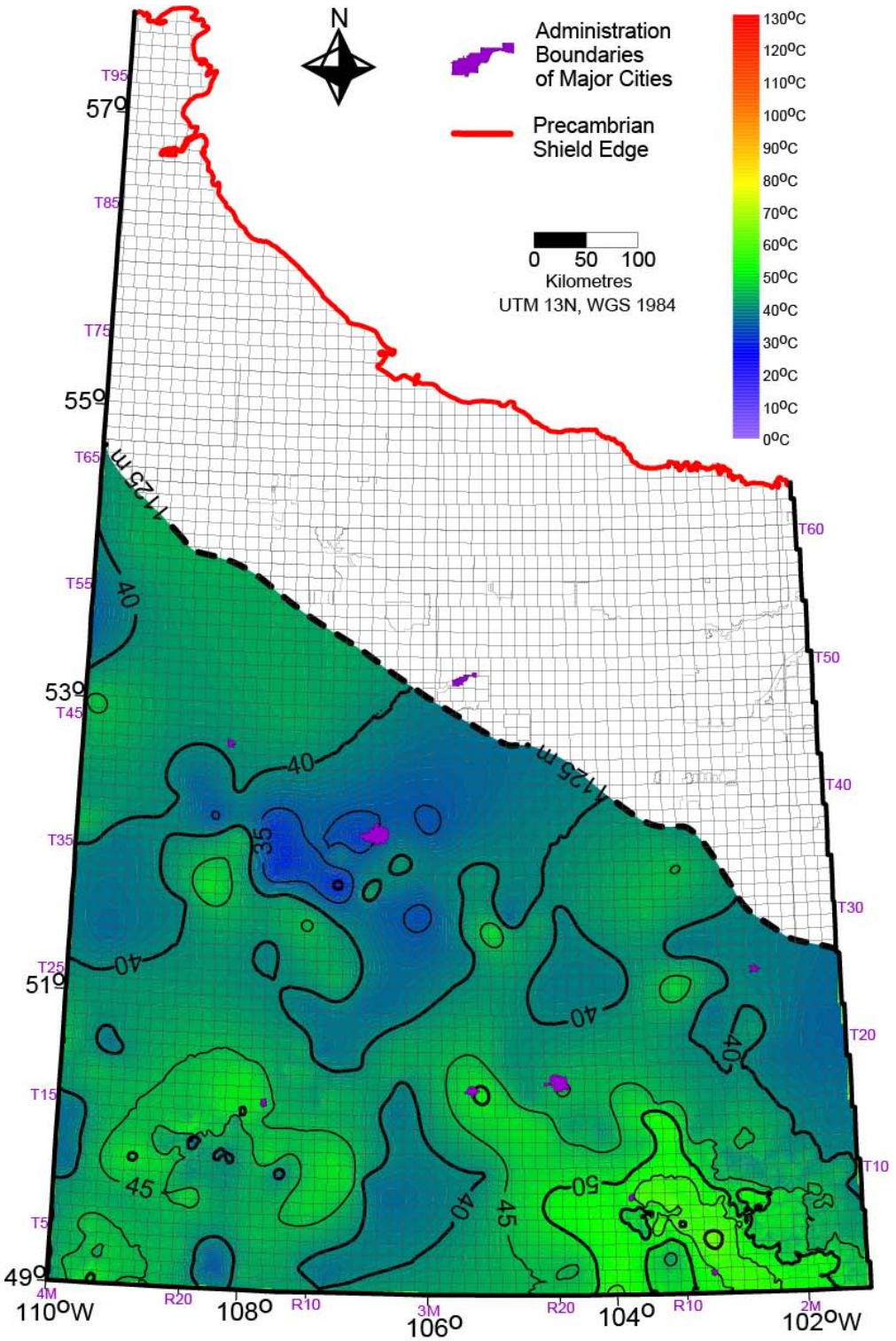

Figure C.6.a. Temperature at 1250 m KB. Data distribution would obscure features thus shown on a separate map, following this. CI: 5 °C.

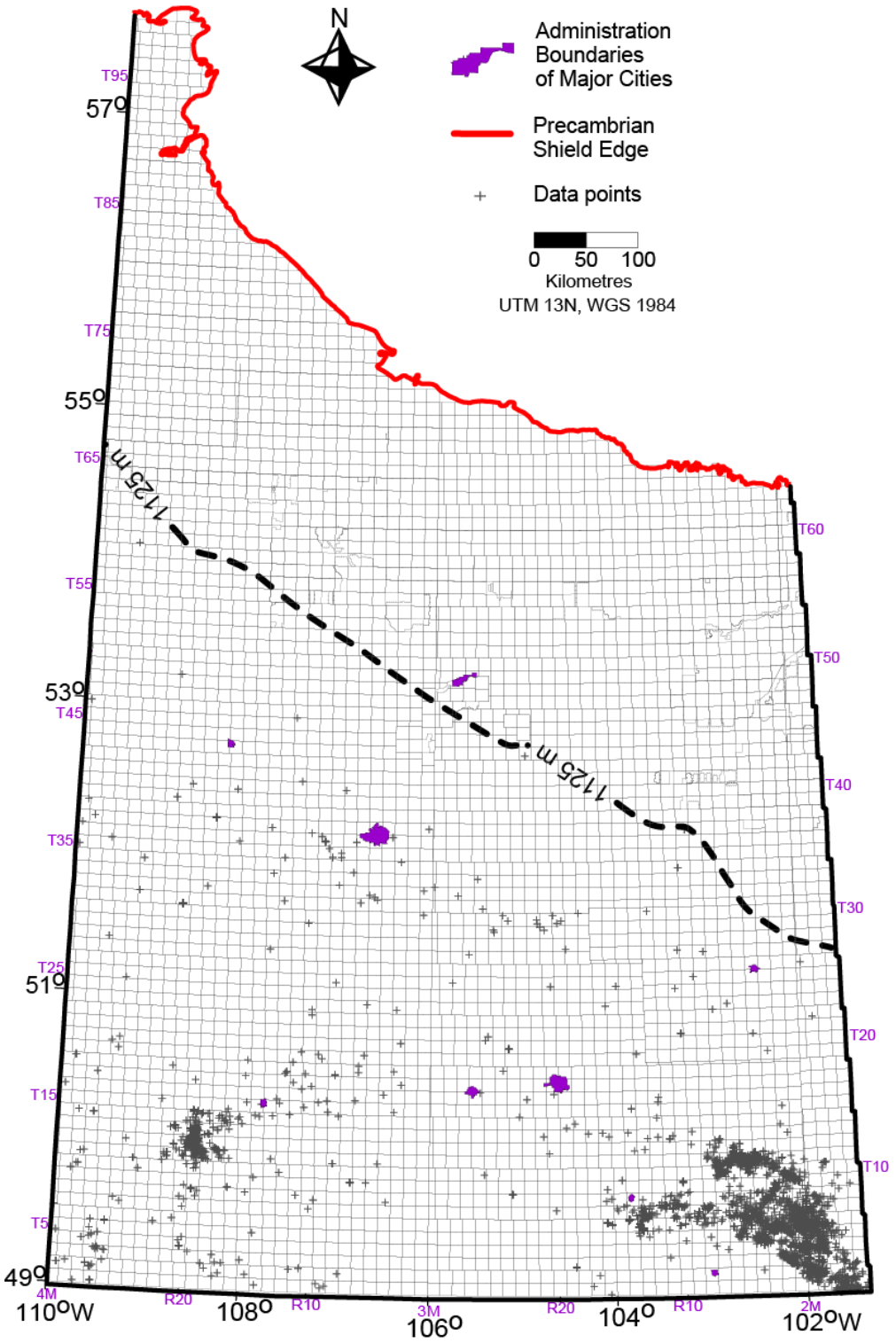

Figure C.6. b. Data distribution at 1250 m KB.

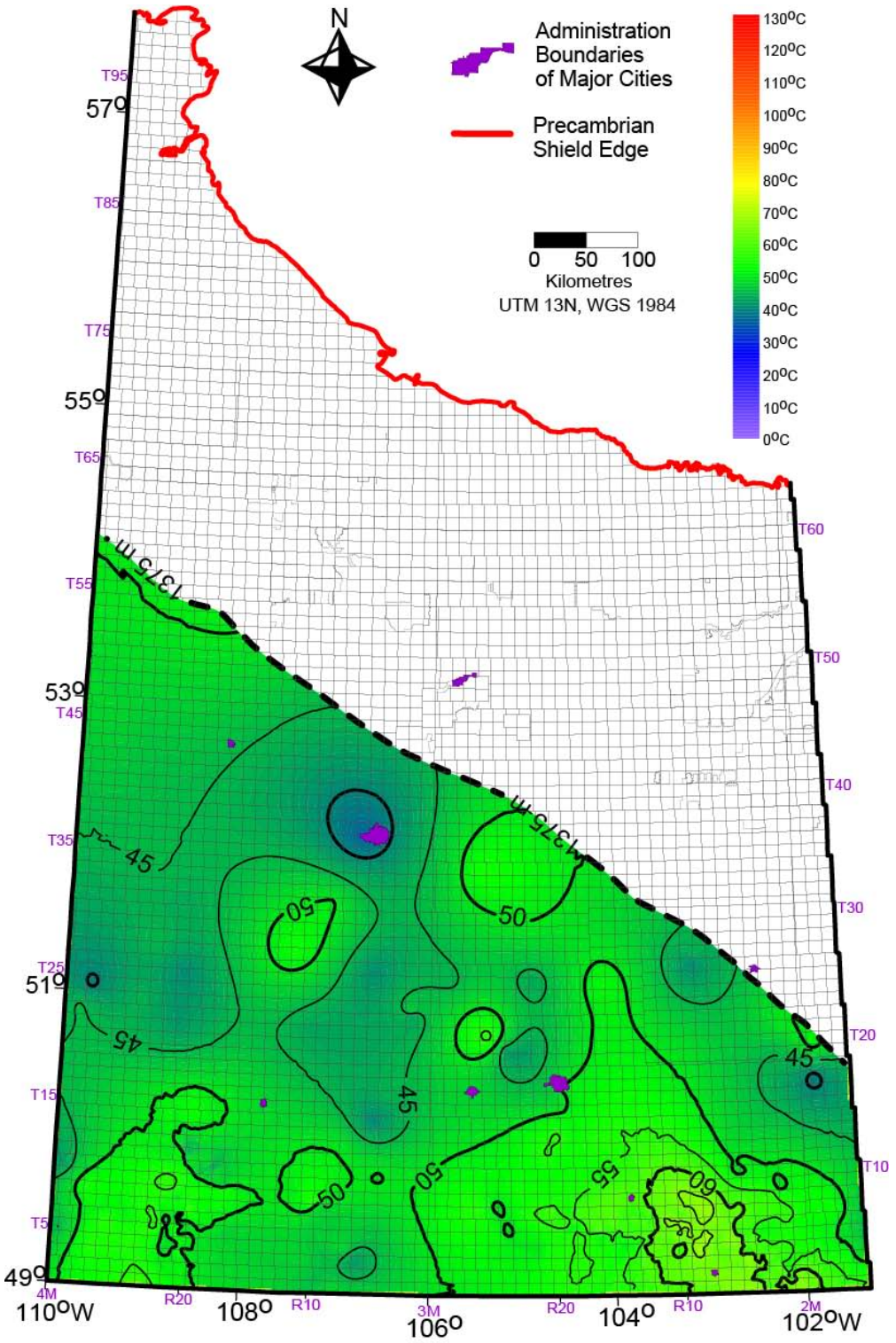

Figure C.7.a. Temperature at 1500 m KB. Data distribution would obscure features thus shown on a separate map, following this. CI: 5 °C.

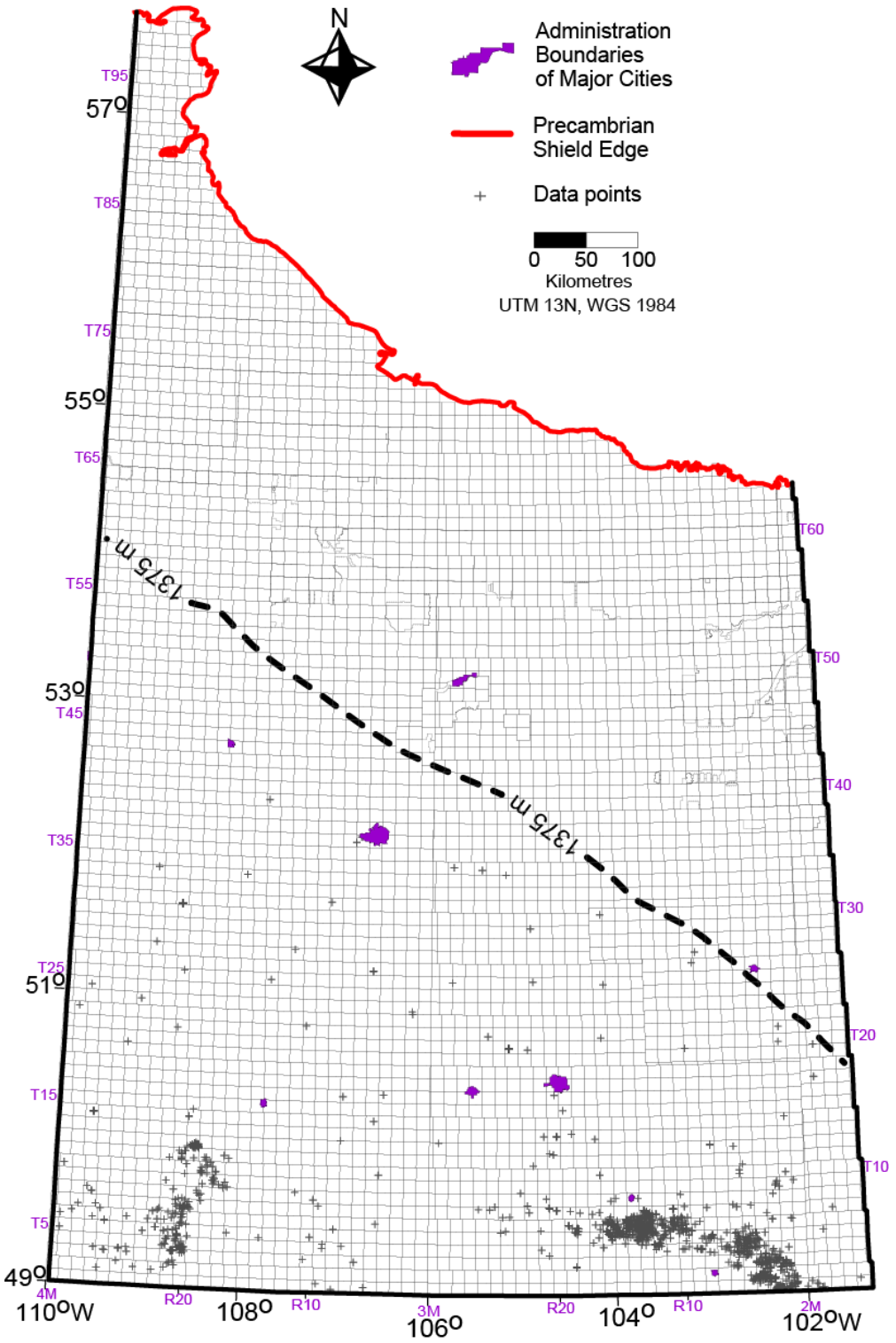

Figure C.7. b. Data distribution at 1500 m KB.

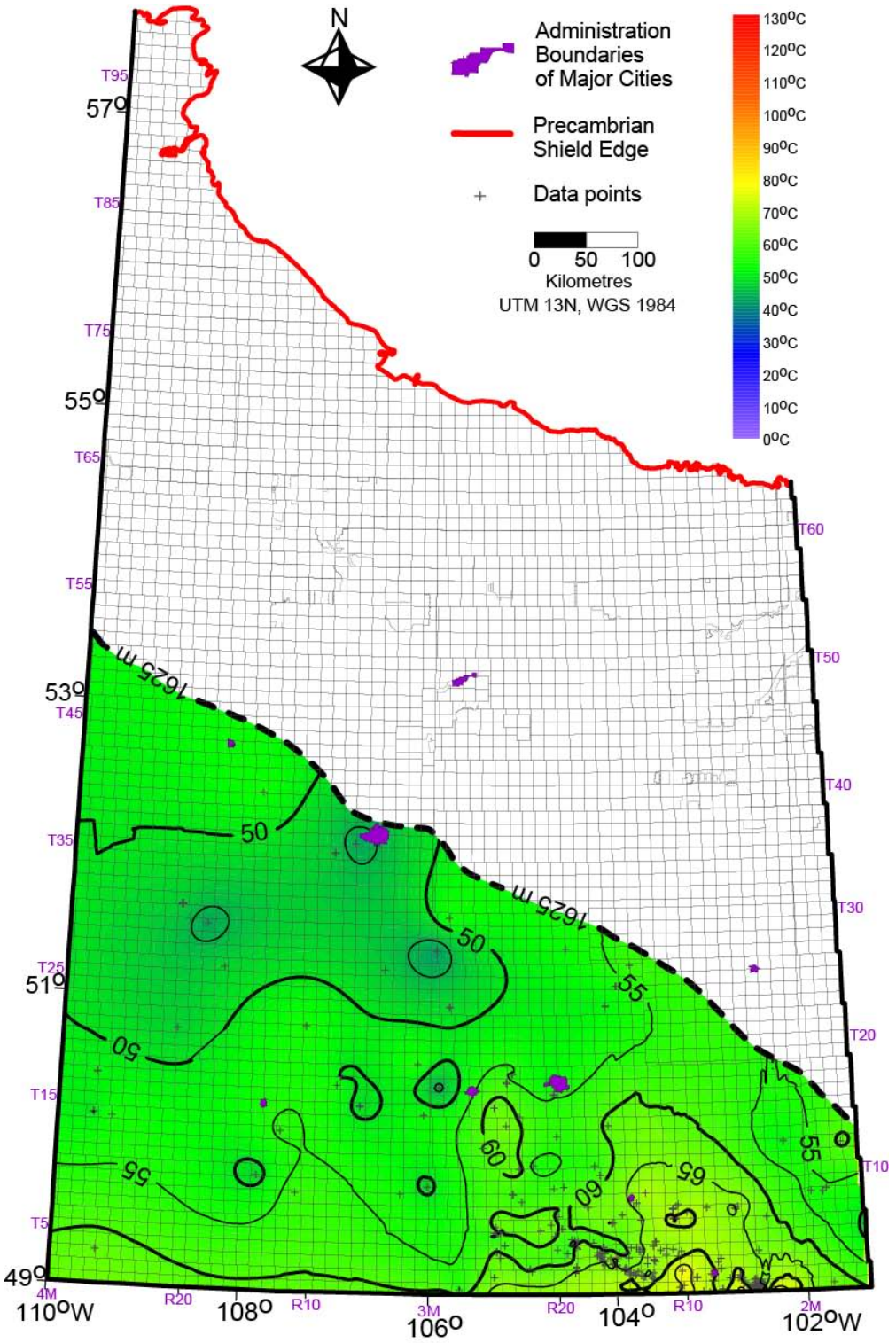

Figure C.8. Temperature at 1750 m KB. CI: 5 °C.

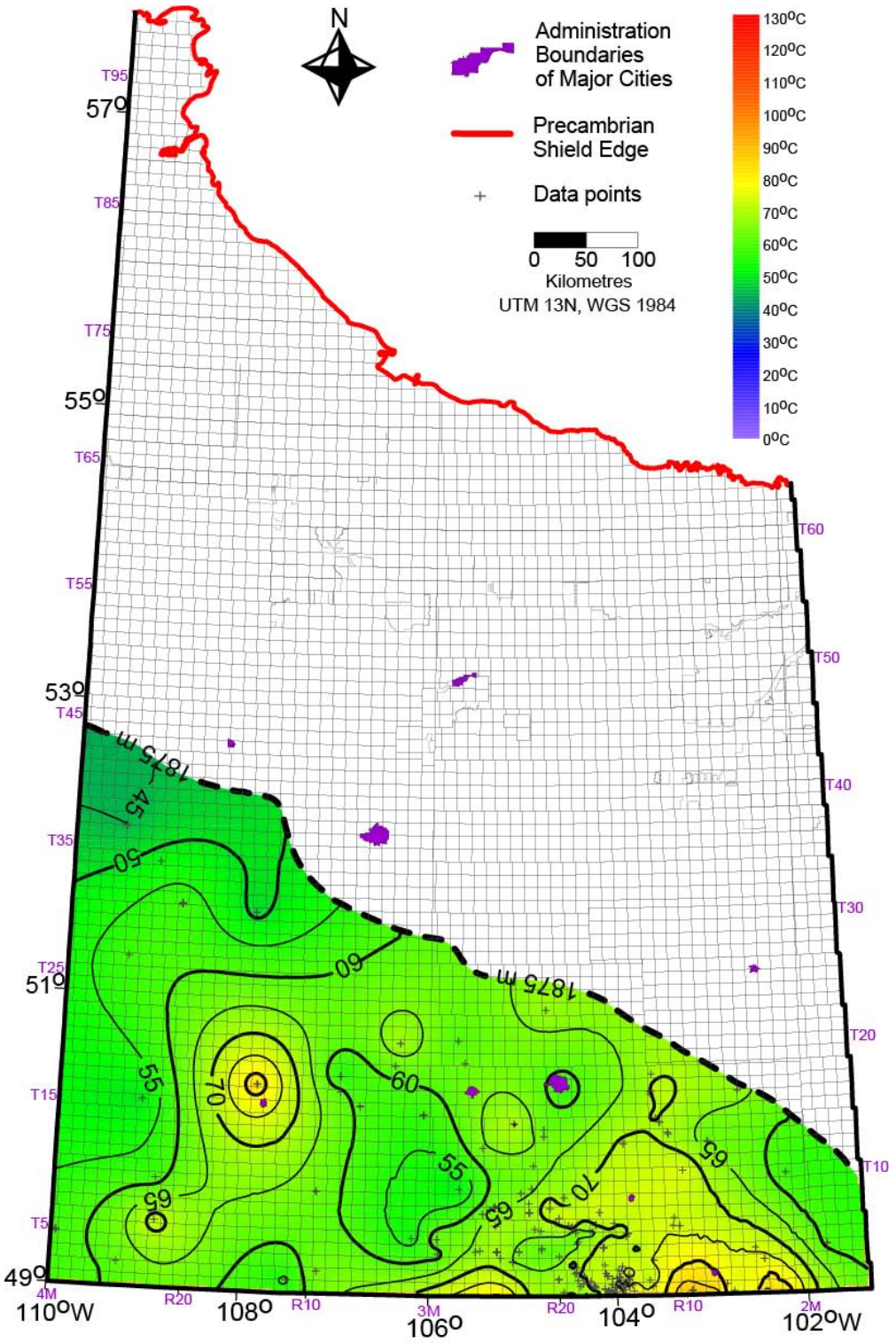

Figure C.9. Temperature at 2000 m KB. CI: 5 °C.

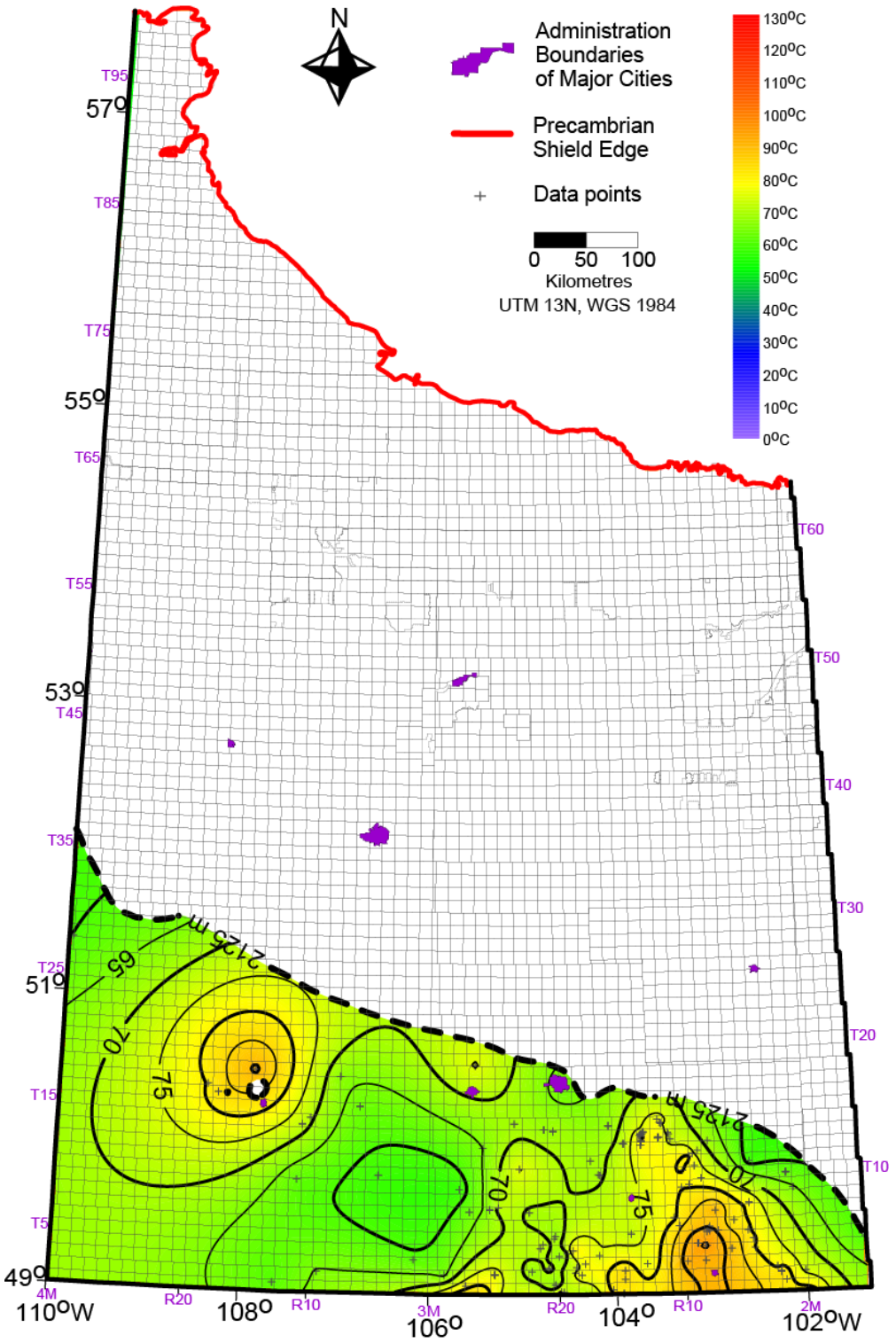

Figure C.10. Temperature at 2250 m KB. CI: 5 °C.

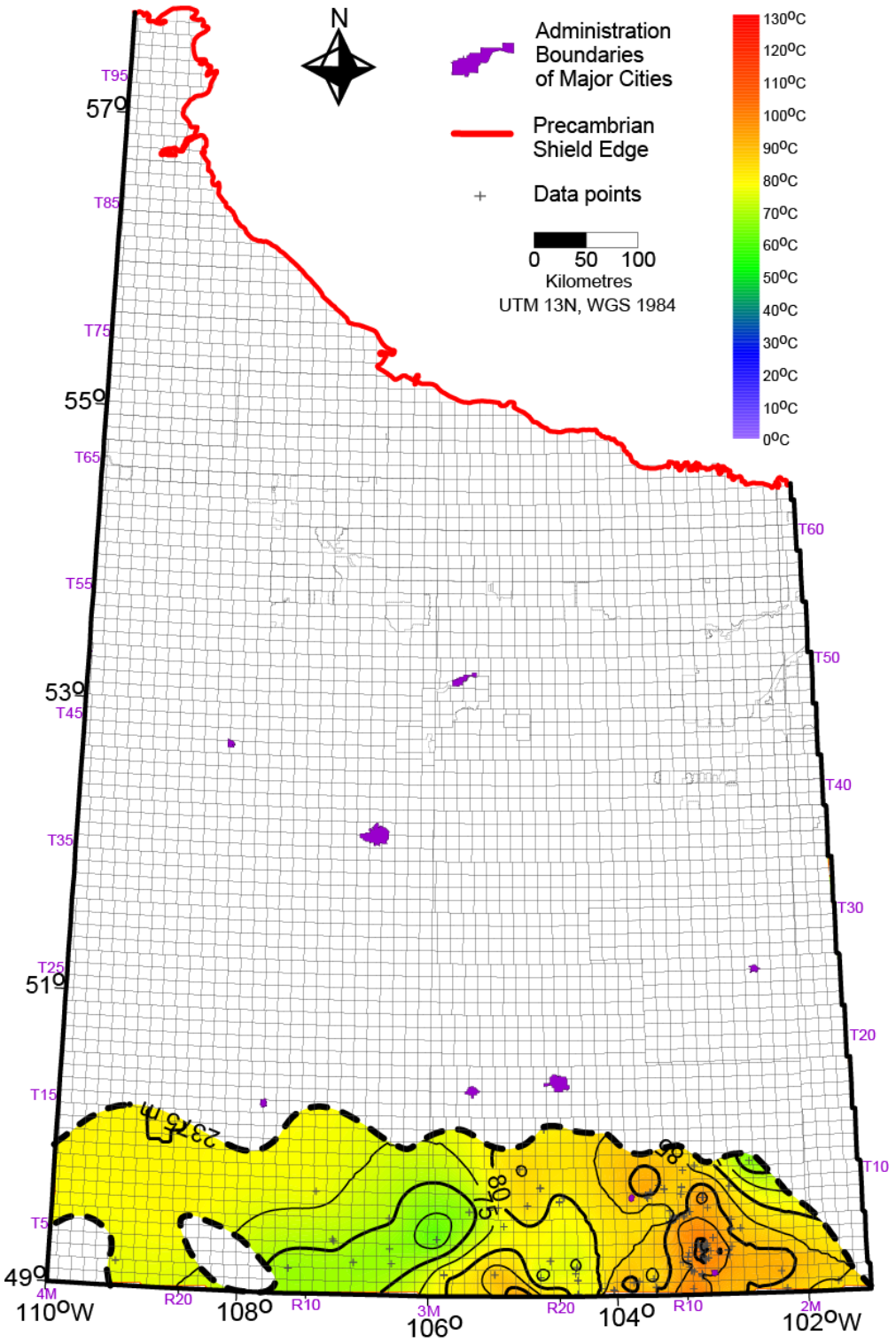

Figure C.11. Temperature at 2500 m KB. CI: 5 °C.

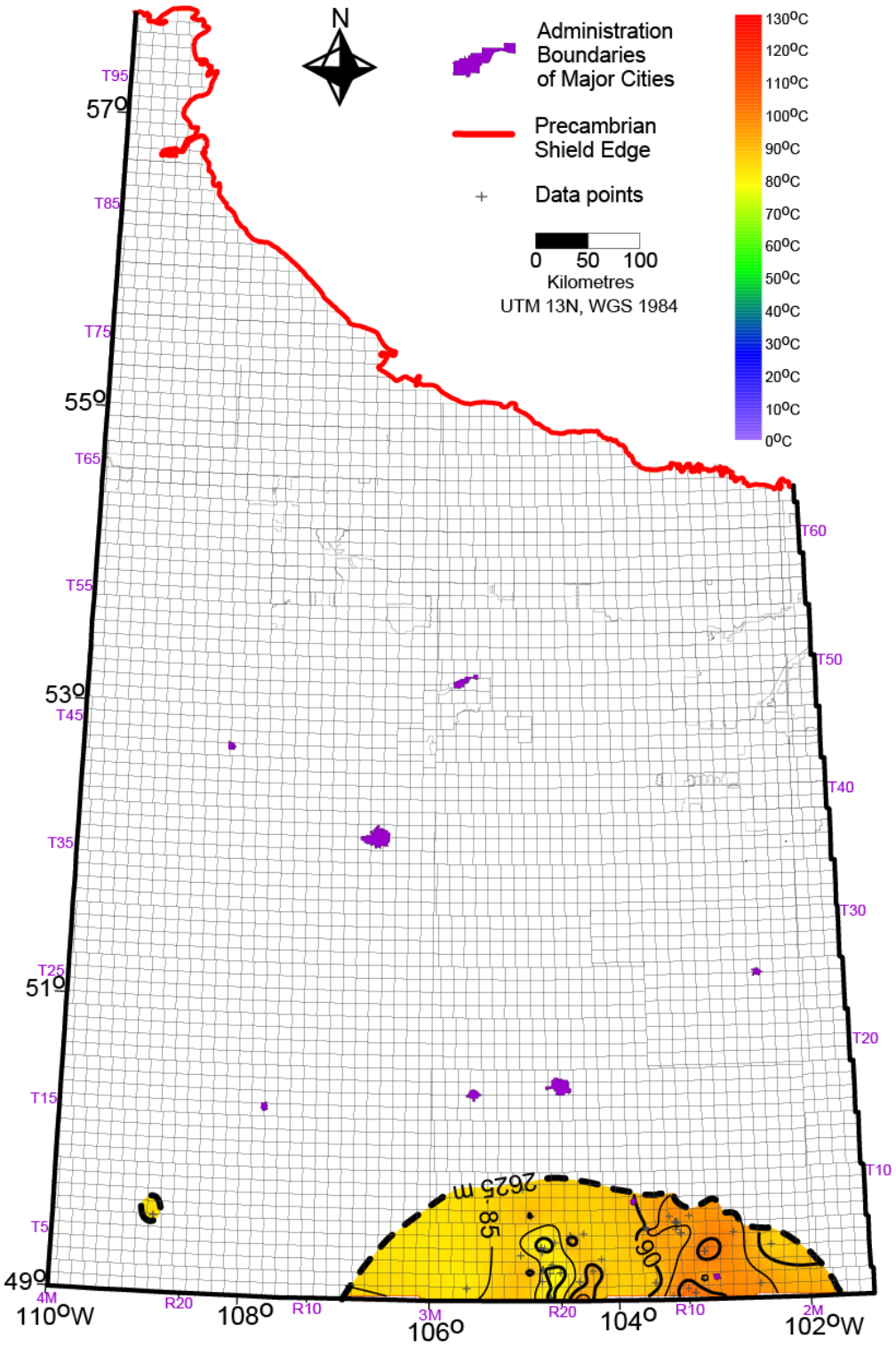

Figure C.12. Temperature at 2750 m KB. CI: 5 °C.

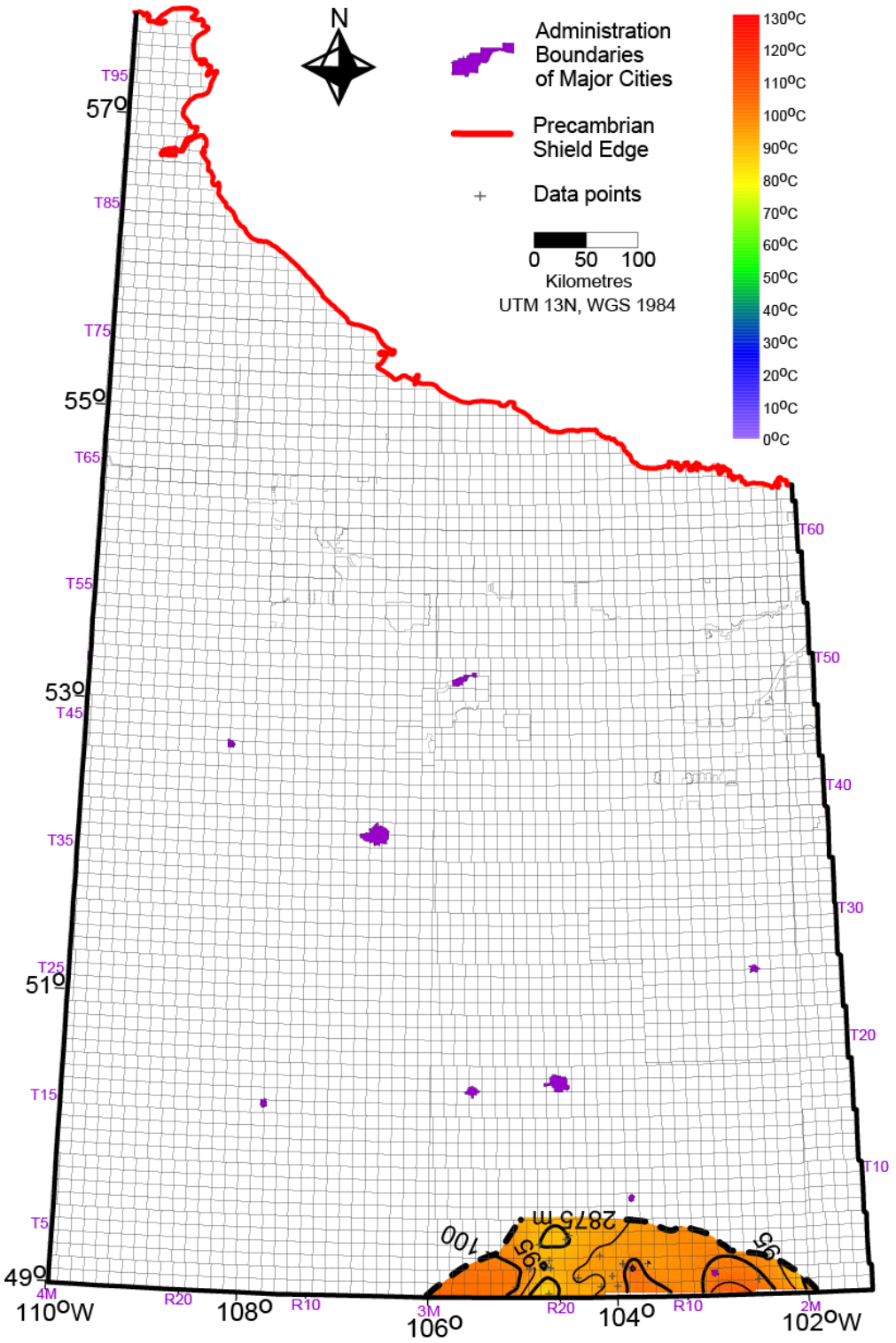

Figure C.13. Temperature at 3000 m KB. CI: 5 °C.

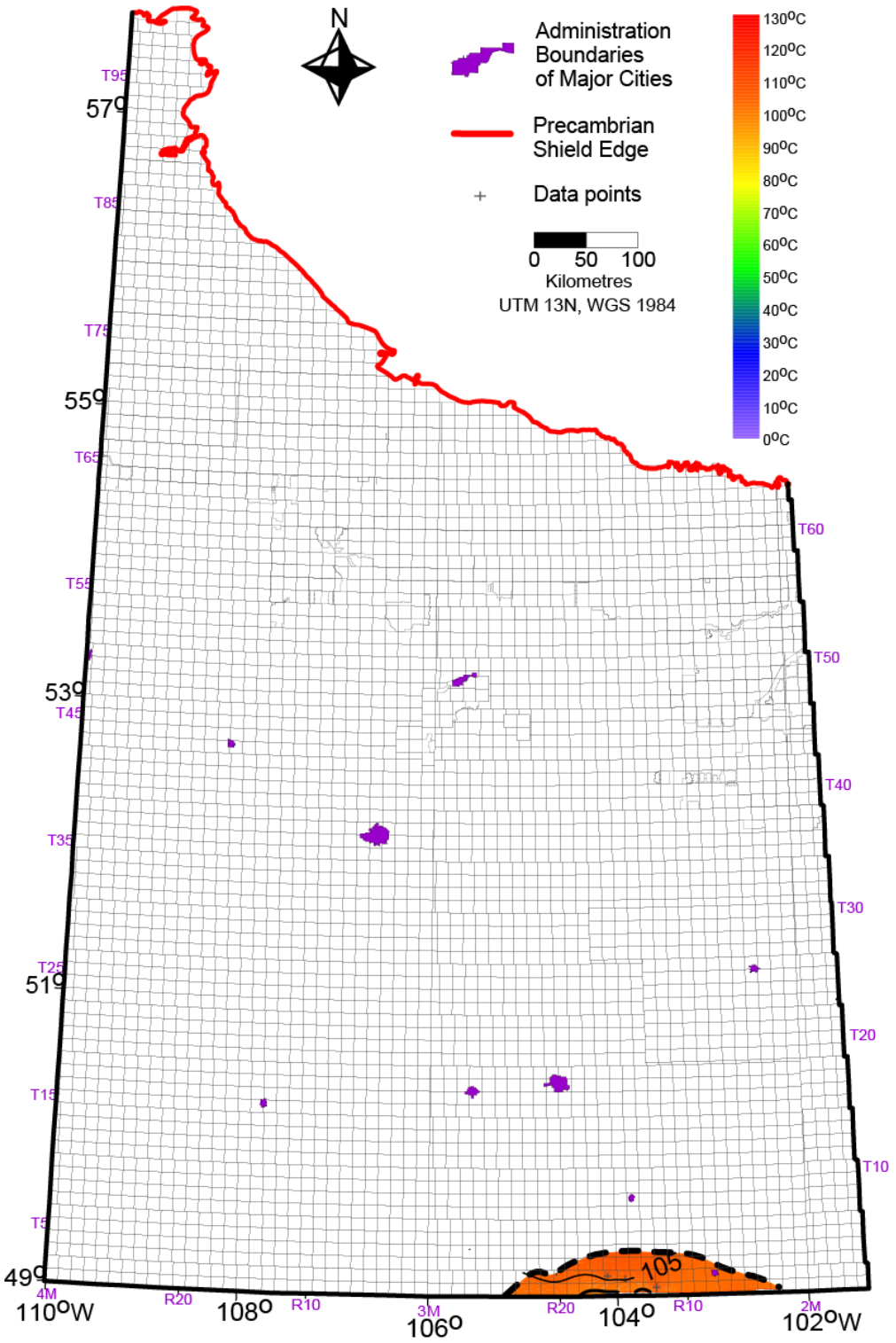

Figure C.14. Temperature at 3250 m KB. CI: 5 °C.

Appendix D. Isothermal maps

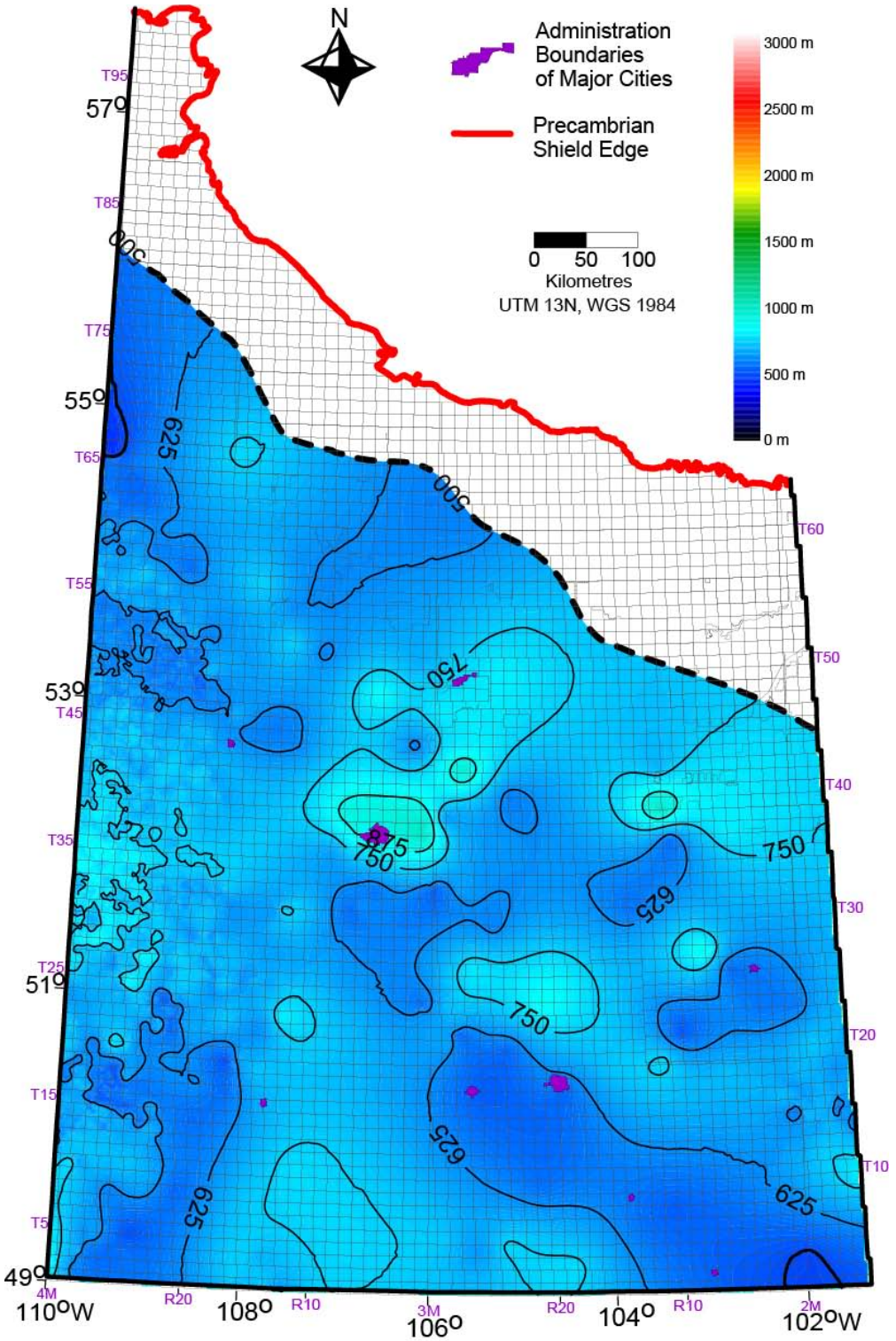

Figure D.1.a 25 °C isothermal depth map. Data distribution would obscure features thus shown on a separate map, following this. CI: 125 m.

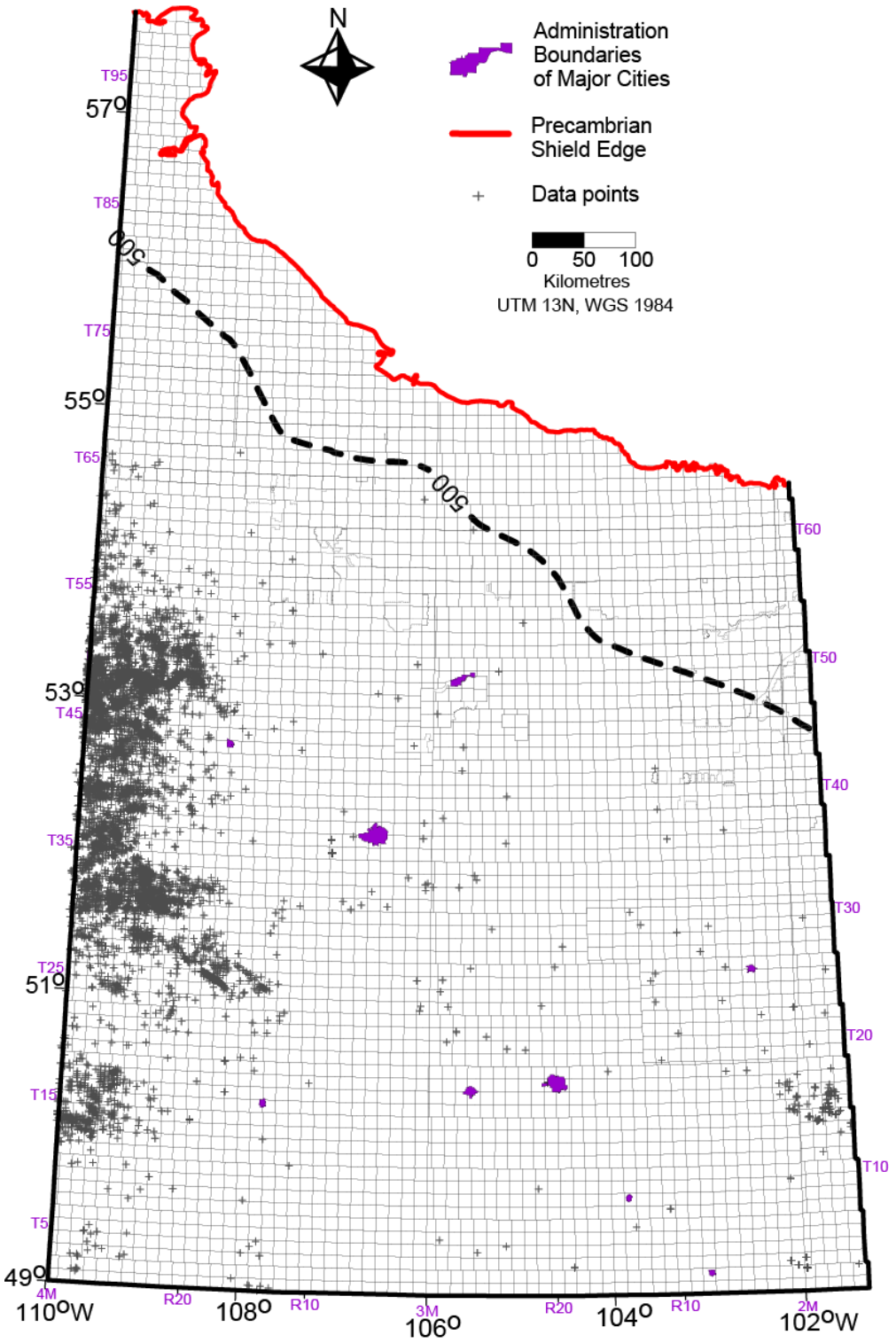

Figure D.1. b Data distribution for the 25 °C isothermal depth map.

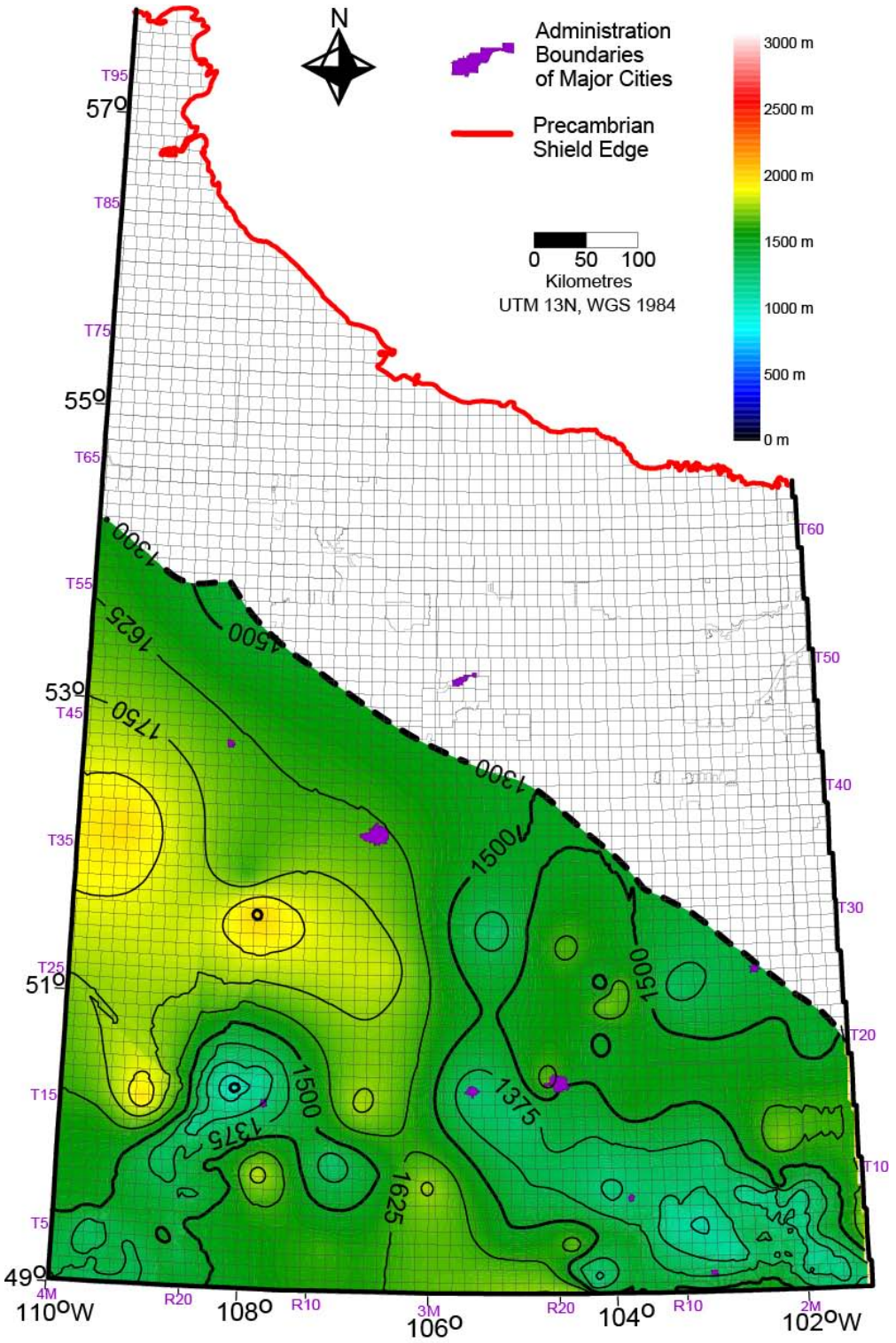

Figure D.2.a 50 °C isothermal depth map. Data distribution would obscure features thus shown on a separate map, following this. CI: 125 m.

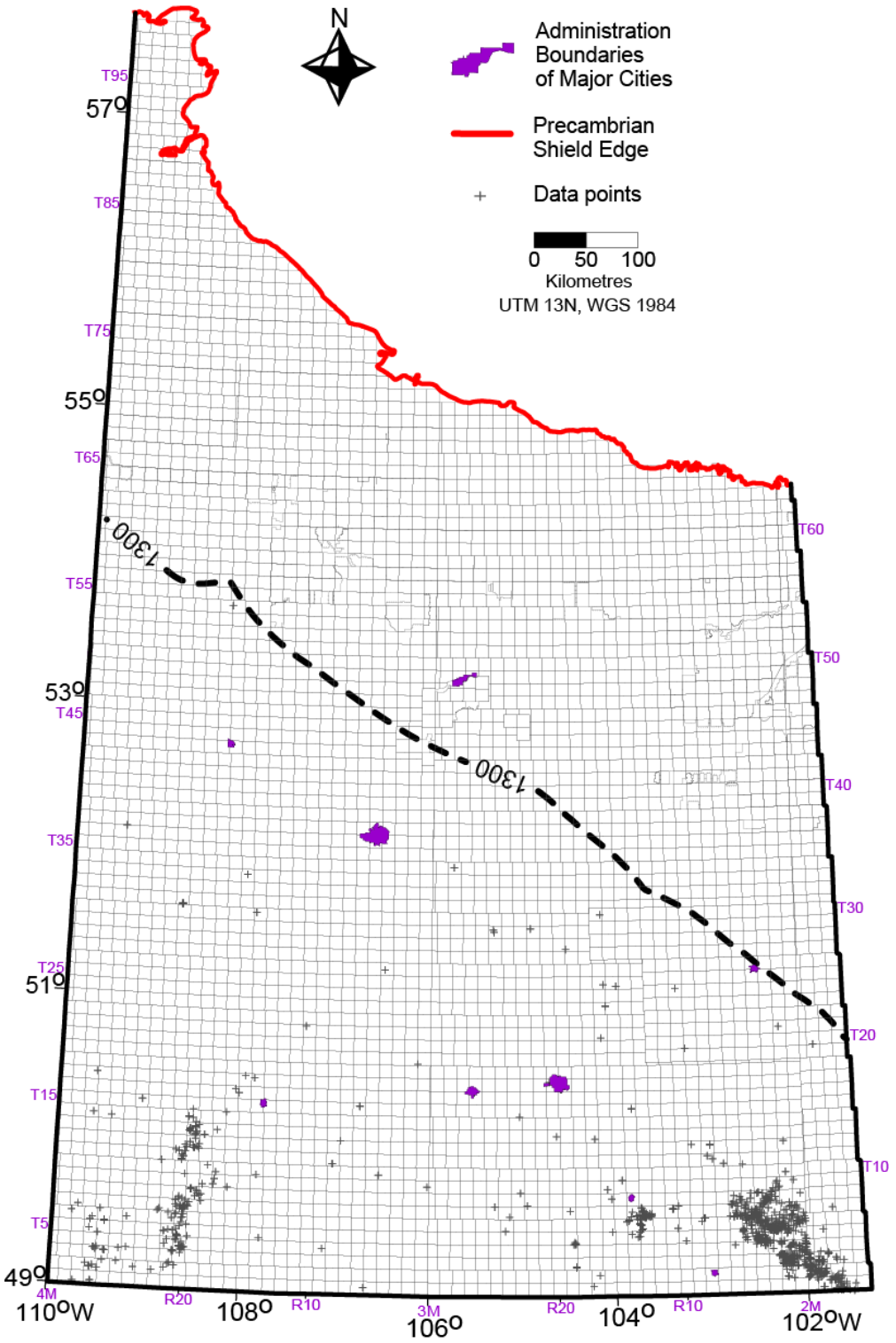

Figure D.2.b Data distribution for the 50 °C isothermal depth map.

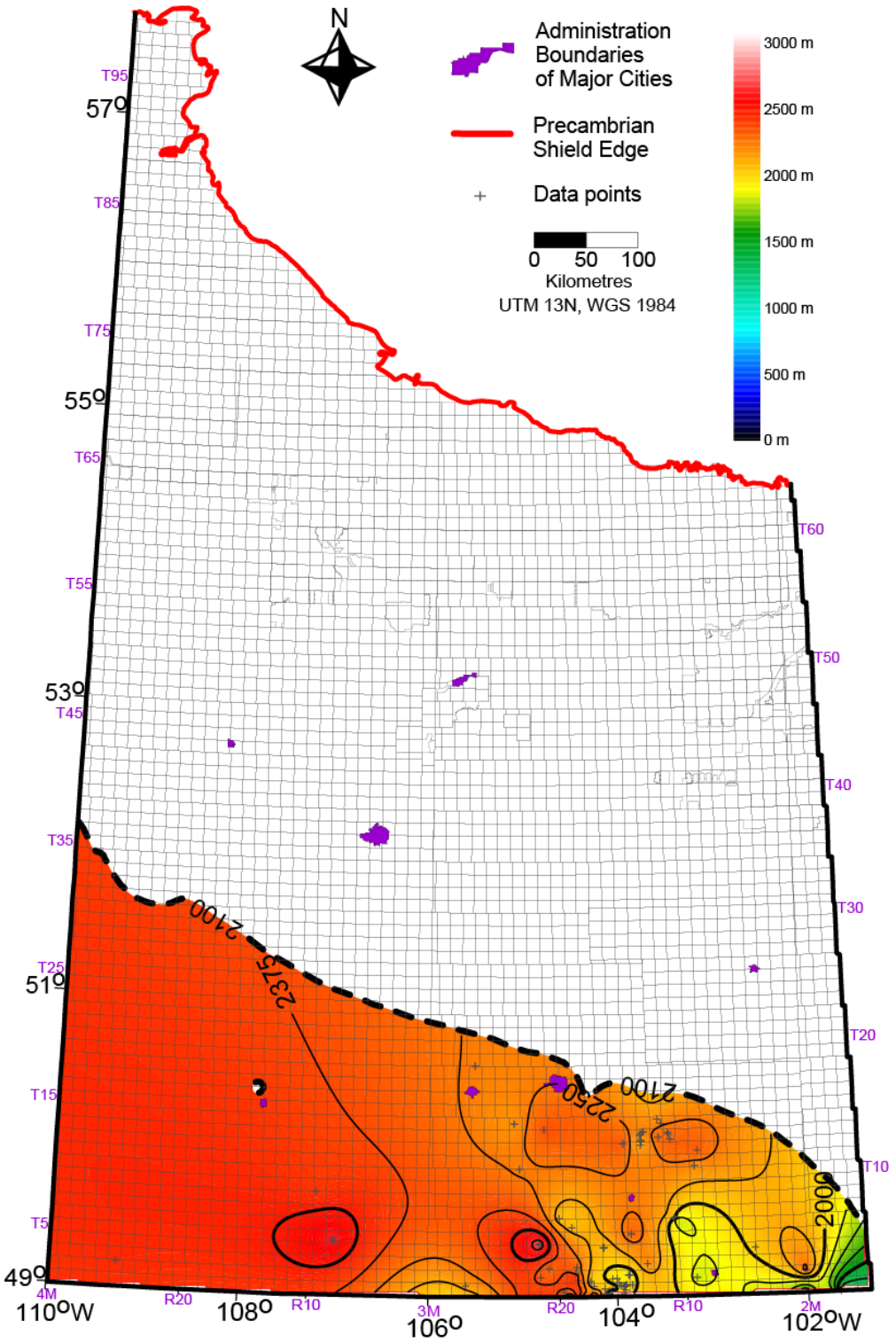

Figure D.3. 75 °C isothermal depth map. CI: 125 m.

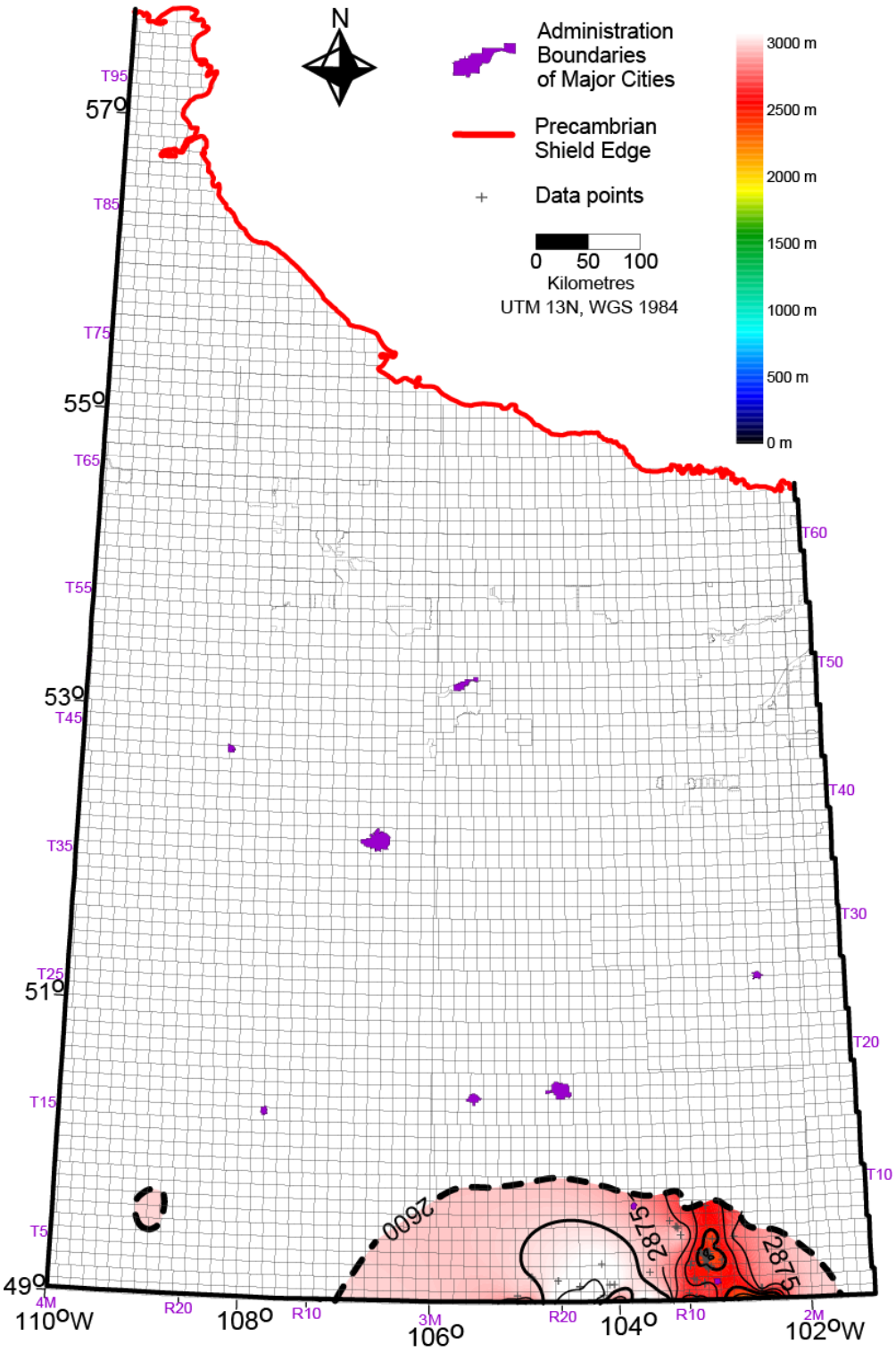

Figure D.4. 100 °C isothermal depth map. CI: 125 m.

Appendix E. Geothermal gradient maps

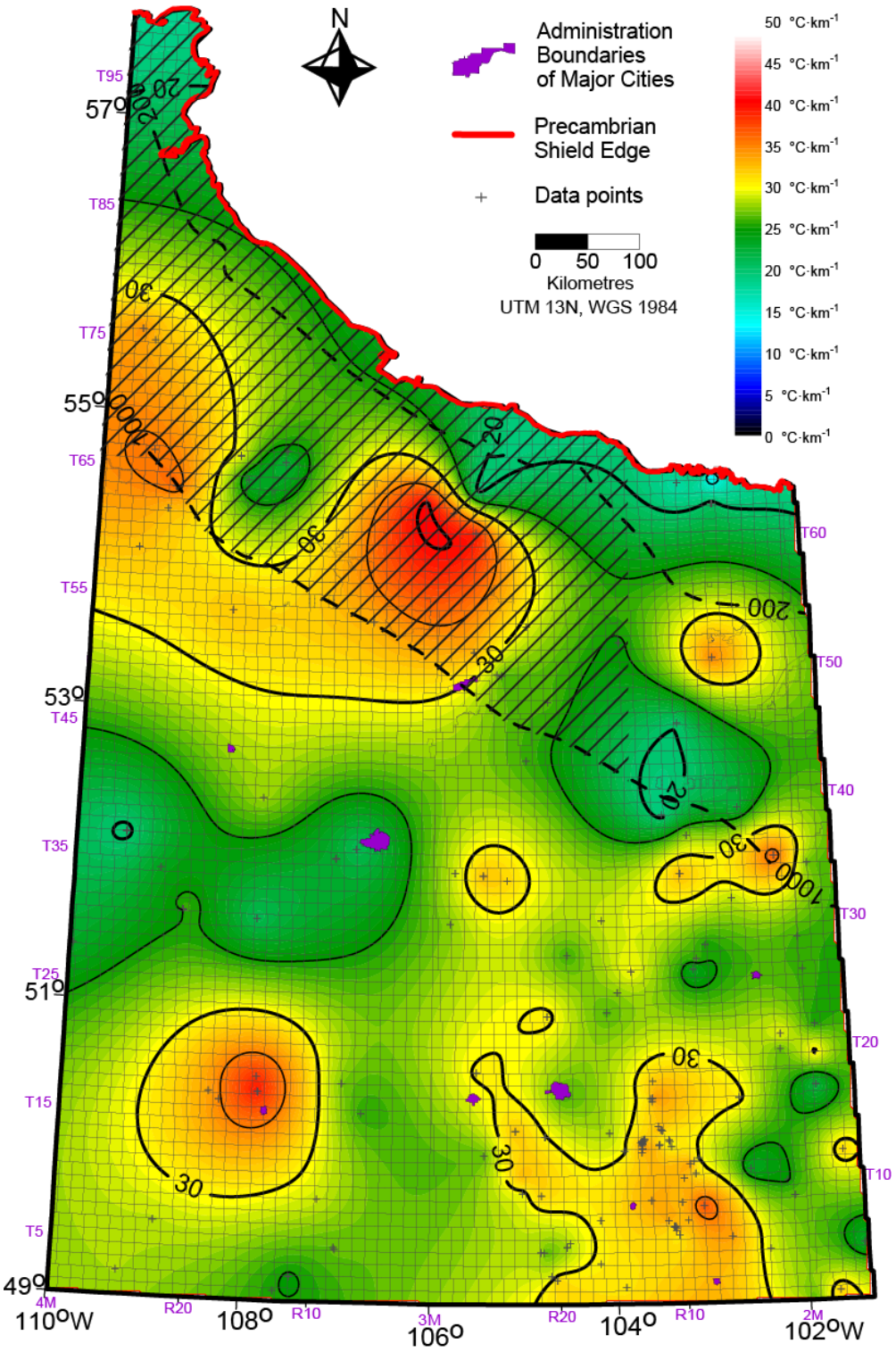

Figure E.1. Integral geothermal gradient map. CI: 5 °C·km^{-1}. Hatched area identifies shallow region supported by few, Quality B measurements.

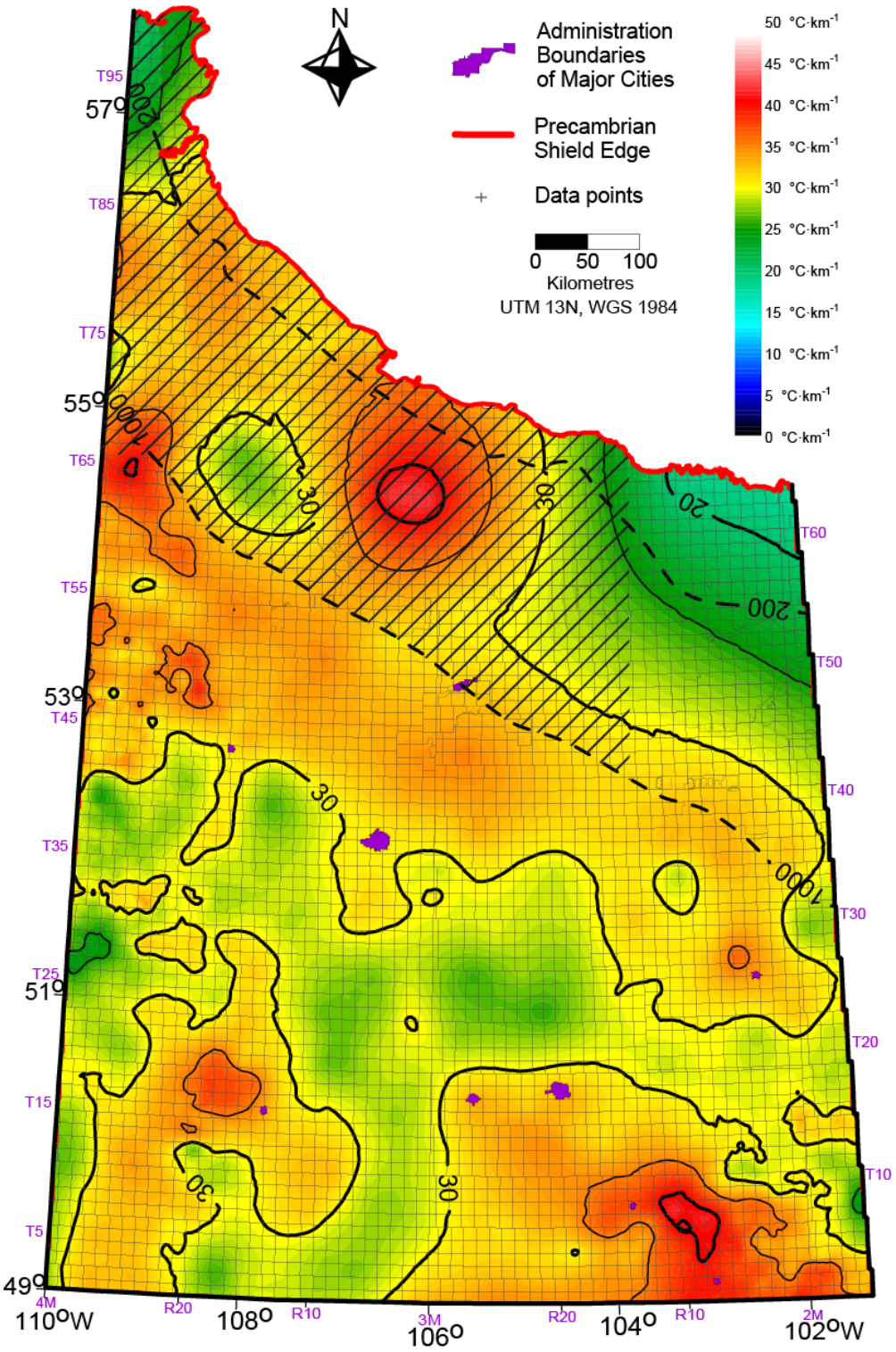

Figure E.2. Mesozoic-Cenozoic interval geothermal gradient map. Nugget effect: 1 $(°C)^2 \cdot km^{-2}$. CI: 5 $°C \cdot km^{-1}$. Data distribution is the same as A.13.b. Hatched area identifies shallow region supported by few, Quality B measurements.

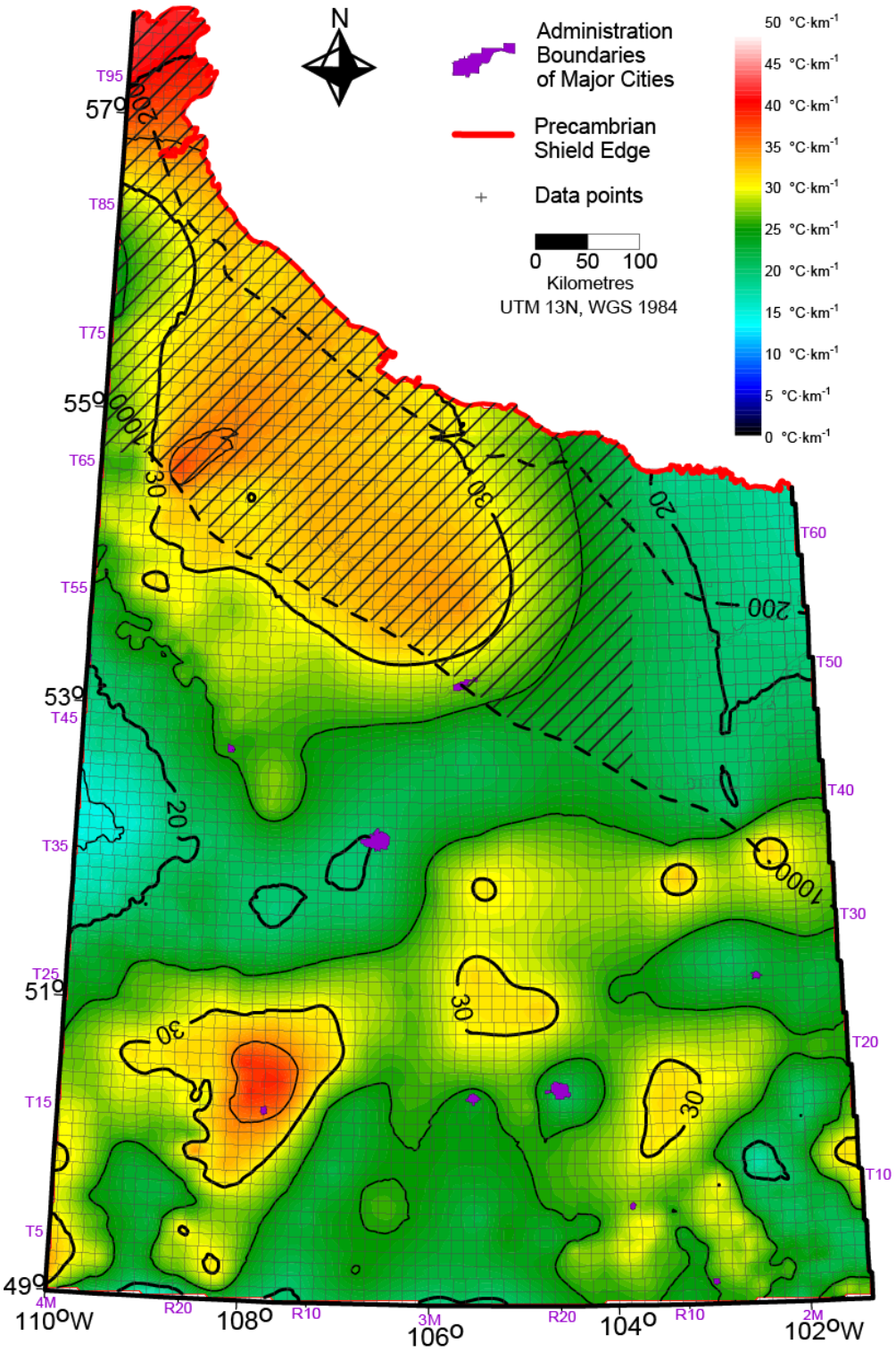

Figure E.3. Paleozoic interval geothermal gradient map. Nugget effect: 1 $(°C)^2 \cdot km^{-2}$. Data distribution is the same as A.13.b. CI: 5 $°C \cdot km^{-1}$. Hatched area identifies shallow region supported by few, Quality B measurements.

Appendix F. Thermal conductivity maps

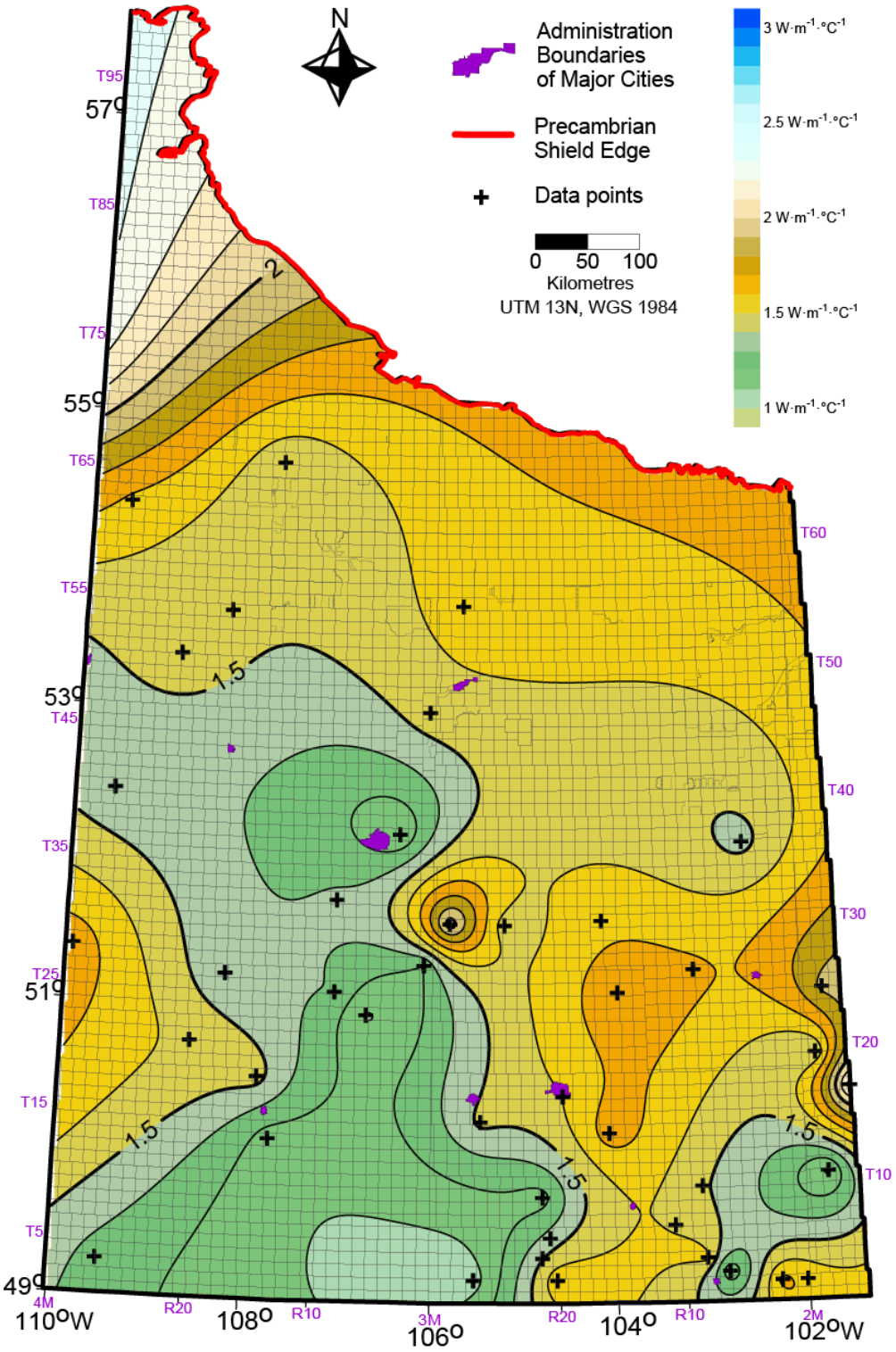

Figure F.1. Integral thermal conductivity map. CI: 0.1 $W \cdot m^{-1} \cdot °C^{-1}$.

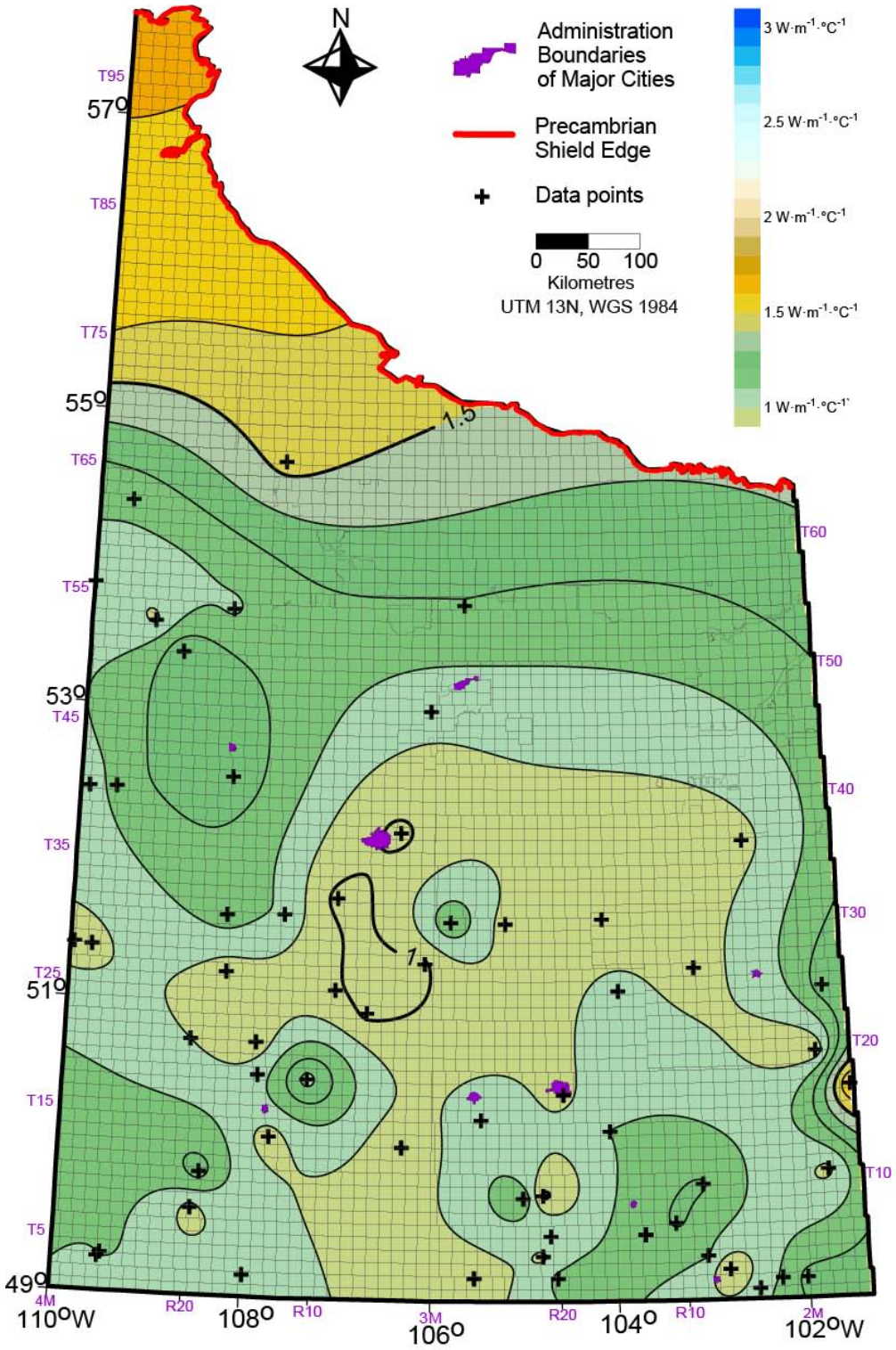

Figure F.2. Mesozoic-Cenozoic interval thermal conductivity map. CI: 0.1 $W \cdot m^{-1} \cdot °C^{-1}$.

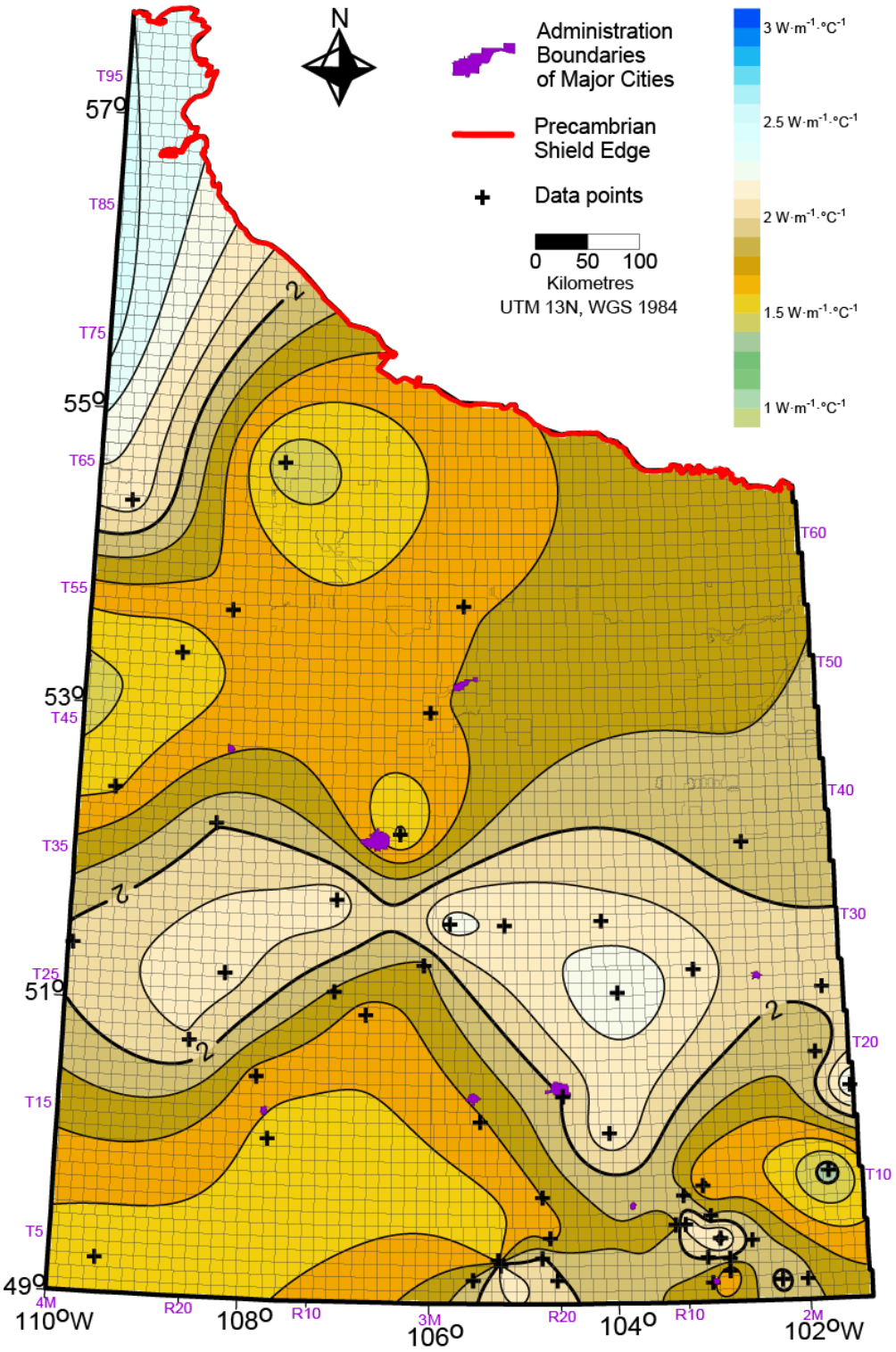

Figure F.3. Paleozoic interval thermal conductivity map. CI: 0.1 $W \cdot m^{-1} \cdot °C^{-1}$.

Appendix G. Heat flow maps

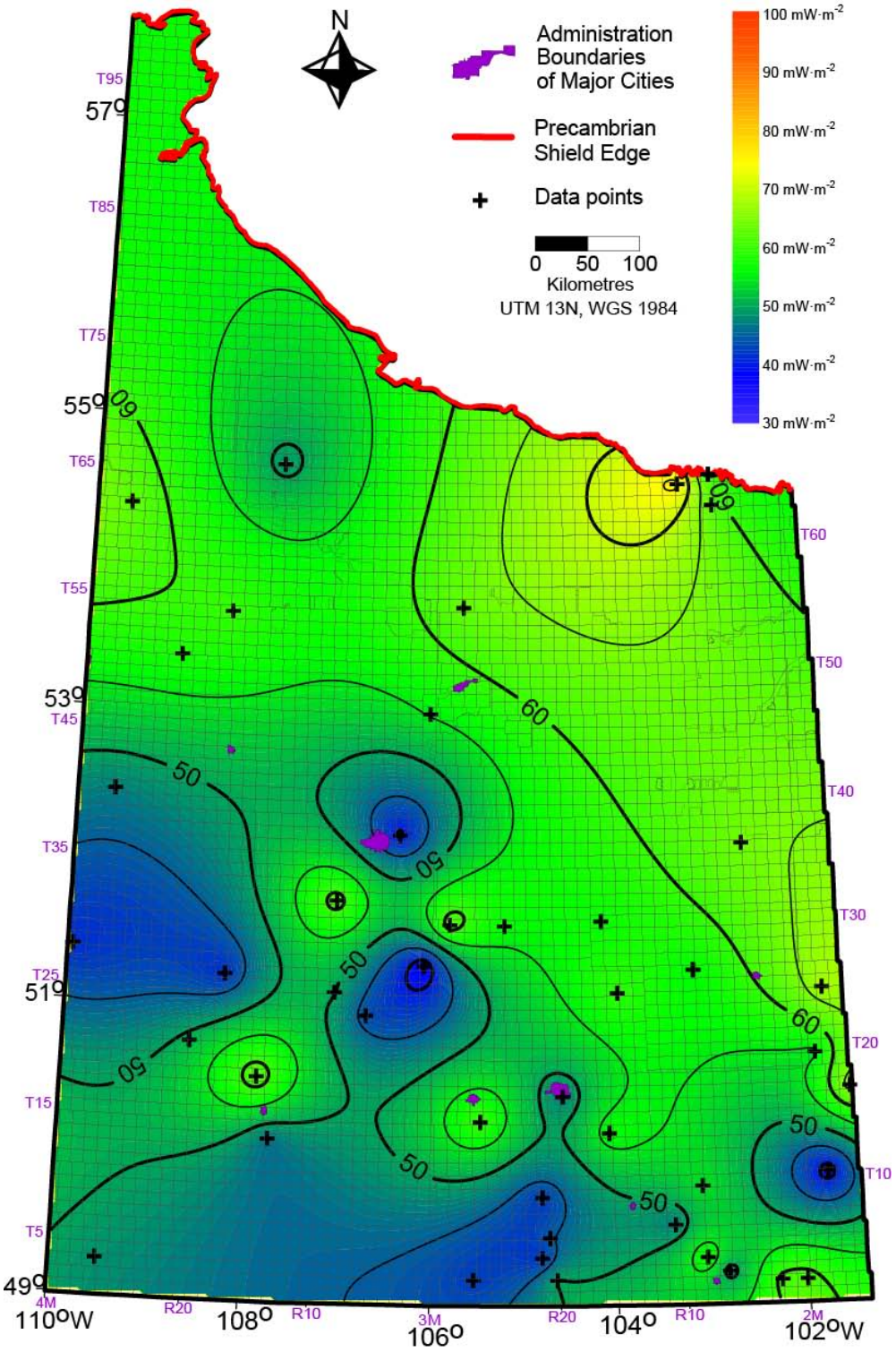

Figure G.1. Integral heat flow map. CI: 5 mW·m^{-2}.

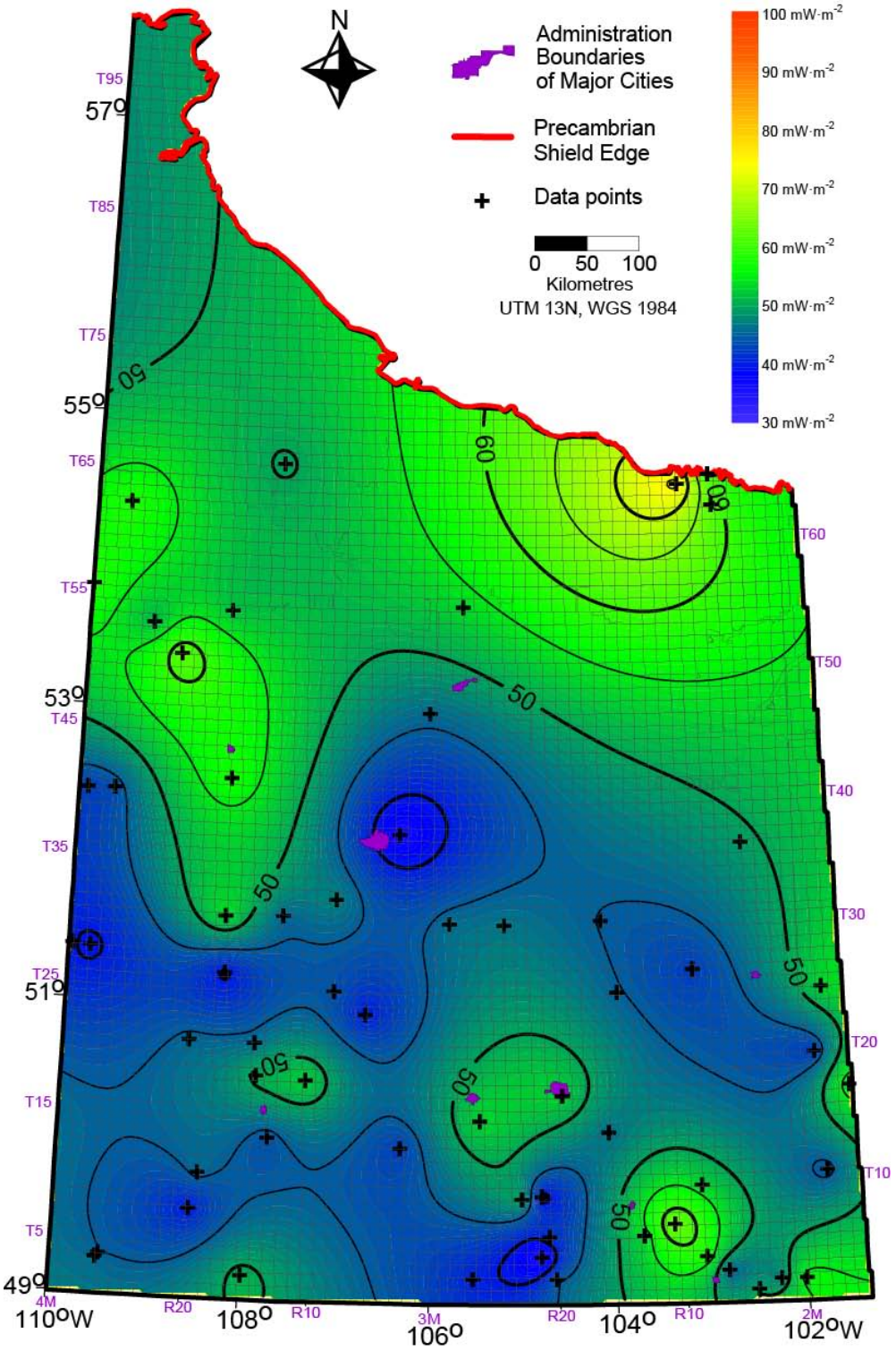

Figure G.2. Mesozoic-Cenozoic interval heat flow map. CI: 5 mW·m^{-2}.

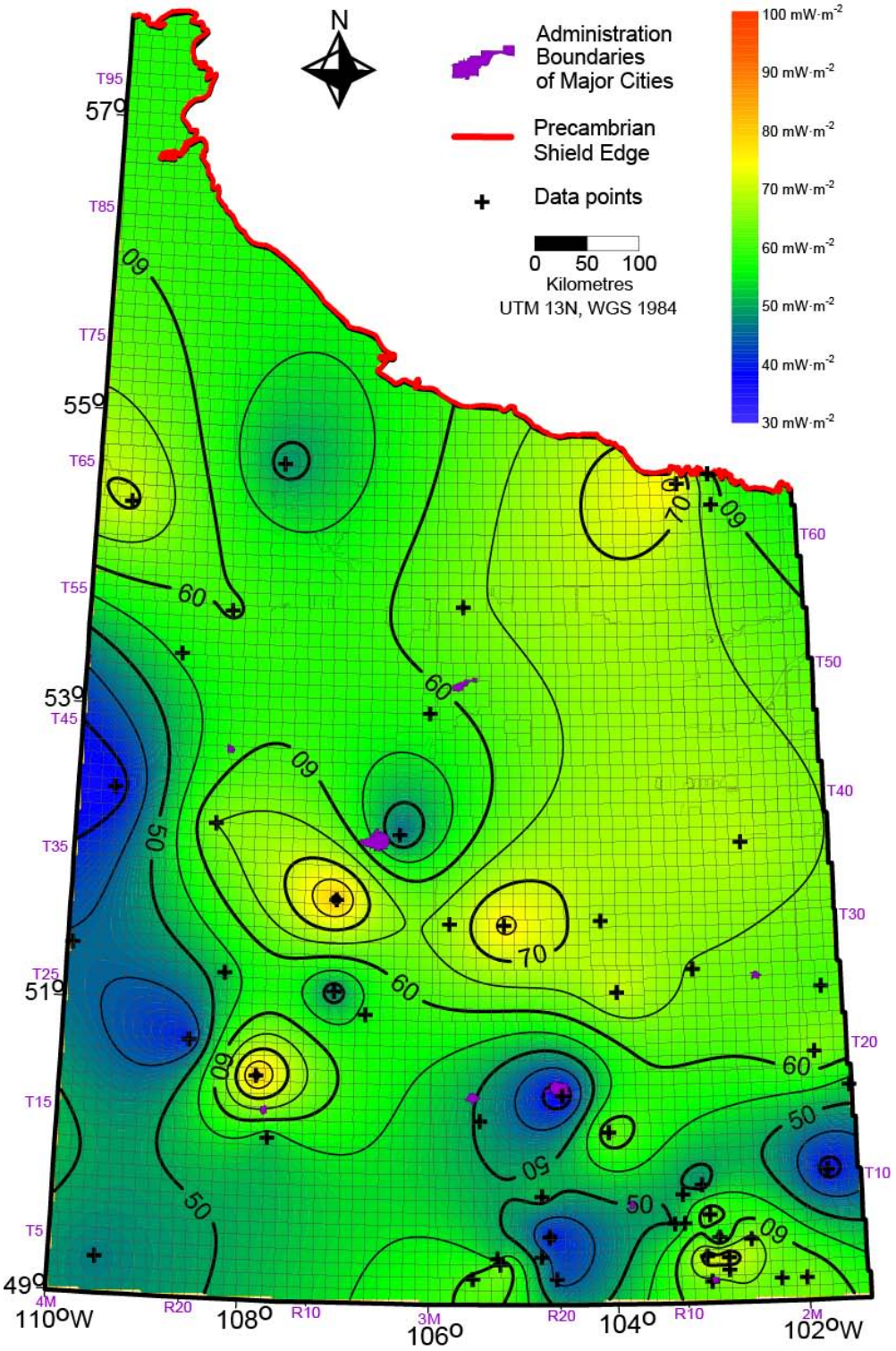

Figure G.3. Paleozoic interval heat flow map. CI: 5 mW·m^{-2}.

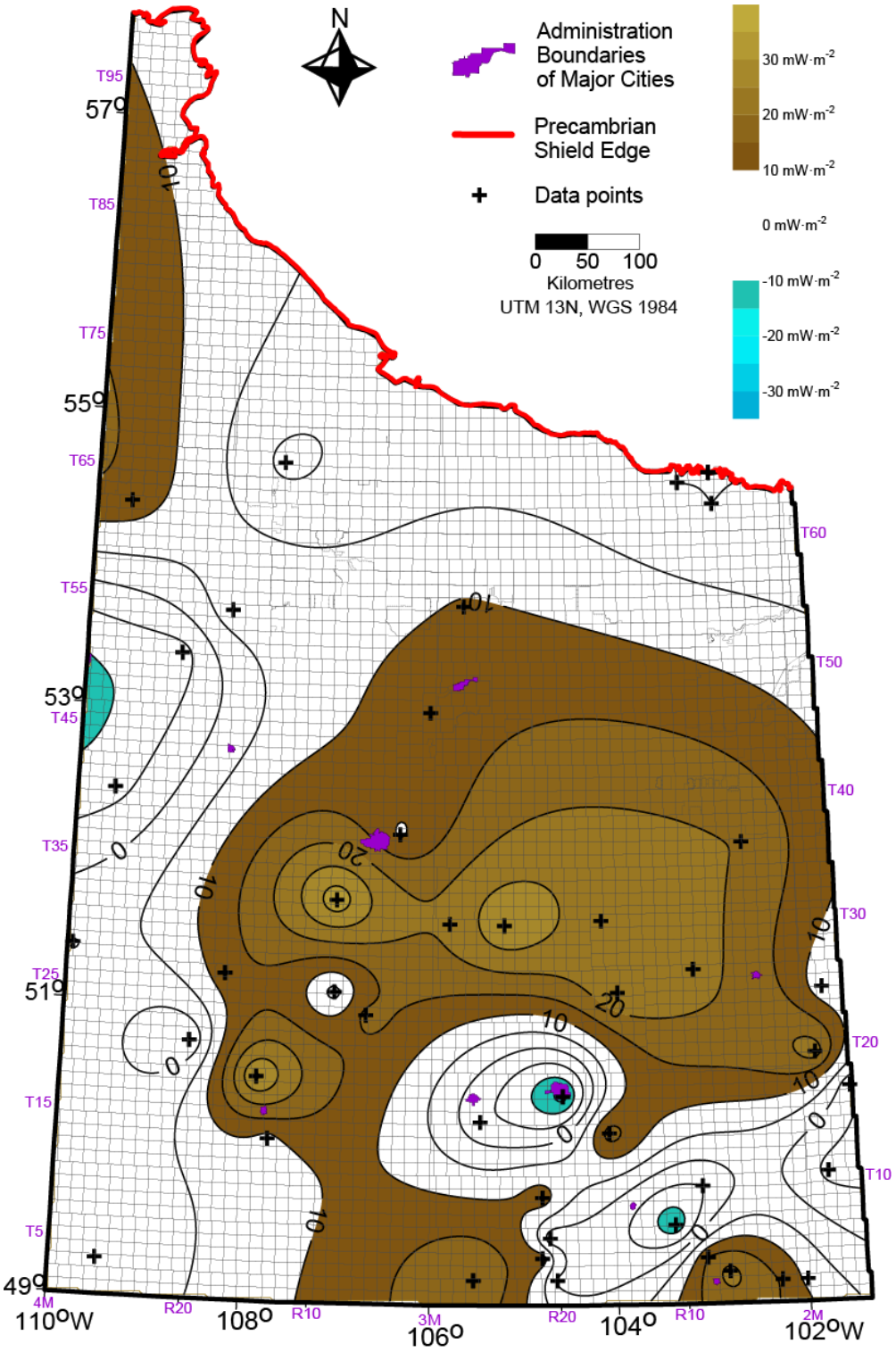

Figure G.4. Heat flow difference map. It was generated via subtracting the Mesozoic-Cenozoic heat flow from the Paleozoic heat flow. CI: 5 mW·m^{-2}.

Appendix H. Heat generation map

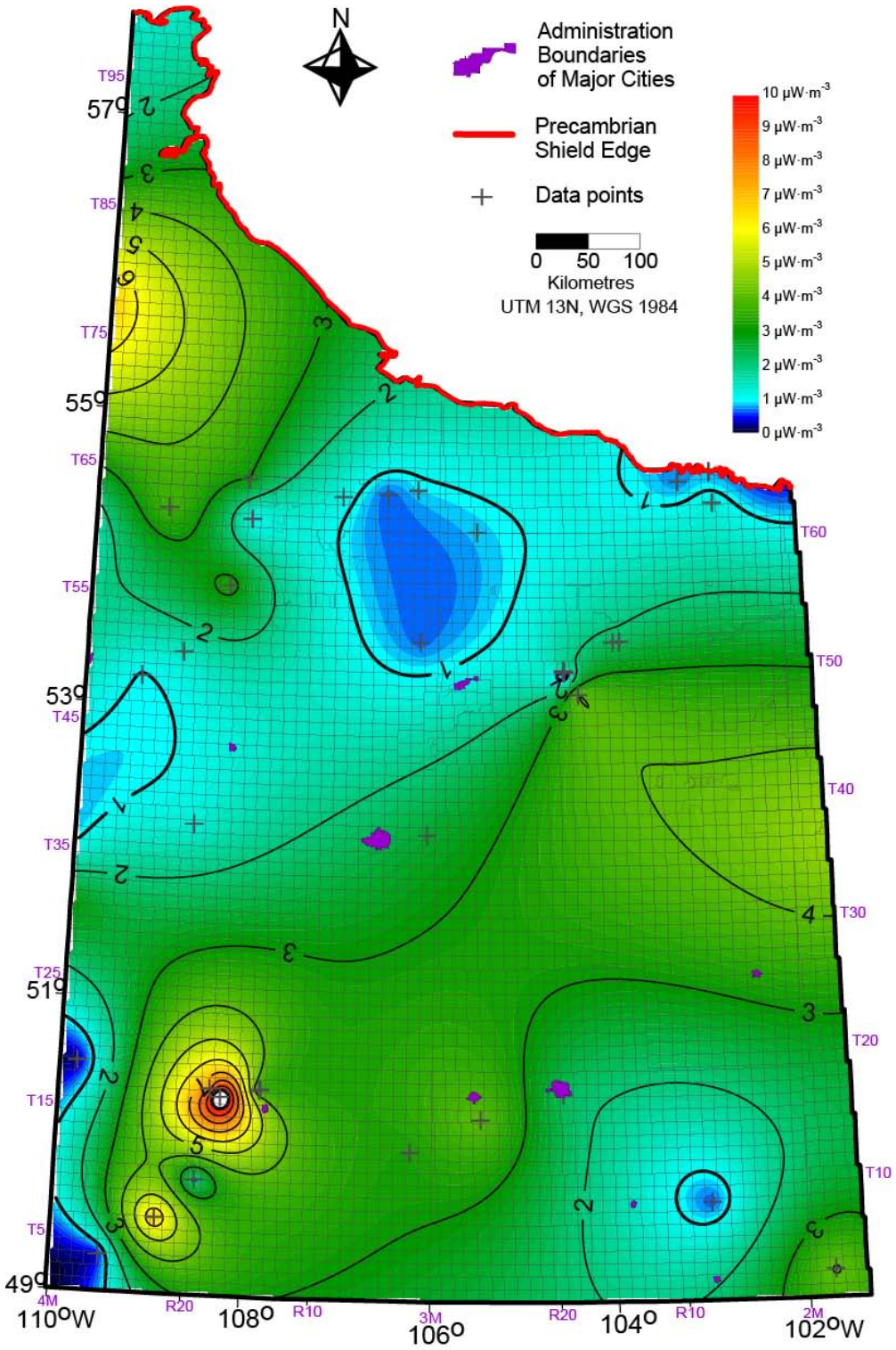

Figure H.1. Top of basement heat generation map. CI: 1 µW·m^{-3}.

Appendix I. Sensitivity to gridding

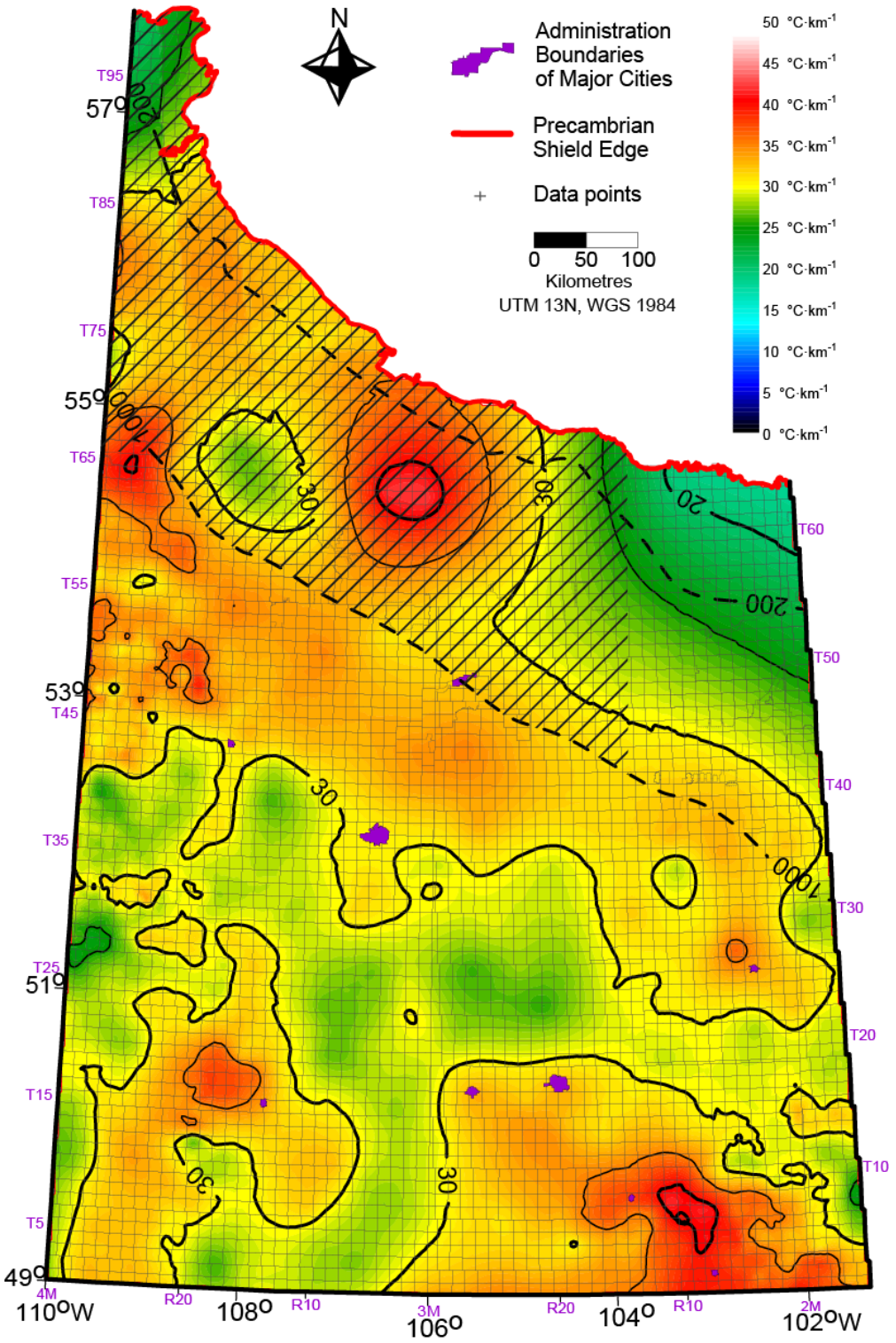

Figure I.1. Cenozoic-Mesozoic geothermal gradient with default kriging. Nugget effect: 1 $(°C)^2 \cdot km^{-2}$. CI: 5 °C/km. Data distribution is the same as A.13.b.

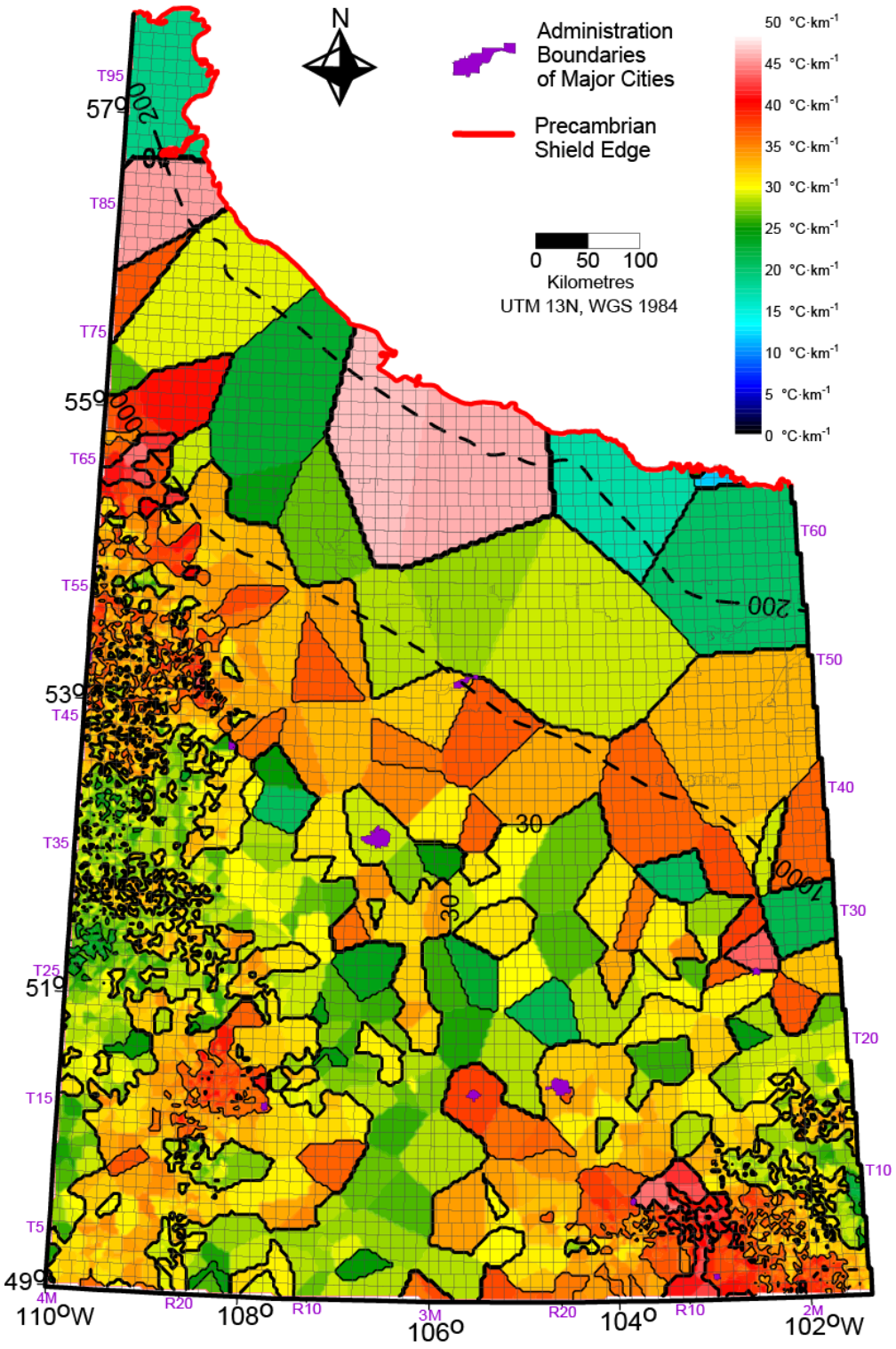

Figure I.2. Cenozoic-Mesozoic geothermal gradient with nearest neighbours. CI: 5 °C/km. Data distribution is the same as A.13.b.

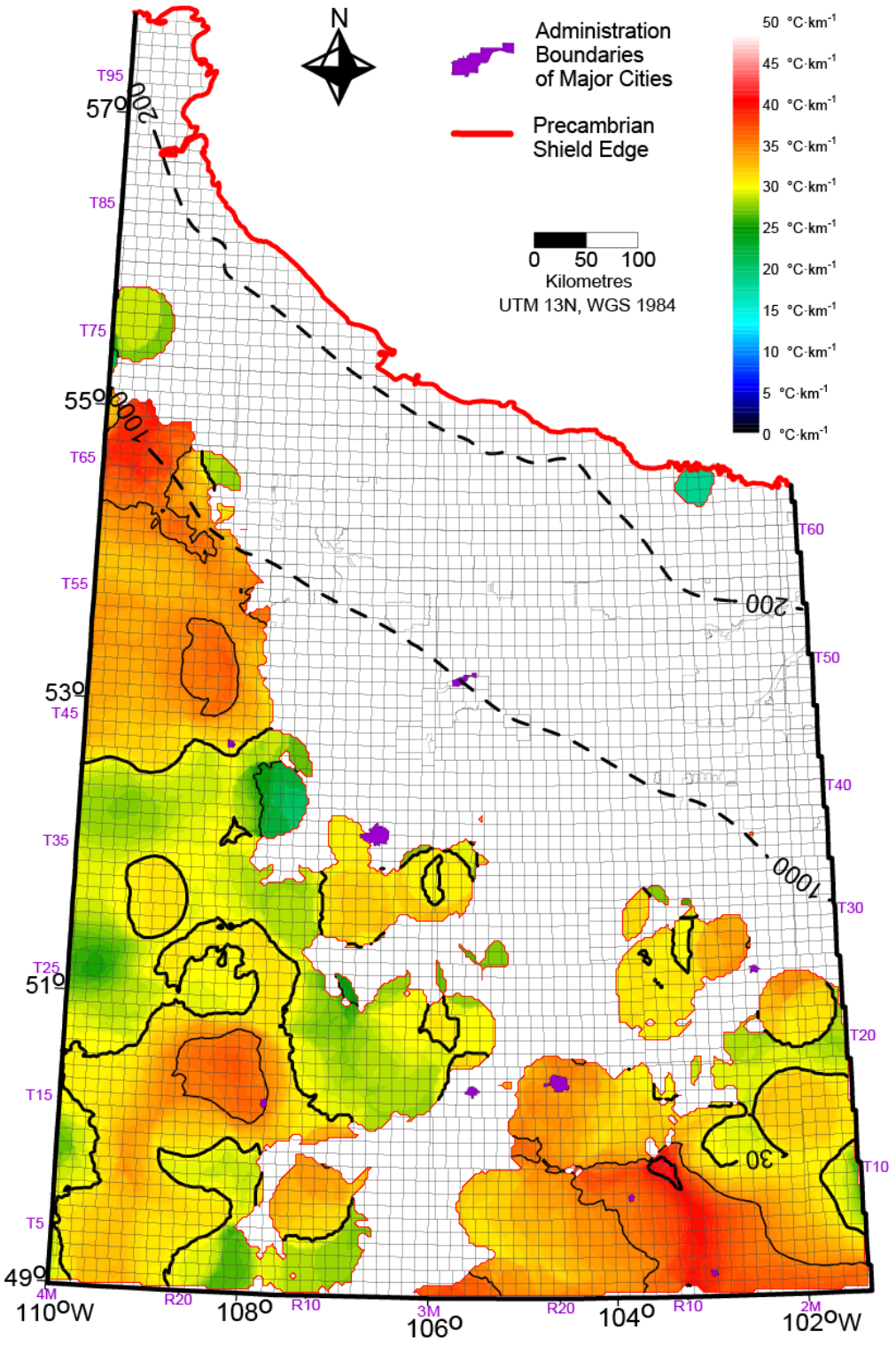

Figure I.3. Cenozoic-Mesozoic geothermal gradient with moving average gridding with 30 km search radius. Minimum number of data: 5. CI: 5 °C/km. Data distribution is the same as A.13.b.

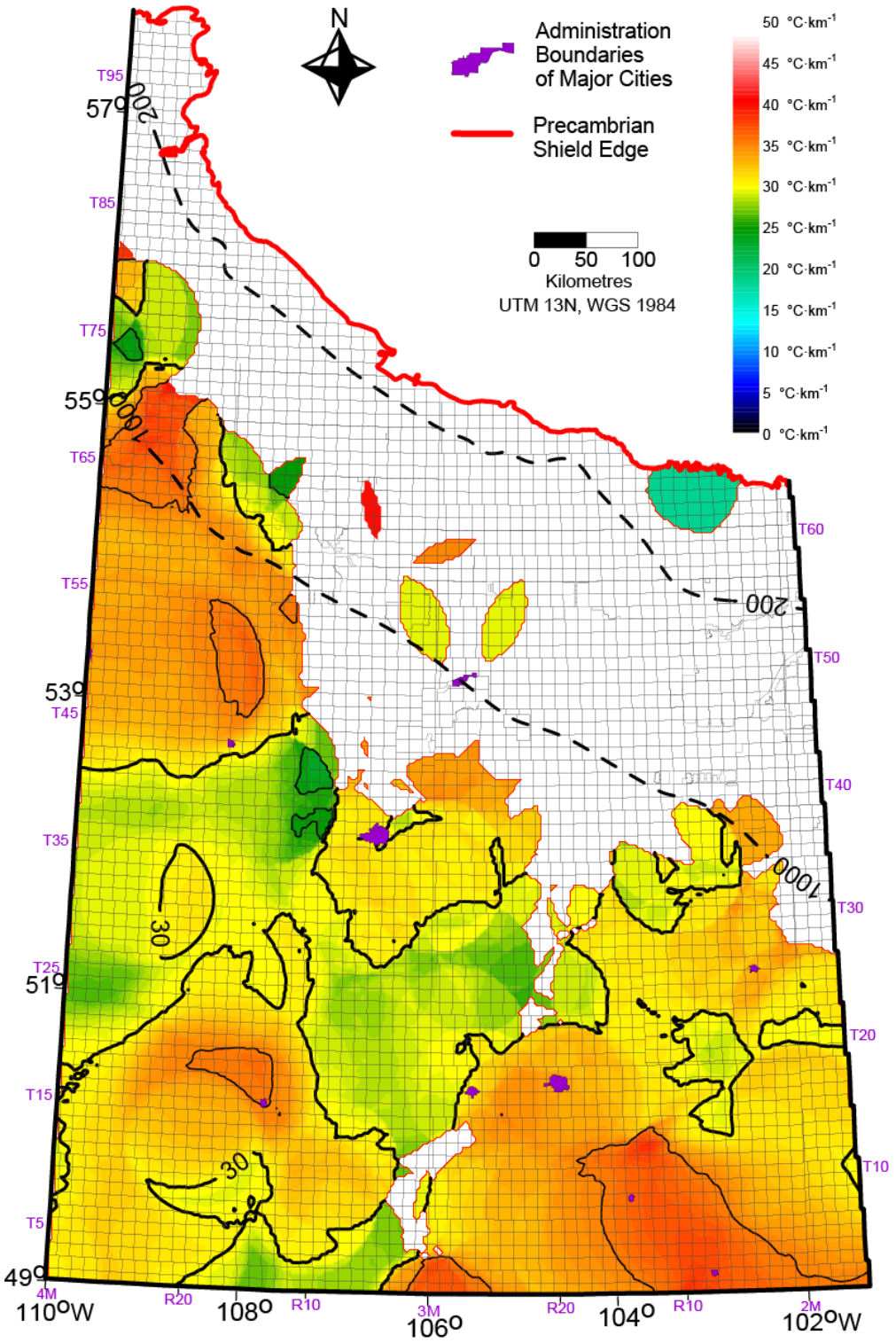

Figure I.4. Cenozoic-Mesozoic geothermal gradient with moving average gridding with 50 km search radius. Minimum number of data: 5. CI: 5 °C/km. Data distribution is the same as A.13.b.

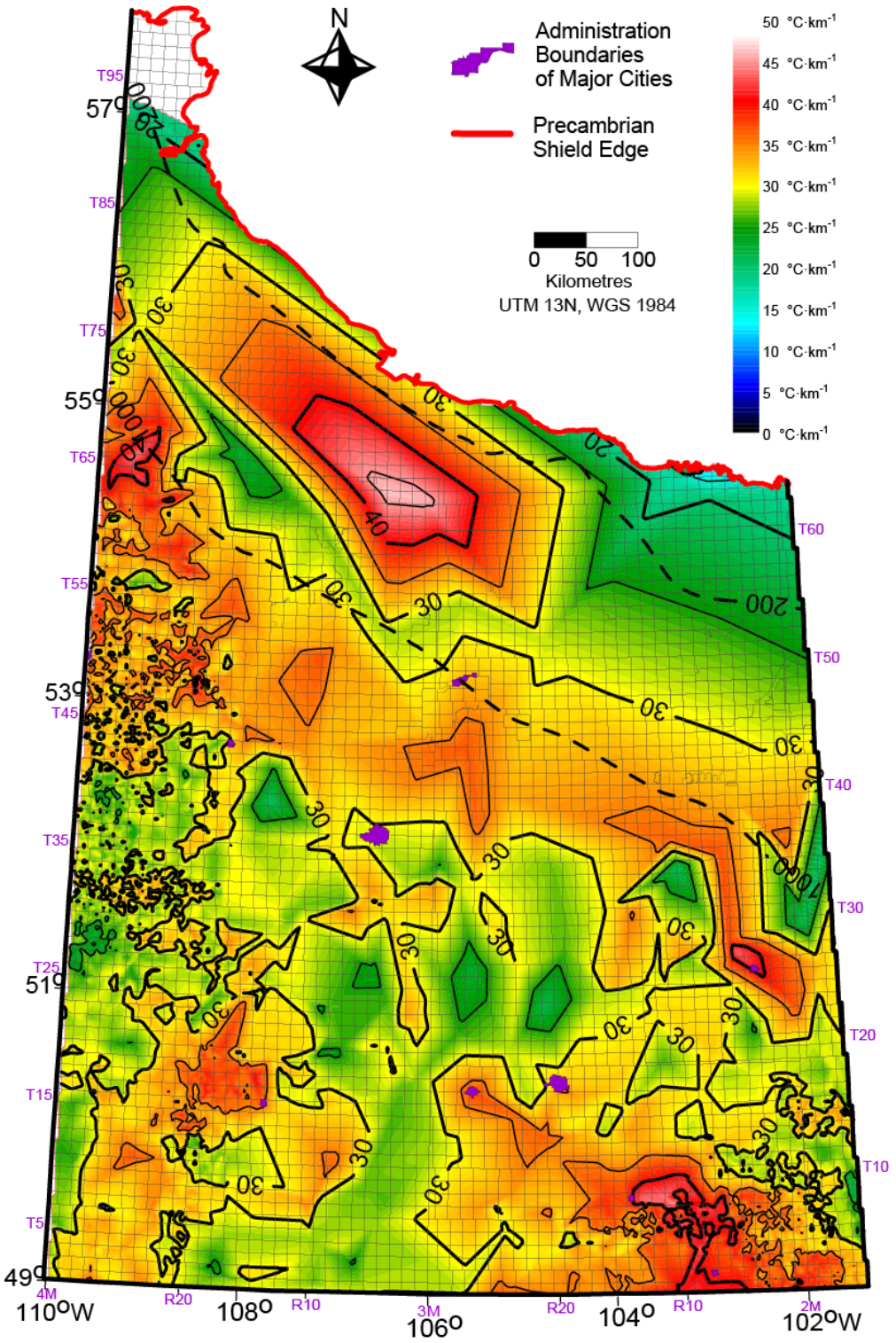

Figure I.5. Cenozoic-Mesozoic geothermal gradient with triangulation with linear interpolation. CI: 5 °C/km. Data distribution is the same as A.13.b.

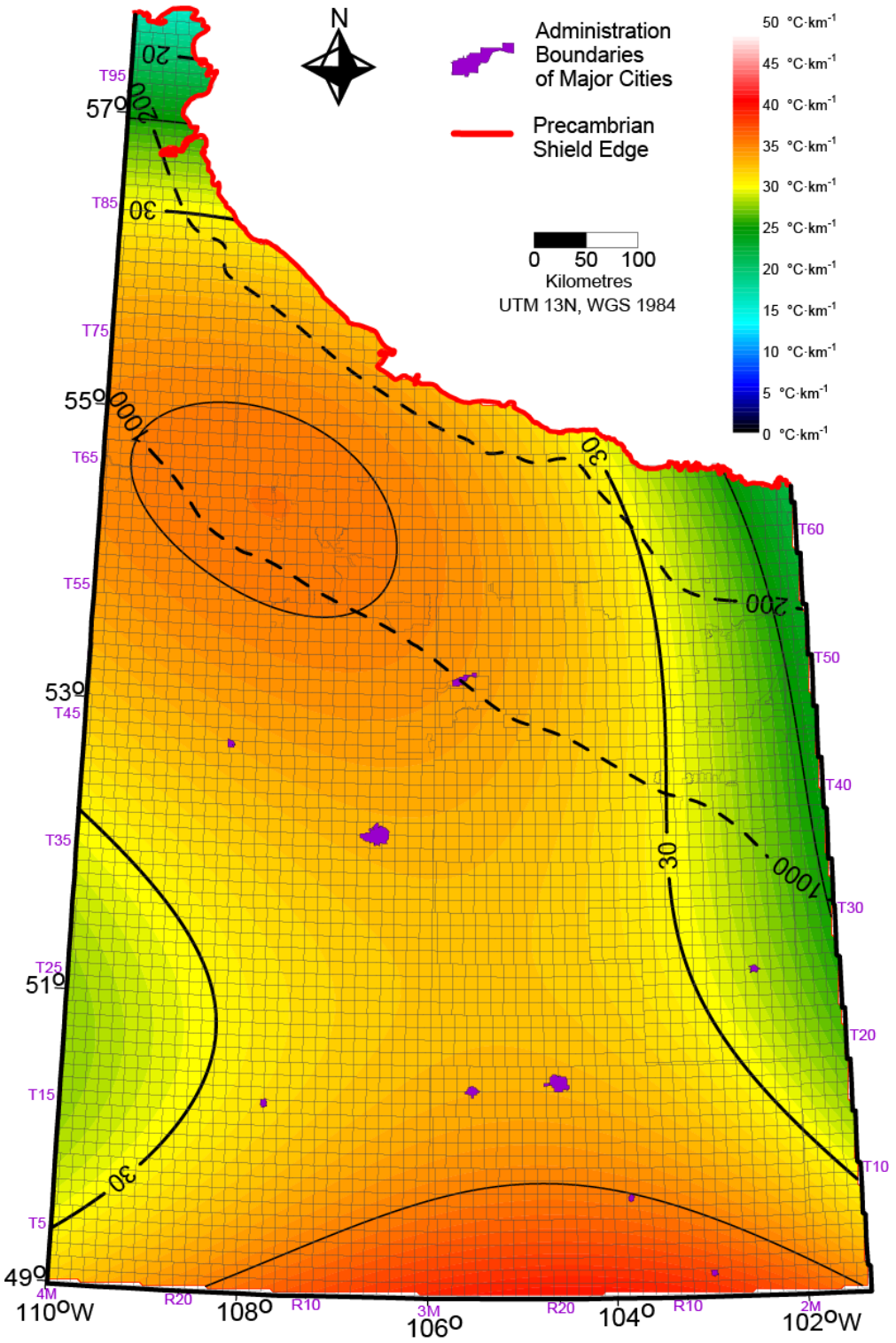

Figure I.6. Cenozoic-Mesozoic geothermal gradient with polynomial regression gridding. Surface definition: cubic surface. CI: 5 °C/km. Data distribution is the same as A.13.b.

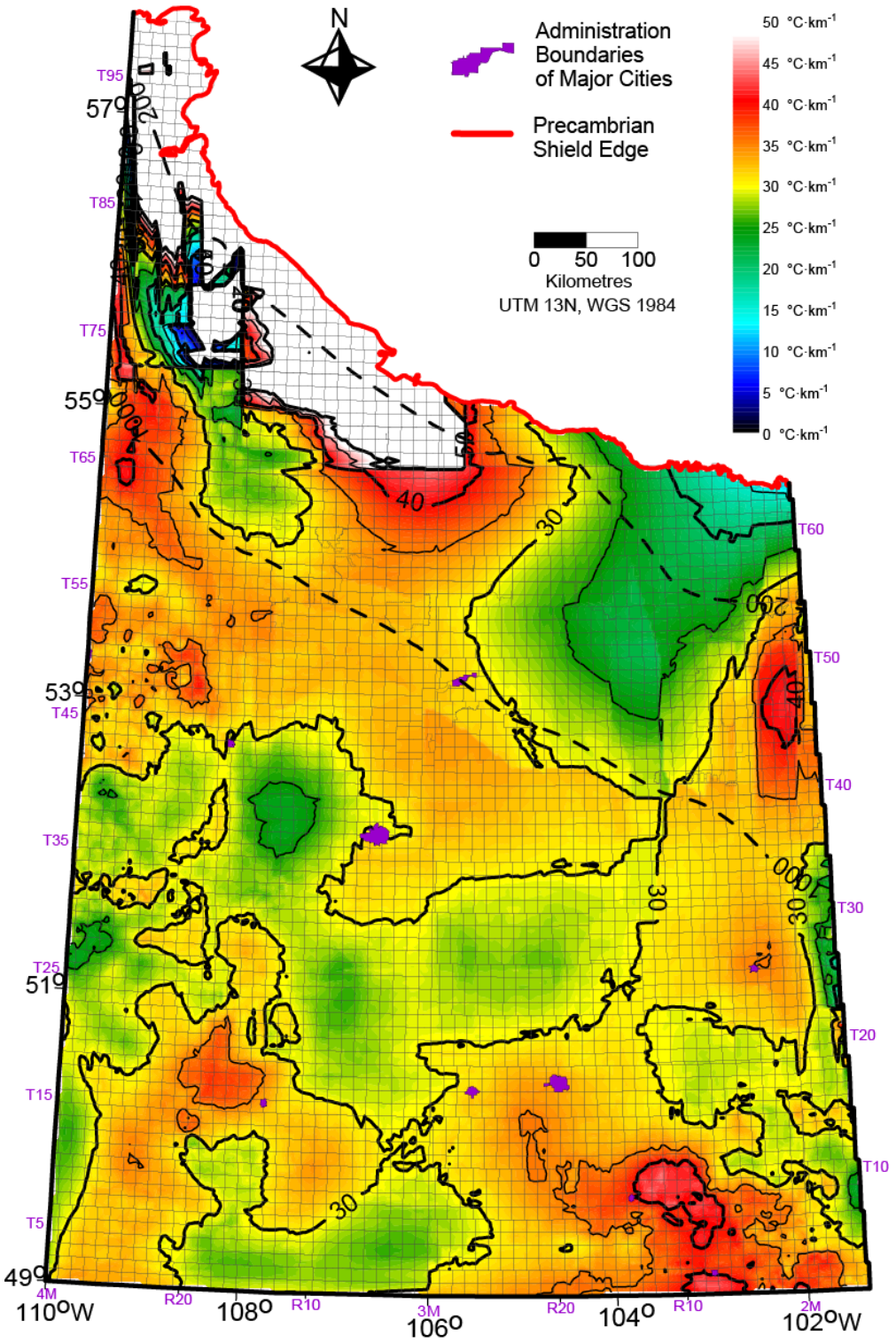

Figure I.7. Cenozoic-Mesozoic geothermal gradient with third order local polynomial regression gridding. CI: 5 °C/km. Data distribution is the same as A.13.b.

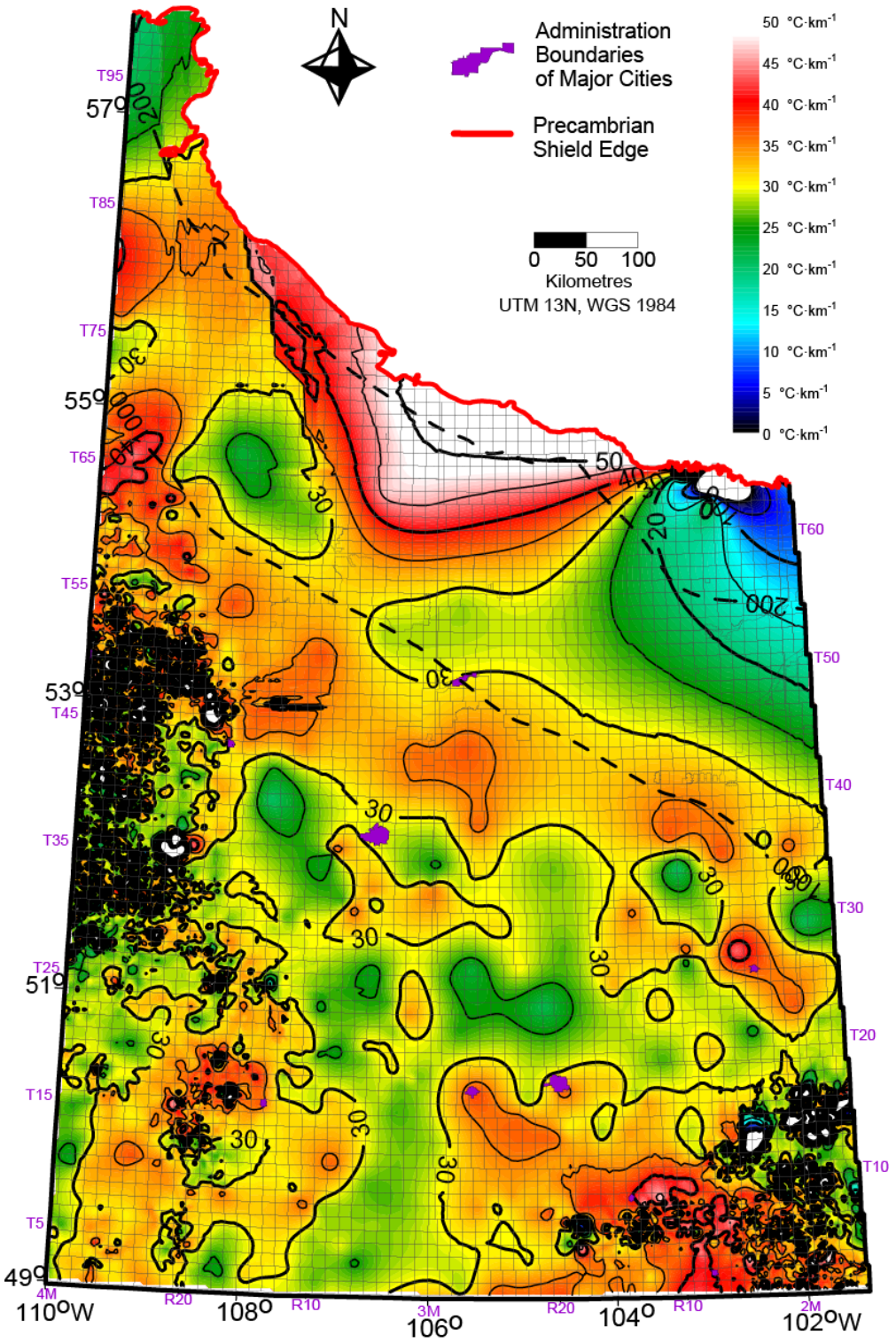

Figure I.8. Cenozoic-Mesozoic geothermal gradient with radial base function. CI: 5 °C/km. Data distribution is the same as A.13.b.

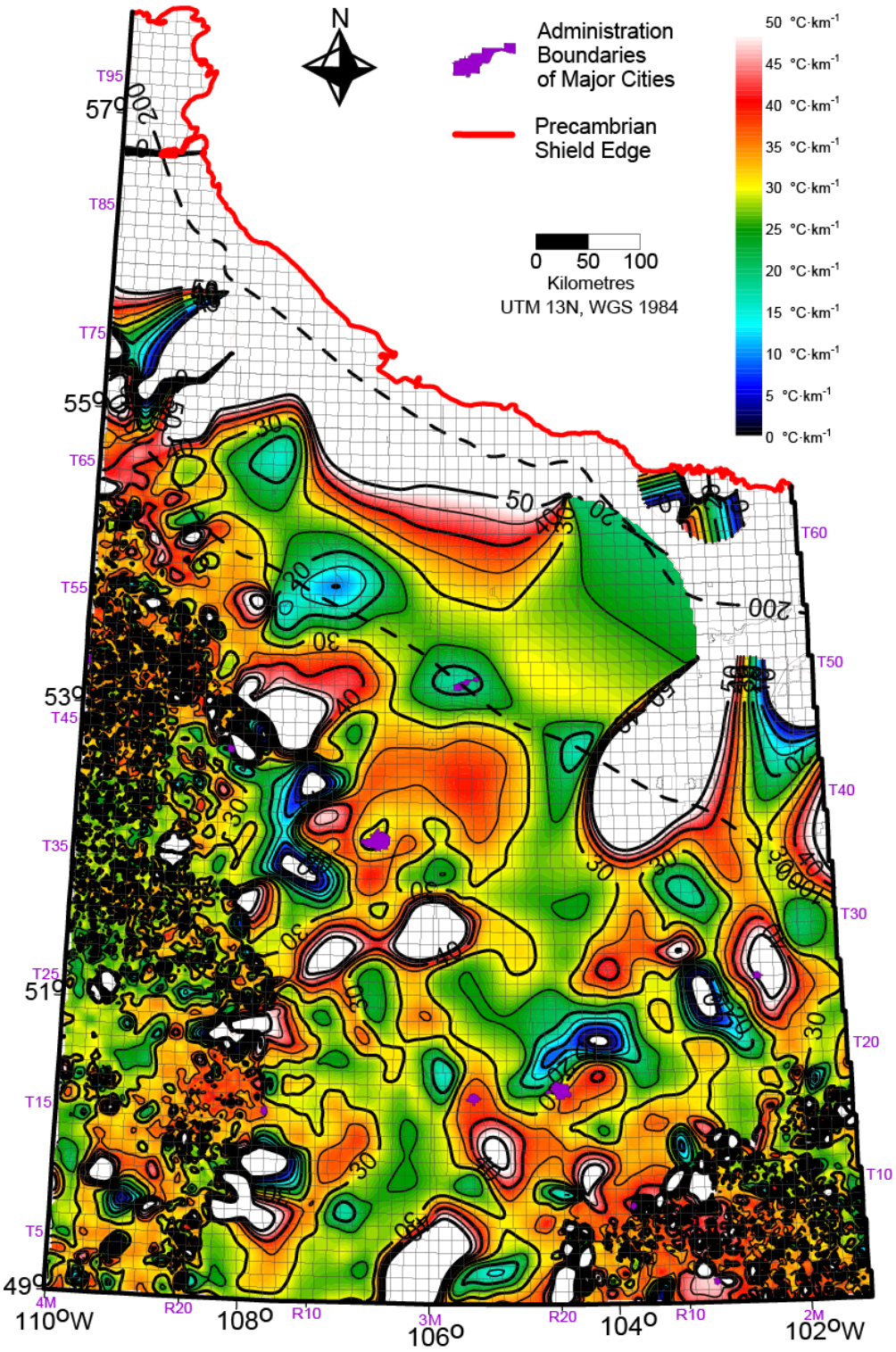

Figure I.9. Cenozoic-Mesozoic geothermal gradient with modified Shepherd's method gridding. CI: 5 °C/km. Data distribution is the same as A.13.b.

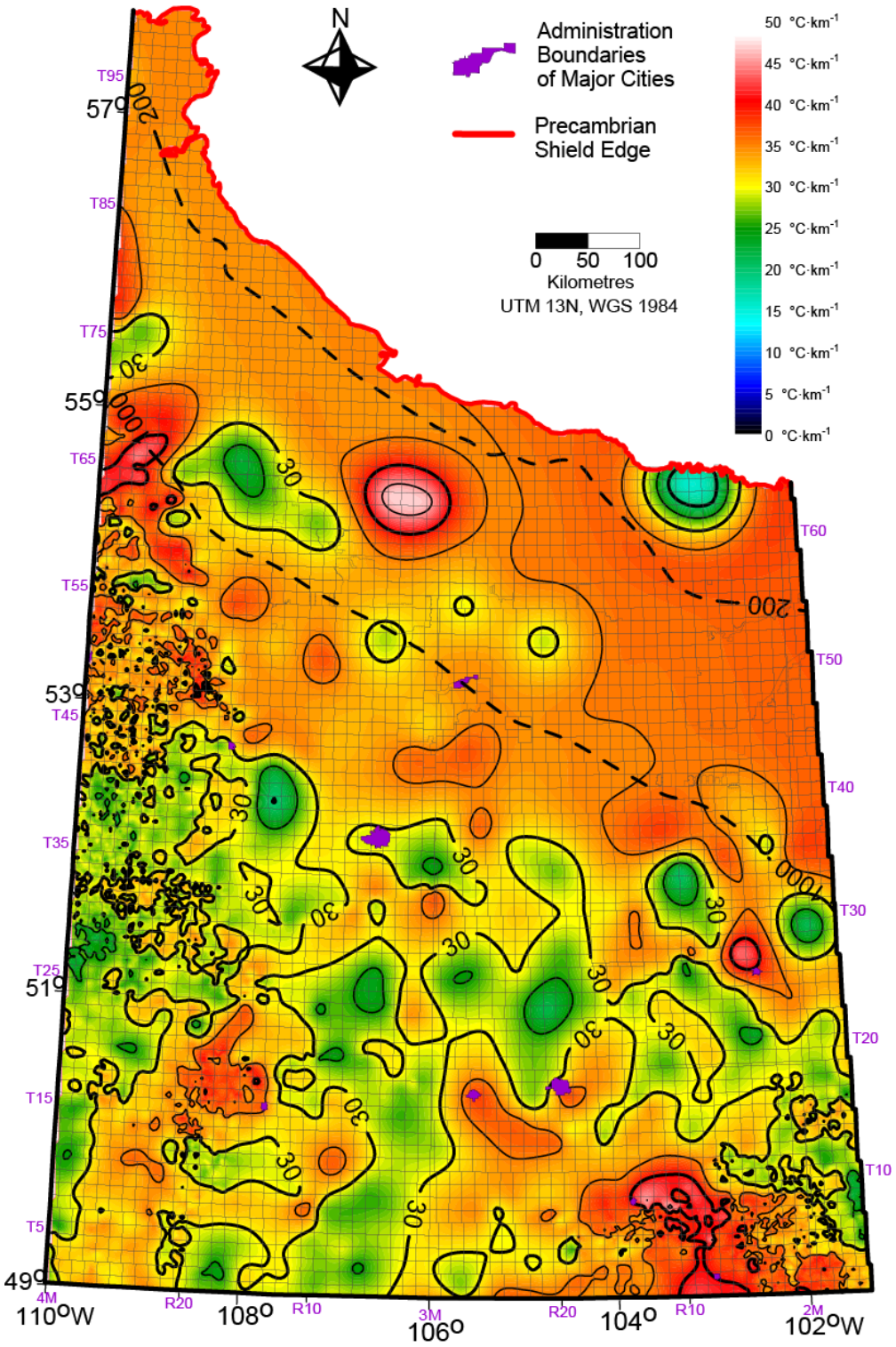

Figure I.10. Cenozoic-Mesozoic geothermal gradient with minimum curvature gridding. CI: 5 °C/km. Data distribution is the same as A.13.b.

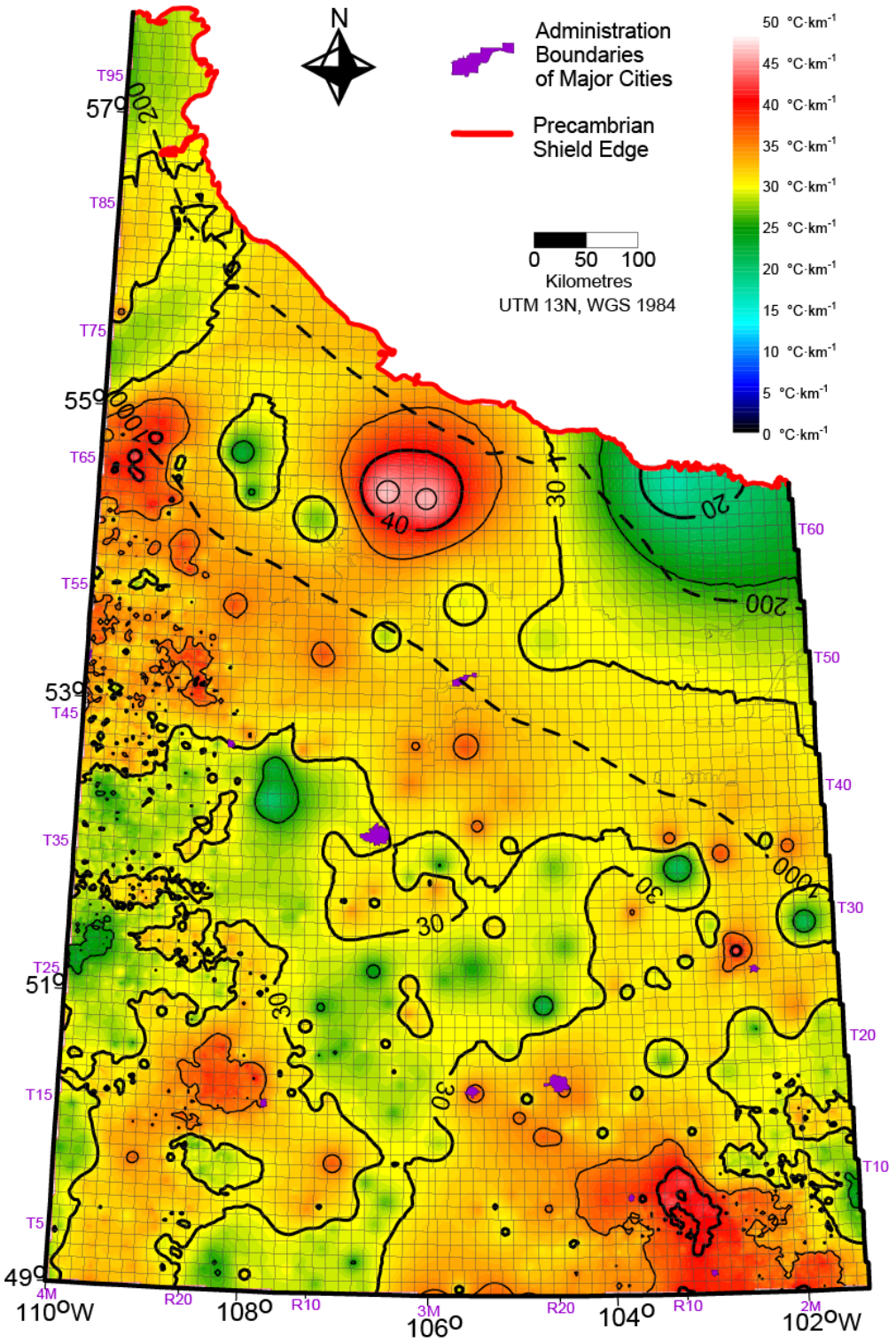

Figure I.11. Cenozoic-Mesozoic geothermal gradient with inverse distance method. CI: 5 °C/km. Data distribution is the same as A.13.b.

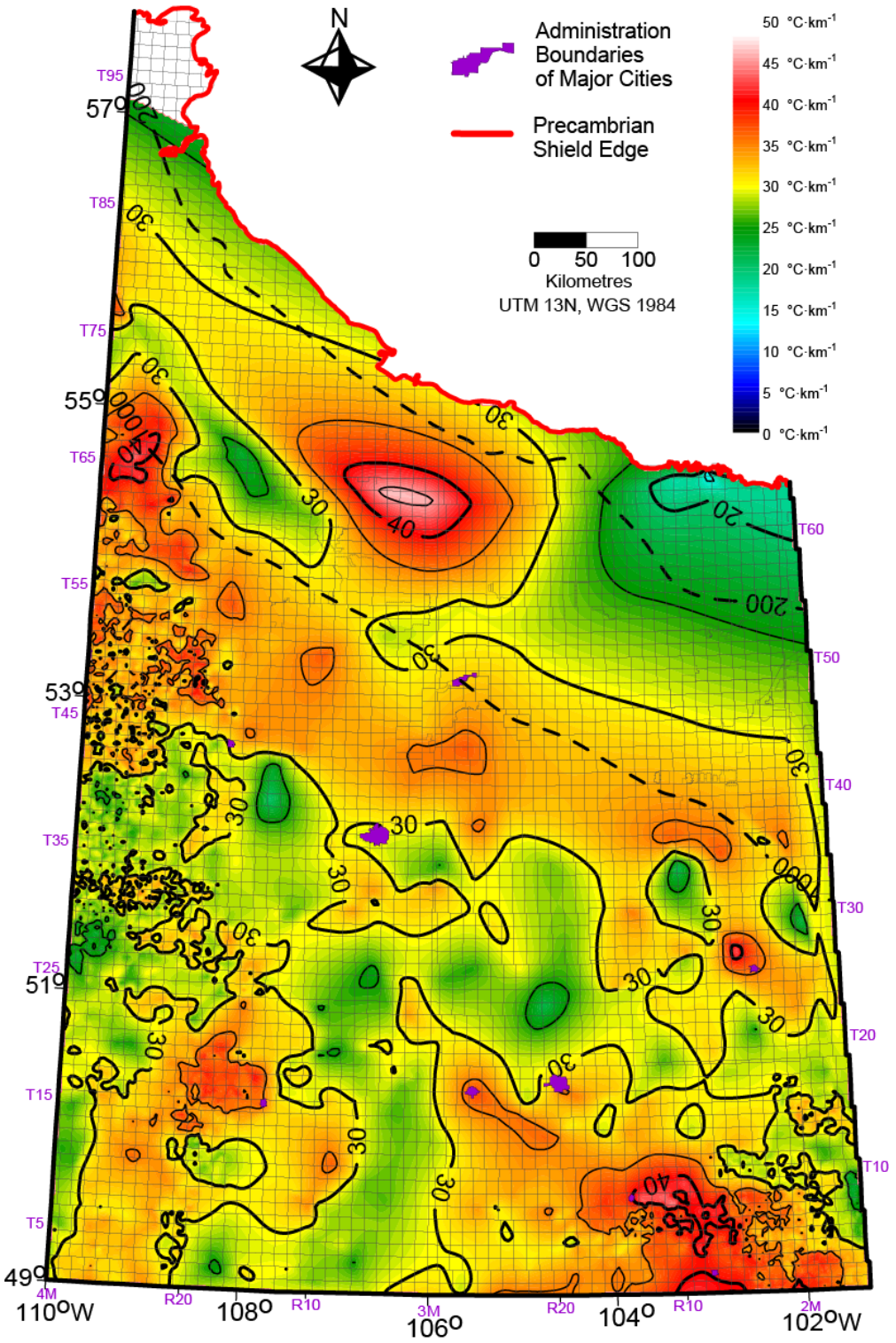

Figure I.12. Cenozoic-Mesozoic geothermal gradient with natural neighbours. CI: 5 °C/km. Data distribution is the same as A.13.b.